Investigating The Functional Consequences Of Expanded Triplet Repeat Sequence In A Mouse Model of Huntington's Disease (HD)

by

Chiung-Mei Chen

Thesis submitted for the degree of Doctor of Philosophy (Ph.D.)

University of Glasgow

Division of Molecular Genetics, Faculty of Biomedical and Life Sciences,

University of Glasgow

Abstract

Huntington's disease (HD) is an autosomal dominant, progressive neurodegenerative disorder, characterised by an array of different psychiatric manifestations, cognitive decline and choreiform movement. The underlying molecular genetic defect is an expanded trinucleotide (CAG)n repeat encoding a polyglutamine stretch in the N-terminus of the huntingtin protein. The mechanisms by which mutant huntingtin causes neuronal dysfunction and degeneration are not clear. The lack of autopsy brain material from patients, especially presymptomatic patients, makes investigation of pathogenesis difficult. Several transgenic and "knock-in" HD mouse models have therefore been generated to enable the exploration of pathological, molecular, and cellular abnormalities in HD. A "knock-in" HD mouse model (Glasgow HD mice), generated by introducing an extended stretch of ~ 80 CAG repeats into the endogenous mouse *Hdh* gene to mimic the molecular findings on human HD chromosomes, has shown neuronal dysfunction and neuropathological findings reminiscent of early stages of HD (Shelbourne et al., 1999; Li et al., 2000a; Usdin et al., 1999). The present study uses the Glasgow HD mice to investigate the early phenotypic and cellular/molecular consequences of the expanded CAG repeats in HD.

One of current limitations of using "knock-in" HD mice as a tool to investigate HD is that robust protocols for measuring modest behavioural phenotypes are less well developed. The combination of the rotarod apparatus and a more sensitive protocol was found to provide a more robust measure of the locomotor performance of the HD mice. Progressive motor deficits in both male and female HD mice were detected from 4 to 18 months of age. These observations occurred in the absence of progressive weight loss or a limb-clasping phenotype that is common in other mouse models.

Although the pathogenesis of HD is not fully understood, several mechanisms that may contribute to neuronal dysfunction and cell death have been suggested. These include defective energy metabolism, mitochondrial abnormalities, increased oxidative stress, and excitotoxicity and the interplay between these different mechanisms. Given that mitochondria could play a central role in these processes, the integrity of mitochondrial DNA (mtDNA) in the tissues of HD mice was investigated. The result of a competitive

PCR strategy showed that number of total mtDNA molecules was significantly decreased (~ 30 %) in the striatum (no reduction in the cortex and cerebellum) of 24-month old HD mice, but not at 15 months of age, when compared to wild-type mice, suggesting mtDNA depletion is a progressive rather than a developmental phenomenon.

In light of the ~ 30 % reduction of total mtDNA in the striatum, expression levels of the mitochondrial DNA-encoded respiratory complex enzymes, cytochrome b (Cytb), cytochrome c oxidase I (COI) and cytochrome c oxidase II (COII) were investigated in different brain regions of HD mice. At ~25 months of age, there were no significant differences in mRNA levels of *CoII* and *Cytb* in any brain region (striatum, cortex and cerebellum) studied when compared to normal littermates. However, HD mice showed significantly decreased CO-I protein levels and marginally decreased *CoI* mRNA levels in the striatum.

Reduced levels of mtDNA may be caused by decreased replication of mtDNA or increased oxidative damage of mtDNA. Increased levels of 8-OHdG, a marker of increased oxidative stress, were detected in the dorsomedial, dorsolateral and ventromedial striatum, but not in the cortex of 24 month-old HD mice providing direct evidence that increased oxidative stress specifically occurs in the striatum of HD mice. As no alterations in the mitochondrial transcription factor (mtTFA) in the striatum of HD mice could be detected, it is likely that mtDNA depletion in the HD mice is caused by increased levels of oxidative stress rather than decreased replication.

In summary, the study shows early and progressive motor deficits and late-onset mitochondrial abnormalities in a "knock-in" HD mouse model. The increased levels of oxidative stress present in HD striatum may be responsible for the mitochondrial abnormalities. The results provide a basis for further studies investigating how mutant huntingtin causes increased levels of oxidative stress and for identifying novel therapeutic targets.

Table of contents

List of tables

List of figures

List of abbreviations

A	Adenine
ANOVA	analysis of variance
ATP	adenosine triphosphate
ATPase	adenosine triphosphatase
bp	base pair
BSA	bovine serum albumin
C	cytosine
°C	degrees Celsius
CAT	chloramphenical acetyltransferase
cDNA	complementary DNA
COI	cytochrome c oxidase I
CoI mRNA	mouse cytochrome c oxidase I mRNA
COII	cytochrome c oxidase II
CoII mRNA	mouse cytochrome c oxidase II mRNA
Cryab mRNA	mouse alpha B crystallin mRNA
Cytb	cytochrome b
Cytb mRNA	mouse cytochrome b mRNA
DAB	3'3' diaminobenzidine tetrahydrochloride
dCTP	deoxycystosine triphosphate
DEPC	diethyl pyrocarbonate
DMSO	dimethylsulfoxide
Dmpk mRNA	mouse myotonic dystrophy protein kinase mRNA
DNA	deoxyribonucleic acid
DNase	deoxyribonuclease
dNTP	deoxyribonucleotide triphosphate
EDTA	ethylenediaminetetraacetic acid
e.g.	examplia gratia (for example)
et al	et alia
EtBr	ethidium bromide
fg	femtogram
G	guanine
Gapdh mRNA	mouse glyceraldehyde-3-phosphate dehydrogenase mRNA
HmoxI mRNA	mouse heme oxygenase-1 mRNA
4-HNE	4-hydroxy-2-nonenal
HO-1	heme oxygenase-1
HSP	mitochondrial heavy strand promoter
IgG	immunoglobulin G
IgG-HRP	IgG-horseradish peroxidase
IPTG	isopropylthio-β-D-galactoside
kb	kilobase
l	litre
LB	Luria-Bertani
LSP	mitochondrial light strand promoter
M	molar
ml	millilitre
µl	microlitre

mM	millimolar
µg	microgram
mg	milligram
min	minute
MOPS	3-(N-morpholino)-propanesulfonic acid
mRNA	messenger ribonucleic acid
mtDNA	mitochondrial DNA
mtTFA	mitochondria transcription factor A
ng	nanogram
nm	nanometer
NMDA	N-methyl-D-aspartate
OD	optical density
8-OHdG	8-hydroxydeoxyguanosine
ORP	overall rotarod performance
PBS	phosphate buffered saline
PCR	polymerase chain reaction
PEG	polyethylene glycol
PFA	paraformaldehyde
pg	picogram
PMSF	phenylmethylsulphonyl fluoride
Pol γ	mitochondrial DNA polymerase γ
RNA	ribonucleic acid
RNase	ribonuclease
RNase MRP	mitochondrial RNA processing endoribonuclease
rpm	revolutions per minute
rRNA	ribosomal RNA
RT	reverse transcriptase
RT-PCR	reverse transcriptase-PCR
s	second
SDS	sodium dodecyl sulphate
SSB	mitochondrial single-stranded DNA-binding protein
SSC	saline sodium citrate
T	thymine
TAE	Tris-acetate-EDTA buffer
TBE	Tris-borate-EDTA buffer
TBS	Tris-buffered saline
TBST	Tris-buffered saline tween 20
Tfam mRNA	mouse mitochondria transcription factor A mRNA
Tm	melting temperature
Tris	Tris(hydroxymethyl)amino methane
tRNA	transfer RNA
Tween 20	polyoxyethylene sorbitan monolaurate
UV	ultraviolet
v/v	volume per volume
w/v	weight per volume
X-Gal	5-Bromo-4-chloro-3-indolyl-β-D-galactoside
YAC	yeast artificial chromosome

To Mum, Dad, Sheng, Ping-I and Mu-Chun

Acknowledgements

I would like to thank the people who have given a lot of support and friendship:

My supervisor, Peggy Shelbourne and Debbie Dewar for offering me the opportunity to undertake the project and their constructive guidance.

My assessor, Darren Monckton and John Clutterbuck for their helpful advice.

Colleagues and staff in the lab on Level 5: Keith Johnson, Mark Bailey, Graham Brock, Graham Hamilton, Peggy Ennis, Liz Evans, Laura Kennedy, Mario Pereira, John McAbney, Jonathan Houseley, Ann Hever, Christine Haworth, Saadia Karim, Demetrius Vouyiouklis, Mary Gardiner, Rami Jarjour.

Richard Wilson for statistical analysis advice.

Colleagues and staff in the Wellcome Surgical Institute, Glasgow and Daniel Cuthill and Jill Fowler for giving me their mouse and rat tissue sections.

Sheng for constantly supporting me whenever I needed, and Ping-I and Mu-Chun for being very cooperatively helpful, without whom the life of this four years could have been harder.

Finally, the Chang Gung Memorial Hospital. Without its financial support, the PhD project would never have started.

Author declaration

I certify this thesis does not contain material previously published or written by any other person. The research reported in this thesis is my own original work except where referred to in the text and the results of this study have not been submitted for any other degree or diploma.

Chiung-Mei Chen

1 Introduction

1.1 Huntington's Disease (HD)

Huntington's disease (HD) is an autosomal dominant, progressive neurodegenerative disorder, characterised by an array of different psychiatric manifestations, cognitive decline and choreiform movement (Harper, 1996). Two forms of HD, juvenile HD and adult HD, have been arbitrarily divided by the age of disease onset. The term 'juvenile HD' is generally applied to cases of HD with onset before 20 years of age. Presentation of juvenile HD is commonly with symptoms of mental disturbance and rigidity rather than choreic movements, while HD presenting in mid life more frequently shows a relatively pure movement disorder. The psychiatric problems include a variety of conditions that range from antisocial personality, psychosomatic disorder, delusional disorder, and affective disorder to schizophrenia. Although chorea is a cardinal sign of HD, other motor abnormalities such as rigidity, bradykinesia, dystonia, cerebellar ataxia and myoclonus are common either in juvenile HD or in the late stage of adult HD. Family studies of HD in the pre-molecular era had documented that most juvenile and early-onset cases of HD were paternally transmitted and that there appeared to be anticipation, i.e. progressively earlier onset in successive generations. HD is a relentlessly progressive disease, and survival ranges between 10 and 17 years from the age at onset. In the late stages of HD, cachexia is a frequent but not invariable symptom, although lack of muscle bulk is often obvious. However, it has been reported that weight loss occurs in patients with HD despite an adequate diet and feeding (Morales et al., 1989; Pratley et al., 2000). Pneumonia and cardiovascular disease are the commonest causes of death in HD and usually result from immobility and dysphagia.

1.1.1 Epidemiology

The prevalence of HD in the UK is 4~ 8 per 100,000 population, whilst in North America it is estimated to be around 4.5 per 100,000. Variation in the prevalence of HD between countries has been recognized with a very low prevalence of HD (0.11 to 0.65 per 100,000) in Japan (Nakashima et al., 1996) and Hong Kong Chinese (Chang et al., 1994).

1.1.2 Psychomotor abnormalities in HD

Behavioural and cognitive changes and motor deficits are central features of HD. Motor dysfunction in HD is thought to result from the disruption of cortico-basal ganglia-thalamic pathways regulating motor control. Motor disturbances include choreiform involuntary movements of limbs and a progressive impairment in the co-ordination of voluntary movements. In juvenile-onset HD, bradykinesia and dystonia are the predominant symptoms. Epileptic seizures and cerebellar signs are often present in juvenile-onset HD (Harper, 1996).

The cognitive impairment in HD is believed to be a consequence of the profound frontostriatal pathology associated with the disease (Vonsattel and DiFiglia, 1998). Frontostriatal dysfunction has been shown in HD patients who display a decline in visuospatial skills, cognitive flexibility, and recall memory (Lange et al., 1995; Lawrence et al., 1998; Lawrence et al., 1996; Lawrence et al., 2000). Deficits in a visual discrimination/set-shifting task by have been shown in both symptomatic HD patients and presymptomatic mutation carriers (Lawrence et al., 1998; Lawrence et al., 2000). They exhibit preservative responses, an inability to disengage their response from a previously positively reinforced stimulus, and this appears to be the result of loss of inhibition function of the frontostriatal pathway.

Common behavioural problems in HD include loss of energy and initiative, poor judgement and quality of work, impaired judgement, poor self-care and emotional blunting. Affective symptoms such as depression, anxiety and irritability are less common but not rare. Psychotic symptoms (hallucinations and delusions) have been occasionally reported (Craufurd et al., 2001; Harper, 1996). Some behavioural changes (such as loss of energy and initiative, poor judgement, poor self-care and emotional blunting) are strongly correlated to the progression of HD, whilst others (such as depression, anxiety, aggression, and inflexibility) are not (Craufurd et al., 2001). The disease progression-related behavioural changes might provide a reliable marker of the onset and overall progression of the disease, which can be used to evaluate the efficacy of therapies in the future.

1.1.3 Neuropathology of HD

Neurodegeneration in HD starts in the striatum, then involves the cortex and in the latter stages, also the globus pallidus, thalamus and amygdala. Astrocytosis follows the path of striatal cell loss, which develops in a topographically ordered manner, spreading along the caudal-rostral, dorsal-ventral and medial-lateral axes (Vonsattel and DiFiglia, 1998). HD neuropathology has been classified from grade 0 to 4 with increasing severity and extent of striatal involvement (Vonsattel et al., 1985). Clinical manifestations can appear in the absence of gross brain abnormalities, neuronal loss, and reactive gliosis in the striatum (grade 0). In grade 4, the striatum is severely atrophic with the loss of more than 95 % of neurons and marked increases in oligodendrocyte density. The majority of HD cases are Grade 3 or 4 at the time of death (Vonsattel and DiFiglia, 1998). The grade of striatal pathology appears to correlate closely with the involvement of other cerebral regions. Non-striatal regions are largely spared in Grade 1 and 2 (Vonsattel and DiFiglia, 1998). In contrast, profound grade 4 changes are more often found in juvenile HD and neuronal loss extends into the regions spared in adult-onset patients, such as the cerebellum, suggesting a more aggressive pathological process in these individuals (Myers et al., 1988).

Different cell subtypes within the striatum also show selective vulnerability to the disease process. Medium spiny projection neurons are commonly lost while large cholinergic interneurons and medium aspiny somatostatin/nitric oxide synthase neurons are otherwise spared (Reiner et al., 1988). The 'indirect pathway' neurons in striatum, which co-express proenkephalin/enkephalin and are enriched in D2 dopamine receptors, appear to be affected earlier than the 'direct pathway' neurons, co-expressing substance P and D1 dopamine receptors (Richfield et al., 1995; Sapp et al., 1995).

1.2 The molecular basis of HD

1.2.1 HD mutation

A novel gene, *IT15* (*HD*), containing a polymorphic trinucleotide (CAG) repeat that is expanded and unstable on HD chromosomes, was identified by the HD Collaborative

Research Group in 1993 (HDCRG, 1993). The mutated gene carrying the expanded CAG repeat lies on chromosome 4 at 4p 16.3. A (CAG)n repeat longer than the normal range was observed on HD chromosomes from 75 disease families examined, comprising a variety of ethnic backgrounds and 4p16.3 haplotypes. The causative gene mutation responsible for HD thus involves an unstable (CAG)n sequence that acts in the context of a novel gene to produce a dominant phenotype. The human *HD* gene has 67 exons, ranging in length from 43 to 341 base pairs (bp), that span 180 kb of genomic DNA (Ambrose et al., 1994). The (CAG)n repeat encoding a polyglutamine tract is in the first exon and is followed by a CCG repeat encoding a polyproline region. The corresponding protein product of the *HD* gene, huntingtin, has an estimated molecular mass of 348 kDa, representing 3144 amino acids.

No clear homology with any existing protein sequence in the databases has been discovered. However, recently a *Drosophila* homologue of *HD* gene has been identified (Li et al., 1999a). The *Drosophila HD* gene has 29 axons, compared with the 67 exons present in vertebrate *HD* gene. The predicted *Drosophila* huntingtin protein has 3853 amino acids and lacks the polyglutamine and polyproline stretches present in its mammalian counterparts. *Drosophila* and vertebrate *HD* sequences show a high degree of similarity in three large, contiguous regions at the N-terminus, middle and c-terminus of the protein and there is an overall identity of 24 % and similarity of 49 % between fly and human sequences.

The mouse orthologue of human *HD* gene is called the *Hdh* gene and has been mapped to chromosome 5 in a region devoid of mutations causing a comparable phenotype. The mouse *Hdh* gene coding sequence is 86 % identical to the human *HD* gene at the DNA level and 91 % at the protein level. The *Hdh* gene possesses an imperfect CAG repeat encoding 7 consecutive glutamines (Barnes et al., 1994).

1.2.1.1 Clinical correlates with the (CAG)n repeat copy number in HD

A progressive increase in the expressivity of an identical mutation over subsequent generations is termed “anticipation”. One of the distinguishing features of trinucleotide repeat mutations is that the (CAG)n repeat allele can undergo ‘dynamic mutation’ in which

the repeat number may change when transmitted from parent to offspring (intergenerational mutation instability). Anticipation results from intergenerational mutation instability and its corresponding impact on phenotype. Quantitative molecular studies of HD families have indicated that both the anticipation and the parent-of-origin differences are mediated principally through the number of CAG repeats (Ranen et al., 1995; Trottier et al., 1994). In both studies, although a small increase in repeat number (up to 7 repeats) was seen in germline transmission by both sexes, larger increases were seen almost exclusively in the offspring of affected males. The largest increases through generational transmission were particularly likely to occur in individuals who themselves had the largest expansions, confirming the size-dependent instability of the HD mutation. In terms of intergenerational changes, it has been noted that the CAG copy number in the HD mutation may decrease as well as increase, although decreases were only found in a small proportion of transmissions (Kremer et al., 1994). In this study a modest decrease of between 1 and 4 in CAG repeats was seen, but no larger decreases were observed in the next generation.

Several studies have shown that there is a significant inverse correlation between age at onset of symptoms and CAG repeat number, a trend that is even stronger within the juvenile group (Brinkman et al., 1997; Duyao et al., 1993; Stine et al., 1993; Trottier et al., 1994). In these studies, it was also observed that the severity of disease is proportional to the number of CAG repeats.

The rate of progression has also been correlated with the size of CAG repeat (Brandt et al., 1996; Illarioshkin et al., 1994), although the findings were not replicated in another study (Kieburtz et al., 1994) that followed the participants over a shorter period of time. Additional studies have revealed that the extent of pathological change in HD is positively related to the CAG mutation size (Furtado et al., 1996; Penney et al., 1997), although in one further study, evidence for this correlation was not forthcoming (Sieradzan et al., 1997).

The (CAG)n repeat region shows a range of 11-35 repeats in normal individuals, while a repeat number of greater than 35 indicates a high probability of developing HD (Rubinsztein et al., 1996). There have been no confirmed reports of persons with repeats in

the range of 29 to 35 expressing HD. There are, however, confirmed cases of paternally transmitted mutation instability such that descendents of fathers with an allele in this intermediate range are known to have inherited an expanded allele in the clinically affected range (Myers et al., 1993). A repeat size of 36 to 39 is considered indeterminate as to whether the person will develop HD at some time in the future. It appears that some persons with repeats in this range develop HD whilst others live into their late 90s without evidence of disease development (Kremer et al., 1994; McNeil et al., 1997; Rubinsztein et al., 1996).

1.2.1.2 Germline and somatic mutation length variability in HD

As previously mentioned (section 1.2.1.1), a larger CAG repeat length is associated with a severe and early-onset clinical picture. Understanding the molecular mechanism that underlies mutation instability may help explain the neuropathological profiles of HD.

The expanded CAG repeat stretch exhibits striking length-dependent intergenerational instability in HD patients. Gametic CAG repeat instability in HD patients (Leeflang et al., 1995; MacDonald et al., 1993) and in HD transgenic (Mangiarini et al., 1997) and "knock in" mice (Shelbourne et al., 1999; Wheeler et al., 1999) has been reported. In contrast, limited mutation length variation has been reported in somatic tissues of most HD patients (Benitez et al., 1995; De Rooij et al., 1995; Giovannone et al., 1997; MacDonald et al., 1993; Zuhlke et al., 1993), suggesting that gametogenesis is the primary source of mutation length variability.

In contrast, a number of studies provide evidence that significant somatic instability is present in HD. Firstly, in one HD post-mortem study, all tissues examined were found to display some repeat mosaicism, with the greatest levels detected in brain and sperm. Regions within the brain showing most obvious neuropathology, such as the basal ganglia and the cerebral cortex, displayed the greatest mosaicism, whereas the cerebellar cortex, which is seldom involved, displayed the lowest degree of CAG instability (Telenius et al., 1994). Secondly, the greatest levels of somatic instability have been observed in the striatum of HD mice with highly expanded CAG repeats (Kennedy and Shelbourne, 2000;

Mangiarini et al., 1997). Thus, it is considered that somatic instability of the CAG mutation may play a role in the cell-specificity of the pathological HD phenotype.

The molecular mechanism underlying germline and somatic repeat instability of trinucleotide repeat mutations is not well understood. Although unequal sister chromatid exchange and template/DNA polymerase slippage during DNA replication have been proposed, a recent study using small pool PCR to detect (CAG)n repeat length in a "knock-in" HD mouse model has shown evidence that somatic trinucleotide repeat instability may occur by mechanisms that are not replication-based (Kennedy and Shelbourne, 2000). The non-replication based mechanism is supported by the study that the transgenic mice carrying exon 1 of a mutant human *HD* genes on a mismatch repair deficient background (*Msh2*-/-) showed a decreased variation in somatic CAG repeat number, suggesting that Msh2 is required for the somatic instability of the CAG repeat (Manley et al., 1999). As Msh2 involved in the mismatch-repair pathway, this finding implies that CAG expansion may occur when DNA undergoes repair. Recently, a study showed that expansion is neither a mitotic nor a meiotic event in male mouse germ cells. Rather, expansion appears to be a post-meiotic event that occurs late in elongating spermatids, as they become spermatozoa (Kovtun and McMurray, 2001). In this study, the authors also showed that Msh2 is implicated in both germline and somatic mutation expansion and proposed that CAG expansion in the germ cells arises by gap repair and depends on a complex containing Msh2. Alternatively, as increased oxidative damage has been shown in the striatum of HD patients (Browne et al., 1997), it is possible that oxidative damage of DNA may initiate DNA repair that lead to mutation expansion.

1.2.2 The *HD* gene

1.2.2.1 Expression patterns of *HD* gene

Two mRNA species (sizes: 10.3 kb and 13.7 kb), originating from the *HD* gene and coding the same huntingtin protein, have been reported (Lin et al., 1993). The two transcripts are thought to arise through differential polyadenylation, which may constitute a mechanism that regulates huntingtin expression through the generating transcripts with different stabilities. The two main mRNA transcripts from the human *HD* gene are present in most

tissues (Lin et al., 1993; Strong et al., 1993), although the larger transcript is more abundant in human brain (Lin et al., 1993). Many studies have shown that the levels of *HD* gene mRNA are highest in cortical layers II-IV, the hippocampus and dentate gyrus, and lower in the area of the basal ganglia that degenerates first and most profoundly in HD (Landwehrmeyer et al., 1995; Lin et al., 1993; Strong et al., 1993). Using *in situ* hybridisation, one study concluded that there was little difference in mRNA expression levels in normal and HD brain, except for that which could be accounted for by tissue loss in the striatum (Landwehrmeyer et al., 1995).

Similar to mRNA studies, most protein studies also indicate ubiquitous expression of huntingtin with higher levels in brain and testis than in other tissues (Gutekunst et al., 1995; Sharp et al., 1995; Trottier et al., 1995). Among the different regions of brain, the cortex and cerebellum appear to show higher levels of huntingtin protein than the striatum (Gutekunst et al., 1995; Sharp et al., 1995; Trottier et al., 1995). Therefore, the wide pattern of the *HD* gene mRNA and huntingtin protein expression in the cytoplasm of a variety of neuronal and non-neuronal cells and tissues does not readily account for the neuronal specificity of HD pathology.

More recently, it appears that huntingtin expression in the brain may be more heterogeneous than suggested previously (Ferrante et al., 1997). The authors conclude that the spiny striatal neurons and the matrix compartment observed in HD is associated with higher levels of huntingtin expression, whereas the large and medium sized aspiny neurons and the striosome compartments is associated with lower levels of huntingtin expression. However these conclusions are not supported by another study showing that more severe neuronal loss was found in the striosomal compartments than the matrix (Hedreen et al., 1995). Further investigation is needed to resolve these conflicting findings.

Mutant huntingtin can be distinguished from the wild-type huntingtin protein on western blot by virtue of its anomalous migration (Aronin et al., 1995; Ide et al., 1995; Jou and Myers, 1995; Persichetti et al., 1995; Trottier et al., 1995). Its increased size in relation to the wild type protein is highly correlated with CAG repeat expansion (Aronin et al., 1995). Although, similar regional distribution of both mutant and wild-type huntingtin is evident, several studies, using a variety of antibodies to detect huntingtin, have noted a modest

reduction in relative expression level of mutant protein in HD (Gutekunst et al., 1995; Ide et al., 1995; Persichetti et al., 1996; Trottier et al., 1995). It has also been noted that the degree of reduction in mutant huntingtin level appeared to be aggravated by increasing CAG repeat allele length (Gutekunst et al., 1995). However, it has also been reported that a longer repeat length can generate a higher level of mutant huntingtin protein expression (Aronin et al., 1995). It has been suggested that the discrepancy in the studies of expression levels of normal and mutant huntingtin may be due to a sensitivity bias favouring detection of the disease isoform by the antiserum used (Aronin et al., 1995; Trottier et al., 1995). In summary, the relationship between the level of huntingtin expression and selective vulnerability to HD is poorly understood at this time.

1.2.2.2 Function of normal huntingtin

The function of huntingtin protein remains unclear. Elucidating the normal function of huntingtin may help to understand some aspects of the disease process, if loss of normal huntingtin function contributes to HD pathogenesis.

Immunocytochemical studies show that huntingtin is exclusively localized in the neuronal cytoplasm, enriched in nerve endings and associated with synaptic vesicles in the human brain (DiFiglia et al., 1995; Gutekunst et al., 1995; Sharp et al., 1995; Trottier et al., 1995). Biochemical evidence suggests that wild-type and mutant huntingtin are present in cytosolic soluble fractions and microsomal membranes and associated with the cytoskeleton (DiFiglia et al., 1995; Gutekunst et al., 1995; Wood et al., 1996). Immunofluorescence studies suggest that huntingtin co-localizes with the transferrin receptor, coated vesicles in cytoplasm and multivesicular bodies that are part of an endosomal-lysosomal system and enriched in Golgi apparatus (Sapp et al., 1997; Velier et al., 1998). Huntingtin also appear to be associated with microtubules and synaptic vesicles suggesting that it plays a role in intracellular organelle trafficking or fast axonal transport (Sapp et al., 1997; Tukamoto et al., 1997).

Studies using mouse models in which targeted disruption of both mouse *Hdh* alleles leads to death of embryos in uterus between embryonic day 7.5 and 10.5, have indicated that huntingtin plays a role in embryonic development during gastrulation (Duyao et al., 1995;

Nasir et al., 1995; Zeitlin et al., 1995). Although, heterozygous loss of huntingtin does not appear to cause any overt abnormalities in some mouse lines (Duyao et al., 1995; Zeitlin et al., 1995), neuronal loss and degeneration in the subthalamus and globus pallidus has been reported in another mutant line with heterozygous loss of huntingtin (Nasir et al., 1995; O'Kusky et al., 1999). Furthermore, in a mouse model where *Hdh* expression is conditionally inactivated at two developmental time points (after embryonic day 15 and after postnatal day 5), elimination of *Hdh* expression in the brain and testis leads to neuronal degeneration, motor phenotypes, early mortality and sterility, suggesting an important role of huntingtin in postnatal neuronal survival (Dragatsis et al., 2000). In cell culture, it has been shown that wild-type huntingtin up-regulates transcription of brain-derived neurotrophic factor (BDNF), a pro-survival factor produced by cortical neurons and necessary for survival of striatal neurons (Zuccato et al., 2001). When huntingtin become mutated, the up-regulation benefit appears to be lost, cortical BDNF production is decreased and striatal neurons are compromised (Zuccato et al., 2001). Evidence of a role for wild-type huntingtin in decreasing the cellular toxicity of mutant huntingtin *in vivo* (Leavitt et al., 2001) and *in vitro* (Ho et al., 2001; Rigamonti et al., 2000; Rigamonti et al., 2001) has also been shown. Over-expression of normal huntingtin significantly attenuates neuronal toxicity induced by both NMDA receptor agonists and mutated huntingtin (Sun et al., 2001). Taken together, these findings suggest that huntingtin may be critical both in embryogenesis and in neuronal survival in the adult.

1.2.3 The molecular pathology of HD

1.2.3.1 Gain of function of mutant huntingtin protein

Several human homozygous HD patients have provided evidence to support the notion that homozygous HD individuals are no more severely affected than their heterozygous HD sibs (Myers et al., 1989; Wexler et al., 1987). This observation is compatible with the theory of a gain of function resulting from the mutant huntingtin protein.

Heterozygous loss of huntingtin in mice does not appear to cause any overt abnormalities, indicating that loss of one *HD* gene copy does not generate the same phenotype as human heterozygous HD patients (Duyao et al., 1995; Zeitlin et al., 1995). This finding also

suggests that a gain of function of the mutated gene is operating in HD. Further supporting evidence is provided by a human case of a chromosome 4 translocation that results in deletion of a copy of *HD* gene without HD symptoms (Ambrose et al., 1994). More direct evidence comes from transgenic HD mouse models. For example, R6/2 mice that express exon 1 of the mutant human *HD* gene (in addition to their two endogenous *Hdh* genes) have a progressive neurological phenotype and neuropathology reminiscent of human HD (Mangiarini et al., 1996).

1.2.3.2 Loss of function of normal huntingtin in HD pathogenesis

As previously mentioned, huntingtin may be critical to neuronal survival in the adult because of its ability to up-regulate BDNF levels and decrease the toxicity of mutant huntingtin (section 1.2.2.2). In addition, when cultured CNS cells overexpressing full-length mutant huntingtin were exposed to apoptotic stimuli, levels of endogenous full-length wild-type huntingtin as well as BDNF production were reduced (Zuccato et al., 2001). Further studies in a symptomatic transgenic HD mouse model have revealed decreased levels of full-length huntingtin expression probably due to the activation of an apoptotic cascade that increases endogenous huntingtin cleavage (Ona et al., 1999). Therefore, these findings highlight the possibility that loss of wild-type huntingtin's function may also contribute to the disease phenotype of HD.

1.2.3.3 Intracellular aggregates in HD brain tissue

One feature of mutant huntingtin is its tendency to form intracellular aggregates, especially following proteolytic cleavage. R6/2 mice that express exon 1 of the mutant human *HD* gene were found to develop pronounced intranuclear aggregates termed neuronal intranuclear inclusions (NIIs), containing mutant huntingtin protein and ubiquitin, prior to developing a neurological phenotype (Davies et al., 1997). NIIs appear as roughly circular pale structures easily identified in toluidine blue-stained semithin sections, with no membrane separating the inclusion from the surrounding nuclear matrix. The NIIs appear to be composed of fine granular material with occasional filamentous structures. Such aggregates can be formed in transfected yeast and cell cultures (Cooper et al., 1998; Krobitsch and Lindquist, 2000; Li and Li, 1998; Martindale et al., 1998; Saudou et al.,

1998), transgenic or knock-in mice expressing various mutant huntingtin constructs of different length and CAG repeat sizes (Hodgson et al., 1999; Li et al., 2000a; Reddy et al., 1998; Schilling et al., 1999; Wheeler et al., 2000; Yamamoto et al., 2000) and in the brains of HD patients (Becher et al., 1998; DiFiglia et al., 1997; Gutekunst et al., 1999; Sieradzan et al., 1999).

Antibodies against internal regions of human huntingtin (amino acids 549-670) do not reveal huntingtin aggregates, suggesting that aggregates are mostly composed of N-terminal huntingtin fragments (Becher et al., 1998; DiFiglia et al., 1997; Sieradzan et al., 1999)). However, in addition to truncated huntingtin fragments, full-length mutant and wild-type huntingtin can also be recruited into nuclear aggregates (Wheeler et al., 2000).

NIIs are frequently present in the striatum, putamen and cortex of HD brains, but are rarely seen in the hippocampus, red nucleus, cerebellum and other brain areas (Becher et al., 1998; Sieradzan et al., 1999). They appear to be present in the nuclei of neurons but not astrocytes. Similar aggregates are also present in the neuropil (neuropil aggregates) or dystrophic neurites in both human and mouse HD brains (DiFiglia et al., 1997; Li et al., 1999b; Li et al., 2000a; Maat-Schieman et al., 1999; Schilling et al., 1999).

The presence of huntingtin aggregates in brains of HD patients and most HD mice raise the possibility that such aggregates may play a role in HD pathogenesis. NIIs in HD brains may interfere with nuclear activity and lead to neuronal dysfunction. The presence of neuropil aggregates suggests that they may be responsible for the degenerative dendritic and exonal changes that lead to functional alteration in HD and the evidence is discussed in later sections.

1.2.3.3.1 Mechanism of formation of aggregates

The hypothesis that glutamine repeats may form a stable beta-pleated sheet via a so-called "polar zipper" held together by hydrogen bonds has been postulated for the formation of aggregates (Perutz, 1996). *In vitro* experiments (Scherzinger et al., 1997) have shown that N-terminal huntingtin with an expanded polyglutamine stretch can form insoluble aggregates with the characteristics of beta-pleated sheets. This mechanism operates above

a certain threshold size of polyglutamine (> 40 residues), and coincides with the threshold repeat length associated with the presentation of HD symptoms.

Another hypothesis postulates that aggregate formation is the result of a tissue transglutaminase (tTG)-catalysed reaction. Because a polypeptide bound glutamine is a tTG substrate, it has been suggested that the addition of glutamine residues beyond a threshold length may result in a protein becoming a tTG substrate causing formation of isopeptide bonds and insoluble aggregates through crosslinking (Kahlem et al., 1998). In support of this hypothesis is the fact that tTG activity and tTG levels are elevated in brain regions affected in HD (Karpuj et al., 1999; Lesort et al., 1999) and that *in vitro*, mutant huntingtin and polyglutamine tract peptides are good tTG substrates (Cooper et al., 1997; Kahlem et al., 1996). However, the distribution of aggregates in HD brains (Vonsattel and DiFiglia, 1998) does not correlate well with the observed increases in tTG levels and activity (Karpuj et al., 1999; Lesort et al., 1999). Further studies in cell culture models have revealed that tTG is totally excluded from the huntingtin aggregates, and modification of the tTG expression level had no effect on the frequency of the aggregates (Chun et al., 2001). Therefore, tTG does not appear to be required for the formation of aggregates, and likely does not play a role in the aggregation process of huntingtin. Further studies need to explore the role of increased tTG in HD.

1.2.3.4 Are intracellular aggregates toxic or protective to neurons?

A number of studies have demonstrated that intracellular aggregates are toxic and hence pathogenic in HD. However, accumulated evidence also suggests that the intracellular aggregates may be protective rather than toxic to cells. The supported and against evidence is discussed in the following sections.

1.2.3.4.1 Evidence supporting toxic intracellular aggregates

In vitro studies have indicated that various N-terminal fragments of mutant huntingtin, rather than the full-length mutant huntingtin, can form aggregates in cytoplasm and nuclei, and that aggregation is prompted by lengthening the glutamine repeat and by shortening the huntingtin amino acid sequence (Cooper et al., 1998; Li and Li, 1998; Martindale et al.,

1998). In these studies, expression of mutant huntingtin results in increased susceptibility to apoptotic stress, which is greater with increasing polyglutamine size, decreasing protein length and formation of aggregates. These studies suggest that the formation of aggregates may mediate the cellular vulnerability to apoptotic stress.

Transgenic mouse studies have shown that the progressive appearance of neuropil aggregates is highly correlated with the development of neurological symptoms (Li et al., 1999b). Further studies also showed that huntingtin aggregates selectively accumulate in striatal medium spiny neurons and are associated with synaptic vesicles in axonal terminals, in 'knock in' HD mice (Li et al., 2000a). It was also shown that glutamate uptake by synaptic vesicles was inhibited by N-terminal fragments of mutant huntingtin *in vitro*. These findings suggest that intracellular aggregates may contribute to the neuronal dysfunction in HD.

In a *Drosophila* HD model, co-expression of an expanded-polyglutamine tract with a bivalent artificial huntingtin binding polypeptide could delay and limit the appearance of aggregates and inhibit both adult lethality and photoreceptor neuron degeneration (Kazantsev et al., 2002). The results also demonstrate a strong correlation between the accumulation and aggregation of polyglutamine protein and subsequent degeneration, showing that a delay in the formation of aggregates caused by the suppressor is highly correlated with protection from degeneration.

1.2.3.4.2 Evidence supporting non-toxic intracellular aggregates

However, there is also evidence that nuclear accumulation of the N-terminally truncated mutant huntingtin rather than aggregates *per se*, can lead to cell dysfunction or death. Indeed, suppression of NII formation can increase cell death *in vitro*, suggesting that NIIs may be consequences of neuroprotective packaging of the toxic soluble huntingtin fragments into less toxic insoluble aggregates (Kim et al., 1999a; Saudou et al., 1998). Also studies of a transgenic mouse model of spinocerebellar ataxia 1 (SCA1) have shown that absence of ataxin-1 in the nucleus as a result of a co-existing mutated nuclear localization signal, results in no pathological changes in their Purkinje cells (Klement et al., 1998). In contrast, SCA1 transgenic mice with a deletion in the self-association region

of ataxin-1 developed profound degenerative changes in Purkinje cells even though NII formation was completely blocked and only soluble ataxin-1 was present in the nucleus.

In HD post-mortem brains, the distribution of huntingtin aggregates does not correspond well to the location of neuropathology. Interestingly, there is a significant positive correlation between nuclear inclusion abundance and CAG repeat length in the cortex of human HD brains but not in the striatum (Sieradzan et al., 1999). Furthermore, NIIs appear to be more frequent in the cortex than in striatum in all pathological grades of HD (DiFiglia et al., 1997; Gutekunst et al., 1999; Sieradzan et al., 1999). In addition, it has been shown that most of the nuclear aggregates in post-mortem striatum are observed in populations of interneurons that are spared in HD (Kuemmerle et al., 1999). Collectively, these findings suggest that huntingtin aggregates per se may not be responsible for initiating the pathological changes in HD.

1.2.3.5 Toxic fragment versus full-length huntingtin hypothesis of HD pathogenesis

The "toxic gain of function" theory postulates that the expanded polyglutamine causes a conformation change and confers novel properties on the mutant huntingtin proteins, which may finally cause detrimental effects on cells. It is not clear whether the pathogenic properties act at the level of the full-length mutant protein or only after its truncation or both.

1.2.3.5.1 Toxic fragment hypothesis of HD pathogenesis

The toxic fragment hypothesis postulates that huntingtin is cleaved within cells by a caspase or other protease into a short protein fragment containing the polyglutamine tract, which is toxic to cells (Wellington et al., 1998). An increasing body of evidence, showing that pure polyglutamine tracts or protein fragments containing glutamine tracts may be toxic to cells, is summarized in the following paragraph.

Cells transfected with the truncated huntingtin constructs, when exposed to apoptotic stimuli display higher levels of death compared with cells that expressed full-length

huntingtin containing the same polyglutamine length (Cooper et al., 1998; Li and Li, 1998; Martindale et al., 1998). These studies also showed that in both truncated and full-length constructs, increasing toxicity is associated with longer polyglutamine tracts. HD mouse models expressing truncated N-terminal fragments of mutant huntingtin have more rapidly progressing phenotypes than those expressing full-length mutant protein (see section 1.4). These findings support the idea that truncated mutant huntingtin fragments play an important role in pathogenesis.

Moreover, HD post-mortem studies have demonstrated that N-terminal fragments of mutant huntingtin can be detected in NIIs, suggesting that huntingtin proteolysis may occur *in vivo* (DiFiglia et al., 1997; Sieradzan et al., 1999). Occurrence of huntingtin proteolysis is evident by the presence of caspase-3 cleaved N-terminal fragments of wild-type in brains of normal individuals and HD patients as well as such fragments of mutant huntingtin in HD patients (Kim et al., 2001). Further supporting studies demonstrated that a distinct pattern of huntingtin fragments generated by a protease acting on protease-susceptible domains of huntingtin exists in human striatum and human HD striatum showed elevated levels of cleaved N- and C-terminal fragments compared with those in controls (Mende-Mueller et al., 2001).

Huntingtin does appear to be a substrate for caspase cleavage and the rate of cleavage by apopain (a proapoptotic cysteine protease) increases with the length of the huntingtin polyglutamine tract (Goldberg et al., 1996). It has also been demonstrated that huntingtin contains at least two caspase-3 and one caspase-1 cleavage sites and when cleaved by caspase 1 or caspase 3, a polyglutamine-containing fragment from huntingtin is released (Wellington et al., 1998). Further studies have shown that inhibiting caspase cleavage of huntingtin by mutagenizing the cleavage sites reduces toxicity in apoptotically stressed neuronal and non-neuronal cells (Wellington et al., 2000). Caspase inhibitors significantly increased cell survival in clonal striatal cells expressing mutant huntingtin (Kim et al., 1999a). Further studies have demonstrated that caspase-1 is activated in HD brains and transgenic HD mice (R6/2) and that inhibiting its activity reduced endogenous huntingtin cleavage in HD mice (Ona et al., 1999). Inactivation of caspase-1 also slowed the progression of pathological features in R6/2 mice (Chen et al., 2000; Ona et al., 1999). However, R6/2 mice do not have caspase-1 cleavage sites in their mutant huntingtin

protein, so it is possible that inhibition of caspase-1 acts in general inhibition of pro-apoptotic pathways rather than increasing the cleavage of huntingtin.

The susceptibility of huntingtin to cleavage by caspase provides a mechanism for generating polyglutamine fragments, which then may lead to cell toxicity. However, it is not clear whether the caspase cleavage of huntingtin is directly involved in the disease or the polyglutamine acts, indirectly by harbouring sites for caspase that, in turn, trigger apoptosis when sequestered into aggregates.

1.2.3.5.2 Does full-length mutant huntingtin contribute to HD pathogenesis?

Although accumulated evidence suggests that truncated mutant huntingtin is more toxic to cells than full-length mutant huntingtin, several studies suggest that the expanded polyglutamine tract triggers HD pathogenesis in the context of full-length protein. In one "knock-in" HD mouse model, the expanded polyglutamine tract appears to alter mutant huntingtin conformation and changes its mobility and reactivity with IF8 (an antibody specific for long soluble polyglutamine tract) (Wheeler et al., 2000). The authors also provided evidence supporting a scenario in which medium spiny neurons, rather than large interneurons, can promote the formation of a distinct version of full-length huntingtin with an accessible N-terminus, rather than stable cleaved N- and C-terminal products. In this scenario, the N-terminal accessible version of the protein appears to be redistributed to the nucleus in mutant medium spiny neurons. The formation of nuclear inclusions and insoluble aggregates occurs at a much later stage. The authors conclude that the altered structure imposed on the 'exposed' N-terminus by an elongated polyglutamine stretch may facilitate the interaction of huntingtin with other critical cellular constituents and/or it may lead to devastating consequences via gradual loss of an essential function of huntingtin in mature striatal spiny neurons. This finding may provide a link between mutant huntingtin and selective vulnerability in HD and suggests that mutant full-length huntingtin and partial loss of normal huntingtin may both play a role in HD pathogenesis.

Further studies have shown that full-length mutant huntingtin is more resistant to proteolysis than normal huntingtin and N-terminal cleavage fragments arising from the processing of normal huntingtin in affected HD brain are sequestrated by full-length

mutant huntingtin (Dyer and McMurray, 2001). These findings support a model in which the expanded polyglutamine tract alters the protein's solubility and renders the mutant protein resistant to proteolysis, This, in turn, allows the full-length mutant protein to accumulate and trigger subsequent pathological changes.

Although full-length mutant huntingtin may be able to initiate neuropathological changes in HD, the toxic fragment theory can't be ruled out. Indeed, a recent study showed that the HD disease process, initiated by full-length mutant protein, is hastened by co-expression of mutant fragment (Wheeler et al., 2002). Therefore, full-length and truncated mutant huntingtin may both contribute to HD pathogenesis.

1.2.3.6 Chaperones, the ubiquitin-proteasome pathway and HD pathogenesis

It has become increasingly well documented that the expansion of a glutamine tract to a length within the pathogenic range results in the misfolding of the protein. This concept is strongly supported by several reports demonstrating that nuclear aggregates of polyglutamine proteins are ubiquitinated (Davies et al., 1997; DiFiglia et al., 1997). Degradation of most proteins by the proteasome requires the conjugation of multiple ubiquitin molecules. Ubiquitinated proteins are then recognized and hydrolysed by the 26S proteasome (Schwartz and Ciechanover, 1999). In addition to ubiqutitin, nuclear aggregates have been shown to contain chaperone proteins, including HSP40 and HSP70 heat shock proteins and components of the proteasome system *in vitro* (Chai et al., 1999; Cummings et al., 1998; Stenoien et al., 1999) and *in vivo* (Chai et al., 1999; Warrick et al., 1999)].

In cell cultures, polyglutamine aggregates appear to sequester heat shock proteins, proteasome components and nuclear proteins and are suppressed by over expression of the HDJ-2 chaperone *vitro* (Cummings et al., 1998; Stenoien et al., 1999) with a parallel decrease in cytotoxicity (Chai et al., 1999). HDJ-2 and HSC70 also co-localize with NIIs in brains of R6/2 HD mice and over-expression of HDJ-1 and HSC70 can suppress the formation of aggregates and cellular toxicity in cell culture (Jana et al., 2000). Hence, most of the studies support the postulation that aggregates accumulate when the capacity of the ubiquitin-proteasome system to degrade misfolded huntingtin is exhausted and over-

expression of some chaperones may promote the degradation of misfolded huntingtin and reduce cell toxicity. Such proposals have also been supported by studies in SCA1 mice. When SCA1 mice were crossbred with mice over-expressing a molecular chaperone (inducible HSP70), high levels of HSP70 in the resulting progeny indeed afforded protection against neurodegeneration (Cummings et al., 2001).

However, aggregate formation is not always inhibited by over-expression of heat shock protein in some systems. For example, over-expression of heat shock protein 40 (HDJ-2) increases polyglutamine inclusion formation in COS-7 cells expressing N-terminal fragment of huntingtin (Wyttenbach et al., 2000). Furthermore, while directed expression of HSP70 suppressed polyglutamine-induced neurodegeneration in a *Drosophila* model of Machado-Joseph disease, it did not have a visible effect on NII formation (Warrick et al., 1999). Further studies demonstrated that chaperone-suppressed cellular toxicity of mutant huntingtin is independent of polyglutamine aggregates, but probably is mediated through its inhibition of caspase-3 and caspase-9 activity (Zhou et al., 2001). These findings suggest that evaluating the therapeutic effects of drugs on HD pathology should not be solely based on their ability to inhibit huntingtin aggregation, since aggregates may not be pernicious to cells.

1.2.3.7 Interaction of huntingtin with cytoplasmic proteins

It has been suggested that selective neuropathological changes in HD may relate to aberrant cell type-specific protein interactions of the mutant huntingtin protein. If such interactions are involved in HD pathogenesis, it could be the regional expression of these proteins and/or the different lengths of polyglutamine tract in different tissues that determine the selective pattern of neurodegeneration.

A number of huntingtin-interacting proteins including glyceraldehyde-3-phosphate dehydrogenase (Burke et al., 1996), calmodulin (Bao et al., 1996), huntingtin-interacting protein1 (HIP1) (Kalchman et al., 1997; Wanker et al., 1997), huntingtin-interacting protein2 (HIP2) (Kalchman et al., 1996), huntingtin-associated protein 1 (HAP1) (Li et al., 1995), huntingtin-associated protein 40 (HAP40) (Peters and Ross, 2001), WW domain

proteins (Faber et al., 1998), cystathionine β-synthase (Boutell et al., 1998) and SH3 containing Grb-like protein (SH3GL3) (Sittler et al., 1998) have been identified.

Glyceraldehyde-3-phosphate dehydrogenase (GAPDH) has been shown to interact directly with the polyglutamine tract of huntingtin (Burke et al., 1996). GAPDH appears to interact preferentially with smaller fragments of huntingtin as opposed to the full-length huntingtin and preferentially with long lengths of polyglutamine (Burke et al., 1996). The strong evidence for energy impairment in HD makes the association with GAPDH intriguing. Such an interaction may be the initial step in the impairment of glycolysis in HD. Although post-mortem HD studies have shown that the activity of GAPDH is normal in brain tissues (Browne et al., 1997; Kish et al., 1998; Tabrizi et al., 1999), further studies analysing GAPDH activity of subcellular fractions demonstrated that the GAPDH activity is reduced in the nuclear fraction of fibroblasts from HD patients despite unchanged *GAPDH* gene expression (Mazzola and Sirover, 2001). Since GAPDH is a multifunctional enzyme with roles in glycolysis, DNA repair and replication and programmed cell death (Ronai, 1993), the reduction of GAPDH activity in the nucleus may cause impaired energy production and the promotion of apoptosis.

HIP1 is the human orthologue of a yeast protein (Sla2p) with a known role in membrane and cytoskeleton function. HIP1 is expressed throughout the brain with highest levels in the cortex and is present in peripheral tissues at low to moderate levels (Kalchman et al., 1997; Wanker et al., 1997). The interaction between HIP1 and huntingtin is modulated by CAG repeat length with preferential binding to the smaller size of polyglutamine stretch (Wanker et al., 1997). Recently, HIP1 has been shown to be an endocytic protein, functioning in clathrin-mediated endocytosis through binding to clathrin and adaptor protein 2 (Metzler et al., 2001). The structural integrity of HIP1 is crucial for maintaining normal clathrin-coated vesicle size and function (Waelter et al., 2001). HIP1 may participate in the transport of endocytic vesicles to target organelles in the cells. Since normal huntingtin is more strongly bound to HIP1 than mutant huntingtin, it is possible that huntingtin is important in endocytosis and mutant huntingtin may compromise this activity. HIP1 is also a pro-apoptotic protein and over-expression *in vitro* results in rapid caspase-3-dependent cell death via the intrinsic pathway of apoptosis (Hackam et al., 2000). It has been suggested that the association of normal huntingtin attenuates the pro-

apoptotic actions of HIP1. Further studies support this proposal (Gervais et al., 2002). The authors identified a novel partner for HIP1, called Hippi (HIP1 protein interactor). The presence of mutant huntingtin favours the formation of Hippi-HIP1 oligomers that can recruit procaspase-8 to form a complex of Hippi, HIP-1, and procaspase-8 and launch the apoptosis pathway.

HAP1 is predominantly a membrane-associated protein that shows a subcellular distribution profile similar to synaptophysin, suggesting that HAP1 associated with the cytoskeleton or synaptic vesicles (Li et al., 1995). In contrast to HIP1, the interaction between huntingtin and HAP1 is modulated in the opposite direction. HAP1 has increased affinity for huntingtin with increasing polyglutamine length (Li et al., 1995). Northern blot analysis shows that expression of *HAP1* mRNA in human is limited to the brain, with maximal expression in the caudate, cortex and hippocampus and lower level in cerebellum (Li et al., 1996). HAP 1 is expressed in several brain regions in a manner that is similar to nitric oxide synthase (nNOS), an enzyme involved in the synthesis of nitric oxide (NO). The correlation of HAPI and nNOS expression pattern suggests that the enhanced interaction of mutant huntingtin with HAP1 might increase the synthesis of NO and render certain neuronal populations more susceptible to excitotoxicity (Li et al., 1996).

The *HIP2* gene encodes human ubiquitin-conjugating enzyme, hE2-25K (Chen and Pickart, 1990). E2 ubiquitinating enzymes have known roles in the turnover of abnormal proteins. The interaction between HIP2 and huntingtin is not influenced by CAG length (Kalchman et al., 1996). hE2-25K is expressed in all assessed human tissues but enriched in brain. The interaction of hE2-25K with huntingtin may provide important clues to the regulated metabolism of huntingtin protein. However, whether the interaction influence the intracellular processing of mutant huntingtin is not clear.

Huntingtin from HD brains appears to bind calmodulin more avidly than wild-type huntingtin (Bao et al., 1996). Calmodulin is an intermediate in many calcium-mediated signalling pathways. Many cellular processes such as vesicle transport or fusion are calcium dependent and altered regulation of protein interactions in this process may have deleterious consequences.

Recently, HAP40 was identified as a 40-kDa protein encoded within intron 22 of the factor VIII gene (Peters and Ross, 2001). In the presence of normal huntingtin, HAP40 is located in the cytosol. However, in the absence of huntingtin, HAP40 is actively transferred to the nucleus (Peters and Ross, 2001). Although, the repercussions of the relationship between HAP40 and huntingtin are not clear, these data indicate that HAP40 may contribute to the function of normal huntingtin and is a candidate for involvement in the aberrant nuclear localization of mutant huntingtin found in HD.

Cystathionine β-synthase has been shown to specifically bind to huntingtin but not other polyglutamine-containing proteins (Boutell et al., 1998). However, the interaction between huntingtin and cystathionine β-synthase is independent of polyglutamine repeat length. Cystathionine β-synthase is a key enzyme in the generation of cysteine from methionine. Absence of cystathionine β-synthase is associated with homocysteinuria, an autosomal recessive disorder, characterized by mental retardation, developmental delay, seizures and psychiatric disorders. Two of the oxidation products of homocysteine, L-homocysteate and L-homocysteine sulphinate, are known to be potent agonists of NMDA receptors (Boutell et al., 1998) It is conceivable that the interaction of mutant huntingtin with cystathionine β-synthase may interfere with the normal function of cystathionine β-synthase, causing increased homocysteine levels that lead to excitotoxicity in HD. To support this postulation, further studies in examining the distribution of homocysteate and other homocysteine oxidation products in the brain tissue of HD patients and HD mice are essential.

SH3 containing Grb-like protein (SH3GL3) preferentially binds to the N-terminal fragment of huntingtin with an expanded polyglutamine tract (Sittler et al., 1998). The formation of huntingtin aggregates is significantly enhanced in the presence of SH3GL3 (Sittler et al., 1998). SH3GL3 plays a major role in the signal transduction from membrane receptors and in the regulation of exo/endocytic cycle of synaptic vesicles (Pawson, 1995). As SH3GL3 is selectively expressed in different brain regions including striatum and cortex (Sittler et al., 1998), the binding of this protein to a huntingtin fragment containing expanded polyglutamine may contribute to the selective vulnerability of neurons in HD. However, whether the normal function of SH3GL3 is affected by the interaction with mutant huntingtin is not known and requires further study.

WW domain proteins are involved in signal transduction, proteolysis and mRNA splicing (Faber et al., 1998), but the effect of polyglutamine length on the interaction between huntingtin and WW domain proteins and the role of such interactions are not clear and need to be explored further.

Most of these huntingtin-interacting or associated proteins are expressed throughout the brain and are not especially enriched in regions most affected in HD. Therefore it remains unclear whether these proteins play a role in the selective vulnerability of neuronal death.

1.2.3.8 Transcriptional dysregulation caused by expanded polyglutamine stretches

The role of the nuclear inclusions in the mechanism of polyglutamine diseases is controversial, as previously mentioned, but evidence from cellular and animal models indicates that nuclear localization of mutant protein is important in toxicity (Klement et al., 1998; Saudou et al., 1998). It is possible that nuclear localization of mutant protein interferes with nuclear transcription factors and co-factors leading to cellular toxicity. Recently, CBP [cAMP-responsive element binding protein (CREB)-binding protein], a cofactor for CREB-dependent transcriptional activation, has been shown to co-localize with the mutant huntingtin in cells co-transfected with expression plasmids containing both genes (Kazantsev et al., 1999; Nucifora et al., 2001). Furthermore, CBP has been found in nuclear inclusions formed in HD mice (Nucifora et al., 2001; Steffan et al., 2000) and in human HD brains (Nucifora et al., 2001).

Several lines of evidence suggest the possibility that expanded polyglutamine repeats could cause aberrant transcriptional regulation through their interaction with nuclear transcription factors. The binding of $TAF_{II}130$ (a cofactor for CREB-dependent transcriptional activation) to expanded polyglutamine stretches has been shown in a cell culture model of polyglutamine disease to strongly suppress CREB-dependent transcriptional activation (Shimohata et al., 2000). It has also been demonstrated that expanded polyglutamine specifically interferes with CBP-activated gene transcription, and over expression of CBP rescues polyglutamine-induced neuronal toxicity (Nucifora et al., 2001). A further study using cell lines expressing N-terminal mutant huntingtin suggests that increased

susceptibility to cell death and decreased neurite outgrowth is partly due to an impaired CRE-transcriptional response (Wyttenbach et al., 2001). A key test of CBP involvement in HD pathogenesis will be to identify the genes that are transcriptionally regulated by this factor, and that have altered expression in cells containing the polyglutamine expansion and displaying pathological changes. A reduction of CRE-mediated transcription is likely in human HD, since reduced levels of the CRE-response genes such as corticotrophin-releasing hormone, proenkephalin and substance P are seen in HD brain tissue compared to control brain tissue (Augood et al., 1996; Desouza, 1995; Sapp et al., 1995). This pathway is also likely to be impaired in HD mouse models, since cAMP-responsive genes are down regulated in R6/2 mice (Luthi-Carter et al., 2000).

It has been postulated that other transcription factors could also be inactivated by expanded polyglutamine tract. At least 12 such proteins have been identified (McCampbell and Fischbeck, 2001a), but the exact role these factors play in disease pathogenesis is unknown. Interestingly, many of these factors are involved in histone acetylation. In a cell culture model of spinobulbar muscular atrophy, histone acetylation was reduced in cells expressing mutant polyglutamine. Reversal of this hypoacetylation, which can be achieved by over expression of CBP or its amino terminus, or by treatment with deacetylase inhibitors, reduced cell loss (McCampbell et al., 2001b). A recent *Drosophila* study also demonstrated that progressive neurodegeneration and early adult lethality, caused by expression of an expanded polyglutamine tract, were arrested by feeding flies with histone deacetylase inhibitors (Steffan et al., 2001). Similar results were shown in a yeast model expressing nuclear expanded polyglutamine (Hughes et al., 2001). These results provide evidence that the use of deacetylase inhibitors could be a viable therapeutic strategy in HD. However, as a first step, it is very important to see what effect these compounds have in HD mouse models.

In addition to reduced CRE-mediated transcription, other transcript expression appears to be altered in polyglutamine disease. Nuclear proteins that interact with expanded polyglutamine stretches include p53 and nuclear receptor co-repressor (N-CoR). *In vitro*, N-CoR preferentially binds to huntingtin protein containing longer polyglutamine repeats (Boutell et al., 1999). The N-CoR protein is known to repress transcription from ligand-activated receptors such as retinoid X-thyroid hormone receptor dimers. *In vivo*, N-CoR is

redistributed to the cytoplasm by mutant huntingtin, suggesting that altered transcriptional regulation may be involved in HD (Boutell et al., 1999). Mutant huntingtin was also found to significantly repress transcription of a p53-regulated promoter (Steffan et al., 2000) and mimic the function of p53. It was postulated that mutant protein, mimicking the p53 function, triggers the apoptotic pathway and this might be partly responsible for the neuronal cell death in HD. *In vitro* studies have recently demonstrated that mutant huntingtin binds strongly to specificity protein 1 (Sp1), a transcription factor, inhibiting the Sp1-dependent transcription of genes such as nerve growth factor receptor (Li et al., 2002). Co-expression of Sp1 and $TAF_{II}130$ in cultured striatal cells from wild-type and HD transgenic mice reverse the transcriptional inhibition of the dopamine D2 receptor gene caused by mutant huntingtin, as well as protects neurons from huntingtin-induced cytotoxicity (Dunah et al., 2002). Further *in vivo* studies demonstrated that soluble mutant huntingtin inhibit Sp1 binding to DNA in post-mortem brain tissues of both presymptomatic and affected HD patients, suggesting that inhibition of Sp1-mediated transcription may be an early molecular event in HD (Dunah et al., 2002).

Studies in HD mice revealed downregulated genes encoding components of neuronal signalling systems including brain derived neurotrophic factor (Ferrer et al., 2000), glutamate transporters (Lievens et al., 2001), neurotransmitter receptors, intracellular signal transducing enzymes, retinoic acid machinery and molecules that control Ca^{2+} homeostasis (Luthi-Carter et al., 2000). Similar results were obtained in transgenic SCA1 mice, in which down-regulation of several genes abundantly expressed in Purkinje cells, occurred before any pathological or neurobehavioral abnormalities (Lin et al., 2000). In this model, several genes for proteins involved in Ca^{2+} homeostasis were downregulated, as was the Purkinje cell-specific glutamate transporter (Lin et al., 2000). It was thus suggested that glutamate neurotoxicity and excessive intracellular Ca^{2+} fluxes may be early pathogenic events in SCA1 and possibly also in other polyglutamine disorders.

1.2.3.9 Channel hypothesis

Recently, the formation of ion channels from long synthetic polyglutamine tracts in artificial planar lipid bilayers has been reported (Hirakura et al., 2000; Monoi et al., 2000). Both studies report that a variety of physiological cations such as K^+, Na^+, Ca^{2+}, and H^+ can

permeate the channel formed by long polyglutamine tracts. The authors thus postulate that channel formation could cause significant leakage in plasma and mitochondrial membranes, leading to degraded membrane potentials and impaired energy stores *in vivo*. Monoi and colleagues, show a threshold of polyglutamine length required for channel formation, i.e. a 40-residue polyglutamine could form channels whereas a 29-residue polyglutamine could not, consistent with the polyglutamine length required for disease development. The authors propose that channel formation would likely cause malfunction and death in affected neurons by altering ion homeostasis, membrane potentials, energy stores and susceptibility to excitotoxicity and apoptosis.

The channel mechanism is well established for microbial toxins and at least six other "amyloid" channels, relevant to diseases such as Alzheimer's and prion disease, have been postulated (Kagan et al., 2001). The remarkable structural resemblance between amyloid and mutant huntingtin-induced aggregates, coupled with the striking similarity of the polyglutamine and amyloid channel properties, lends credence to the channel hypothesis as a cytotoxic mechanism in both diseases (Kagan et al., 2001).

1.2.4 Neuronal dysfunction in HD

The possibility that early stages of HD may be primarily due to cell dysfunction rather than cell death is suggested by the observation that some symptomatic HD patients have no discernable neuropathological abnormalities (Myers et al., 1988). This notion is further supported by studies in HD mouse models, which display phenotypes and cellular dysfunction in the absence of overt cell death (Davies et al., 1997; Lin et al., 2001; Schilling et al., 1999; Shelbourne et al., 1999; Wheeler et al., 2000). Several mechanisms involved in neuronal dysfunction have been suggested, although these mechanisms may ultimately contribute to cell death.

1.2.4.1 Excitotoxicity in HD

Excitotoxicity has long been implicated in the pathogenesis of HD (Beal et al., 1991; Hantraye et al., 1990). Excitotoxicity refers to neuronal death resulting from exposure to excitatory amino acids like glutamate. The striatum receives abundant glutamatergic input

from cortex and all ionotropic glutamate receptors, including N-methyl-D-aspartate (NMDA), kainate and ∝-amino-3-hydroxy-5-methyl-4-isoxasole propionate (AMPA) receptors. They contribute to excitatory postsynaptic potentials recorded from striatal neurons after cortical stimulation. In conditions of acute glutamate overload, NMDA receptors are activated and cause intracellular influx of Ca^{2+}, which can lead to the generation of nitric oxide and other free radicals, damage to vital cellular structures and ultimately cell death.

Several lines of evidence suggest that glutamate excitotoxicity is involved in HD pathogenesis. Selective neuronal loss, resembling the pattern seen in HD, may be induced by the NMDA agonist (quinolinic acid) (Beal et al., 1991; Ferrante et al., 1993; Huang et al., 1995). In addition, post-mortem analysis of human HD brains has suggested that striatal neurons with high NMDA receptor expression show increased vulnerability to degeneration (Albin et al., 1990; Young et al., 1988). The membrane depolarisation and inward current produced by exogenous glutamate receptor agonists are significantly larger in medium spiny neurons than in large aspiny cholinergic interneurons, suggesting that medium spiny neurons are more sensitive to glutamate receptor agonist stimulation (Calabresi et al., 1998). Indeed, both striatal and cortical projection neurons in culture are highly vulnerable to NMDA agonists, while interneurons are relatively spared (Figueredo-Cardenas et al., 1994). This may account for the cell type-specific vulnerability of striatal neurons in HD, if glutamate excitotoxicity is involved in HD pathogenesis. There are different subtypes of glutamate receptors in different striatal neurons. NR1A/NR2B is the predominant NMDA receptor subtype in striatal medium spiny neurons. Further studies showed that NMDA-induced apoptotic death by full-length mutant huntingtin is enhanced in NR1A/NR2B-expressing neurons, but not in NR1A/NR2A-expressing cells (Zeron et al., 2001).

A recent study has shown that normal huntingtin binds to post-synaptic density 95 (PSD-95), a protein that binds to the NMDA receptor and regulates NMDA-dependent long-term potentiation and depression, resulting in the inhibition of NMDA receptor activity (Sun et al., 2001). The polyglutamine expansion inhibits huntingtin binding to PSD-95, resulting in increased susceptibility to glutamate-induced excitotoxicity. Over-expression of the normal N-terminal fragment of huntingtin significantly attenuates neuronal toxicity induced by both NMDA receptor agonists and the mutant huntingtin (Sun et al., 2001). The association

of huntingtin with PSD-95 may thus provide a crucial link between glutamate-induced excitotoxicity and the mutant huntingtin protein.

Pathological changes in presynaptic inputs involved in excitotoxicity have also been shown in a number of studies. Changes in cortical projection neurons and the corticostriatal input have been observed in HD (DiFiglia et al., 1997). Cytoplasmic accumulation of mutant huntingtin occurs in pyramidal neurons and is associated with degeneration of the corticostriatal pathway (Sapp et al., 1999). In this study, the authors also raise the possibility that huntingtin preferentially damages the corticostriatal pathway leading to excessive synaptic release of glutamate and excitotoxicity to striatal cells. Indeed, accumulated evidence suggests that huntingtin is associated with neuronal terminal vesicles and several exo/endocytic vesicle proteins such as HIP-1, HAP-1 and SH3GL3 (section 1.2.3.7). It is therefore reasonable to hypothesize that aberrant interaction of mutant huntingtin with these proteins may interfere with the regulation of exo/endocytic cycle of synaptic vesicles and lead to glutamate-induced excitotoxicity.

1.2.4.2 Increased oxidative stress in HD

A role for oxidative damage in neurodegenerative diseases including HD, is gathering increasing experimental support. Damage caused by oxidative stress includes lipid peroxidation, protein oxidation, and DNA mutation. Immunostaining for 3-nitrotyrosine (3-NT), a marker for peroxynitrite-mediated protein nitration, and malondialdehyde (MDA), a marker for oxidative damage to lipid, has been shown to increase in the striatum of HD brains (Browne et al., 1999). Increased immunostaining for heme oxygenase-1, formed in a compensatory response to oxidative stress, has also been found in the striatum of HD brains (Browne et al., 1999). Furthermore, levels of 8-hydroxydeoxyguanosine (8-OHdG), an oxidative damage product of DNA, in nuclear DNA were significantly increased in HD caudate (Browne et al., 1997). Manganese superoxide dismutase-2 (SOD-2) up-regulation has been shown in cells expressing truncated huntingtin containing 150 glutamines (Li et al., 1999c). Recently, oxidative stress caused by N-terminal fragments of mutant huntingtin has been suppressed by overexpression of heat shock protein 27 in a HD cellular model (Wyttenbach et al., 2002). Collectively, these findings implicate an important role of increased oxidative stress in HD pathogenesis.

1.2.4.3 Metabolic deficits in HD

Several lines of evidence have indicated that abnormalities of energy metabolism are involved in HD pathology.

Studies of cerebral glucose metabolism using F-18 fluorodeoxyglucose positron emission tomography (FDG-PET) provide strong evidence for an impairment of energy metabolism. In HD patients and those at risk of developing this disorder, decreased cerebral metabolic rates for glucose were shown in the caudate and putamen as well as in frontal and parietal cortex (Alavi et al., 1986; Goto et al., 1993; Hayden et al., 1986; Young et al., 1986; Andrews and Brooks, 1998). A further study showed that basal ganglia metabolism is highly correlated with the functional capacity of individual patients and the degree of their motor dysfunction (Young et al., 1986). Using magnetic resonance spectroscopy (MRS) imaging, increased lactate levels have been observed in the striatum and occipital cortex of HD patients, suggesting a compensatory glycolytic response to impaired mitochondrial function (Jenkins et al., 1993). Recently, a proton magnetic resonance spectroscopy study of cerebrospinal fluid from HD patients showed reduced levels of both lactate and citrate, suggesting an impairment of both glycolysis and tricarboxylic acid cycle function in HD patients (Garseth et al., 2000).

The basal ganglia are particularly susceptible to mitochondrial toxins such as 3-nitropropionic acid (3-NP), which is an inhibitor of succinate dehydrogenase. Accidental ingestion of 3-nitropropionic acid (3-NP) in man produces selective basal ganglia lesions and dystonia (Ludolph et al., 1992). Extensive behavioural and neuropathological evaluations showed that a partial but prolonged energy impairment induced by 3-NP in rodents and non-human primates is sufficient to replicate most of the clinical and pathophysiological hallmarks of HD, including choreiform movements, cognitive deficits, and progressive selective striatal degeneration (Borlongan et al., 1997; Guyot et al., 1997; Vis et al., 1999). Further supportive evidence for a metabolic deficit in HD comes from transgenic mouse studies that report progressive weight loss despite increased caloric intake (Mangiarini et al., 1996).

1.2.4.4 An interplay between excitotoxicity, metabolic deficits, and oxidative stress via mitochondrial dysfunction in HD

It is widely accepted that defective energy metabolism, oxidative stress, and excitotoxicity and the interplay between these different mechanisms may contribute to HD pathogenesis.

Excitotoxicity and oxidative stress may both occur as direct consequences of energy failure (Beal, 1998). An inability to maintain cellular ATP levels may lead to partial neuronal depolarisation, relief of the voltage-dependent Mg^{2+} block of the NMDA receptor and persistent receptor activation by ambient glutamate levels. Energy failure also impairs calcium buffering and results in an influx of calcium, which leads to nitric oxide ($NO^{\bullet}$) and superoxide ($O_2^{\bullet}$) generation. The reaction of $NO^{\bullet}$ and $O_2^{\bullet}$ can generate peroxynitrite ($ONOO^{-}$), which is a key mediator of oxidative stress (Beckman and Crow, 1993).

Although there are a number of intracellular sources of free radicals, the mitochondria are thought to be the most important. Mitochondria can buffer increased intracellular calcium by fast sequestration through the electrochemical gradient across the inner mitochondrial membrane. Exposure of mitochondria to an overload of calcium influx leads to mitochondrial generation of hydroxyl and other free radical species (Dykens, 1994). Several *in vitro* studies have linked a glutamate-induced increase in mitochondrial calcium to mitochondrial free radical generation and have argued that mitochondria are the main sink for calcium accumulation and major source of excitotoxic reactive oxygen species (Nicholls and Budd, 1998). When energy failure or mitochondrial dysfunction occurs, the calcium-buffering ability will be diminished and more free radicals will be generated. Therefore, production of reactive oxygen species (ROS) induced by excitotoxicity is augmented by mitochondrial dysfunction. Recently, it has been demonstrated that inhibition of mitochondrial complex II, but not complex I, induces a long-term potentiation of NMDA-mediated synaptic excitation in striatal spiny neurons (Calabresi et al., 2001). However, this inhibition has no effect on excitatory synaptic transmission in striatal cholinergic interneurons and pyramidal neurons. 3-NP-induced long-term potentiation is also critically dependent on endogenous dopamine acting through D2 receptors. In summary, it is possible that mitochondrial dysfunction can mediate selective neuronal vulnerability to oxidative stress via excitotoxicity.

Apoptosis induced by oxidative stress has been well documented, and it may be a mechanism for eliminating ROS-producing cells. Apoptosis is also a possible mechanism of cell death in HD. Mitochondria harbour two nuclear-encoded components, cytochrome c and an "apoptosis-inducing factor" (AIF), which are released upon a Ca^{2+}-induced opening of the mitochondrial transition pore. This event plays a major role in the apoptotic cell death cascade (Susin et al., 1999).

Taken together, several lines of evidence suggest that mitochondria play a central role in excitotoxicity, energy failure and oxidative stress, all of which may be involved in HD pathogenesis.

1.2.4.5 Mitochondrial abnormalities in human HD

Severe defects in the activities of the mitochondrial respiratory chain, especially complex II/III, have been identified in caudate and putamen of HD patients, but not in cortex, cerebellum or fibroblasts (Brennan et al., 1985; Browne et al., 1997; Gu et al., 1996; Tabrizi et al., 1999). In addition, aconitase activity is decreased by 92 % in HD caudate, 73 % in putamen, and 48 % in cortex, but normal in HD cerebellum and fibroblast (Tabrizi et al., 1999). Aconitase is particularly vulnerable to free radicals such as $NO^{\bullet}$ and $ONOO^{-}$, and the decrease of aconitase activity is more prominent than that of complex II/III activity when cells are exposed to $NO^{\bullet}$. Therefore, the decreased aconitase activity in HD striatum may be caused by $NO^{\bullet}$, $ONOO^{-}$and other free radicals usually generated through excitotoxicity.

Mitochondrial DNA (mtDNA), which encodes 13 subunits of mitochondrial respiratory enzyme complex, is particularly susceptible to oxidative damage, due to its proximity to the respiratory chain, limited repair mechanisms, few non-coding sequences, and absence of histones (Richter et al., 1988). If increased oxidative stress occurs in HD, it is reasonable to expect that mtDNA might also be compromised. Indeed, a significant increase in 8-OHdG in mtDNA of the parietal cortex was found in late stage (Vonsattel grade 3-4) HD patients, while no such increase was found in frontal cortex or cerebellum (Polidori et al., 1999). In addition, a marked increase in mitochondrial DNA deletion level has been reported in the temporal and frontal cortex of HD patients (Horton et al., 1995).

Another possible consequence of increased oxidative damage on mtDNA is the reduction of mtDNA content. If mtDNA is depleted, it is possible that expression levels of mitochondrial mRNA may be decreased. Indeed, decreased expression levels of cytochrome c oxidase I mRNA has been recently shown in striatum, external globus pallidus and putamen of HD brain (Gourfinkel-An et al., 2002).

1.2.5 Models of cell loss in HD

Even though many lines of evidence argue strongly for a period of protracted cellular dysfunction prior to cell death, the neuropathological hallmark of HD is striatal cell loss. It has been argued that understanding the mechanism of cell death may help identify therapeutic strategies. Therefore, evidence supporting different mechanisms that may account for the cell death in HD is discussed in the following sections.

1.2.5.1 Apoptosis in HD

Although the precise biochemical mechanisms underlying cell loss in HD are not yet completely understood, the available evidence supports an apoptotic, rather than necrotic, mode of cell death. Apoptosis is programmed cell death-a conserved cellular mechanism initiated by diverse stimuli that leads to activation of aspartate-specific proteases (caspases) and culminates in DNA fragmentation and cell death. A subset of neurons and glia in the neostriatum of post-mortem HD brains, assayed with terminal transferase-mediated deoxyuridine triphosphate-biotin nick-end labelling (TUNEL), have shown DNA strand breaks typical of apoptosis (Dragunow et al., 1995; Portera-Cailliau et al., 1995; Thomas et al., 1995). Further studies have shown that proteins with expanded polyglutamine tracts kill cells through apoptotic pathways (Sanchez et al., 1999; Saudou et al., 1998; Sawa et al., 1999). Huntingtin protein itself has been shown to be an apoptotic substrate and is cleaved in a CAG repeat-length dependent manner by apopain (Goldberg et al., 1996). The presence of activated caspase-8 in the insoluble fraction of affected brain regions from HD patients has also been demonstrated (Sanchez et al., 1999). Furthermore, intranuclear mutant huntingtin increases activity of caspase-1 and caspase-3, and promotes cytochrome c release, leading to apoptosis in cell culture (Li et al., 2000b). Further studies have shown that caspase-1 inhibition delays the onset of disease and prolongs survival in

R6/2 HD mice (Ona et al., 1999). These lines of evidence suggest that caspase- induced apoptosis may be involved in the cell death associated with HD.

1.2.5.2 Endosomal-lysosomal-vacuolar pathway (autophagy)-induced cell death in HD

It has been shown that in dying neurons in the HD brain, huntingtin aberrantly accumulates in perinuclear regions and in numerous punctuate cytoplasmic structures that resemble endosomal-lysosomal organelles (Sapp et al., 1997). The endosomal-lysosomal-vacuolar pathway has been implicated in the handling of other disease proteins, such as prions (Taraboulos et al., 1992) and Aβ peptide 1-42 (Cataldo et al., 1996), and cell death by autophagy, a process whereby cells remove cytosolic proteins and organelles and degrade themselves from within. Autophagy may precede and coexist with apoptosis, and may contribute to cell death in neurons through the regulation of lysosomal proteases cathepsin B and D (Ohsawa et al., 1998).

In clonal mouse striatal cell lines transiently transfected with mutant and normal human huntingtin, exogenous wild-type and mutant huntingtin accumulated diffusely in the cytoplasm, forming vacuoles or nuclear and cytoplasmic inclusions (Kim et al., 1999a). The vacuoles had the ultrastructural features of an autophagosome and proved to associate with exogenous huntingtin and the lysosomal enzyme cathepsin D (Kegel et al., 2000). In this study, transfected cells that developed huntingtin-positive vacuoles became shrunken and developed nuclear invaginations, which are features observed in human HD brains (Tellez-Nagel et al., 1974) and in HD transgenic mice (Davies et al., 1997). A recent study, using a postnatal striatal cell culture system composed predominantly of DARPP-32 (dopamine- and cyclic AMP-regulated phosphoprotein of a molecular weight of 32 kDa)-expressing neurons, showed that mutant huntingtin-containing neurons were far more susceptible to dopamine-induced stress, leading to a cascade of oxyradical formation and induction of neuronal autophagy (Petersen et al., 2001). Moreover, autophagy has been shown to be involved in the degradation of aggregate-prone proteins, since they accumulates when cells are treated with different inhibitors acting at distinct stages of the autophagy-lysosomal pathway and their appearance is reduced when cells are treated with rapamycin, a substance that can stimulate autophagy (Ravikumar et al., 2002). These

findings suggest that an autophagic process, induced by the cytoplasmic accumulation of mutant huntingtin, may contribute to HD neuropathology.

1.3 Other triplet repeat diseases

An increasing number of inherited neurodegenerative diseases including HD are caused by the expansion of unstable trinucleotide repeat tracts. Common features shared by these diseases include: 1) the mutant repeats show both somatic and germline instability, frequently expanding rather than contracting in successive transmissions through the generations of a family; 2) an earlier age of onset and increasing severity of phenotypes in subsequent generations (a phenomenon known as anticipation) that correlates with larger repeat lengths; 3) the parental origin of the disease allele can often influence anticipation, with paternal transmission carrying a greater risk of expansion for many of the disorders.

Trinucleotide repeat diseases can be categorized into two subclasses based on the relative location of the trinucleotide repeat in the gene. The first subclass has its repeat in non-coding sequences. The second subclass, the so-called polyglutamine diseases, is characterized by exonic (CAG)n repeats that code for polyglutamine tracts.

1.3.1 Non-coding trinucleotide repeat diseases

The non-coding trinucleotide-repeat diseases are characterized by large variable repeat expansions that result in multiple tissue dysfunction and degeneration. At least 7 diseases of this category have been identified (Table 1.1). The pathogenic mechanism varies from disease to disease, depending on the consequences of the lost function of the respective protein, or the gain of function of a toxic transcript, or both. Despite the various pathogeneses, a number of similarities exist within this group of diseases. For example, the non-coding-repeat diseases are typically multi-system disorders involving dysfunction or degeneration of many different tissues. In addition, the size and variation of the repeat expansions are much greater in the non-coding trinucleotide-repeat diseases than in the polyglutamine diseases.

Disease	Gene/locus	Protein	Schematic representation	Possible pathogenic mechanism
Fragile X syndrome	FMR1 Xq27.3	FMR1 protein		Loss of function
Fragile XE mental retardation	FMR2 Xq26	FMR2 protein		Loss of function
Friedreich's ataxia	X25 9q13-21.1	Frataxin		Loss of function
Myotonic dystrophy	DMPK 19q13	DMPK		Loss and/or gain of function Reduced DMPK expression Silencing in the DM region Dominant effect on RNA processing
Spinocerebellar ataxia type 8	SCA8 13q21	None		Loss of function? Abnormal RNA regulation?
Spinocerebellar ataxia type 12	SCA12 5q31-33	PPP2R2B		Loss of function? Disruption in phosphatase activity?

Table 1.1 Diseases caused by expansion of non-coding trinucleotide repeats. Upper and lower sizes represent the copy number of CAG repeat associated with disease and normal alleles, respectively. This table is based on Table 1 in Cummings and Zoghbi., 2000.

1.3.2 Polyglutamine diseases

All eight known polyglutamine disorders (Table 1.2) are characterized by progressive neuronal dysfunction that typically begins in mid-life and results in severe neurodegeneration. Although the mutant proteins do not share any homology outside the polyglutamine tract, the polyglutamine diseases have several similar features and probably share common pathogenic mechanisms. Despite the ubiquitous expression of all eight genes, only a certain subset of neurons is vulnerable in each disease. All the diseases are probably caused by a gain of function mechanism conferred by the expanded polyglutamine tract. However, the selective neuronal vulnerability is probably influenced by aspects of the respective gene involved.

There are several families and individuals with HD-like symptoms who do not have the HD mutation (Andrew et al., 1994). One such family affected by an early onset, autosomal recessive disorder resembling juvenile-onset HD was reported recently (Kambouris et al., 2000). The manifestations include choreoathetosis, ataxia, dystonia, seizure, spasticity, mutism, and general intellectual impairment. Brain magnetic resonance imaging findings included progressive frontal cortical and bilateral striatal atrophy. The gene responsible for this disease has been localized to 4p15.3, distinct from the *HD* gene location at 4p16.3 (Kambouris et al., 2000).

Another large pedigree with an autosomal dominant disorder that is clinically similar to HD has been reported to arise from a different CAG expansion mutation (Margolis et al., 2001). The disorder termed Huntington's disease like-2 (HDL2) is characterized by onset in the fourth decade, involuntary movements and abnormalities of voluntary movement, psychiatric symptoms, weight loss, dementia, and a relentless course with death about 20 years after disease onset. Brain magnetic resonance imaging scans and autopsy studies revealed marked striatal atrophy and moderate cortical atrophy, with striatal neurodegeneration that occurs in a dorsal to ventral gradient and occasional intranuclear inclusions. Affected individuals have a CAG repeat expansion of 50 to 60 triplets. Unexpanded allele sizes range from 6 to 27 triplets. The expansion is unstable in vertical transmission, but the range of repeat length among family members is narrow. More recently, the CAG repeat was found to be located in the non-coding strand between exon 1

and 2 of the gene encoding junctophilin-3 (*JPH3*) (Holmes et al., 2001). Therefore, the expanded triplet sequence in the gene *JPH3* is (CTG)n. Junctophilin-3 is a component of the junctional complex that anchors the plasma membrane to endoplasmic reticulum and may be involved in the functional coupling between cell-surface voltage sensors and intracellular calcium channels (Holmes et al., 2001). It is not clear whether the pathogenesis of HDL2 is different from that of HD and other neurodegenerative disorders caused by CAG repeat expansion (Holmes et al., 2001).

Disease	Gene	Locus	Protein	CAG repeat size	
				Normal	Disease
Spinobulbar muscular atrophy	*AR*	Xq13-21	Androgen receptor	9-36	38-62
Huntington's disease	*HD*	4p16.3	Huntingtin	6-35	36-121
Dentatorubral-pallidoluysian atrophy	*DRPLA*	12p13.31	Atrophin-1	6-35	49-88
Spinocerebellar ataxia type 1	*SCA1*	6p23	Ataxin-1	6-44	39-82
Spinocerebellar ataxia type 2	*SCA2*	12q24.1	Ataxin-2	15-31	36-63
Spinocerebellar ataxia type 3	*SCA3*	14q32.1	Ataxin-3	12-40	55-84
Spinocerebellar ataxia type 6	*SCA6*	19q13	α_{1A}-voltage-dependent calcium channel subunit	4-18	21-33
Spinocerebellar ataxia type 7	*SCA7*	12q12-13	Ataxin-7	4-35	37-306
Spinocerebellar ataxia type 17	*TBP*	6q27	TATA-binding protein	29-42	47-55

Table 1.2 Diseases caused by expanded polyglutamine tracts.
This table is modified from Table 2 in (Cummings and Zoghbi, 2000).

1.4 Tools to study HD pathogenesis

The pathogenesis that causes selective neurodegeneration in HD remains unknown. HD is a devastating illness and at present there are no effective therapies to prevent onset and progression of the disease. The ultimate aim of scientific research in the field is to find treatments that can cure the disease or at least prevent its progression. In order to achieve the aim, determining the detailed molecular changes associated with the disease is important. However, the lack of brain tissues from patients, especially presymptomatic patients, makes investigation of early pathogenesis difficult. For this reason, researchers have developed appropriate model systems to investigate the molecular basis of HD.

1.4.1 *In vitro* models of HD

Various cell culture systems have been established as *in vitro* models of HD to study aspects of the pathology such as the potential role of the N-terminal fragments of mutant huntingtin, mechanisms involving protein misfolding and aggregation, and interactions between huntingtin and other proteins.

The advantages of cell culture systems are as follows: 1) they are easily manipulated to overexpress or inhibit different genes within short periods of time; 2) they are generally a single cell type, therefore presenting less confounding factors that might influence the experimental results. However, cell models also have disadvantages: 1) cells expressing mutant gene may not reproduce the phenotypes of HD except the cytotoxicity and cell death; 2) consequences of overexpressed mutant huntingtin in cells do not necessarily reflect the consequences in the organism; 3) overexpression of mutant full-length huntingtin in cell culture is not associated with aggregate formation, suggesting differences between *in vivo* and *in vitro* models; 4) most cellular models overexpress N-terminal fragments of mutant huntingtin, suggesting the pathogenic role of full-length mutant huntingtin may not be investigated in these model.

1.4.2 Invertebrate models of HD

Invertebrate model systems such as *Drosophila melanogaster* and *Caenorhabditis elegans* also offer experimental advantages that can potentially address some of the questions regarding the pathogenic processes underlying HD. Recently, Drosophila was shown to be a useful system for studying polyglutamine-induced diseases. An N-terminal fragment of huntingtin containing 2, 75 or 120 polyglutamine repeats was expressed in fly eyes (Jackson et al., 1998). Late onset neurodegeneration and nuclear inclusions that were dependent on the length of the glutamine repeat in the expressed transgene were observed. Another study using a *Drosophila* model, expressing short (20 repeat) and long (127 repeat) polyglutamine tracts (fused to an HA epitope) in fly eyes, also demonstrated polyglutamine-induced eye degeneration (Kazemi-Esfarjani and Benzer, 2000). Crossing these transgenic strains to a series of *de novo* P-element insertion strains resulted in the recovery of 30 eye degeneration suppressor and 29 eye degeneration enhancer mutations.

Two of the suppressor mutations were identified as dHDJ1 and dTPR2, both encoding proteins with "J" domains, homologous to the mammalian DNA J chaperone protein.

N-terminal huntingtin fragments containing polyglutamine tracts of various sizes were also expressed in the sensory neurons of *C. elegans* (Faber et al., 1999). In this study, phenotypes were observed predominantly in worms expressing the longest (150 repeat) polyglutamine tract. GFP::polyglutamine repeat fusion proteins were also expressed in *C. elegans* body wall muscle (Satyal et al., 2000). Fusion proteins containing a long (82 repeats) but not a short (19 repeats) polyglutamine tract formed cytoplasmic aggregates, causing a delay in larval to adult development and inducing expression of a small heat shock protein. The toxic effect of the polyglutamine expression and the formation of aggregates could be reversed by co-expression of the yeast chaperone Hsp104.

The experimental benefit of invertebrate model systems over cell culture systems is that they have complex organ structure and can express phenotypes other than only cellular toxicity. The experimental advantages of invertebrate model systems over mouse model include forward genetic screens to identify suppressor and enhancer genes, which have been performed in *Drosophila* model studies (Fernandez-Funez et al., 2000; Kazemi-Esfarjani and Benzer, 2000). However, there are disadvantages associated with invertebrate model systems. First, the *Drosophila* model has a very short life expectancy which may not express the age-associated nature of the HD. Second, most of the invertebrate models that have been generated are expressing truncated huntingtin, which do not permit the investigation of molecular pathological changes involving mutant full-length protein. Finally, most *Drosophila* models express mutant huntingtin in their eyes, which have different physiological nature from that of striatal neurons. Thus, the mutant huntingtin-induced pathological changes in *Drosophila* models may not reflect that of human brains.

1.4.3 HD mouse models

Mouse models have several advantages over the previously mentioned systems. These include the biological and genetic similarities with humans and the abundance of tissue for analysis. It is therefore not surprising that several transgenic and knock-in HD mouse

models have been generated to enable the exploration of early pathological, molecular, and cellular abnormalities in HD. In addition, these models may be used to test different approaches to delay the onset or slow the progression of HD.

Given that the similarity between human *HD* and mouse *Hdh* genes and their products (section 1.2.1), it is probable that the function of mouse huntingtin is similar to that of human huntingtin. Indeed, the lethality associated with a mouse 'knock-out' model carrying targeted deletion of both *Hdh* gene copies can be rescued by human huntingtin (Hodgson et al., 1996).

Two types of HD mice have been generated. The first category is transgenic mice (Table 1.3a), in which the mutant gene, or part of it, is inserted randomly into the mouse genome, leading to the expression of a mutant protein in addition to endogenous huntingtin. The second category is 'knock-ins' (Table 1.3b), in which the mutation is inserted into the mouse *Hdh* gene. This is achieved by targeted modification of the gene in mouse embryonic stem (ES) cells by homologous recombination. Knock-in mice express the mutation under the influence of the endogenous *Hdh* promoter and in the appropriate genomic context.

1.4.3.1 Transgenic mouse models of HD

The phenotypes and neuropathological changes of the transgenic HD models appear to be highly variable, which is probably due to the different genetic backgrounds the HD mouse models are maintained on, different expression levels of mutant huntingtin, different sizes of N-terminal fragments of mutant huntingtin, different lengths of polyglutamine tracts and the different techniques used to assay the mice.

For example, the expression levels of mutant huntingtin among the transgenic HD models vary greatly from line to line, in part due to the different promoters used in different models. The strong CMV promoter in the HD89 mice drives high-level expression of mutant protein. In contrast, the transgene in the YAC72 mice appears to produce full-length mutant protein at about 30-50 % the level of endogenous mouse huntingtin. In the remaining models that express truncated fragments of huntingtin, the level of mutant

(a) Transgenic mouse models of HD

Mouse line	Genetic background	Htt expressed	Pro	Number of CAG repeats	Expression of m/e (%)	Earliest motor deficits	NIIs (mo)	Neuropathology	Life span (mo)	Ref
R6/1	CBA xC57BL/6	Exon 1	HD	115	31	~4.5 months$^{\phi}$	5	NR	~10	A
R6/2	CBA x C57BL/6	Exon 1	HD	145	75	5-6 weeks$^{\phi}$	1	Cell loss from 14 weeks	3-4	A
R6/5	CBA xC57BL/6	Exon 1	HD	128-156	77	NR	13-14	NR	15-18	A
N171-82Q	C3H xC57BL/6	Exon 1-4	Mouse Prion protein	82	10-20	3-4 months$^{\phi}$	6.5	No overt cell loss	5-11	B
HD94-tet	CBA xC57BL/6	Exon 1	*CamK//α -tTA*	94	> 100	~2.5 months$^{@}$	2	GFAP -positive from 4.5 mo	>24	C
HD100	SJLx C57BL/6	1000 amino acids of huntingtin	Rat neuron specific enolase	100	~20	3-4 months$^{\phi}$	7	20% of cell loss in striatum from 8 months	>18	D
YAC-72	Fvb/n	Full	HD	72	30-50	7 months$^{\&}$	12	40 % cell loss in striatum from 12 months	>12	E
HD89	Fvb/n	Full	CMV	89	400-500	~2 months$^{@}$	> 3	20% of cell loss in striatum from 6 months TUNEL and GFAP -positive	8-20	F

(b) "knock-in" mouse models of HD

Mouse line	Genetic background	Htt expressed	Pro	Number of CAG repeats	Expression of m/e (%)	Earliest motor deficits	NIIs (mo)	Neuropathology	Life span (mo)	Ref
Hdh^{Q111}	CD1	Full	*Hdh*	111	100	24 months$^{\#}$	~10	No overt cell loss	>24	G, H
Hdh/Q80 (Glasgow HD mice)	Fvb/n, DBA/2, C57BL/6	Full	*Hdh*	80	<100	4 months$^{\phi}$	~11	No overt cell loss	>24	I, J
CAG94	C57BL/6	Full	*Hdh*	94	100	2 months$^{\&}$	>18	No overt cell loss (up to 8 mo)	>12	K, L
$Hdh^{(CAG)150}$	C57BL/6	Full	*Hdh*	150	<100?	> 10 months$^{\#}$	~10	No overt cell loss, gliosis	>12	M
Hdh77Q	C57BL/6	Full	*Hdh*	77	<100?	NR	NO	No overt cell loss, gliosis	>13	N

Table 1.3 Transgenic (a) and "knock-in" (b) mouse models of HD.
Abbreviations: Pro, promoter; m/e, mutant huntingtin/endogenous huntingtin; htt, huntingtin; Ref, reference; CMV, cytomegalovirus; NIIs, neuronal intranuclear inclusions; GFAP, glial fibrillary acid protein; mo, month; TUNEL, terminal transferase-mediated (TdT) deoxyuridine triphosphate (d-UTP)-biotin nick end labelling; NR, not reported; NO, not observed; ϕ indicates that motor deficit was detected using rotarod. & indicates that motor deficit was detected by assessing dark phase activity. @ indicates that motor deficit was detected by observation. # indicates that motor deficit was detected by gait analysis.
A: Mangiarini et al., 1996. B: Schilling et al., 1999. C: Yamamoto et al., 2000. D: Laforet et al., 2001 E: Hodgson et al., 1999. F: Reddy et al., 1998. G: Wheeler et al., 2000. H: Wheeler et al., 2002. I: Shelbourne et al., 1999. J: Li et al., 2000. K: Levine et al., 1999. L: Menalled et al., 2000. M: Lin et al., 2001. N: Ishiguro et al., 2001.

protein is much more difficult to assess because of the technical challenges involved. These include the fact that the small mutant peptide needs to be compared with the very large endogenous huntingtin protein on the same blot and there may be differences in antibody affinity for human and mouse epitopes.

Great variability of phenotypes, expression levels of mutant huntingtin and pathology exist in the transgenic HD mouse models and makes comparison between the different mouse lines difficult. However, the studies do suggest that levels of the mutant huntingtin expression and/or the length of glutamine repeats have profound effects on the severity of the disease and mice with longer repeat expansions have more widespread neuronal pathology than those with shorter repeat expansions.

1.4.3.2 'Knock-in' mouse models of HD

The expression level of mutant huntingtin in knock-in models appears to be similar, and this is not surprising since their respective endogenous promoters are identical. Consistent features of the knock-in mice include nuclear staining and microaggregates of huntingtin in the brains of mice at 2-6 months of age, NIIs only observed when mice are older (10-18 months depending on the model) and no significant levels of cell death in the brains.

When 'knock in' and transgenic mouse models of HD are compared, it appears that full-length mutant huntingtin is less pathogenic than polyglutamine-containing N-terminal huntingtin fragments. For example, the phenotype of the $Hdh^{(CAG)150}$ repeat mice (Lin et al., 2001) is not as severe as that seen in the R6/2 transgenic mice (Mangiarini et al., 1996). These results suggest that a polyglutamine tract of a given length is more toxic when it appears in the context of a smaller protein, underlying the importance of polyglutamine tract length as a determinant of disease severity. Mice with longer repeats have more severe phenotypes and widespread neuropathology than those with shorter repeat expansions.

In summary, 'knock in' mouse models showed mild and late onset of behavioural phenotypes and late occurrence of intracellular inclusions without overt neuronal death,

suggesting they are modelling early stages of human HD. They are therefore useful tools for investigating early pathological events in HD.

1.4.3.3 Psychomotor abnormalities in mouse models of HD

Because psychomotor abnormalities are cardinal features of human HD, studies of psychomotor abnormalities of HD mice may help provide a basis for correlating molecular changes to clinical symptoms and to test potential treatments.

All transgenic HD models have shown early and progressive psychomotor abnormalities (Carter et al., 1999; Dunnett et al., 1998; Hodgson et al., 1999; Laforet et al., 2001; Lione et al., 1999; Luesse et al., 2001; Schilling et al., 1999). Various tools were used to assess the psychomotor function of mice in these studies, including a swimming tank, rotarod apparatus, raised beam walking, paw-print pattern analysis, spontaneous activity measures, prepulse inhibition and the Morris watermaze. Psychomotor abnormalities detected in HD mice include hyperactivity and decreased spontaneous explorative behaviour, impaired motor aspects of swimming, poor four-limb co-ordination and balancing, abnormal sensorimotor gating control and visuospatial learning. As previously mentioned (section 1.4.3.1), the different tools used to assess the mice, the different genetic backgrounds the HD mouse models are maintained on, the different expression levels of mutant huntingtin, the different sizes of N-terminal fragments of mutant huntingtin, and the different lengths of polyglutamine tracts make it difficult to directly compare psychomotor abnormalities in these mouse models.

Motor deficits have been found in HdhQ111 mice at 24 months of age using gait analysis. Motor abnormalities have been found in CAG94 mice at 2 months of age by observation of their daily activity. Deficits in gait analysis in $Hdh^{(CAG)150}$ mice at 10 months of age have been reported. Behaviour abnormalities (aggressive behaviour) were found in the Glasgow HD mice at 3 months of age. However, similar experiments have not been carried out in other 'knock in' mouse models. The discrepancy found in the onset of the motor deficits of knock-in models is probably due to the different CAG repeat length, different genetic backgrounds of mice and different methods used to detect the motor abnormalities. Since 'knock in' HD mice are probably modelling early stages of HD, extensive studies on

motor, behavioural, and cognitive function on these mice are warranted not only to correlate the early phenotypic abnormalities to early pathological and molecular changes, but also to provide more reliable markers for testing the efficacy of potential treatments that might prevent early pathological events in the future.

1.4.3.4 Excitotoxicity in HD mouse models

Post-synaptic and pre-synaptic abnormalities of the corticostriatal pathway have been shown to be involved in glutamate-induced excitotoxicity in human HD (section 1.2.4.1). Further studies in HD mouse models have provided further evidence of glutamate-induced excitotoxicity in HD.

Striatal and cortical neurons in transgenic and "knock-in" HD mouse models (R6/2 and CAG94 respectively) displayed more rapid and increased neuronal swelling in response to NMDA agonist exposure than those in controls (Levine et al., 1999). An enhancement of NMDA receptor current as well as an enhancement of intracellular Ca^{2+} influx induced by selective activation of NMDA receptors have been reported in both symptomatic and pre-symptomatic R6/2 mice (Cepeda et al., 2001). These findings indicate that alterations in NMDA receptor function in HD may predispose the striatal neurons to excitotoxic damage, leading to subsequent neuronal degeneration. Indeed, increased sensitivity to NMDA receptor-mediated excitotoxicity has been shown in YAC72 HD mice (Zeron et al., 2002). Importantly, NMDA receptor-mediated excitotoxicity of cerebellar granule neurons was not enhanced, consistent with cell-type and NMDA receptor subtype specificity.

However, contrasting results were observed in R6/1 and R6/2 HD mice that appear to be strongly protected from acute striatal excitotoxic lesions (Hansson et al., 2001; Hansson et al., 1999). A recent study has shown that expression of an N-terminal fragment of huntingtin has less NMDR-induced excitotoxicity than full-length huntingtin in a cell line (Zeron et al., 2001). Indeed, a recent study showed that HD100 transgenic mice that express 33 % of the full length of huntingtin (R6/2 mice express around 3 % of the length of huntingtin) retain sensitivity to NMDR-induced excitotoxicity, suggesting that the sensitivity to NMDR-induced excitotoxicity is probably huntingtin length dependent (Petersen et al., 2002). Furthermore, the development of nuclear inclusions and more

efficient handling of increased Ca^{++} are correlated with the appearance of resistance to NMDR-induced excitotoxicity in R6/2 mice. Collectively, the differential sensitivity to NMDR-induced excitotoxicity of R6/2 and YAC72 mice is probably due to: 1) R6/2 mice express only a small fragment of mutant huntingtin protein, whereas YAC72 mice express the full length mutant protein and thus R6/2 mice may bypass the initial steps of pathogenesis mediated by mutant full-length huntingtin; 2) the size of polyglutamine stretch is twice as large in R6/2 mice compared to YAC72 mice 3) R6/2 mice show widespread and abundant intranuclear inclusions, whereas those found in brains of YAC72 mice are more sparse and restricted in distribution.

Increasing evidence supporting the idea that presynaptic changes in the striatum may also contribute to excitotoxicity comes from studies using HD mouse models. Recently, the inhibitory effects of mutant huntingtin on vesicular glutamate uptake have been shown in the knock-in HD mouse line, Hdh4/Q80 (Li et al., 2000a). Further studies have also shown that impaired glutamate uptake activities in the striatum of R6/2 mice (Lievens et al., 2001). In addition, changes in cortical pyramidal neurons, which may result in presynaptic changes, take place early in the disease in a transgenic HD mouse model (Laforet et al., 2001). Decreased striatal ascorbate release has been shown in transgenic R6/2 HD mice (Rebec et al., 2002). Striatal ascorbate release depends on the activation of glutamate-releasing afferents from the cortex, most likely involving heteroexchange with glutamate during glutamate uptake (O'Neill, 1995). The decreased striatal ascorbate is probably due to the decreased heteroexchange with glutamate, resulting from a failure of glutamate re-uptake (Rebec et al., 2002).

1.4.3.5 Increased oxidative stress in HD mouse models

A role for increased oxidative damage in HD pathogenesis has been addressed in HD mouse model studies. R6/1 mice showed a progressive increase in striatal lipid peroxidation that parallels the worsening of neurological phenotypes (Perez-Severiano et al., 2000). Increased levels of inducible nitric oxide synthase and 3-nitrotyrosine (3-NT) immunostaining in the striatum were also found in the R6/2 mice but not in the control mouse brains (Tabrizi et al., 2000). Furthermore, increased concentrations of 8-hydroxydeoxyguanosine (8-OHdG) was found in the urine, plasma and striatal

microdialysates of R6/2 mice and immunohistochemical studies in brain showed increased staining during late stages of the illness (~ 12 weeks) (Bogdanov et al., 2001). It is interesting to note that increased 8-OHdG staining was present throughout the brain in both cortical and subcortical areas, and not confined to the striatum of R6/2 mice. In contrast, increased levels of carbonyl proteins or lipid peroxidation products, and loss of aconitase were not found in the forebrain of end stage N171-82Q mice (mice died at 5-6 months of age), suggesting that increased oxidative stress did not contribute to the phenotypes demonstrated by these transgenic mice (Schilling et al., 1999). A possible explanation for the absence of increased oxidative stress in N171-82Q mice is that the mice died in early life and so the mice did not develop time-dependent levels of increased oxidative stress. In addition, the tissue examined is forebrain, but not striatum that usually degenerates first in human HD.

1.4.3.6 Mitochondrial abnormalities in HD mouse models

Several lines of evidence from studies in HD mouse models have suggested that mitochondrial abnormalities are involved in HD pathogenesis. A significant reduction of aconitase activity in the striatum and a decrease in complex IV activity in the striatum and cortex have been shown in R6/2 mice at ~12 weeks of age (Tabrizi et al., 2000). Cyanide (complex IV enzyme inhibitor)-induced, but not complex II or III inhibitor-induced mitochondrial depolarisation is greater in the lymphocytes of HD89 mice compared to controls, suggesting a selective mitochondrial dysfunction in the lymphoblasts of HD89 mice (Sawa et al., 1999).

1.5 Mitochondrial Biology

Many lines of evidence suggest that mitochondrial abnormalities play an important role in HD pathogenesis. As part of the present study involves the investigation of mitochondrial integrity in HD mice, mitochondrial biology is briefly reviewed.

1.5.1 The structure of mitochondria

Each mitochondrion is bound by two highly specialised membranes that create two separate compartments: the internal matrix space and a much narrower intermembrane space. The major working part of the mitochondrion is the matrix and the inner membrane that surrounds it.

The inner membrane is folded into numerous cristae, which greatly increase its total surface area. It contains proteins with three types of function: 1) those that carry out the oxidation reactions of the respiratory chain, 2) an enzyme complex called ATP synthase that makes ATP, and 3) specific transport proteins that regulate the passage of metabolites into and out of the matrix.

The matrix contains a highly concentrated mixture of hundreds of enzymes, including those required for the oxidation of pyruvate and fatty acids and for the citric acid cycle. The matrix also contains several identical copies (5-10) of the mitochondrial DNA genome, special mitochondrial ribosomes, tRNAs, and various enzymes required for the expression of the mitochondrial genes. The intermembrane space contains several enzymes that use the ATP passing out of the matrix to phosphorylate other nucleotides.

1.5.2 Energy generation by mitochondria

The citric acid cycle, also known as the tricarboxylic acid cycle or the Krebs cycle, oxidizes the acetyl group of pyruvate or fatty acids to generate CO_2 and high-energy electrons, which pass via NADH and $FADH_2$ to the respiratory chain. The high-energy electrons move along the respiratory chain, eventually combining with O_2 to produce H_2O and energy.

Mitochondria trap this energy in the form of ATP by the process of the oxidative phosphorylation (OXPHOS). The proteins involved in OXPHOS are located within the inner membrane and include the electron transport chain (ETC) component, ATP synthase and the adenine nucleotide translocator (ANT). The high-energy electrons borne on NADH are transferred to complex I (NADH dehydrogenase) and then to coenzyme Q_{10} (CoQ). The

electrons from succinate in the TCA cycle are transferred to complex II (succinate dehydrogenase, SDH) and to CoQ. From CoQ, the electrons are passed to complex III (cytochrome b-c_1), then to cytochrome c (cyt c), then to complex IV (cytochrome c oxidase). The energy released is used to pump protons (H^+) out of the inner membrane to create an electrochemical gradient (Delta Psi) that is positive and acid on the outside, and negative and alkaline on the mitochondrial matrix side. This creates a capacitor that can be depolarised by the transport of protons back into matrix through a proton channel in the F_0 membrane component of ATP synthase (ATPase). The proton flux drives the ADP and P_I (inorganic phosphate) to make ATP, which is then exported to the cytosol in exchange for the spent ADP by the ANT. In this way, oxygen consumption by the ETC is coupled to ADP phosphorylation by the ATPase through the electrochemical gradient (Wallace, 1999).

1.5.3 The mitochondrial genome

In addition to the genetic information housed in the cell nucleus, most animal cells also contain a mitochondrial genome. In vertebrates, mitochondrial DNA (mtDNA) is present in multiple copies (usually 10^3-10^4 copies/cell). Vertebrate mtDNA is a circular double stranded DNA ~16-18 Kb in length, coding for seven of the 43 subunits of complex I (ND1, 2, 3, 4, 4L, 5, and 6), one of the 11 subunits of complex III (cytocchrome b, cyt b), three of the 13 subunits of complex IV (COI, COII, and COIII) and two of 16 subunits of ATPase (ATPase 6 and 8). It also codes for the small and large rRNAs and 22 tRNAs (Shadel and Clayton, 1997).

1.5.4 Mitochondrial transcription

The two mtDNA strands can be separated on denaturing cesium chloride gradients, owing to a strand bias in G+T content. They are thus designated the heavy strand (H-strand) and the light strand (L-strand). Transcription of each strand occurs from one or two promoters (depending on the species). These promoters are designated as either a light-strand promoter (LSP) or a heavy-strand promoter (HSP), depending on which mtDNA strand serves as the template for transcription. Transcriptional initiation appears to require only a few nuclear-coded protein factors. Transcription of the H-strand begins at the light-strand

promoter. This involves the core mtRNA polymerase, the transcription factor mtTFA, and most likely a second transcription factor. Large polycistronic transcripts are produced from each strand that are then processed to generate mature tRNAs, rRNAs and mRNAs (Clayton, 1991).

Transcripts made on the H strand are extensively cleaved by RNA processing events to yield two rRNAs, 14 tRNAs, and 10 poly A-containing RNAs (Doersen et al., 1985). In contrast, the L strand transcript is processed to produce only 8 tRNAs and 1 small poly A-containing RNA. The remaining 90 % of this transcript apparently contains no useful information (being complementary to coding sequences synthesised on the other strand) and is degraded. The poly A-containing RNAs are the mitochondrial mRNAs. Although they lack a cap structure at their 5' end, they carry a poly-A-tail at their 3' end that is added post-transcriptionally by a mitochondrial poly A polymerase (Clayton, 1991).

The mRNA species corresponding to all the protein-coding regions have been identified; and in each case, an initiation codon lies within six bases of start of the transcript. The codon used for initiation apparently can be AUG, AUA, or AUU, which is different to those used for initiation of nuclear transcription. Non-translated 5'and 3' regions of transcripts are virtually absent. Almost all of the genes are expressed in the clockwise direction (transcripts made on H strand) (Fig. 1.1). In only one case are two clockwise coding regions found in the form of contiguous genes (ATPase 6 and CO3) (Fig. 1.1). In every other case, at least one tRNA gene separates adjacent coding regions. The punctuation of rRNA- and protein-coding regions by tRNA genes does not leave room for promoters such as those found in eukaryotic nuclei. A single promoter for clockwise transcription is located in the D-loop of the H-strand (Fig. 1.1). Transcription starts just before the tRNA gene in front of the 12S rRNA gene, and continues almost all the way around the circle, to terminate in the D-loop. The significance of the alternation of tRNA genes with rRNA- and protein-coding genes is that the tRNAs indicate sites of cleavage. By cleaving the primary transcript, which is mediated by a mitochondrial RNase P, on either side of each tRNA gene, all of the genes except ATPase 6 and CO3 give rise to monocistronic products (Doersen et al., 1985). The rRNA molecules appear to be synthesized in greater amounts than the mRNAs. This could be caused by premature termination of some proportion of the transcripts at some point after the two rRNA genes

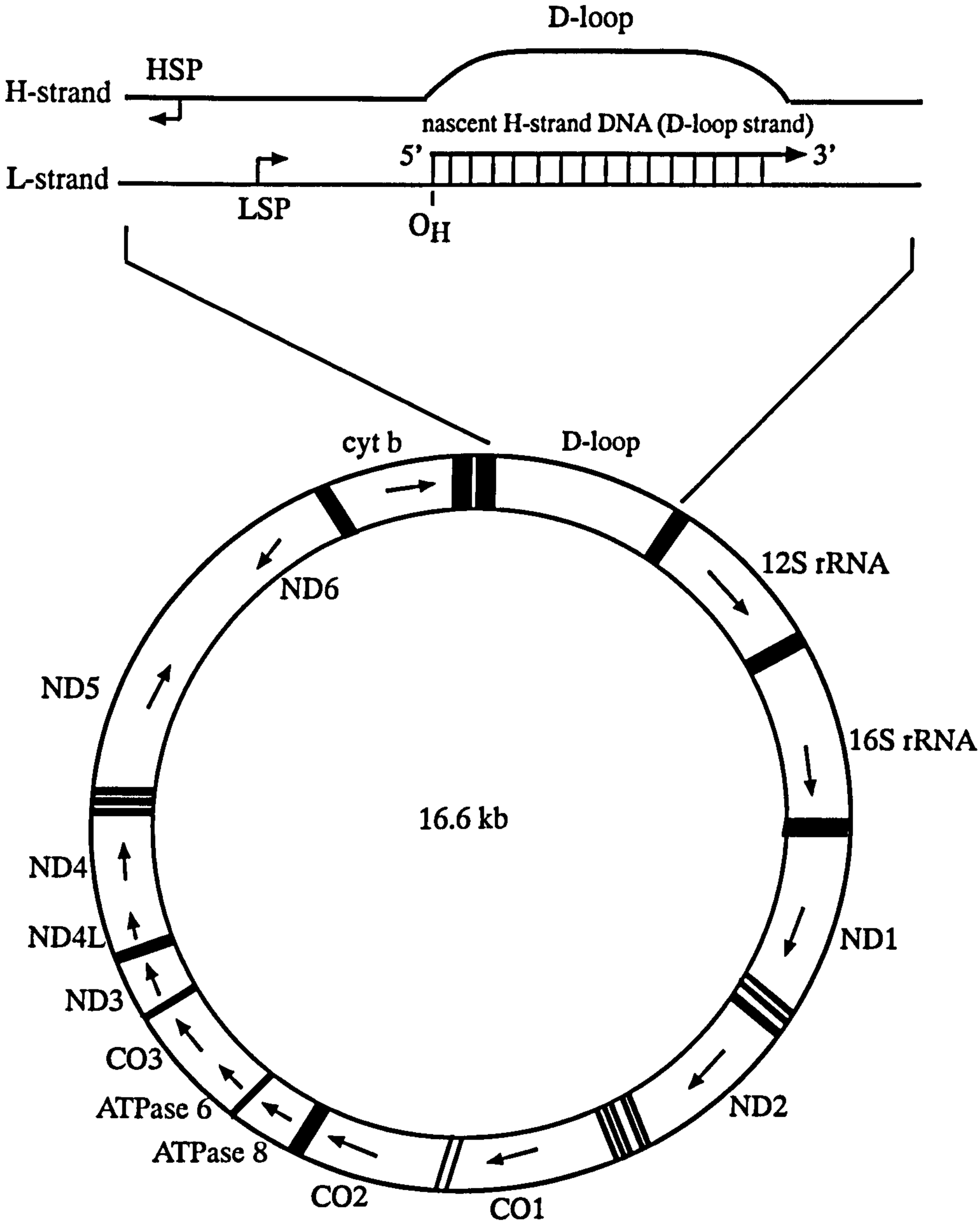

Figure 1.1 Schematic representation of a vertebrate mitochondrial genome. Vertebrate mitochondrial DNA contains 22 tRNA genes, 2 rRNA genes, and 13 protein-coding regions. 12 of the 13 protein-coding and 2 rRNA-coding regions and 14 of the tRNA genes are transcribed in the clockwise direction. 1 protein-coding gene and 8 tRNA genes are read counter clockwise. ▬ indicates tRNA genes. Thin arrows indicate orientation of the gene coding sequence 5'-3'. CO: cytochrome c oxidase. ND: NADH dehydrogenase. The D-loop form of mtDNA is shown with the D-loop regulatory region expanded at the top of figure. The mtDNA H-strand and L-strand are depicted as heavy and thin lines, respectively. The nascent H-strand (D-loop strand, thick arrow) is shown bound (dashed lines) to the parental L-strand and displacing the parental H-strand (bubble) to form the D-loop. The origin of H-strand (O_H) synthesis is labeled. The heavy-strand promoter (HSP) and light strand promoter (LSP) are depicted as bent arrows in the D-loop regulatory region. This figure is modified from Figure 1 in Shadel et al., 1997 Annu. Rev. Biochem. 66:409-435.

have been transcribed. This idea has been supported by the observation that the polymerase transcribing the rRNA genes more frequently stops at the 3' end of 16S rRNA due to the binding of a mitochondrial transcription termination factor (mTERF) to mtDNA (Kruse et al., 1989). Mitochondrial DNA therefore presents the closest analogy to a bacterial operon in eukaryotes. It is transcribed from a single region, but individual tRNAs, rRNAs, and mRNAs are released from the transcript. Processing of the transcript therefore becomes the central event in gene expression. The correct production of 5' and 3' ends of mitochondrial mRNA is important for mRNA stability. Incorrectly processed mRNA is often either unstable or untranslatable.

1.5.5 Replication of mitochondrial DNA

In all vertebrates examined to date, the mtDNA molecule contains a non-coding region that harbours the promoters for transcription initiation and a closely associated origin of H-strand DNA replication. In this region, a unique displacement-loop (D-loop) form of the mtDNA molecule arises from the template-directed termination of H-strand DNA synthesis soon after initiation. The arrested nascent H-strand remains stably hybridised to the circular parental molecule, forming a triple-strand structure characterised by the displaced parental H-strand. Because the promoters and leading-strand origin are located near the 5'-boundary of the D-loop structure, this entire locus is commonly referred to as the D-loop regulatory region or mtDNA control region (Fig. 1.1).

Mammalian mtDNA replication begins at O_H, which is located directly downstream of the LSP in the D-loop region of the molecule. This fact coupled with biochemical analysis of early replication intermediates, has led to a model in which RNA transcripts derived from the LSP are processed to yield primers for H-strand DNA replication (Clayton, 1991).

Mammalian mitochondrial promoters have a bipartite structure consisting of one region encompassing the site for transcription initiation, and a second region upstream that is the binding site for a transcription factor, mtTFA (Chang and Clayton, 1984). The mtTFA molecule has the ability to bend and unwind the DNA upon binding (Fisher et al., 1992). Therefore, the ability of mtDNA to activate transcription requires binding to, and

presumably bending or unwinding of the DNA immediately upstream of the transcription initiation site.

In all vertebrates, transcription initiation from mitochondrial promoters *in vitro* requires a mitochondrial RNA polymerase (mtDNA polymerase), mtTFA and likely a second transcription factor, mtTFB (Chen et al., 1996) (Fig. 1.2a). Precise mapping of RNA and DNA species in the D-loop region provided evidence that RNA derived from the LSP can serve as a primer for H-strand DNA replication (Chang et al., 1985). As transcription proceeds across the origin, a RNA/DNA hybrid forms which involves some subsets of the conserved sequence blocks (termed CSBI, CSBII, CSBIII) (Fig. 1.2b). Evidence has accumulated suggesting that the CSBs are involved in forming a properly configured RNA substrate for the activities that process the mitochondrial primer RNA (Xu and Clayton, 1996). Formation of a stable RNA-DNA hybrid structure at O_H is an important feature for H-strand replication (Xu and Clayton, 1996).

For a RNA molecule to serve as a primer for initiating DNA replication it must provide a donor 3'-hydroxyl group for extension by DNA polymerase. To provide a properly positioned primer, the LSP transcript must either terminate or be processed at sites near O_H. A site-specific mitochondrial RNA processing endoribonuclease (RNase MRP) with this activity was identified in mouse and human cells. RNase MRP does not cleave single-strand, origin-containing RNAs (Bennett et al., 1992). Evidence has suggested that the substrate for RNA processing is likely the triple RNA-DNA hybrid rather than single-strand RNA and shown that cleavage of RNA-DNA hybrid were completely dependent on the presence of CSB I (Lee and Clayton, 1997) (Figure 1.2c).

In vertebrates, apparently only one DNA polymerase, pol γ, is devoted to mtDNA synthesis (Figure 1.2d). Pol γ is distinguished from other cellular DNA polymerases by certain chemical criteria, including high activity using synthetic RNA templates *in vitro*, inhibition by both N-methylmaleimide and dideoxynucleoside triphosphates (ddNTPs), resistance to aphidicolin and stimulation by salt. Pol γ from all sources contain 3'-5' exonuclease activity (Gray and Wong, 1992). Mutations in the exonuclease domain result in increased mtDNA mutation rates in vivo, consistent with a role for this region in proofreading misincorporated nucleotides. As is the case of nuclear DNA polymerase, pol

a) Transcription initiation at LSP

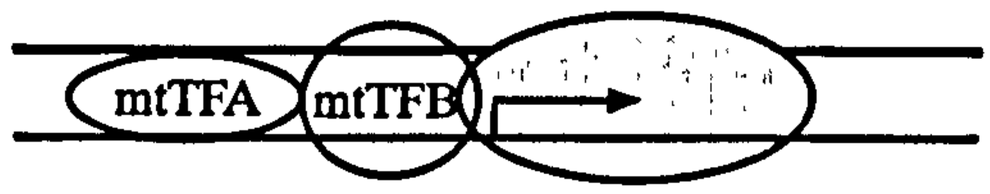

b) R-loop formation (RNA/DNA dybrid)

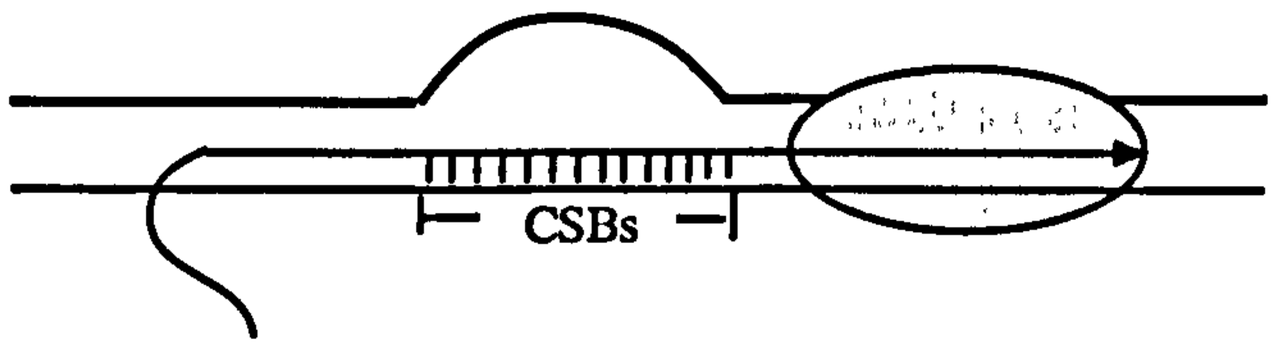

c) RNA primer processing in R-loop

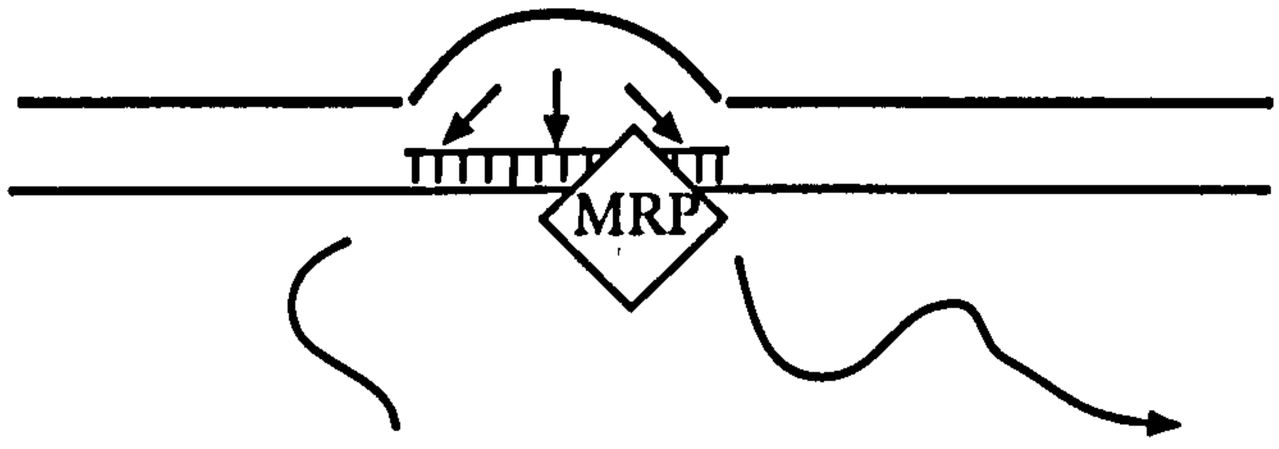

d) Initiation of H-strand synthesis

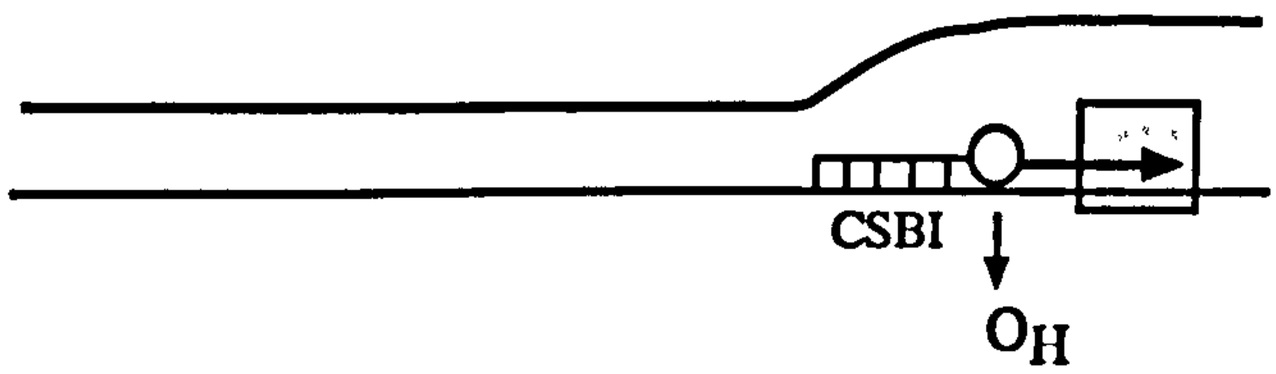

Figure 1.2 A general model for initiation of vertebrate H-strand replication. The parental mtDNA H-strand and L-strand are depicted as parallel heavy and thin lines, respectively. Nascent light strand promoter (LSP) RNA transcripts and nascent DNA H-strands are depicted as thin and heavy arrows respectively. The bubble represents the displaced parental H-strand. The initiation mechanism is divided into four steps (a-d). a) The process begins with the initiation of transcription at a light-strand promoter. This involves the core RNA polymerase (grey oval), mtTFA (white oval), and most likely a second transcription factor, mtTFB (white circle). b) As transcription proceeds across the region, a RNA/DNA hybrid (dashed lines) forms involving a subset of the CSBs (CSB I, II, and III). c) The RNA/DNA hybrid ultimately forms a stable R-loop configuration that creates the substrates for RNA processing activities (arrows) that lead to the formation of RNA primers. The cleavage pattern generated by RNase MRP (grey diamond) on synthetic R-loop substrates suggests that it is an important mtRNA primer processing activity in mitochondria. d) Initiation of H-strand replication (heavy arrow with attached circle) through extension of an RNA primer (thin line attached to circle) by DNA polymerase γ (grey rectangle), initiates near CSB I (O_H). This figure is based on Figure 2 in Shadel et al., 1997 Annu. Rev. Biochem. 66:409-435.

γ needs to associate with accessory factors. Mitochondria from several organisms contain a single-stranded DNA-binding protein (SSB) that is similar to *E.coli* SSB, both in amino acid sequence and DNA-binding properties. Consistent with a role in mtDNA replication, SSB stimulates pol γ activity *in vitro* (Williams and Kaguni, 1995) and functions in helix destabilization (Van Tuyle and Pavco, 1985). Also, mtDNA helicase activity has been isolated from bovine brain tissue and is predicted to act on the mtDNA template ahead of pol γ (Hehman and Hauswirth, 1992).

The triplex D-loop is a conserved feature of mtDNA in vertebrates, which suggests that it plays a crucial role in mtDNA metabolism. Possible roles for the stable D-loop include maintaining a given number of mtDNA molecules in a state primed for subsequent DNA replication (Clayton, 1982), and providing a mtDNA configuration that is necessary either for transcription regulation (King and Low, 1987) or for mtDNA segregation. In some cell types, increased D-loop frequency has been correlated with increased oxidative demand (Annex and Williams, 1990). In *Xenopus laevis,* elevated D-loop frequency is observed when mtDNA proliferates during oogenesis (Callen et al., 1983). Such findings suggest that D-loop formation and frequency is regulated. The D-loop-containing form of mtDNA arises from premature termination of H-strand synthesis downstream of O_H. The terminated nascent H-strand remains associated with the parental duplex. 3'-ends of D-loop DNA strands occurs at specific locations that are apparently directed by short (15 bp) template sequences (Doda et al., 1981). These termination-associated sequences (TASs) are well conserved in vertebrates and are found at similar positions upstream of the D-loop DNA 3'-ends that have been mapped (Foran et al., 1988). These findings suggest that nascent D-loop strand termination is a template-directed event and may represent one potential control point for regulating D-loop formation *in vivo*.

1.5.5.1 Regulation of mtDNA replication

Linkage of transcription to H-strand mtDNA replication in vertebrates suggests that mtDNA copy number may be controlled ultimately by the frequency of transcription initiation at the LSP. Because of its documented role in transcription initiation, much attention has been directed toward understanding mtTFA structure, function, and regulation. Human mtTFA contains two high-motility-group (HMG) boxes, and a C-

terminal tail. Studies on the mechanism of transcriptional activation of mtTFA have revealed that human mtTFA (h-mtTFA) forms a specific DNA-binding complex, mediated by both HMG-box domains and stabilised by the C-terminal tail, which promotes a specific bent structure in the DNA that allows the mitochondrial RNA polymerase to initiate transcription (Dairaghi et al., 1995).

Regulation of mitochondrial DNA (mtDNA) expression is crucial for mitochondrial biogenesis during development and differentiation. Mitochondrial transcription factor (mtTFA) has been demonstrated to regulate mtDNA copy number *in vivo* and is essential for mitochondrial biogenesis and embryonic development (Larsson et al., 1998). Consistent with a role in regulating mtDNA copy number, the level of h-mtTFA varies concomitantly with the level of mtDNA in human cells. Firstly, cultured human cells, depleted of mtDNA by treatment with ethidium bromide, contain extremely low levels of human-mtTFA (h- mtTFA) (Davis et al., 1996). Secondly, h-mtTFA is reduced in tissues from patients who exhibit a mtDNA-depletion phenotype (Poulton et al., 1994) and is elevated in tissues from patients who have an accumulation of mtDNA. The authors suggested that h-mtTFA deficiency in these patients might be due to reduced production or stability of the h-mtTFA protein in tissues with diminished mtDNA. Some studies have shown that mRNA of h-mtTFA can be elevated in cells depleted of mtDNA (Miranda et al., 1999). However, in other studies, no increased or decreased levels of mtTFA mRNA were detected after mtDNA depletion by ethidium bromide (Moraes et al., 1999). Although previous studies have revealed some conflicting results, there are several lines of evidence to suggest that mtDNA replication is regulated by coordinating signals from the nucleus and mitochondria.

Recently, pol γ has been examined as a potential mtDNA regulatory factor. Mitochondrial DNA depletion in AIDS patients appears to be caused by the inhibition of pol γ activity by antiviral drugs (Benbrik et al., 1997). However, in cells lacking mtDNA, and hence mtDNA replication, pol γ was expressed in a stable form and at normal levels, suggesting that pol γ level is not responsive to the amount of mtDNA in a cell (Davis et al., 1996). This study did not implicate pol γ as a major regulator of mtDNA copy number. These findings indicate that other nuclear-encoded proteins such as SSB, mitochondrial RNA

processing endoribonuclease and DNA helicase may also play a significant role in regulating mtDNA replication.

1.5.6 Regulation of mitochondrial biogenesis

The OXPHOS capacity can vary widely in different tissues of the body. Thus, during development from a fertilised oocyte to a multicellular organism, mitochondrial biogenesis is regulated and OXPHOS capacity is adapted to the different energy demands of particular cell types. In addition, adult animal cells can also adjust OXPHOS capacity to changing energy demands caused by various physiological or pathological conditions.

Increased transcription of mtDNA seems to be a hallmark of mitochondrial biogenesis as an adaptation to changes of energy demands caused by various physiological or pathological conditions. For example, the number of mitochondria increases through foetal life, accompanied by increases of both mtDNA copy number and mitochondrial transcript levels (Ostronoff et al., 1996). In addition, in many instances of mitochondrial biogenesis stimulated by various physiological challenges, increased levels of mRNAs for both nuclear- and mitochondrial-encoded OXPHOS subunits are also found, emphasizing the important role of transcriptional regulation. Examples where this occurs include endurance training of skeletal muscle (Hood et al., 1989; Williams, 1986), hyperthyroidism in liver and skeletal muscle (Wiesner et al., 1992) and hyperglucocorticoidism in colon epithelium (Rachamim et al., 1995). In contrast, during cold adaptation in brown tissue (Klingenspor et al., 1996) and during heart hypertrophy induced by thyroid hormones, the increase of functional mitochondrial mass is brought about not only by elevated levels of such transcripts, but at the same time by an additional, specific stimulation of mitochondrial translational capacity (Leung and McKee, 1990; Wiesner et al., 1994). Similarly, the rapid rise of OXPHOS capacity around birth in developing rat liver was attributed mainly to stimulation of translation, both in the cytosol and mitochondrial compartments (Ostronoff et al., 1996). It remains to be shown whether such a stimulation of mitochondrial translation also occurs during the adaptive processes mentioned above, in which mitochondria increase in both number and size (training of skeletal muscle), or size only (hyperthyroid state of liver and muscle). With the exception of some forms of skeletal muscle training and heart hypertrophy induced by thyroid hormones, the copy number of

mtDNA was found to be unchanged under most conditions, emphasising that up-regulation of mtDNA copy number is probably of minor importance for adaptive stimulation of mitochondrial biogenesis (Wiesner, 1992b).

1.5.7 Reactive oxygen species and regulation of mitochondrial biogenesis

Levels of mtTFA mRNA is elevated in cells experiencing increased oxidative stress (Miranda et al., 1999). Levels of cytochrome c_1 and cytochrome b mRNA also increase after exposure to oxidative stress mediated by antimycin A, an inhibitor of the mitochondrial cytochrome bc_1 complex (Suzuki et al., 1998). Furthermore, in the hearts of rats or patients with defects in energy production, mRNAs of both nuclear DNA- and mtDNA-encoded OXPHOS genes and mtTFA mRNA have been shown to increase, and it has been suggested that this is mediated through ROS (Heddi et al., 1999; Wiesner et al., 1999). All of above studies support the idea that, in principle, reactive oxygen species could stimulate expression of OXPHOS genes and mtTFA and they may form part of a mitochondrion-nucleus regulatory signalling pathway.

However, there is still some uncertainty about whether the ROS stimulates or represses the biogenesis of mitochondria. For example, one study demonstrated that an oxidative insult specifically decreased levels of a mitochondrial transcript which is an incompletely processed product of the mitochondrial genome encompassing ATPase subunit 6 and 8 plus the adjacent gene for cytochrome c oxidase (Elliott et al., 1999). In addition, mtDNA depletion and a compensatory increase of mtDNA transcription rates have been shown in liver after alcohol administration that caused oxidative stress (Mansouri et al., 1999). Similarly mtDNA depletion has been shown in Freidriech's ataxia, a condition associated with increased oxidative stress (Bradley et al., 2000). Reduced mtDNA transcription has been reported in a senescent rat heart (Andreu et al., 1998), despite the fact that mtDNA content appears to increase with aging (Lee et al., 1998). Since age is a condition associated with increased oxidative stress, these studies suggest that the responses of mtDNA replication and mtDNA transcription to increased oxidative stress may be different.

1.5.8 Coordination of nuclear and mitochondrial gene expression

Mitochondria biogenesis requires the ordered synthesis of the requisite proteins and lipids and delivery of each component to correct organelle subcompartments. While most of the proteins in mitochondria are encoded by nuclear DNA, some are encoded by mtDNA and synthesized on ribosomes within the mitochondria. Contributions from the two genetic systems to the construction of mitochondria are closely coordinated in the cell (Poyton and McEwen, 1996).

The nuclear genome exerts a great deal of control over mitochondrial gene expression and the protein import, export, and assembly pathways required for biogenesis of functional mitochondria. One study has shown that transcription of human mtTFA is activated by NRF-1 (nuclear respiratory factor 1) and NRF-2 (nuclear respiratory factor 2), two general transcription factors that regulate expression of several cellular proteins including subunits of mitochondrial respiratory proteins encoded by nuclear DNA (Virbasius and Scarpulla, 1994). It is therefore possible that the expression of nuclear and mitochondrial genes in mammals could be co-regulated globally through NRF-1 and NRF-2 proteins.

Biogenesis of mitochondria, either during development or in response to an alteration in physiological or pathological processes, is controlled through interactions of the nuclear and mitochondrial genomes, although the signal transduction pathways that connect the two genomes are not well understood. Both of the nuclear and mitochondrial genomes contribute essential subunit polypeptides to mitochondrial proteins and they collaborate in the synthesis and assembly of these proteins.

1.6 The aims of study

As previously reviewed, whilst many aspects of HD remain unresolved, several lines of evidence suggest that mitochondria play a central role in excitotoxicity, energy failure and oxidative stress, all of which have been implicated in HD pathogenesis. Further studies of mitochondrial function in HD may shed light on the mechanism and molecular pathology of HD. To this end, a HD "Knock-in" mouse model (termed the Glasgow HD mice and

described in Shelbourne et al., 1999) was used to study the functional consequences of the full-length mutant huntingtin protein.

The Glasgow HD mice were generated by introducing an HD-like mutation (an extended stretch of 72-80 CAG repeats) into the endogenous mouse *Hdh* gene. Histological examination of Glasgow HD mouse brains revealed that mutant brains, on average, were 10-15 % smaller than normal at 4-6 and 16-17 months of age, although no significant neuronal loss was detected (Shelbourne et al., 1999). Mutant mice also display aggressive behaviour at 3 months of age and electrophysiological deficits (a significant reduction in long-term potentiation) at 8 months of age (Usdin et al., 1999), suggesting learning and memory impairments. However, studies of locomotor performance including beam walking and rope tests did not show significant differences between HD mice and wild-type littermates at 17 months of age (Peggy Shelbourne, unpublished data).

Glasgow HD mice also display progressive formation of nuclear aggregates in the striatum when immunodetected with EM48 antibody (Li et al., 2000a). At 4 months of age, only weak nuclear staining was seen in the striatum, but by 11 months of age, this nuclear staining had become more intense, with small puncta. By 21-27 months, many nuclear aggregates had appeared and nuclei often contained a single, large aggregate. At the same time, the striatum also contained neuropil aggregates aligned in linear arrays reminiscent of processes. However, these neuropil aggregates appeared much later than intranuclear aggregates and were prominent in older mice. In addition to intranuclear aggregates, medium spiny neurons also formed aggregates in their processes and axonal terminals and they might interfere with the synaptic vesicle function of glutamate uptake (Li et al., 2000a). This finding suggests that the axonal terminal aggregates may contribute to the excitotoxicity in HD. Investigation of the repeat size of individual mutation alleles in tissues of Glasgow HD mice has shown that the mutation becomes very unstable in striatal tissue and repeat instability may occur by mechanisms that are not replication-based (Kennedy et al., 2000). It has been postulated that oxidative damage of DNA may initiate DNA repair that lead to mutation expansion.

Given that the Glasgow HD mice have detectable phenotypes and pathological changes reminiscent of early stages of human HD, more thorough experiments investigating motor

function and molecular pathology in these mice were performed and the aims of the study were:

1) to investigate and quantify the phenotypic features of the HD mice including motor function, weight profile and limb clasping;

2) to investigate mitochondrial function and increased oxidative stress as early molecular changes in HD mouse brain;

3) to correlate the phenotypic consequences and molecular changes in the HD mice, with a view to providing information for developing therapeutic strategies in the future.

2 Materials and methods

2.1 Materials

2.1.1 Chemicals and reagents

Chemicals of molecular biology grade were obtained from Merck Ltd. (BDH Laboratory Supplies), except for the following:

Boric acid, sodium dodecyl sulphate (SDS), Trizma base, polyethylene glycol 8000 (PEG), 3-N-morpholino-propanesulfonic acid (MOPS), Triton X-100, sodium acetate, polyoxyethylene sorbitan monolaurate (Tween 20), dextran sulphate, diethyl pyrocarbonate (DEPC), paraformaldehyde, hydrogen peroxide, sodium hydroxide, salmon sperm DNA, isopropylthio-β-D-galactoside (IPTG), 5-bromo-4-chloro-3-indolyl--β-D-galactoside (X-gal), glycerol, Ficoll, dimethylsulfoxide (DMSO) and poly-L-lysine were obtained from Sigma Chemical Company Ltd.

Diaminoethanetetra-acetic acid disodium salt (EDTA), sucrose, chloroform, methanol, and disodium hydrogen orthophosphate dihydrate were obtained from Fisher Scientific International Company.

Bovine serum albumin (fatty acid free, BSA) was obtained from Boehringer Mannheim UK Ltd.

G-50 Sephadex, G-25 Sephadex were supplied by Amersham Pharmacia Biotech, UK, Ltd.

Nonidet®P-40 was obtained from Calbiochem.

Hematoxylin and eosin were obtained from Surgipath.

DPX mounting medium was purchased from Lamb.

Histoclear was supplied by National Diagnostics.

2.1.2 Membranes and radiochemicals

The following nylon membranes and radiochemicals were obtained from Amersham Pharmacia Biotech, UK, Ltd: Hybond N, 20 cm wide roll; Hybond N plus, 20 cm wide roll; [γ-^{32}P] ATP (5000 Ci/mmol, 10 μCi/μl); [α-^{32}P] dCTP (3000 Ci/mmol, 10 μCi/μl).

Biodyne B membranes, 30 cm x 3 m, for northern blot analysis were obtained from Pall Gelman Laboratory. PVDF membranes, Immobilon™-P, for western blotting analysis were obtained from Millipore. 3MM chromatography paper was supplied by Whatmann.

2.1.3 Polymerase chain reaction (PCR)

All PCR amplifications were carried out in a thermal cycler (GeneAmp PCR System 9700, PE Applied Biosystem), in thin walled 200 μl tubes (Anachem).

2.1.4 DNA, RNA, and Protein markers

All DNA samples that were electrophoresed on gels were measured against the 1 kb DNA size ladder or the 1 kb plus DNA size ladder (GibcoBRL).

All RNA samples electrophoresed on gels were measured against the 0.24-9.5 kb RNA ladder (GibcoBRL).

All protein samples that were electrophoresed on gels were measured against the Sea Blue Standard (Novex, Invitrogen).

2.1.5 Gel electrophoresis

Agarose was obtained from Roche Diagnostics. Formamide was purchased from Scientific Imaging System, Eastman Kodak Company. Formaldehyde was from Sigma. Electrophoresis tanks for agarose and northern blot gels and Power Pac 300 were from Biorad. The NuPage™ electrophoresis system used for western blotting was purchased from Novex, Invitrogen.

2.1.6 Photography, autoradiography and image analysis for immunohistochemistry

A gel documentation system (UVP 7500) and thermal paper K65HM-CE (Mistubishi) were used to take gel photographs. Fuji RX X-ray film was obtained from Genetic Research Instrumentation Ltd. X-ray film was developed using X-Ograph Compact X_2 (X-Ograph, Ltd). The intensity of bands on the gel photographs or on X-ray film was measured with Kodak Digital Science ID software from Kodak. Images of immunohistochemistry sections were taken using a Leica DMRB microscope connected to a digital camera (Cool Snap-Pro, Media Cybernetics) and a computer with image analysis software (Image Pro Plus 4.5, Media Cybernetics).

2.1.7 Oligonucleotides

The oligonucleotides were supplied by Sigma-Genosys. The sequences of oligonucleotides used are listed below:

Table 2.1 Oligonucleotide information Tm = (A+T) x 2°C + (G+C) x 4°C.

Oligonucleotide	Sequence, 5'→3'	Tm (°C)	Annealing to
MHD 16	CCCATTCATTGCCTTGCTGCTAAG	62	Mouse *Hdh* gene (Fig. 4.19)
MHD 18	GACTCACGGTCGGTGCAGCGGTTCC	70	Mouse *Hdh* gene (Fig. 4.19)
L1	CGCTCTACCT CACCATCTCT T	62	Mouse mitochondrial DNA (Fig. 4.1)
H1	TGCTTACCTT GTTACGACTT A	57	Mouse mitochondrial DNA (Fig. 4.1)
L2	ACCAACAGCT ACCATTACAT T	58	Mouse mitochondrial DNA (Fig. 4.1)
H2	TGATTGGGTT TATGAGGTCT G	62	Mouse mitochondrial DNA (Fig. 4.1)
F3	CAAGTCCATGACCATTA ACTGG	58	Mouse mitochondrial DNA (Fig. 4.1)
MIMICL1	CGCTCTACCT CACCATCTCT TAGAAGTTGT CCATATTGGC C	79	*Ecoli* CAT gene (Fig 4.7 and Fig. 4.8)
MIMICH1	TGCTTACCTT GTTACGACTT A ATAACCAGA CCGTTCAGCT G	78	*Ecoli* CAT gene (Fig 4.7 and Fig. 4.8)
MIMICL2	ACCAACAGCT ACCATTACAT T CGCAGTACTG TTGTAATTC	75	*Ecoli* CAT gene (Fig 4.10 and Fig. 4.8)
MIMICH2	TGATTGGGTT TATGAGGTCT GATCACTGGA TATACCACCG	79	*Ecoli* CAT gene (Fig 4.10 and Fig. 4.8)
mGDH-A	CACTTGAAGGGTGGAGCCAAAC	69	Mouse *Gapdh* mRNA (Fig. 5.3a)
mGDH-BR	TGGGTGGTCCAGGGTTTCTTAC	68	Mouse *Gapdh* mRNA (Fig. 5.3a)
CLW2F	GAATTCAGGCTTAAGGAGGTCCGA CTG	61	Mouse *Dmpk* exon 2 (Fig. 5.3b)
CLW4R	GAATTCGCAAAATGCAGCTGTGTG ATC	61	Mouse *Dmpk* exon 4 (Fig. 5.3b)
TFA1	TCGCATCCCCTCGTCTATCAG	69	Mouse *Tfam* mRNA (Fig. 5.4a)
TFA2	TCGCATCCCCTCGTCTCTCG	67	Mouse *Tfam* mRNA (Fig. 5.4a)
COIF	CTGAGCGGGAATAGTGGGC	65	Mouse *CoI* mRNA (Fig. 6.1a)
COIR	GCAAGCTCGTGTGTCTACC	63	Mouse *CoI* mRNA (Fig. 6.1a)
COIIF	CTACAAGACGCCACATCCCC	67	Mouse *CoII* mRNA (Fig. 6.1a)
COIIR	CTAGGACAATGGGCATAAC	62	Mouse *CoII* mRNA (Fig. 6.1a)
CytbF	CATTCATTGACCTACCTGCC	65	Mouse *Cytb* mRNA (Fig. 6.1a)
CytbR	CTGGGTCTCCTAGTATGTG	58	Mouse *Cytb* mRNA (Fig. 6.1a)
HOF	CGTCCACAGC CCGACAGCAT	73	Mouse *Hmox* 1 mRNA (Fig.7.2a)
HOR	GGAGCGGTGT CTGGGATGAG	69	Mouse *Hmox* 1 mRNA (Fig.7.2a)
CROF	ATGGACATCGCCATCCACCAC	62	Mouse *Cryab* mRNA (Fig.7.4)
CROR2	AAGCTTCAGCACTAGTCACAG	58	Mouse *Cryab* mRNA (Fig.7.4)

2.1.8 Enzymes

Restriction enzymes were obtained from GibcoBRL, Boehringer Mannheim, or New England Biolabs. Sources of other enzymes are indicated in the following table:

Table 2.2 Enzyme information

Enzyme	Supplier
HPLC pure klenow	Amersham Pharmacia Biotech
Amplitaq Gold	Perkin Elmer
Taq polymerase	Promega
Proteinase K	Boehringer Mannheim
RNasin	Promega
Superscript™ II reverse transcriptase	GibcoBRL
T4 DNA polynucleotide kinase	Promega
RQ1 RNase free DNase	Promega

2.1.9 Primary antibodies

The sources of primary antibodies used in this study are indicated in the following table:

Table 2.3 Primary antibody information

Antibody	Concentration of antibody supplied	Dilution typically used in study	Supplier
Monoclonal anti-porin antibody	Not known	1:5000	Calbiochem
Monoclonal anti-β tubulin III antibody	Not known	1:25000	Promega
Polyclonal anti-mtTFA antibody	Not known	1:15000	A gift from David Clayton, Department of Developmental Biology, Beckman Center for Molecular and Genetic Medicine, Stanford University
Monoclonal anti-cytochrome c oxidase subunit I (COI), 1D6-E1-A8	Lyophilised powder (100μg)	4 μg/ml	Molecular Probes
Monoclonal anti-8-OH-deoxyguanosine (8-OHdG)	Lyophilised powder (100μg)	1μg/ml	Nikken Foods Co, Japan
Polyclonal anti-4-hydroxynonenal (4-HNE)	Not known	1:2000	Calbiochem
Polyclonal anti-heme oxygenase 1 (HO-1), SPA-895	Not known	1:1500	Stressgen

2.1.10 Secondary antibodies

The sources of secondary antibodies used in this study are indicated in the following table:

Table 2.4 Secondary antibodies

Antibody	Concentration of antibody supplied	Dilution typically used in study	Supplier
Donkey anti-rabbit IgG-horseradish peroxidase (IgG-HRP)	Not known	1:4000	Amersham
Goat anti-mouse IgG-HRP	Not known	1:60000	Jackson Lab
Horse biotinylated anti-mouse secondary antibody	1.5 mg/ml	1:500	Vector
Goat biotinylated anti-rabbit secondary antibody	1.5 mg/ml	1:100	Vector

2.1.11 Kits

The sources of kits used in this study are indicated in the following table:

Table 2.5 Kit information

Kit	Supplier
ABI PRISM™ Dye Terminator Cycle Sequencing Ready Reaction kit	Perkin Elmer
Random Primers DNA Labeling System	GibcoBRL
QIAquick Gel Extraction kit	Qiagen
QIAgen Plasmid DNA Miniprep kit	Qiagen
QIAgen Plasmid DNA Midiprep kit	Qiagen
TOPO™ TA Cloning	Invitrogen
SUPERSCRIPT™ Preamplification System for the First Strand cDNA Synthesis Kit	GibcoBRL
TRI REAGENT™	Sigma
ExpressHyb Hybridisation Solution	Clontech
SuperSignal West Pico Chemiluminescent Substrate	Pierce
3'3' diaminobezidine tetrahydrochloride (DAB) kit	Vector
VECTASTAIN® Elite ABC kit	Vector
Vector® M.O.M. Immunodetection Kits	Vector

2.1.12 Normal serum

Normal goat serum, normal horse serum, and normal donkey serum were from Vector.

2.1.13 Medium and antibiotics

Luria- Bertani (LB) broth: 10 g Tryptone, 5 g yeast extract, 10 g NaCl and dH_2O added to a final volume of 1 litre.

LB agar: 10 g Tryptone, 5 g Yeast extract, 10 g NaCl, 15 g Agar, and dH_2O added to a final volume of 1 litre.

Ampicillin: Stock solution: 50 mg/ml in dH_2O. Store at -20°C. Working solution: 50 µg/ml

2.1.14 Bacterial host strains

DH5α: F-, φ80d*lac*ZΔM15, Δ(*lac* ZYA-*arg*F), U169, *deo*R, *rec*A1, *end*A1, *hsd*R17 (r_{K}-, m_{K+}), *sup*E44, λ-, *thi*-1, *gyr*A96, *rel*A1 (Life Technologies Ltd).

TOP10F': F'{*lac*I^{q}Tn*10* (Tet^{R})} mcrA Δ (*mrr-hsd*RMS-*mcr*BC) Φ80*lac*ZΔM15 Δ*lac*X74 *rec*A1 *deo*R *ara*D139 Δ(ara-leu)7697 *gal*U *gla*K *rps*L (Str^{R}) *end*A1 *nup*G (Invitrogen)

2.1.15 Vectors

pCR®2.1-TOPO® in TOPO™ TA Cloning kit was used for cloning (Invitrogen).

2.1.16 Storage of bacterial culture containing recombinant plasmids

Long-term storage of recombinant plasmid was achieved by mixing equal volumes of an overnight culture of the host containing the recombinant clone and sterile glycerol. These stocks were stored at -70°C, where they can remain viable for several years.

2.1.17 Solutions

Aprotinin: Stock solution: 10 mg/ml. Working solution: 10 µg/ml

Blocking solution for western blot: 0.2 % casein solution in 1 X TBS (Pierce), 0.1 % normal goat or donkey serum.

10 mM Citric acid, pH6.0: 2.1 g/l, pH to 6.0 with 10 M NaOH.

Cryoprotectant for free-floating sections: 1.37 g NaH_2PO_4, 5.46 g Na_2HPO_4, 300 ml glycerol, 300 ml ethylene glycol and 400 ml water. Store at -20°C.

100 X Denhardts solution (Denhardt, 1966): 2 g Ficoll, 2 g polyvinylpyrrolidone, 2 g BSA, and dH_2O to 100 ml.

Denaturing solution: 1.5 M NaCl, 0.5 M NaOH

Depurinating solution: 0.25 M HCl.

5 X DNA loading dye: 0.5 % (w/v) SDS, 0.25 % (w/v) xylene cyanol, 0.25 % (w/v) bromophenol blue, 1.5 % (w/v) Ficoll®400, 3 X TBE.

Ethidium bromide (EtBr): Stock solution: 10 mg/ml, working solution: 200 ng/ml.

EBC lysis buffer: 5 ml 1M Tris-HCl, pH 8.0, 2.4 ml 5 M NaCl, 1 ml NP-40 made up to 100 ml with water and stored at 4°C.

Formaldehyde gel: 15 mls 10 X MOPS, pH 8.0, 15 ml formaldehyde, 120 ml DEPC water, and 1.95 g agarose.

Homogenizing medium A for purification of cell nuclei: 0.25 M sucrose, 5 mM $MgCl_2$, 10 mM Tris-HCl, pH 7.4.

Homogenizing medium B for purification of cell nuclei: 2.2 M sucrose, 1 mM $MgCl_2$, 10 mM Tris-HCl, pH 7.4.

Hybridization buffer for Southern blot: 5 X SSPE, 5 X Denhardts, 0.5 % (w/v) SDS, 7 % (w/v) Dextran sulphate and 100 µg/ml salmon sperm DNA in distilled water.

Hybridization buffer for using a synthetic oligonucleotide as probe: 15 mls 20 X SSPE, 1 ml 50 X Denhardts, 2 ml 10 % (w/v) SDS, and 100 µl of 50 mg/ml yeast t-RNA in 32 ml distilled water.

IPTG (Isopropylthio-β-D-galactoside): Stock solution: 300 mg/ml in dH_2O. Working solution: 30 µg/ml.

Leupeptin: Stock solution: 1 mg/ml. Working solution: 10 μg/ml.

10 X MOPS (pH 7 or pH 8): 0.2 M 3-(N-morpholino)-propanesulfonic acid (MOPS), 50 mM sodium acetate, 10 M EDTA, pH to 7.0 or 8.0 with 10 M NaOH, wrap with foil and stored at 4°C.

Neutralizing solution: 1.5 M NaCl, 0.5 M Tris, adjust to pH 7.0 with HCl.

Oligo labelling buffer: Oligo labelling buffer was made up to the ratio 2A: 5B: 3C and stored at -20°C. Solution A: 1.2 M Tris (pH8), 121 mM $MgCl_2$, 0.48mM dATP, 0.48 mM dGTP, 0.48 mM dTTP, 18 μl of 2-β-mercaptoethanol in a final volume of 1033 μl. Solution B: 2M Hepes, pH 6.6 with NaOH (4°C). Solution C: Pharmacia Biotech Ultrapure dNTP's set suspended in 0.2 mM EDTA (pH7.0) to an optical density of 90 OD unit ml^{-1} (-20°C).

Orange G: 0.06 % (w/v) Orange G, 50 % (v/v) glycerol.

20 % Paraformaldehyde (PFA), pH7.4: Dissolve 20 g PFA in 100 ml 1 X PBS adjust pH to 7.4 with NaOH, filter through 0.8 μm filter and stored at -20°C.

4 % Paraformaldehyde (PFA), pH7.4: Thaw 20 % PFA, pH7.4 and dilute to 4 % PFA with 1 X PBS.

PEG solution for precipitating DNA: 26.2 % polyethylene glycol (PEG) 8000, 66 mM $MgCl_2$, 0.6 M NaOAc, pH 5.2, and autoclave.

Pepstatin: Stock solution: 1 mg/ml. Working solution: 10 μg/ml.

Phenol: Phenol saturated in 10 mM Tris (pH 7.5), 1 mM EDTA (pH8.0)

Phenol: chloroform: isoamyl alcohol, 25:24: 1: Phenol: chloroform: isoamyl alcohol, 25:24: 1 saturated in 10 mM Tris, pH 7.5, 1 mM EDTA, pH8.0.

Phenylmethylsulphonyl fluoride (PMSF): Stock solution 100 mM in propan-2-ol (stored at -20°C). Working solution: 0.1-1 mM.

10 X Phosphate buffered saline (PBS): 1.4 M NaCl, 0.027 M KCl, 0.1 M Na_2HPO_4, 0.021 M KH_2PO_4 adjust to pH 7.4 with HCl.

Pre-hybridisation buffer for Southern blot: 5 X SSPE, 5 X Denhardts, 0.5 % (w/v) SDS, and 100 μg/ml salmon sperm DNA in distilled water.

Pre-hybridisation buffer for using a synthetic oligonucleotide as probe: 15 ml 20 X SSPE, 5 ml 5 X Denhardts, 2 ml 10 % (w/v) SDS, and 100 μl of 10 mg/ml salmon sperm DNA in 28 ml distilled water.

Proteinase K: working stock of 20 mg/ml in filter sterilized H_2O.

Proteinase K lysis buffer: 100 mM Tris (pH8.5), 200 mM NaCl, 0.2 % (w/v) SDS, 5 mM EDTA pH8.0, 100 μg/m.

RNA loading buffer: 12 μl of ethidium bromide stock solution (10 mg/ml), 300 μl of 10 X MOPS, pH 8.0, 80 μl of formaldehyde, 900 μl of deionised formamide [37-40 % (w/v)].

Sephadex G25: Sephadex G25, equilibrated with TE, pH7.6.

Sephadex G50: equilibrated with TE, pH7.6.

20 X SSC: 6 M NaCl, 0.6 M $Na_3C_6H_5O_7.2H_2O$, and autoclave.

20 X SSPE: 0.2 M $NaH_2PO_4.2H_2O$, 3 M NaCl, 0.02 M EDTA (pH8.0) and adjust pH to 7.4 with HCl.

10 % (w/v) SDS: 10 % (w/v) SDS in H_2O.

Slot blot loading buffer: 1 ml deionised formamide, 324 μl of 37 % (w/v) formaldehyde and 200 μl 10 X MOPS.

1 X TAE: 0.04 M Trizma base, 0.04 M acetic acid, 0.001 M EDTA, pH8.0.

1 X TBE: 0.09 M Trizma base, 0.09 M boric acid, 0.001 M EDTA, pH8.0.

10 X TBS: 1 M Trizma base, 1.5 M NaCl, pH to 7.5 with HCl and autoclave.

1 X TBST: 0.6 % Tween-20 in 1 X TBS.

TE: 10 mM Tris (pH 7.5), 1 mM EDTA (pH 8.0), and autoclave.

1 M Tris (pH7.5): 1 M Trizma base, add HCl to pH 7.5 and filter sterilize.

1 M Tris, (pH8.3): 1 M Trizma base, add HCl to pH 8.3 and filter sterilize.

1 M Tris, (pH8.0): 1 M Trizma base, add HCl to pH 8.0 and filter sterilize.

Tris buffer for free-floating section staining: 6.05 g Trizma base, 6.76 g NaCl and water to a final volume of 1 l.

X-gal (5-Bromo-4-chloro-3-indolyl-β-D-galactoside): Stock solution: 50 mg/ml (in dimethylformamide) and wrap in foil. Working solution: 50 μg/ml.

2.1.18 Mouse lines

The mice used in this study were generated by inserting a HD-like mutation (an extended stretch of 72-80 CAG repeats) into the endogenous mouse *Hdh* gene to mimic the molecular findings on human HD chromosome by Dr. Peggy Shelbourne (Shelbourne et al., 1999). The resulting mice were maintained on different genetic backgrounds as indicated in Table 2.6.

Table 2.6 Summary of mice used in the study

Designation in the text of this study	Mouse line described in Shelbourne et al., 1999	Mutant huntingtin protein expressed	Genetic backgrounds	Experiment where mice used
HD or Glasgow HD mice	*Hdh6/Q72*	Full length	Fvb/n	The integrity of mtDNA in HD mice, the cause of striatal mtDNA depletion, the effects of mtDNA depletion and the direct evidence of increased oxidative stress in the striatum of HD mice
HD or Glasgow HD mice	*Hdh6/Q72*	Full length	C57BL/6	Locomotor study

2.2 Methods

2.2.1 DNA isolation

2.2.1.1 Genomic DNA isolation

The tissue samples taken from mice were immediately placed on dry ice or kept at -80°C before proceeding to DNA extraction. The DNA was extracted by adding 700 µl of lysis buffer containing 35 µl of 2 M Tris (pH 8.5), 28 µl of 5 M NaCl, 14 µl of 10 % (w/v) SDS, 7 µl of 0.5 M EDTA (pH 8.0), 0.7 µl of proteinase K (100 mg/ml) and 615 µl of distilled

water. The mixture was incubated overnight with shaking at 55°C, then vortexed hard, and centrifuged for 10 min at 10,000 X *g*. The supernatant was transferred to a clean, labelled eppendorf tube containing 700 µl isopropanol (propan-2-ol) to precipitate the DNA. The DNA pellet was resuspended in 1 X TE overnight at 4°C.

2.2.2 Phenol/chloroform extraction of DNA solutions

A DNA solution is extracted with a 1:1 phenol/chloroform mixture in order to remove protein contamination. The organic solvents precipitate proteins, and these are left as a coagulated, white mass at the interface between the aqueous and organic phases after centrifugation.

An equal volume of phenol/chloroform (phenol: chloroform: octanol = 25: 24:1) was added to the DNA solution and emulsified by mixing. The organic and aqueous phases were separated by centrifugation (10,000 X *g*, 10 min) and the aqueous phase transferred to a clean tube. A final extraction with an equal volume of 24:1 chloroform/octanol was performed to remove any remaining phenol that might inhibit subsequent enzyme reactions.

2.2.2.1 Extraction of plasmid DNA

1) Small scale preparation

Plasmid DNA preparation was prepared by the alkali-lysis method (Sambrook et al., 1989) using the Qiagen QIAprep miniprep kit. An overnight culture of the host bacteria harboring the recombinant clone was grown in LB broth at 37°C in a shaking incubator. Cells from 1.5 ml of this culture were collected by centrifugation at 6,000 X *g* for 5 min and resuspended in 250 µl buffer P1 and subjected to the protocol specified in the manufacturer's instructions. The DNA was finally eluted from the column with distilled water.

2) Large scale preparation

Plasmid DNA was prepared using the QIAgen midiprep kit according to the manufacturer's instructions. Briefly, 5 ml LB broth culture containing 100 µg/ml ampicillin was inoculated

with a single transformed bacteria colony. After overnight incubation, 0.4 ml culture was used to inoculate 200 ml LB broth (containing 100 µg/ml ampicillin) that was then incubated at 37°C overnight with shaking (300 rpm). Bacterial cells were harvested by centrifugation (Beckman, J2-MC) at 6,000 X *g* for 15 min at 4°C. The pellet was gently resuspended in buffer P1 and incubated on ice for 5 minutes. Buffer P2 was added and the mixture was gently inverted until it turned clear. This mixture was incubated on ice for a further 5 min. Buffer P3 was added and the solution mixed gently until a heavy white protein precipitate was formed. The solution was incubated on ice for 15-20 min and then centrifuged at 20,000 X *g* for 30 min in a Beckman rotor at 4°C. The supernatant was applied to a QIAGEN-tip 100 column equilibrated with 4 ml buffer QBT and was allowed to flow through the column by gravity. Under these conditions, the plasmid DNA binds to the resin whereas protein and RNA do not. 30 ml buffer QC was added to the column and allowed to flow through by gravity. The plasmid DNA was eluted with buffer QF and the elutant mixed with 0.7 volumes of isopropanol to precipitate the plasmid DNA. The mixture was centrifuged at 10,000 X *g* for 30 min followed by one wash in 70 % (v/v) ethanol. The plasmid DNA pellet was resuspended in 200 µl TE buffer.

2.2.2.2 Preparation of nuclear DNA from mouse brain

A quarter of a mouse brain was chopped finely with scissors in cold homogenizing medium A (0.25 M sucrose, 5 mM $MgCl_2$, 10 mM Tris-HCl pH 7.4). The homogenizing medium A was poured off and the chopped tissue was resuspended in 9 volumes of fresh homogenizing medium A (5 ml). The suspension of chopped tissue was homogenized using a Heidolph homogenizer (Labplant) with a loose-fitting (0.1 mm clearance) Teflon pestle driven at 1000 r.p.m. Approximately 40-50 up and down strokes were performed to obtain complete cell breakage. The homogenate was filtered through four layers of muslin taking care not to squeeze the muslin to obtain the last few drops of liquid. The homogenate was then centrifuged at 600 X *g* for 10 min, 4°C. The supernatant was poured off and the pellet resuspended in half the original volume of homogenizing medium A. The resuspended nuclei were centrifuged at 600 X *g* for 10 min at 4°C. The supernatant was discarded, leaving a pellet of crude nuclei.

The pellet of crude nuclei was resuspended in 9 volumes (5 ml) of homogenizing medium B (2.2 M sucrose, 1 mM $MgCl_2$, 10 mM Tris-HCl pH 7.4) and homogenized using the Heidolph homogenizer with a loose-fitting (0.1 mm clearance) Teflon pestle with 5-6 up and down strokes driven at 1000 rpm. The solution was transferred to a centrifuge tube (13 X 51 mm, polyallomer Quick-seal centrifuge tube, Beckman) using a glass pipette. The tube was sealed and centrifuged at 60-80,000 X *g* for 80 min at 4°C in a fixed angle rotor (35,000 rpm in TLA100.4, Beckman). After centrifugation, the nuclei formed a cream or white coloured fine pellet at the bottom of the tube. The seal of tube was cut, and any skin that might have formed at the top of the dense sucrose was removed using a stainless steel spatula. The tubes were emptied by rapid inversion and any remaining sucrose was wiped out with a tissue wrapped around a glass rod or spatula. The nuclei were resuspended in homogenizing medium A and stored at -20°C.

To check there was no contamination of cytoplasm, the nuclei were stained with 1 % (w/v) methylene blue. The nuclei appeared clean without any membrane adhering to the outside of the nucleus.

Promega PCR buffer was diluted 1 in 10 to get the composition of 10 mM Tris-HCl, 50 mM KCl, 0.1 % (v/v) Triton, and 2.5 mM $MgCl_2$. Proteinase K was added to the solution to a final concentration of 100 μg/ml. The resuspended nuclei in homogenizing medium were centrifuged at 600 X *g* for 10 min. 500 μl PCR buffer containing 100 μg/ml Proteinase K was added to the pellet and incubated at 55°C for 3-4 hours. After incubation, the nuclear DNA was purified by phenol and chloroform extraction.

2.2.2.3 Concentration of DNA samples

Ethanol precipitation can increase the concentration of DNA and also remove short chain and monomeric nuleic acid components. Either of the following protocols was used:

1. Addition of 0.1 volume of 3 M CH_3COONa (pH 4.8) followed by 2 volumes of absolute ethanol.
2. Addition of 0.1 volume of 3 M CH_3COONa (pH 4.8) followed by equal volume of isopropanol that has been equilibrated at room temperature.

After the addition of ethanol or isopropanol, the solution was mixed and placed at -20°C for at least 30 min. The DNA pellet was recovered after centrifugation (10,000 X *g*, 15 min), washed in 70 % (v/v) ethanol to remove excess salt, and centrifuged again to pellet the DNA, which was dried and resuspended in 1 X TE buffer. If required, the tube containing the DNA pellet was left at 37°C in a water bath for 30-120 min to resuspend the DNA.

2.2.3 Quantification of DNA or RNA

Spectrophotometric determination is used to quantify the amount of DNA. Readings are taken at wavelength of 260 nm and 280 nm. The reading at 260 nm allows calculation of the concentration of nucleic acid in the sample. An OD of 1 corresponds to approximately 50 μg/ml for double-stranded DNA, 40 μg/ml for single stranded DNA and RNA, and ~20 μg/ml for single stranded oligonucleotides. The ratio between the readings at 260 nm and 280 nm (OD_{260}/OD_{280}) indicates the purity of the nucleic acid. Pure preparation of DNA and RNA have OD_{260}/OD_{280} values of 1.8 and 2.0 respectively. If contamination with protein or phenol is present, the OD_{260}/OD_{280} will be significantly less than the values indicated. For double stranded DNA or RNA the concentration was calculated using the following equations:

Concentration of DNA=OD_{260} X 50 X Dilution factor (μg/ml)

Concentration of RNA=OD_{260} X 40 X Dilution factor (μg/ml)

2.2.4 Digestion of DNA with restriction enzymes

Restriction digests of most plasmids and genomic DNA were carried out in 30 μl reactions for 2 -15 hours (depending on the enzyme used) at the temperature suitable for the specific enzyme. 3-5 μg DNA was digested in the presence of 3 μl of BSA (100 μg/ml), 3 μl of 10 X reaction buffer, 1-2 μl (20-30 units) of restriction enzyme and distilled water to a total volume of 30 μl.

2.2.5 Polymerase chain reaction (PCR)

2.2.5.1 PCR primer design

Oligonucleotides that were 20 to 21 nucleotides long and had melting temperatures (Tm={(A+T) x 2°C + (G+C) x 4°C})(Suggs et al., 1981) between 55°C and 68°C were designed. Both PCR primers in a set were designed to have a similar Tm, not to be complementary at their 3' end, not self-complementary and not to contain repeated sequences. The programs GeneJockey II (Biosoft, Cambridge, UK) were used to aid the design of the primer sets.

2.2.5.2 Amplification of mitochondrial DNA (mtDNA)

A pair of primers L1/H1 (Table 2.1) was chosen to amplify total mtDNA using the following PCR conditions: 1) 94°C, 5 min; 2) 24 cycles of 94°C, 40 s; 55°C, 20 s; 72°C, 40 s; 3) 72°C, 8 min. In all PCR for total mtDNA amplification, 5-15 ng of tissue DNA was amplified in the presence of 2.0 mM $MgCl_2$ PCR buffer, 1.2 μM primers, 2.0 units of *Taq* polymerase (Promega), 200 μM dNTP, in a total reaction volume of 20 μl.

Mitochondrial DNA molecules containing a deletion between a pair of direct repeats spaced 3867 base pairs apart were specifically amplified with primers L2/H2 (Table 2.1) using a short PCR cycle to prevent synthesis of a full-length product from undeleted mtDNA: 1) 94°C, 10 min; 2) 30 cycles of 94°C, 35 s; 55°C, 20 s; 72°C, 35 s; 3) 72°C, 8 min. In all PCR assays for deleted mtDNA amplification, 75 to 300 ng of tissue DNA was amplified in the presence of 1.5 mM $MgCl_2$ PCR buffer, 1.2 μM primers, 2.0 units of *Taq* polymerase (AmpliTaq Gold, Perkin Elmer), 200 μM dNTP, 5 % (v/v) DMSO, in a total reaction volume of 20 μl.

2.2.5.3 Amplification of mouse *Hdh* gene

The CAG repeat sequence in the mouse *Hdh* gene was amplified using published primers, MHD16 and MHD 18 and PCR conditions (Shelbourne et al., 1999). Briefly, a touchdown PCR protocol was used: 1) 94°C, 5 min; 2) 20 cycles of 94 °C, 30 s; 71 °C to 61 °C for 30 s

(ramping down -0.5 °C per cycle); 72°C, 35 s; 3) 10 cycles of 94°C, 30 s; 60°C; 30 s; 72°C, 30 s; 4) 72 °C, 7 min. 1, 2, 5 ng of DNA extracted from purified cell nuclei was amplified in the presence of 1.5 mM $MgCl_2$ PCR buffer, 1.2 μM primers, 2.0 units of *Taq* polymerase (Sigma), 200 μM dNTP, 10 % (v/v) DMSO in a total reaction volume of 10 μl.

2.2.5.4 Amplification of first strand cDNA

PCR was used to amplify first strand cDNA to generate hybridization probes for northern blots or to check RNA samples for DNA contamination. PCR was carried out using ~150 ng equivalent of RNA as a template and each of the following primers (see Table 2.1) to amplify the following gene sequences:

A) Mouse glyceraldehyde-3-phosphate dehydrogenase (*Gapdh*) mRNA: The PCR conditions were as follows: 1) 94°C, 10 min; 2) 34 cycles of 94°C, 50 s; 65 °C; 50 s, 72°C, 50 s; 3) 72°C, 8 min. The pair of primers, mGDH-A/mGDH-BR, was used to amplify first strand cDNA from the mouse *Gapdh* mRNA to check the RNA template for DNA contamination.

B) Mouse myotonic dystrophy protein kinase (*Dmpk*) mRNA: The PCR conditions were as follows: 1) 94°C, 10 min; 2) 30 cycles of 94°C, 60 s; 61°C, 60 s; 72°C, 60 s; 3) 72°C, 7 min. The primer CLW2F is in the exon 2 of mouse *Dmpk* gene and the primer CLW4R is in the exon 4 of mouse *Dmpk* gene. This pair of primers, CLW2F/CLW4R, was used to amplify first strand cDNA from the mouse *Dmpk* mRNA to check the RNA sample for DNA contamination.

C) Mouse mitochondrial transcription factor A (*Tfam*) mRNA: The PCR conditions were as follows: 1) 94°C, 10 min; 2) 34 cycles of 94 °C, 50 s; 68°C, 50 s; 72°C, 50 s; 3) 72 °C, 10 min. This pair of primers, TFA1/TFA2, was used to amplify first strand cDNA from mouse *Tfam* mRNA.

D) Mouse cytochrome b (*Cytb*) mRNA: The PCR conditions were as follows: 1) 94°C, 10 min; 2) 32 cycles of 94°C, 40 s; 62°C, 60 s; 72°C, 60 s; 3) 72°C, 7 min. This pair of primers, cytbF/cytbR, was used to amplify the first strand cDNA from mouse *Cytb* mRNA.

E) Mouse cytochrome c oxidase subunit I (*CoI*) mRNA: The conditions of PCR were as follows: 1) 94°C, 10 min; 2) 32 cycles of 94°C, 40 s; 65°C, 60 s; 72°C, 60 s; 3) 72°C, 7 min. This pair of primers, COIF/COIR, was used to amplify first strand cDNA from mouse *CoI* mRNA.

F) Mouse cytochrome c oxidase subunit II (*CoII*) mRNA: The conditions of PCR were as follows: 1) 94°C, 10 min; 2) 32 cycles of 94°C, 40 s; 62°C, 60 s; 72°C, 60 s; 3) 72°C, 7 min. This pair of primers, COIIF/COIIR, was used to amplify first strand cDNA from mouse *CoII* mRNA.

G) Mouse heme oxygenase-1 (*HmoxI*) mRNA: The PCR conditions were as follows: 1) 94°C, 10 min; 2) 32 cycles of 94°C, 30 s; 65°C, 50 s; 72°C, 50 s; 3) 72°C, 10 min. This pair of primers, HOF/HOR, was used to amplify first strand cDNA from mouse *HmoxI* mRNA.

H) Mouse α-B crystallin (*Cryab*) mRNA: The PCR conditions were as follows: 1) 94°C, 10 min; 2) 32 cycles of 94°C, 30 s; 55°C, 45 s; 72°C, 45 s; 3) 72°C, 10 min. This pair of primers, CRF/CROR2, was used to amplify the first strand cDNA from mouse *Cryab* mRNA.

In all PCR reactions, first strand cDNA was amplified in the presence of 1.5 mM $MgCl_2$ PCR buffer, 1.2 μM primers, 2.0 units of *Taq* polymerase (Perkin Elmer), 200 μM dNTP. All PCR products were visualised after electrophoresis through an EtBr-stained agarose gel (1.5 %). PCR products using primers TFA1F/TFA2R, CytbF/CytbR, COIF/COIR, COIIF/COIIR and HOF/HOR were visualized on the gel, cut, gel purified and cloned using TOPO™ TA cloning kit from Invitrogen, indicated in section 2.2.9.

2.2.6 Agarose gel electrophoresis of DNA

DNA fragments were electrophoresed on 0.8-2.5 % (depending on the size of fragment) agarose gels using Biorad gel electrophoresis systems. Most gels were cast and electrophoresed in 1 X TBE buffer. All gels contained ethidium bromide at a concentration of 0.1-0.2 μg/ml. Electrophoresis conditions varied depending on the level of resolution required.

Enzyme-digested genomic DNA for Southern blot analysis was electrophoresed in 0.8-1 % agarose gels at 1.5 volts/cm, 4°C, overnight or longer depending on the resolution level required.

Plasmid DNAs and their restriction fragments were typically electrophoresed on 1 % agarose gels. Appropriate band resolution was normally achieved after electrophoresis at 6-8 volts/cm for 2 hours.

2.2.6.1 Sizing DNA fragments on agarose gels

Gel electrophoresis will separate different-size DNA molecules, with the smallest molecules travelling the greatest distance towards the positive electrode. The formula that links migration rate to molecular weight of the DNA fragment is

$$D=a-b\ (logM)$$

Where D is the distance moved, M is the molecular weight and a and b are constants that depend on the electrophoresis conditions.

In general, a DNA marker, comprising fragments of known size, was introduced into a lane of each agarose gel. By plotting the size of the marker fragments against the distance they migrated on semi-log paper, a calibration curve for that gel was constructed. This was used for estimating the size of an unknown fragment from the distance it had migrated.

2.2.7 Purification of DNA fragments from agarose gels

In order to extract and purify DNA fragments from agarose gels, one of two methods were used:

1) QIAquick gel extraction kit (Qiagen): the PCR products or plasmid DNA fragments after restriction enzyme digest were resolved on a 1 % agarose gel. The DNA fragment from the agarose gel was excised with a clean scalpel blade. 3 volumes of buffer QG were added to 1

volume of gel (100 mg = 100 µl), followed the protocol recommended by the manufacturer. Finally distilled water was added to elute the DNA from the column.

2) The DNA fragment was excised from the agarose gel with a clean scalpel blade. A piece of glass wool was packed tightly in between two sheets of 3 MM paper and placed in an eppendorf tube with a small hole at the bottom. The gel slices were placed in the tube and the tube was placed into another eppendorf tube and centrifuged at 9,000 X *g* for 10 min. Purification and concentration of the DNA was achieved with PEG solution (section 2.1.17). An equal volume of PEG solution was added to the DNA, vortexed thoroughly and incubated at room temperature for at least 10 min before centrifugation at 10,000 X *g* for 10 minutes. After centrifugation, the pellet was rinsed with 1 ml of 100 (v/v) % alcohol. The DNA was centrifuged, air-dried and resuspended in distilled water.

2.2.8 Transformation

2.2.8.1 Preparation of competent cells

A 50 ml culture inoculated with 500 µl overnight culture was grown with aeration in medium A [LB with 10mM $MgSO_4$.7H2O, 0.2 % (w/v) glucose] to mid logarithmic phase. The cells were kept on ice for 10 min, and pelleted at 1,500 X *g* for 10 min at 4°C. The cells were resuspended gently in 500 µl of pre-cooled medium A, then 2.5 ml storage solution B [36 % (w/v) glycerin, 12 % (w/v) PEG (MW 7500), 12 mM $MgSO_4$.7H2O added to LB (pH7.0)] was added and mixed well without vortexing. The competent cells were divided into aliquots of 100 µl each and stored at -80°C until use.

2.2.8.2 Transformation procedure

100 µl of competent cells were mixed with 1 µl of diluted plasmid DNA and put on ice for 30 min. The cells were heat shocked at 42°C for 1 min and put back on ice for a further 2 min. 0.5 ml pre-warmed LB broth (no antibiotic) were added to the transformation mix, mixed well and incubated in a 37°C water bath for 1 hour. The mix was then plated out on selective plates and incubated overnight at 37°C.

2.2.9 Cloning of amplified DNA

DNA fragments generated by PCR or RT-PCR and isolated by gel purification were cloned using the TOPO™ TA cloning kit (Invitrogen). The plasmid vector (pCR®2.1-TOPO) is supplied linearized with a single 3' thymidine (T) overhang for TA cloning and topoisomerase covalently bound to the vector (Shuman, 1994). *Taq* polymerase has a non-template-dependent terminal transferase activity that adds a single deoxyadenosine (A) to the 3'end of the PCR products. This allows PCR fragments to ligate efficiently with the vector. Generally, the molar ratio of insert to vector used was 2:1. Cloning reactions were performed by adding 2 μl (10 ng/μl) PCR product into a total volume of 5 μl in the presence of 1 μl (10 ng/μl) of pCR®2.1-TOPO vector. After mixing gently and incubating for 5 min at room temperature, the mixture was subjected to transfomation using TOP10F' One Shot™ competent cells according to the manufacturer's instructions. After transformation, two volumes of each transformation mixture (one tenth and nine tenths) were spread onto selective plates (LB plate with 50 μg/ml of X-Gal, 30 μg/ml IPTG and 50 μg/ml of ampicillin) and incubated overnight at 37°C.

Recombinant and nonrecombinant colonies were differentiated by insertional inactivation of a marker gene. This method of selection is based on the fact that the bacteria containing recombinant plasmids with insert DNA inactivating the *lacZα* gene of the plasmid vector cannot synthesize the corresponding β-galactosidase protein that convert X-Gal to a blue product. Therefore, cells containing recombinant plasmids vector are colorless in the presence of X-Gal, while cells containing non-recombinant plasmids are blue. A white colony was selected, inoculated into LB broth and incubated overnight at 37°C with shaking (300 rpm) for subsequent mini-preparation of plasmid DNA.

2.2.10 DNA Sequencing

After the required template has been cloned and purified, DNA sequencing was performed on either an ABI 373A or an ABI 377 sequencer by the Molecular Biology Support Unit at the University of Glasgow. Reactions were performed as stated in the ABI PRISM™ Dye Terminator Cycle Sequencing Ready Reaction kit protocol. The kit is based on the dideoxy

chain termination method of Sanger and colleagues (Sanger et al., 1977). Ethanol precipitation protocol 1 was used for purifying extension products.

The dideoxy sequencing reactions are performed with fluorescent dye-labeled primers or 3'-dye labeled dideoxynucleotide terminators. AmpliTaq® or T7 DNA polymerase is used for primer extension during cycle sequencing. Four different fluorescent dyes distinguish the products from each of the four dideoxy sequencing reaction. These reactions are performed in a PCR tube and loaded into one lane on the gel. The dye-labeled DNA fragments are electrophoresed through an acrylamide gel and separated according to the size. When the fragments reach a fixed position above the lower buffer chamber, the dye fluorescence is excited by light from a laser, which scans back and forth across this area of the gel. A photomultiplier tube detects four different wavelengths of fluorescent light and converts it into electrical signals. These signals are then transmitted to a computer and stored for subsequent analysis.

DNA sequences were edited and aligned using Sequence Navigator (Applied Biosystems). If necessary, the resulting DNA sequence was compared to the GenBank and EMBL nucleotide databases at the National Centre for Biotechnology Information (NCBI) using the BLAST program accessed via the online service.

2.2.11 Preparation of labelled probes from DNA templates

2.2.11.1 Random primed labeling of DNA probes

Radiolabeling of DNA probes for Southern or northern blots was achieved by a random-primers DNA labeling kit (Gibco BRL) (Feinberg and Vogelstein, 1983). 20-30 ng DNA template was heated for 5 min and quenched on ice for 2 min. This was then mixed with 15 µl buffer, 1 µl (3 units) Klenow fragment, 5 µl (50 µCi) [α ^{32}P] dCTP, 2 µl of 1 kb plus ladder (0.1 ng/µl), and water added to a final volume of 50 µl. The mixture was incubated at 25°C for at least one hour. Non-incorporated nucleotides were removed by passing the reaction mixture through a Sephadex G-50 column.

2.2.11.2 End-labeling of DNA probes

Oligonucleotides or primers were 5' end-labeled using T4 polynucleotide kinase (Promega) and [γ-^{32}P] ATP (Amersham). This was performed by adding 48 pmole primer or oligonucleotide to a 20 µl solution in the presence of 2 µl 10 X polynucleotide kinase buffer (500 mM Tris-HCl, pH 7.5, 0.1 M DTT, 0.1 M $MgCl_2$), 20 µCi [γ-^{32}P] ATP (3000 Ci/mmol, 10 µCi/µl), and 10 units of T4 polynucleotide kinase. The mixture was incubated at 37°C for 90 min. The unincorporated nucleotides were removed by passing reaction mixture through a Sephadex G-25 column.

2.2.12 Southern blotting and hybridization

2.2.12.1 Southern blotting

DNA fragments in an agarose gel were transferred onto a nylon membrane using the method described by Southern (Southern, 1975). Following electrophoresis, the gel was immersed in denaturing solution for one hour. After a brief rinse in H_2O, the gel was soaked in neutralization solution for a further hour. The gel was placed on two sheets of 3 MM Whatmann paper on a platform, which were pre-wetted in 2 X SSPE and made to function as a wick by dipping into a reservoir containing 20 X SSPE. The edges of the gel were shrouded by plastic film in order to prevent the 20 X SSPE bypassing the gel into the blotting materials. A Hybond N, or Hybond N plus membrane (Amersham) and two sheets of 3 MM Whatmann paper were cut to the size of the gel and soaked in 2 X SSPE. The blotting membrane was carefully placed over the gel, avoiding trapping any air bubbles between them. The two sheets of 3 MM Whatmann paper were similarly placed over the nylon membrane. A pack of dry paper towel was laid on top of the Whatmann paper. Finally, a weight (~ 1 Kg) was placed on the towels. Transfer was carried out overnight at room temperature. The membrane was then rinsed in 2 X SSPE and baked at 80°C for 2 hours to fix the DNA to the membrane.

2.2.12.2 Competition of probes

To prevent repetitive sequences within a probe hybridising to non-target DNA, the probes was competed with an excess of low molecular weight DNA before hybridisation. The method used is based on that described by Sealey and colleagues (Sealey et al., 1985). *Cot*I mouse DNA (GibcoBRL) was used as low molecular weight DNA to compete a probe. The labelled probe was added to 125 µl 20 X SSPE, 100 µl *Cot*I DNA, and H_2O to a total volume of 450 µl, heated at 100°C for 15 min, and then incubated at 65°C for at least 4 hours before use.

2.2.12.3 Hybridisation of Southern blots

For pre-hybridisation, the membrane was sealed in a Hybaid hybridisation bottle with hybridisation solution at 65°C for at least 5 hours and usually overnight. A 20 X 20 cm membrane required 10 ml hybridisation solution. If the labelled probe was not competed with mouse *Cot*I DNA, it was denatured prior to hybridisation by boiling for 5 min, followed by rapid cooling on ice. The denatured probe or the competed probe was then added directly to the bottle containing the membrane. The hybridisation was performed at 65°C in a Hybaid rotating oven for 16-24 hours. After hybridisation, the membrane was subjected to two washes of 2 X SSPE, 0.1 % (w/v) SDS at 65°C for 15-20 min. High stringency washes were performed, where necessary, in 0.1 X SSPE, 0.1 % (w/v) SDS at 65°C in a Hybaid oven with shaking. After washing, the membrane was left to air dry, wrapped in cling film and exposed to X-ray film at -70°C in the presence of intensifying screen.

2.2.12.4 Hybridisation using synthetic oligonucleotide

Before adding radio-labelled oligonucleotides, the membrane was pre-hybridised in pre-hybridisation solution containing 6 X SSPE, 5 X Denhardt's solution, 0.4 % (w/v) SDS and 100 µg/ml denatured salmon sperm DNA at x°C (x = Tm of oligonucleotide-5°C) for at least 5 hours.

The temperature of hybridisation was calculated based on the formula 2(A+T) +4 (G+C)= Tm, where Tm is the melting temperature of the DNA (Itakura et al., 1984). Hybridisations were carried out at 5°C below the Tm in the presence of 6 X SSPE, 5 X Denhardt, 0.4 % (w/v) SDS and 100 µg/ml yeast t-RNA. After hybridisation, the membrane was washed in 6 X SSPE, 0.1 % (w/v) SDS at the same temperature used for hybridization. More stringent washes were achieved by decreasing the salt concentration of the washing solution. Membranes were then wrapped in cling film and exposed to X-ray film at -70°C in the presence of intensifying screens.

2.2.13 Removal of probe from membranes

Southern blot or northern blot membranes could be reused if the unwanted probe was removed. To achieve this, the membrane was immersed in a solution of boiling 0.1 % (w/v) SDS and allowed to cool to room temperature over 30 min on a shaking platform. The membrane was finally rinsed in 2 X SSPE or 2 X SSC and stored damp in a sealed plastic bag.

2.2.14 Western blot analysis

2.2.14.1 Preparation of protein lysates from mouse brain

Tissue (4-5 mg) was homogenized in a 500 µl EBC lysis buffer containing 5 µl PMSF (100 mM), 5 ul Leupeptin (1 mg/ml), 5 µl pepstatin (1 mg/ml) and 0.5 µl aprotinin (10 mg/ml) at 4°C using a sterile 0.5 mm probe driven at 9,000 rpm (Polytron Kinematica AG PT-3000 Homogeniser). To ensure complete lysis of the cells, the sample tube was then put on a rotary mixer at 4°C for 30 min. After complete lysis, the homogenate was centrifuged (at 4°C) with 19,000 X *g* for 15 min. The supernatant was removed and stored at -70°C.

2.2.14.2 Preparation of the standard curve for the Coomassie blue protein assay

Diluted BSA standards were prepared from 2.0 mg/ml BSA stock using distilled water as the diluent. Two replicates of each standard were prepared. 1.0 ml of each standard was added to appropriately labelled tubes and 1.0 ml of the diluent alone was used for the

control tube. 1 ml of Coomassie blue reagent (Pierce) was added to each tube and mixed well. The absorbance of each tube versus the control was measured. A standard curve was generated by plotting the average control-corrected 595 nm reading for each BSA standard versus its concentration in μg/ml. The standard curve was used to determine the protein concentration.

1 μl of protein lysate (unknown concentration) was added to 999 μl distilled water, followed by 1.0 ml of Coomassie blue reagent. The absorbance of the sample at 595 nm was measured against the control. The concentration was determined using the standard curve and multiplied by 1000 (to take into account of the dilution factor of the sample).

2.2.14.3 Western blot gel electrophoresis and blotting of protein

10-20 μg of protein lysate was loaded on a NuPage 10 % Bis-Tris gel (Novex) and subject to the NuPage™ electrophoresis system (Novex). Blotting of the proteins onto PVDF membrane was achieved using a Novex western transfer apparatus according to the manufacturer's instructions. After blotting, the membrane was washed twice with 1 X TBST for 5 min, air dried and sealed in a plastic bag.

2.2.14.4 Immunodetection of blotted protein

The dried PVDF membrane was wetted with methanol followed by two washes in 1 X TBST for 10 minutes. The membrane was then incubated in a blocking solution [0.2 % (w/v) casein solution (Pierce), in 1 X TBS + 0.1 % (v/v) normal goat serum or normal donkey serum depending on the secondary antibody] at 4°C overnight.

The membrane was incubated in primary antibody (see Table 2.3) diluted with 1 X TBST at room temperature with shaking for 3-4 hours. After washing with 1X TBST (4 x 15 min) at room temperature, the membrane was incubated in secondary antibodies diluted with 1 X TBST (see Table 2.4) at room temperature for 2 hours. After washing in 1x TBST (4 x 15 minutes) at room temperature, the membrane (size: 8 x 8 cm) was immersed to 3 ml of chemiluminescent substrate (SuperSignal West Pico, Pierce), and exposed to X-ray film for 15-60 seconds depending on the antibody used.

2.2.14.5 Removal of antibody from western blot membrane

Stripping of antibody from the western blot membrane was achieved by incubating the membrane in the solution containing 6.25 ml of 1 M Tris, pH 6.7, 20 mls of 10 % (w/v) SDS, 73.05 ml water and 700 µl β-mercaptoethanol at 50°C for 30-40 min. After stripping, the membrane was washed in 1 X TBST for two 10-min periods, air-dried and sealed in a clean plastic bag.

2.2.15 Northern blot analysis

2.2.15.1 Extraction of RNA from mouse tissue

As RNA is vulnerable to degradation from nucleases, the following precautions were taken: the restriction of RNA work to a dedicated bench, the use of dedicated equipment wherever possible and the use of gloves at all times. All solutions required for RNA related techniques were made using DEPC-treated water. DEPC was added to a concentration 0.1 % (v/v), mixed and allowed to stand overnight before inactivation by autoclaving. All plasticware was soaked in DEPC-treated water before autoclaving. Each tissue was frozen immediately on dry ice after dissection, followed by storage at -70°C.

When preparing RNA, 5-50 mg tissue was defrosted on ice in a bijou before adding 1 ml of Sigma TRI REAGENT™. The tissue was homogenized using a sterile 0.5 mm Polytron probe driven at 20,000 rpm (Kinematica AG PT-3000 homogeniser). RNA was then prepared according to the Sigma TRI REAGENT™ protocol and resuspended in 40 µl of DEPC-treated water. If necessary, the RNA was incubated at 65°C for 30 min to achieve resuspension. To avoid genomic DNA contamination, 15 µl of RQ1 (RNase free DNase, Promega, 1 unit/µl) and 10 µl of 10 X buffer were added to the RNA sample and made up 100 µl with DEPC-treated water. This mixture was incubated at 37 °C for 30 min before being made up to 400 µl with DEPC-treated water and extracted using an equal volume of phenol: chloroform: isoamyl alcohol. After vortexing, the mixture was centrifuged at 10,000 X *g* for 10 min and the upper layer was removed. The RNA was precipitated by adding 0.1 volume of 3 M CH_3COONa (pH 4.8) followed by 2 volumes of absolute ethanol. The RNA was pelleted by centrifugation at 10,000 X *g* for 10 min, rinsed in 75 % (v/v) ethanol and

air dried for not more than 30 min before being resuspended in 30-40 µl 1 X TE, 0.1 % (w/v) SDS. The RNA concentration was determined by spectrophotometry by diluting 1/80 with distilled water to a final volume of 400 µl and measuring the absorbance of the RNA at λ 260 nm.

2.2.15.2 RNA visualization by agarose gel electrophoresis

A 1 % agarose gel containing 0.1 % (w/v) SDS was made with 1 X TAE buffer (DEPC-treated). 10 µl of 10 mg/ml EtBr was added to 200 ml melted agarose gel. 5 µg of each RNA sample was added to 5 X loading buffer, loaded on the gel and electrophoresed at 10 volts/cm for ~ 1 hour.

2.2.15.3 First Strand cDNA synthesis

First strand cDNA was synthesized using a protocol modified from the SUPERSCRIPT™ Preamplification System for First Strand cDNA Synthesis (GibcoBRL). 1 µl Oligo (dT) 12-18 base primers (GibcoBRL) was added to 2.5 µg total RNA and made up to a final volume of 9.5 µl with DEPC-treated water. A control reaction containing no reverse transcriptase (RT) was made up to a final volume of 11.5 µl. The tubes were heated at 70°C for 10 min, centrifuged briefly, and placed on ice before adding 20 units of RNasin (Promega), 10 mM of DTT, 1 mM of dNTPs and 5 X Superscript II buffer. The final volume of the test reaction was 18 µl (20 µl for no-RT control). Each sample was mixed and incubated at 42 °C for 2 min before 2 µl (400 units) of Superscript II reverse transcriptase was added to the positive reaction tubes only. The tubes were incubated at 42°C for a further 50 min. The reaction was stopped by heating at 70°C for 15 min. 20 µl of DEPC-treated water was added to each sample before storing the cDNA at -70°C.

2.2.15.4 Northern blotting

A 1.2 % (w/v) denaturing formaldehyde-agarose gel was generated by boiling agarose in 120 ml DEPC-treated water and adding 15 ml 10 X MOPS (pH 8) and 15 ml 37 % (w/v) formaldehyde before pouring into the gel former. 8 µl of RNA (10-15 µg) was added to 6 µl denaturing buffer (300 µl of 10 X MOPS, pH 8, 80 µl of formaldehyde, 900 µl formamide,

and 12 µl of EtBr 10 mg/ml) and 4 µl of 5 X loading dye. This mixture was heated at 65°C for 10 min, cooled on ice, loaded into the wells and electrophoresed in 1 X MOPS buffer, pH 7 at 10 volts/cm for 3-4 hours in a fume food.

Before proceeding with the transfer process, the integrity of the separated RNA was checked by visualising the RNA under UV light and looking for the intact 28S and 18S ribosomal RNA bands. The gel was photographed with a fluorescent ruler aligned along the side of the gel and then soaked in 6 X SSC for 30 minutes before transferring to a Biodyne B membrane (Pall Gelman Laboratory) overnight by capillary action in 10 X SSC. After the transfer process, the membrane was baked at 80°C for 2 hours.

2.2.15.5 Hybridisation of northern blot membranes

The northern blot membrane was prehybridised in 5 ml ExpressHyb hybridisation solution (Clontech) at 68°C for 1-2 hour, after which the denatured radiolabelled probe was added and hybridised for a further 1-3 hours. The membrane was washed to a final stringency of 0.1 X SSC, 0.1 % (w/v) SDS at 65-68°C for 10 min-1 hour (depending on the probe used). After washing, the membrane was sealed in a plastic bag and exposed to X-ray film at -70°C in the presence of intensifying screen.

2.2.16 Slot blot analysis of total RNA

Slot blotting is a less time consuming technique than northern blotting because it does not involve electrophoresis and transferring RNA. However, genomic DNA contamination must be avoided to prevent confounding hybridisation signals from DNA.
The slot blot equipment, Minifold II (Schiender and Schell) was treated with 3 % (v/v) H_2O_2 for 20 min and then thoroughly rinsed with DEPC-treated water to removed any RNases. 5 µg of each RNA sample was resuspended in 11 µl of TE / 0.1 % (w/v) SDS. 33 µl of loading buffer (section 2.1.17) was added to each sample, followed by incubation at 65°C for 10 min. After quenching on ice, 11 µl of 20 X SSC was added to each sample. The slot blot equipment was assembled with two pieces of pre-wetted 3 MM Whatmann paper underlying the nylon Biodyne B membrane (Pall Gelman Laboratory) (cut to size and pre-soaked in 1 X TAE for 30 min). 500 µl of 1 X TAE was added and aspirated through the

slot twice using a low-power vacuum (Fisher) before sample loading. After loading 55 µl of each sample in the slot, the vacuum was applied for 5 min. When the samples had been aspirated through, 500 µl of 4 X SSC was added and aspirated through the slot twice. The membrane was then baked for 2 hours at 80°C, hybridised and washed using the procedures described for northern blotting (section 2.2.15.5).

2.2.17 Immunohistochemistry

2.2.17.1 Perfusion and fixation of mouse tissue

Each mouse was anaesthetised with 0.1 ml Euthetal (Rhone Meriex, Ltd) via intraperitoneal injection. Following the absence of a reflex response to pain stimulation, the mouse was perfused transcardially with 50 ml 2 % (w/v) xylocaine in 1 X PBS for 2 min to dilate the blood vessels. This was followed by 120 ml 4 % (w/v) paraformaldehyde (PFA) in 1 X PBS, pH 7.4. After perfusion, the whole head of mouse was immersed in 4 % (w/v) PFA at 4°C overnight. The next day the skull was removed and the brain left in 4 % (w/v) PFA for a further 2-3 hours.

2.2.17.2 Preparation of free-floating sections

The fixed brain was left in 30 % (w/v) sucrose in 1 X PBS until it sank to the bottom of the container. The sucrose-protected brain was immersed in isopentane cooled with dry ice at -42°C for 2-5 min. The brain was then mounted on a chuck with Cryomatrix (Shandon). Immediately, after the Cryomatrix solidified completely, the brain was cut. 30 µm serial coronal sections were cut with a Cryotome, immersed in the wells of Nunc multidish (Nunc International) containing cryoprotectant (section 2.1.17) and stored at -20°C.

2.2.17.3 Preparation of paraffin-embedded tissue sections

The fixed brain was kept in 1 X PBS for 1-3 days prior to paraffin-embedding procedures. Fixed brains were cut into three coronal blocks using a rodent brain matrix. Individual blocks were placed into labelled embedding cassettes (Surgipath). The cassettes were

processed for wax embedding using the following programme of a Shandon Citadel 1000 automatic processor:

1. 70 % (v/v) ethanol, 35°C	1 hour
2. 80 % (v/v) ethanol, 35°C	1 hour
3. 96 % (v/v) ethanol, 35°C	1 hour
4. 100 % ethanol, 35°C	1 hour
5. 100 % ethanol, 35°C	1 hour
6. 100 % ethanol, 35°C	1 hour
7. 100 % ethanol, 35°C	1 hour
8. 100 % ethanol/Histoclear (1:1), 35°C	1 hour
9. Histoclear	1 hour
10.Histoclear	1 hour
11.Paraffin wax 60°C	1 hour X 3

Stainless steel moulds were prepared by cleaning with Histoclear (National Diagnostics). They were then placed on a hotplate and the inside surface coated with a thin film of glycerine. The moulds were then filled with liquid wax and returned to the hotplate. The embedding cassettes containing brain blocks were put into the wax moulds and removed from the hotplates. Sufficient melted wax was added to ensure that cassette and mould remained securely connected.

6 μm serial coronal sections of paraffin-embedded tissue blocks were cut with a microtome (Leica RM 2135). The resulting ribbons of sections were floated on a water bath (42°C) for several minutes to allow them to relax and stretch into their normal conformation after cutting. A microscope slide (poly-L-lysine coated) was then placed in the water beneath the end of the ribbon. Two single brain sections were cut from the ribbon using a scalpel blade and mounted on the slide.

2.2.17.4 Immunostaining of free-floating tissue sections

The free-floating sections kept in cryoprotectant were transferred to new wells containing 1 X PBS and incubated for 5 min. The sections were permeabilized with 0.2 % (v/v) Triton in 1 X PBS on a shaking platform for 30 min. After two 5-min washes in 1 X PBS, the sections were treated with 3 % (v/v) hydrogen peroxide in 1 X PBS for 20 min. After two 5-min washes in 1 X PBS, the sections were incubated in a blocking solution [10 % (v/v)

normal goat serum (Vector) and 0.5 % (w/v) bovine serum albumin in 1 X PBS for polyclonal primary antibodies; 10 % (v/v) normal horse serum (Vector) and 0.5 % (w/v) bovine serum albumin in 1 X PBS for monoclonal primary antibodies] for an hour. Tissues sections were incubated in primary antibody (see Table 2.3) overnight at 4°C. The next day, sections were subjected to two 10-min washes in 1 X PBS, followed by 1 hour incubation in biotinylated secondary antibody [anti-mouse secondary antibody for monoclonal primary antibodies (1:100; Vector) and anti-rabbit secondary antibody for polyclonal primary antibodies (1:100; Vector)]. Sections were then subjected to two 5-min washes in 1 X PBS and incubated for 1 hour in an avidin biotinylated enzyme complex (VECTASTAIN® ABC kit, Vector). Finally, the sections were subjected to two 5-min washes in 1 X PBS and the signal developed by using 3'3 -diaminobenzidine tetrahydrochloride (DAB; Vector) as the chromogen. After the sections appeared brown, the DAB were washed away with two 5-min washes in distilled water. After incubation in Tris buffer (section 2.1.17) for 10 min, the sections were mounted on microscope slides and air-dried overnight. The next day, the sections were rinsed in running water for 1 hour, and then dehydrated through serial concentrations of ethanol and Histoclear [2 min in 70 % (v/v) ethanol, 2 min in 90 % (v/v) ethanol, two 2-min periods in absolute ethanol and two 2-min periods in Histoclear]. A cover slide was then applied using DPX mounting medium. Controls for the specificity of the immunostaining, by omitting the primary antibody, were included in each experiment.

2.2.17.5 Immunnostaining of paraffin-embedded tissue sections

Paraffin-embedded tissue sections were dewaxed at 60°C for 20 min and then immersed in Histoclear for two 10-min periods. Sections were then dehydrated in 100 % ethanol for two 5- min periods.

For antigen retrieval, tissue sections were pre-treated by microwaving at full power in a 10 mM citric acid buffer (pH 6.0) for two 5-min periods. After a cooling period of 40 min, the sections were treated with 3 % (v/v) hydrogen peroxide in methanol for 30 min to block the endogenous peroxidase activity. After rinsing in running water for 20 min, sections were washed with 1 X PBS for two 5-min periods. Sections were then incubated in a blocking solution [10 % (v/v) normal goat serum (Vector) and 0.5 % (w/v) bovine serum albumin in 1 X PBS for polycolnal primary antibodies; or a mouse IgG blocking reagent kit from

Vector® M.O.M (Vector) for monoclonal primary antibodies] for 1 hour. Tissues sections were incubated in primary antibody (see Table 2.3) overnight at 4°C. The next day, sections were subjected to two 5-min washes in 1 X PBS, followed by a 20 min incubation in biotinylated anti-mouse secondary antibody for monoclonal primary antibodies (1:100 or 1:500; Vector) and 1 hour in biotinylated anti-rabbit secondary antibody for polyclonal primary antibodies (1:100; Vector). Sections were then subjected to two 5-min washes in 1 X PBS and incubated for 1 hour in an avidin biotinylated enzyme complex (Vectastain® Elite ABC kit, or Standard ABC kit, Vector). Finally, the sections were subjected to two 5-min washes in 1 X PBS and the signal developed by using 3'3' -diaminobenzidine tetrahydrochloride (DAB; Vector) as the chromogen with (when stained with anti-HO-1, anti-4-HNE, and anti-8-OHdG antibodies) or without Nickel enhancement (when stained with anti-COI antibody). After the sections appeared brown, the DAB was washed away with running water for 10 minutes. After dehydrating the sections in serial concentrations of ethanol and Histoclear [2 min in 70 % (v/v) ethanol, 2 min in 90 % (v/v) ethanol, two 2-min periods in absolute ethanol and two 2-min periods in Histoclear], a cover slide was applied using DPX mounting medium. Controls for the specificity of the immunostaining, by omitting the primary antibody, were included in each experiment.

2.2.18 Assessing locomotor performance of mice using a rotarod apparatus

Motor coordination and balance of mice were measured using a rotarod apparatus (Dunham and Miya, 1957; Rozas and Labandeira Garcia, 1997). The rotarod was built in house by the workshop in the University of Glasgow. The rotarod consists of a revolving rod that can rotate at different speeds, a power source for controlling the rod speed and 4 separators placed along the rod at suitable intervals to divide the rod into equal-sized compartments for simultaneous testing of 4 mice. Four timer sets corresponding to 4 compartments were built into the device, and are used to measure the latency of the mouse to fall off the rod. The diameter of the revolving rod is 3.5 cm and it is covered with a layer of rubber. The rod is about 60 cm height from the floor of the device. The floor of the device is made of a rubber-like material. The protocol used in the study is outlined in Table 2.7. The latency to fall off the rotarod was recorded and used in subsequent analyses. The maximal time for each trial

was 1 min. Each mouse was tested at three time points, 4, 12 and 18 months of age. During the week prior to the 2nd and 3rd time point test, each mouse was retrained by subjecting it to three trials per day at 20 rpm (maximum 1 min) for 2 consecutive days.

Table 2.7 Protocol for locomotor experiment

Rotarod speed (rpm)	Maximum time/trial (min)	Trials/day	Number of consecutive days
Acclimatisation: day 1			
0	1	1	1
5	1	1	1
10	1	1	1
15	1	1	1
20	1	1	1
Training: day 2-4			
20 rpm	1	3	3
Testing: day 8-10			
5	1	1	3
10	1	1	3
15	1	1	3
20	1	1	3
25	1	1	3
30	1	1	3
35	1	1	3
40	1	1	3

3 Investigating the phenotypic features of HD mice

3.1 Introduction

As mentioned previously in the chapter 1, the aims of the study were to investigate the pathological changes at molecular and cellular levels of HD mice and the phenotypic consequences of the HD mutation. In previous studies, it has been shown that the HD mice display abnormal social behaviour at 3 months of age (Shelbourne et al., 1999) and electrophysiological deficits (a significant reduction in long-term potentiation) at 8 months of age (Usdin et al., 1999), suggesting learning and memory impairments. However, studies of locomotor performance including beam walking and rope tests did not show significant differences between HD mice and wild-type littermates at 17 months of age (Peggy Shelbourne, unpublished data). The clasping of limbs, which is commonly present as a phenotypic abnormality in some HD mouse models (Mangiarini et al., 1996; Hodgson et al., 1999; Reddy et al., 1999; Yamamoto et al., 2000), was not noticed in the HD mice. Also, HD mice could not be distinguished from normal mice by observing the daily activity at any point during their lifespan. Since motor dysfunction plays a prominent role in early stages of HD (Harper et al., 1996), it was decided that the locomotor function of HD mice should be investigated further. A rotarod apparatus (Dunham and Miya, 1957; Rozas and Labandeira Garcia, 1997) that gives the tested mice a more challenging task, thus providing a more sensitive measure of locomotor performance, was used to assess four limb motor coordination, balance and muscle strength of HD mice. By assessing the rotarod performance of HD mice at different time points, the aims of the study were: 1) to determine whether the locomotor dysfunction is present in HD mice as a functional consequence of the *HD* gene mutation; 2) to determine when the onset of locomotor dysfunction occurs in HD mice and whether motor function progressively deteriorates; 3) to relate molecular and cellular findings to locomotor dysfunction; 4) to investigate the use of rotarod performance as a "biomarker" to assess the efficacy of potential therapies in the future.

3.2 Investigating the locomotor function of HD mice using a rotarod apparatus

Eight male HD mice and 8 male wild-type littermates, and 8 female HD and 8 female wild-type littermates were tested in the study (see details of the mouse cohorts in section 2.1.18). Mice were housed together according to litter order and sex rather than genotype, and rotarod experiments were performed in numerical order of mouse identification tags. As HD mice could not be distinguished from normal littermates by appearance in their home cage, the rotarod experiments were performed in a manner that was effectively blind to genotype.

Although 8 male HD mice were used at the beginning of study, 1 male HD mouse died after the first time point of the experiment (4 months of age) and another male HD mouse died after second time point of the experiment (12 months of age). Therefore, only 7 and 6 male HD mice were used at the second (12 months of age) and third time points respectively (18 months of age).

Locomotor assessments commenced at 4 months of age. All mice were subjected to handling twice a week from 5 weeks of age until the rotarod assessments began, because it was felt that this would decrease the handling stress imposed on mice when they were performing the rotarod task. During the week prior to testing, each mouse received a training course (section 2.2.18), which again was designed to reduce the handling stress and allow each mouse to learn the task and reach a steady baseline level of performance. Each mouse was then tested at 8 increasing speeds from 5-40 rpm, 1 trial per speed per day for 3 consecutive days. Each mouse was tested at three time points: 4, 12 and 18 months of age. The latency to fall off the rod for each trial of each mouse was recorded after each trial was completed. The performance of each mouse was also videotaped for data backup purposes.

Since each mouse has 3 data points per speed per time point for 8 speeds and 3 different ages, a complex data set was produced and so a number of alternative methods of data analysis were explored.

3.2.1 Analysis of rotarod data using individual mean latencies to fall off the rod at each speed

Initially, the rotarod performance of male HD and male wild-type cohorts at each of 8 different speeds (5-40 rpm) at 4, 12 and 18 months of age was analysed. The mean time staying on the rod (from 3 trials) at each speed for each mouse at each time point was determined. The data points from HD and wild-type littermates were combined respectively and compared in a pair-wise fashion using Student's *t* test (Fig. 3.1). No significant differences between male HD and male wild-type mouse groups were observed at any speed at 4 months of age (Fig. 3.1a). Male HD mice showed worse rotarod performances at speeds of 10-40 rpm at 12 months of age when compared with male wild-type littermates (Fig. 3.1b). Male HD mice showed worse rotarod performances at speeds of 15-20 and 40 rpm at 18 months of age when compared to male wild-type littermates (Fig. 3.1c). The results revealed that male HD mice showed worse performances at 7 speeds and 3 speeds at 12 and 18 months of age respectively, when compared to male wild-type littermates.

The same method was used to compare the rotarod performance of female HD and female wild-type cohorts. No significant differences between female HD and female wild-type mouse groups were observed at any speed at 4 months of age. Female HD mice showed worse rotarod performances at speeds 15-40 rpm, and 15-30 and 40 rpm at 12 and 18 months of age respectively when compared to female wild-type littermates. However, as the data set obtained from each cohort was complex, it was difficult to draw an overall conclusion about performance deficits and their relationship with age.

3.2.2 Analysis of the rotarod data using a measure of overall performance

Since the pair-wise comparison generated many data points for each mouse, alternative representations of the data were considered.

The sum of the time periods staying on the rod at 8 speeds was used to represent the overall rotarod performance (ORP) of each mouse. Since each mouse performed 3 trials (1 trial per

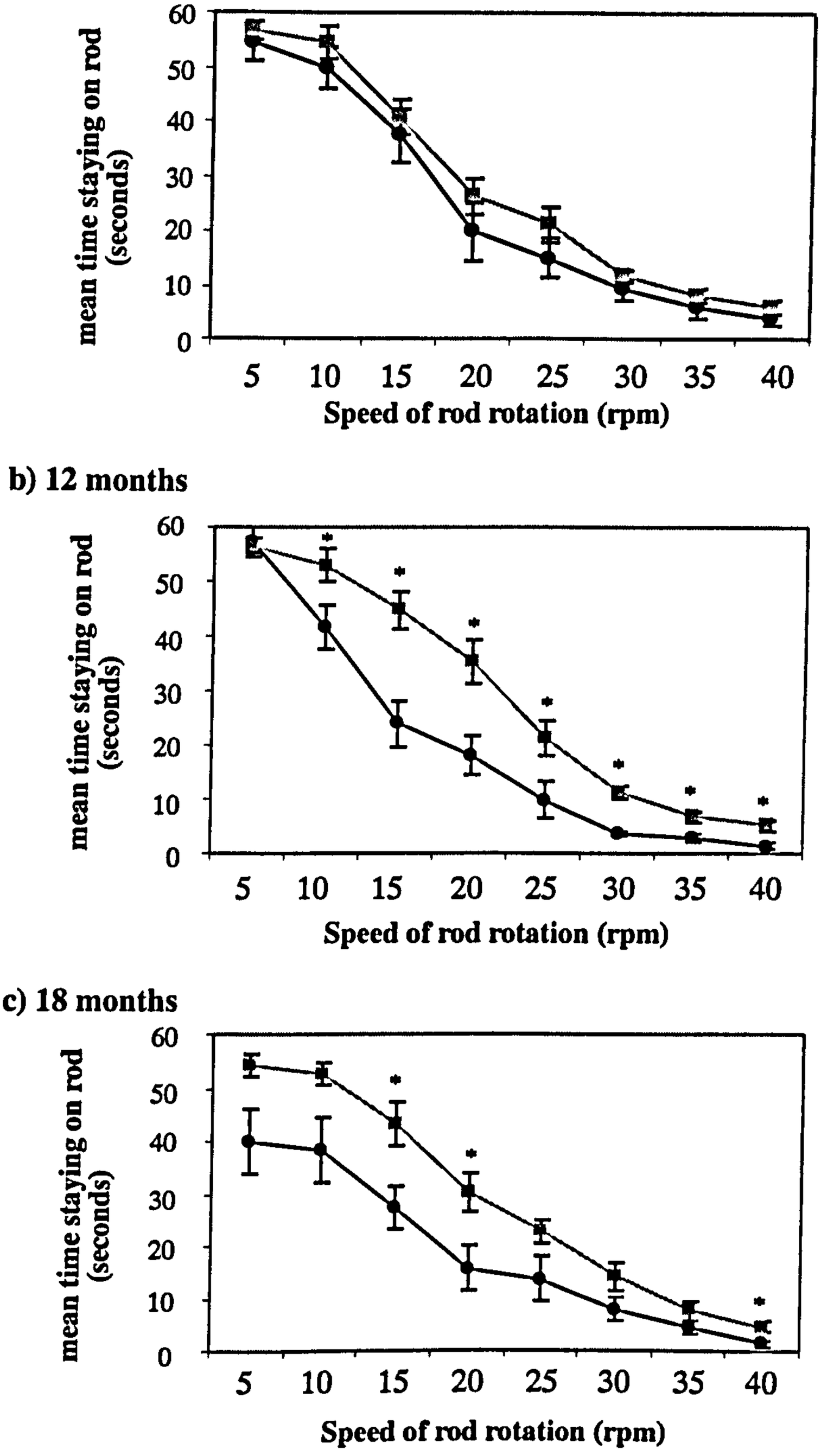

Figure 3.1 Pair-wise comparisons of rotarod performances of 8 male HD mice (black circle) and 8 wild-type littermates (grey square) at various speeds (5-40 rpm) at 4 (a), 12 (b) and 18 months of age (c). The male HD mice showed worse performances ($p < 0.05$ and indicated by symbol*) at speeds of 10-40 rpm at 12 months of age and 15, 20 and 40 rpm at 18 months of age when compared to the male wild-type littermates using the Student's *t* test (two-tailed) for statistical analysis. All values are expressed as mean ± S.E.

day for 3 consecutive days) at each speed, either of two different measurements (the sum of the mean or the maximum time staying on the rod from 3 trials at each speed) can be used to represent ORP. The data were analysed using both methods to investigate the outcome of using the different measurements.

3.2.2.1 Analysis of the rotarod data using the sum of the mean time staying on the rod from 3 trials at each speed

The sum of the mean time staying on the rod from 3 trials at each speed (termed 'mean ORP') of each mouse at 4, 12 and 18 months of age was determined. A comparison of mean ORP of HD mice and wild-type littermates at each time point was performed using the Student's *t* test (two tailed). In addition, the differences in mean ORP between 4 and 12 months of age and between 12 and 18 months of age for each mouse cohort were determined. The deterioration of overall rotarod performance of HD mice with age was also compared to wild-type littermates.

The results revealed that female HD mice showed worse mean ORP at 12 ($p = 0.002$) and 18 months ($p = 0.001$) of age when compared with female wild-type littermates (Fig. 3.2a). The mean ORP of female HD mice appeared to deteriorate significantly from 4 to 12 months of age ($p = 0.04$), but not after 12 months of age (Fig. 3.2b).

Male HD mice showed a significantly worse mean ORP at 12 ($p = 0.007$) and 18 months of age ($p = 0.01$) when compared to male wild-type littermates (Fig. 3.2c). Male HD mice displayed a trend toward a decreased mean ORP with age from 4 to 12 months ($p = 0.09$), when compared to wild-type littermates (Fig. 3.2d). However, the mean ORP of male HD mice did not appear to decline significantly after 12 months of age.

3.2.2.2 Analysis of the resulting data using the sum of the maximum time staying on the rod from 3 trials at each speed

The sum of the maximum time that a mouse stayed on the rod from 3 trials at each speed (termed 'maximum ORP') of each mouse at 4, 12 and 18 months of age was determined.

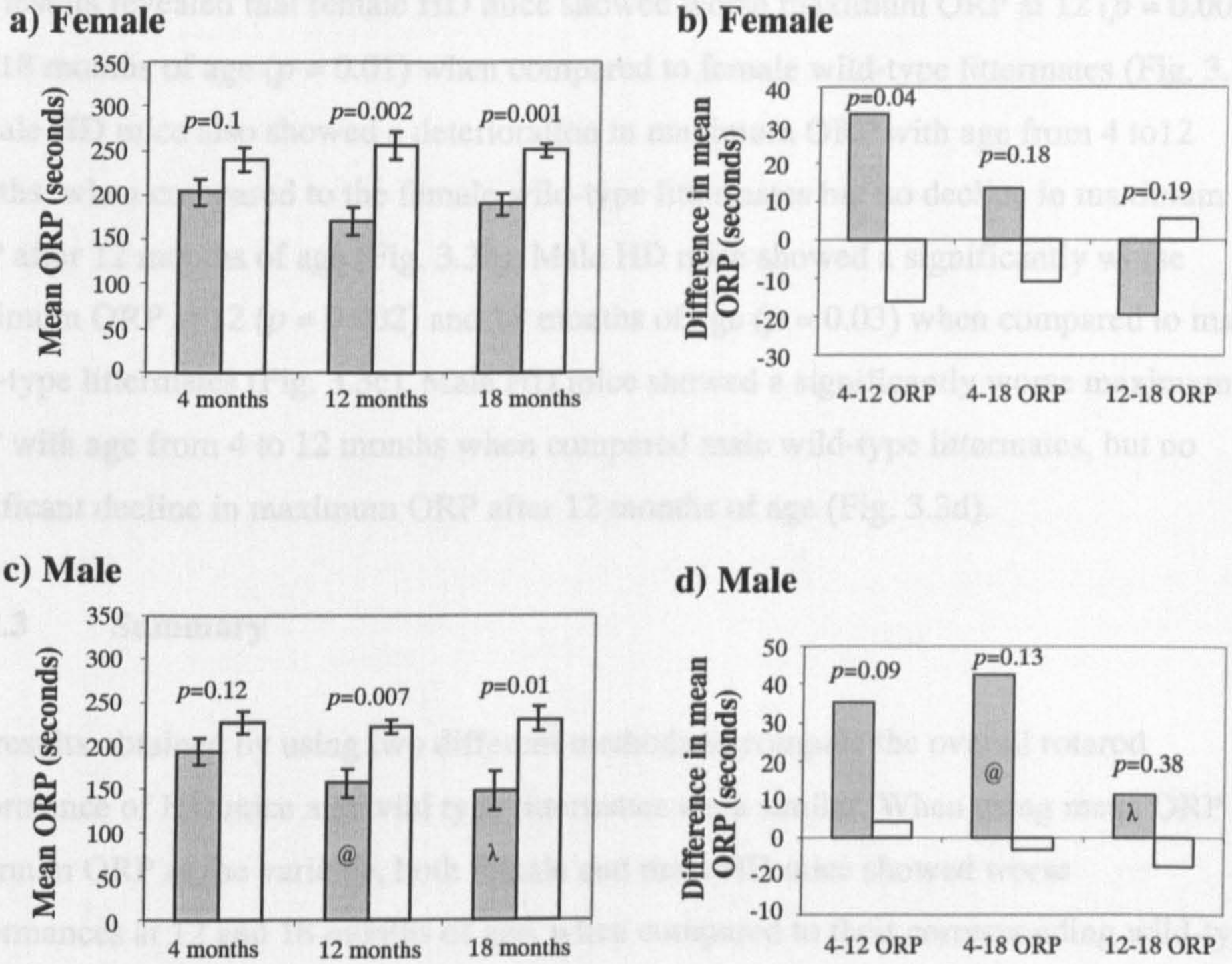

Figure 3.2 Comparisons of the mean overall rotarod performances (mean ORP) of 8 female HD and 8 female wild-type littermates (a and b) and 8 male HD and 8 male wild-type littermates (c and d) at 3 time points using the sum of mean time on the rod from 3 trials at each speed as the mean ORP. Female HD mice showed worse performances at 12 and 18 months of age compared to the female wild-type littermates. The performances of female HD mice declined from 4 to 12 months of age. Male HD mice showed worse performances at 12 and 18 months of age, when compared to male wild-type littermates. Male HD mice also showed a trend toward decline in ORP from 4 to 12 months of age, but not from 12 to 18 months of age. Data are expressed as mean ± S.E. @ indicates the mean value was obtained from 7 animals. λ indicates the mean value was obtained from 6 animals. The *p* values indicated were obtained from comparing the results obtained with HD mice (grey column) and wild-type littermates (open column) using the Student's *t* test (two-tailed) for statistical analysis. The decrease in ORP of each mouse group from 4 to 12, 4 to 18 and 12 to 18 months of age is indicated by 4-12 ORP, 4-18 ORP and 12-18 ORP respectively.

Comparisons of the maximum ORP of HD mice and wild-type littermates at 3 time points were performed using the same statistical methods as described in section 3.2.2.

The results revealed that female HD mice showed worse maximum ORP at 12 ($p = 0.001$) and 18 months of age ($p = 0.01$) when compared to female wild-type littermates (Fig. 3.3a). Female HD mice also showed a deterioration in maximum ORP with age from 4 to12 months, when compared to the female wild-type littermates but no decline in maximum ORP after 12 months of age (Fig. 3.3b). Male HD mice showed a significantly worse maximum ORP at 12 ($p = 0.002$) and 18 months of age ($p = 0.03$) when compared to male wild-type littermates (Fig. 3.3c). Male HD mice showed a significantly worse maximum ORP with age from 4 to 12 months when compared male wild-type littermates, but no significant decline in maximum ORP after 12 months of age (Fig. 3.3d).

3.2.2.3 Summary

The results obtained by using two different methods to compare the overall rotarod performance of HD mice and wild type littermates were similar. When using mean ORP or maximum ORP as the variable, both female and male HD mice showed worse performances at 12 and 18 months of age, when compared to their corresponding wild-type littermates. Both female and male HD mice showed a significant deterioration in mean and maximum ORP with age from 4 to 12 months, when compared with their corresponding wild-type littermates (male HD mice showed a trend toward decline in mean ORP from 4 to 12 months of age). However, the mean and maximum ORP of both female and male HD mice did not significantly decline after 12 months of age.

3.2.3 Analysis of the resulting data using ANOVA

Three-way ANOVA was the final method used to analyse the data because it uses all raw data points, takes into account different factors that might influence the rotarod performance, and reveals the relationship between different factors. The Minitab software package was used for data analysis.

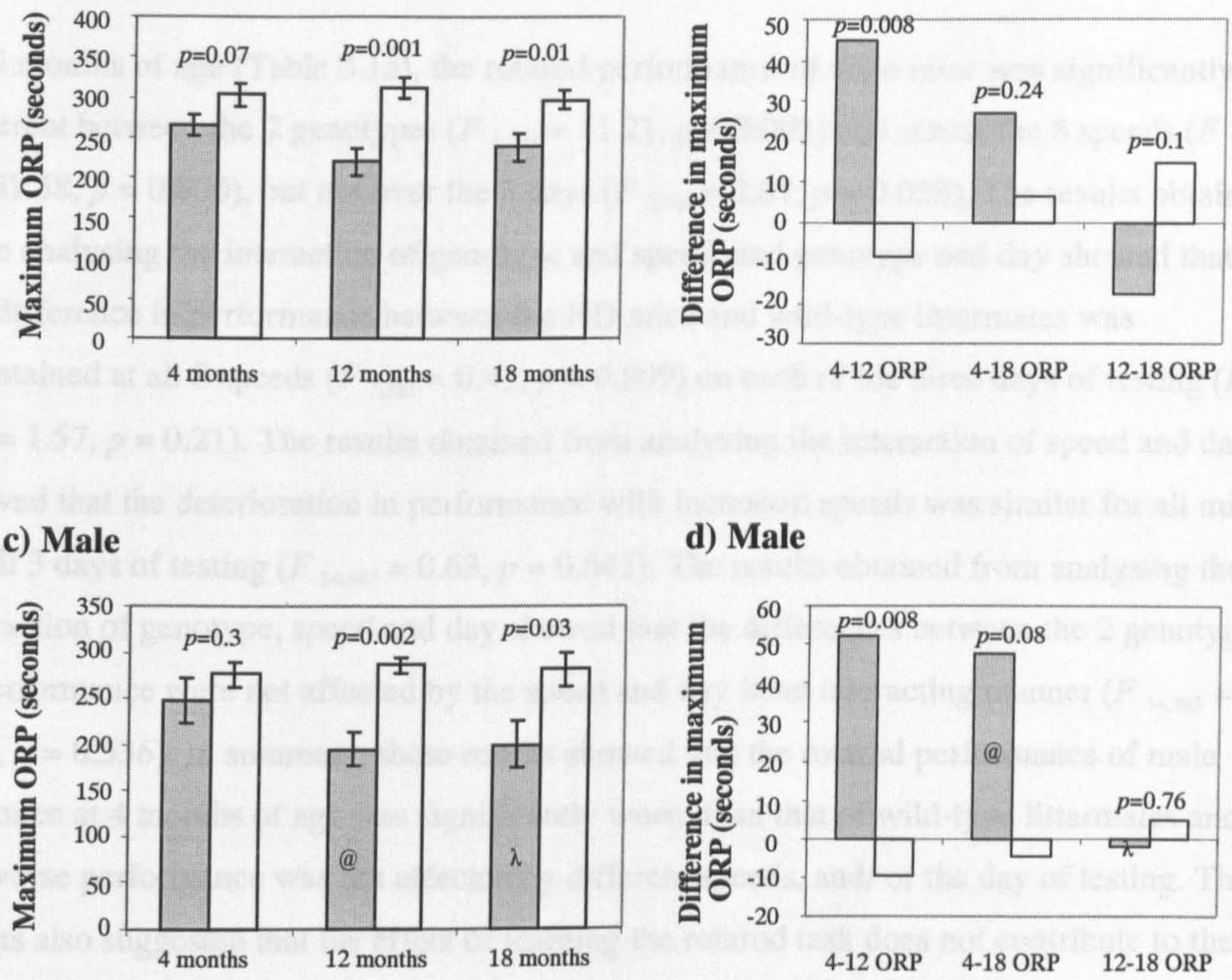

Figure 3.3 Comparisons of the maximum overall rotarod performances (maximum ORP) of 8 female HD and 8 female wild-type littermates (a and b) and 8 male HD and 8 male wild-type littermates (c and d) at 3 time points using the sum of maximum time on the rod from 3 trials at each speed as the maximum ORP. Female HD mice showed worse performances at 12 and 18 months of age, when compared to female wild-type littermates. Female HD mice showed a decline in ORP from 4 to 12 months of age, but not from 12 to 18 months of age. Male HD mice showed worse performances at 12 and 18 months of age, when compared to male wild-type littermates. Male HD mice showed a significant decline in ORP from 4 to 12 months of age, but not from 12 to 18 months of age. Data are expressed as mean ± S.E. @ indicates the mean value was obtained from 7 animals. λ indicates the mean value was obtained from 6 animals. The *p* values indicated were obtained from comparing the results obtained with HD mice (grey column) and wild-type littermates (open column) using the Student's *t* test (two-tailed) for statistical analysis. The decrease in ORP of each mouse group from 4 to 12, 4 to 18 and 12 to 18 months of age is indicated by 4-12 ORP, 4-18 ORP and 12-18 ORP respectively.

To compare the rotarod performances of HD mice and their corresponding wild-type littermates at 3 time points using three-way ANOVA, genotype (2 genotypes: HD and wild-type), speed (8 speeds) and day (3 consecutive days) were used as 3 factors. The results from data obtained with male mice at 4, 12 and 18 months of age are shown in Table 3.1.

At 4 months of age (Table 3.1a), the rotarod performance of male mice was significantly different between the 2 genotypes ($F_{1,383} = 11.21, p = 0.001$) and across the 8 speeds ($F_{7,383} = 151.58, p = 0.000$), but not over the 3 days ($F_{2,383} = 2.87, p = 0.058$). The results obtained from analysing the interaction of genotype and speed, and genotype and day showed that the difference in performance between the HD mice and wild-type littermates was maintained at all 8 speeds ($F_{7,383} = 0.41, p = 0.899$) on each of the three days of testing ($F_{2,383} = 1.57, p = 0.21$). The results obtained from analysing the interaction of speed and day showed that the deterioration in performance with increased speeds was similar for all mice on all 3 days of testing ($F_{14,383} = 0.63, p = 0.841$). The results obtained from analysing the interaction of genotype, speed and day showed that the differences between the 2 genotypes in performance were not affected by the speed and day in an interacting manner ($F_{14,383} = 0.92, p = 0.536$). In summary, these results showed that the rotarod performance of male HD mice at 4 months of age was significantly worse than that of wild-type littermates and the worse performance was not affected by different speeds, and/ or the day of testing. The results also suggested that the effect of learning the rotarod task does not contribute to the worse performance of HD mice, since the performance of all mice did not differ over the 3 days of testing.

The results from analysing the data obtained with male mice at 12 months of age (Table 3.1b) were similar to that at 4 months of age except for the results from analysing the interaction of genotype and speeds. The performances of different genotypes showed different responses to different speeds i.e. the differences in performance between the HD mice and wild-type littermates were exaggerated at some speeds, but not maintained at other speeds ($F_{7,359} = 5.22, p = 0.000$). A greater significant difference between the HD mice and wild-type littermates at 12 months of age ($F_{1,359} = 71.75, p = 0.000$) than 4 months of age was noted. In summary, these results suggested that the rotarod performance of male HD mice at 12 months of age was significantly worse than that of wild-type littermates and that the worse performance of male HD mice at 12 months of age was

a) Male at 4 months of age

Source	DF	Adj SS	Adj MS	F	P
Genotype	1	1449.3	1449.3	11.21	< 0.001***
Speed	7	137192.	19598.9	151.58	< 0.001***
Day	2	742.2	371.1	2.87	0.058
Genotype♦Speed	7	367.1	52.4	0.41	0.899
Genotype♦day	2	405.6	202.6	1.57	0.210
Speed♦day	14	1139.0	81.4	0.63	0.841
Genotype♦speed♦day	14	1668.3	119.2	0.92	0.536
Error	336	43443.0	129.3		
Total	383				

b) Male at 12 months of age

Source	DF	Adj SS	Adj MS	F	P
Genotype	1	7945.2	7945.2	71.75	< 0.001***
Speed	7	129035	18433.6	166.47	< 0.001***
Day	2	517.3	258.6	2.34	0.098
Genotype♦speed	7	4046.1	578.0	5.22	< 0.001***
Genotype♦day	2	251.8	125.9	1.14	0.322
Speed♦day	14	1250.9	89.4	0.81	0.662
Genotype♦speed♦day	14	507.4	36.2	0.33	0.990
Error	312	34549.1	110.7		
Total	359				

c) Male at 18 months of age

Source	DF	Adj SS	Adj MS	F	P
Genotype	1	8511.0	8511.0	68.78	< 0.001***
Speed	7	85988.9	12284.1	99.27	< 0.001***
Day	2	822.7	411.3	3.32	0.037*
Genotype♦speed	7	2071.7	296.0	2.39	0.022*
Genotype♦day	2	21.8	10.9	0.09	0.916
Speed♦day	14	2394.9	171.1	1.38	0.160
Genotype♦speed♦day	14	1376.4	98.3	0.79	0.675
Error	288	35637.2	123.7		
Total	335				

Table 3.1Comparison of the rotarod performance of 8 male HD and 8 male wild-type littermates at 4 (a), 12 (b) and 18 (c) months of age using three-way ANOVA.
The rotarod performance of mice is significantly different between the 2 genotypes and across the 8 speeds, but not over the 3 days of testing at 4 and 12 months of age. The rotarod performance of mice is significantly different between the 2 genotypes, across the 8 speeds and over the 3 days of testing at 18 months of age. The differences in performance between the 2 genotypes at 12 and 18 months of age were exaggerated at some speeds but not maintained at other speeds (source: genotype♦speed). DF: degree of freedom, Adj SS: adjusted sum of square, Adj MS: adjusted mean of square, F: *F* ratio, P: *p* value.
♦ indicates interaction between factors.

exaggerated at some speeds but not maintained at other speeds. This emphasizes that choosing the right speeds for the rotarod test is important, if only a few speeds (less than 8 speeds) are to be tested to reveal the differences in performance between different genotypes of mice in the future.

The results from analysing the data obtained with male mice at 18 months of age (Table 3.1c) were similar to that at 12 months of age except from that the performance of male mice was significantly different over the 3 days of testing ($F_{2,335} = 3.32, p = 0.037$). Since the F ratio was not high, it suggested that male mice at 18 months of age had some but not huge learning of rotarod test. Also, it was not known whether the difference is due to the improvement or deterioration over the three days of testing, and whether genotype and/or fatigue (because of old age) contributed to the difference. Therefore, the learning effect might not or have little impact on the difference in perfomances between HD mice and wild-type littermates.

The results from data obtained with female mice at 4, 12 and 18 months of age are shown in Table 3.2a, 2b, and 2c respectively.

At 4 months of age (Table 3.2a), the performance of female mice was significantly different between the 2 genotypes ($F_{1,383} = 14.5, p = 0.000$), across the 8 speeds ($F_{7,383} = 135.07, p = 0.000$), and over the 3 days ($F_{2,383} = 4.52, p = 0.012$). The difference in performance between the HD mice and wild-type littermates was maintained at all 8 speeds ($F_{7,383} = 0.84, p = 0.556$) and on all 3 days ($F_{2,383} = 0.96, p = 0.386$) of testing. The deterioration in performances of mice with increased speeds was different over the 3 days of testing ($F_{14,383} = 2.42, p = 0.003$). The differences between the 2 genotypes in performance were not affected by the speed and day in an interacting manner ($F_{14,383} = 0.32, p = 0.992$). In summary, these results suggested that the rotarod performance of female HD mice at 4 months of age was significantly worse than that of wild-type littermates and the worse performance was not affected by different speeds, and/or days of testing. It was also noted that female mice at 4 months of age showed difference in performance over the 3 days of testing and the difference was affected by the speeds tested. However it was not known whether the difference is due to the improvement or deterioration over the three days of testing, and whether the genotype of mice contributed to the difference. Since the F ratio

a) Female at 4 months of age

Source	DF	Adj SS	Adj MS	F	P
Genotype	1	2081.3	2081.3	14.5	< 0.001***
Speed	7	135718	19388.4	135.07	< 0.001***
Day	2	1297.4	648.7	4.52	0.012*
Genotype♦speed	7	841.9	120.3	0.84	0.556
Genotype♦day	2	274.4	137.2	0.96	0.386
Speed♦day	14	4869.3	347.8	2.42	0.003**
Genotype♦speed♦day	14	633.6	45.3	0.32	0.992
Error	336	48229.0	143.5		
Total	383				

b) Female at 12 months of age

Source	DF	Adj SS	Adj MS	F	P
Genotype	1	11169.4	11169.4	81.97	< 0.001***
Speed	7	148012	21144.6	155.17	< 0.001***
Day	2	301.0	150.5	1.10	0.333
Genotype♦speed	7	2602.9	371.8	2.73	0.009**
Genotype♦day	2	697.5	348.8	2.56	0.079
Speed♦day	14	1368.9	97.8	0.72	0.757
Genotype♦speed♦day	14	1309.5	93.5	0.69	0.788
Error	336	45786.1	136.3		
Total	383				

c) Female at 18 months of age

Source	DF	Adj SS	Adj MS	F	P
Genotype	1	5490.4	5490.4	59.39	< 0.001***
Speed	7	160023	22860.5	247.30	< 0.001***
Day	2	283.4	141.7	1.53	0.217
Genotype♦speed	7	3485.7	498.0	5.39	< 0.001***
Genotype♦day	2	345.6	172.8	1.87	0.156
Speed♦day	14	1973.6	141.0	1.53	0.1
Genotype♦speed♦day	14	1394.7	99.6	1.08	0.377
Error	336	31059.5	92.4		
Total	383				

Table 3.2 Comparison of the rotarod performance of 8 female HD and 8 female wild-type littermates at 4 (a), 12 (b) and 18 (c) months of age using three-way ANOVA.
The rotarod performance of female mice is significantly different between the 2 genotypes, across the 8 speeds, and over the 3 days at 4 months of age. The rotarod performance of female mice is significantly different between the 2 genotypes, across the 8 speeds, but not over the 3 days at 12 and 18 months of age. The deterioration in performances with increased speeds for all mice is different over the 3 days of testing at 4 months of age. The differences in performance between the 2 genotypes at 12 and 18 months of age were exaggerated at some speeds but not maintained at other speeds (source: genotype♦speed).
DF: degree of freedom, Ad SS: adjusted sum of square, Adj MS: adjusted mean of square, F: F ratio, P: *p* value. ♦ indicates interaction between factors.

was not high ($F_{2,383} = 4.52, p = 0.012$), it suggested that female mice at 4 months of age had some learning of the rotarod task. Therefore, the learning effect might not or have little impact on the difference in perfomances between female HD mice and female wild-type littermates. The results from analysing the data obtained with female mice at 12 (Table 3.2b) and 18 months of age (Table 3.2c) were similar to that of male mice at 12 months of age (Table 3.1b).

Three-way ANOVA was also used to analyse the deterioration of rotarod performance of each mouse group with age. Age (3 time points; 4, 12 and 18 months), speed (8 speeds), and mouse (individual mice in the cohort) were used as 3 factors.

The results from analysing the data obtained with male HD mice are shown in Table 3.3a. The rotarod performance of male HD mice significantly deteriorated with age ($F_{2,431} = 12.6, p = 0.000$), and increased speed ($F_{7,431} = 205.73, p = 0.000$). Male HD mice showed a great variability in performance within the group ($F_{5,431} = 24.98, p = 0.000$). The results obtained from analysing the interaction of mouse and age, and mouse and speed showed that the performance deficits of male HD mice with age ($F_{10,431} = 4.02, p = 0.000$) and increased speeds ($F_{35,431} = 3.85, p = 0.000$) were exaggerated in some mice but not maintained in other mice. The results obtained from analysing the interaction of age and speed showed that the deterioration of performance of male HD mice with age was exaggerated at some speeds but not maintained at other speeds ($F_{14,431} = 3.07, p = 0.000$). Different ages, speeds and mice affected the performance in an interacting way ($F_{70,431} = 1.59, p = 0.005$). In summary, the rotarod performance of male HD mice significantly deteriorated with age. However, a huge variability in performance was present among individual mice within the male HD group and it was noted that some mice showed a more prominent deterioration in performance with age, but some did not show any decline at all. This variability in performance suggested that a longitudinal study testing the same mice at different ages is probably more appropriate rather than using different mice of different ages to investigate the deterioration of rotarod performance with age. Also, the deterioration of performance of male HD mice with age was exaggerated at some speeds but not maintained at other speeds, suggesting that the rotarod test at some speeds is more sensitive in detecting the deterioration of performance with age.

The results from analysing the data obtained with female HD mice (Table 3.3c) were similar to those with male HD mice except from that the deteriorations of performance of female HD mice with age were maintained at all speeds ($F_{14,575} = 1.31, p = 0.2$) and the performance of female HD mice was not affected by the interaction of different ages, speeds and mice ($F_{98,575} = 0.91, p = 0.699$).

The results of the performance of male and female wild-type littermates are shown in Table 3.3b and 3.3d respectively. Both groups of wild-type mice like both groups of HD mice showed a great variability in performance within the group and the variability were influenced by the different speeds and ages. The performance of male wild-type littermates (Table 3.3b) did not decline with age but that of female wild-type littermates (Table 3.3d) deteriorated slightly with age ($F_{2,575} = 3.28, p = 0.039$). However, the deterioration of HD female rotarod performance ($F_{2,575} = 5.62, p = 0.004$) was greater than that of wild-type littermates ($F_{2,575} = 3.28, p = 0.039$).

3.2.3.1 Summary

Two main conclusions were drawn from the results obtained by using ANOVA to analyse the rotarod performance data. Firstly, both male and female HD mice showed worse performances at 4, 12 and 18 months of age, when compared with their wild-type littermates. Secondly, both male and female HD mice showed a significantly greater deterioration in rotarod performance with age than their wild-type littermates.

All methods indicated differences between HD and wild-type cohorts at 12 and 18 months of age but the results obtained by using ANOVA and by using overall rotarod performance to analyse the data were different at 4 months of age. The fact that ANOVA tests reveal a difference in the performance of both male and female HD mice at 4 months of age confirms that ANOVA is probably a more powerful data analysis approach because it uses all raw data points and takes into account different factors that might influence the rotarod performance.

a) Male HD

Source	DF	Adj SS	Adj MS	F	P
Age	2	2154.3	1077.1	12.6	< 0.001***
Mouse	5	10681.9	2136.4	24.98	< 0.001***
Speed	7	123156.9	17593.8	205.73	< 0.001***
Age♦mouse	10	3435.9	343.6	4.02	< 0.001***
Age♦speed	14	3678.9	262.8	3.07	< 0.001***
Mouse♦speed	35	11537.2	329.6	3.85	< 0.001***
Age♦mouse♦speed	70	9499.5	135.7	1.59	0.005**
Error	288	24630.0	85.5		
Total	431				

b) Male wild-type

Source	DF	Adj SS	Adj MS	F	P
Age	2	161.7	80.9	1.05	0.353
Mouse	7	5238.4	754.8	9.76	< 0.001***
Speed	7	214015.7	30575.1	395.2	< 0.001***
Age♦mouse	14	5126.9	366.2	4.73	< 0.001***
Age♦speed	14	807.6	57.7	0.75	0.728
Mouse♦speed	49	6612.8	135	1.74	0.002**
Age♦mouse♦speed	98	8441.3	86.1	1.11	0.239
Error	384	29707.3	77.4		
Total	575	270166.8			

c) Female HD

Source	DF	Adj SS	Adj MS	F	P
Age	2	1153.6	576.8	5.62	0.004**
Mouse	7	10351.2	1478.7	14.42	< 0.001***
Speed	7	222382.1	31768.9	309.69	< 0.001***
Age♦mouse	14	3884.4	277.5	2.70	0.001**
Age♦speed	14	1876.2	134.0	1.31	0.2
Mouse♦speed	49	9375.0	191.3	1.87	0.001**
Age♦mouse♦speed	98	9194.4	93.8	0.91	0.699
Error	384	39392.0	102.6		
Total	575				

d) Female wild-type

Source	DF	Adj SS	Adj MS	F	P
Age	2	698.1	398.1	3.28	0.039*
Mouse	7	5943.6	5943.6	7.98	< 0.001***
Speed	7	224332.7	224332.7	31.033	< 0.001***
Age♦mouse	14	4408.4	4408.4	2.96	< 0.001***
Age♦speed	14	2094.3	2094.3	1.41	0.147
Mouse♦speed	49	7074.2	7074.2	1.36	0.062
Age♦mouse♦speed	98	9360.9	9360.9	0.90	0.736
Error	384	40839.3	40839.3		
Total	575	294751.6			

Table 3.3 Comparing the rotarod performances over 3 time points (4, 12 and 18 months of age) for male HD (a) and wild-type (b) and female HD (c) and wild-type (d) mice using three-way ANOVA.
The rotarod performance of male and female HD mice significantly deteriorated with age (source: age). Both male and female HD mice show significantly different performances among individual mice within the group (source: mouse). The rotarod performance of male and female HD mice significantly deteriorated with increased speeds (source: speed). The deterioration of performance with age is exaggerated in some mice, but not maintained in other mice within both male and female HD groups of mice (source: Age♦mouse). The deterioration of performances with increased speeds is different in some mice in both male and female HD groups of mice (source: mouse♦speed). The deterioration of performance of male HD mice with age is exaggerated at some speeds, but not maintained at other speeds (source: age♦speed). Different ages, speeds and individual mice affect the performance in an interacting manner in male HD group (source: age♦mouse♦speed). DF: degree of freedom, Adj SS: adjusted sum of square, Adj MS: adjusted mean of square, F: *F* ratio, P: *p* value. ♦ indicates interaction between factors.

3.2.4 Investigating possible confounding influences affecting the rotarod performance of HD mice

Although the rotarod paradigm is used to measure locomotor function in mice, the performance of the rotarod task is also influenced by body weight, age and cognitive function including memory, learning, attention and motivation. It is essential to determine whether confounding influences affect the rotarod performance of HD mice before drawing any conclusions from the data about motor performance. Therefore, possible confounding factors affecting the rotarod performance of HD mice were investigated.

3.2.4.1 Investigating cognitive effects on rotarod performance

During the week prior to the test experiment, each mouse received a training course (section 2.2.18), and appeared to reach a steady baseline level of performance. The pre-test training was therefore expected to reduce the confounding effects of possible cognitive defects on rotarod performance results. To determine whether there was any evidence of learning of the rotarod test after the pre-test training, two ANOVA methods were performed. Firstly, compared the overall rotarod performance (ORP) of each group of mice over the 3 day period of testing at each age. Secondly, compared individual performances of the mice over the 3 day period of testing at each age.

For the first comparison, the sum of the time periods of staying on the rod at 8 different speeds (ORP) on day 1, day 2 and day 3 at each age tested for each group was determined. Analysis using one-way ANOVA and post hoc Tukey test indicated that there was no significant difference observed in day 1, day 2 and day 3 performances for any group of mice at any age tested, although most of the mice did appear to spend slightly more time on the rod on day 3, compared to day 1 (Fig. 3.4). The results using the ORP as the measure suggested that none of the cohorts of mice used in the study showed significant learning of the rotarod test during the three days of assessment at any time point.

a) Female wild-type littermates

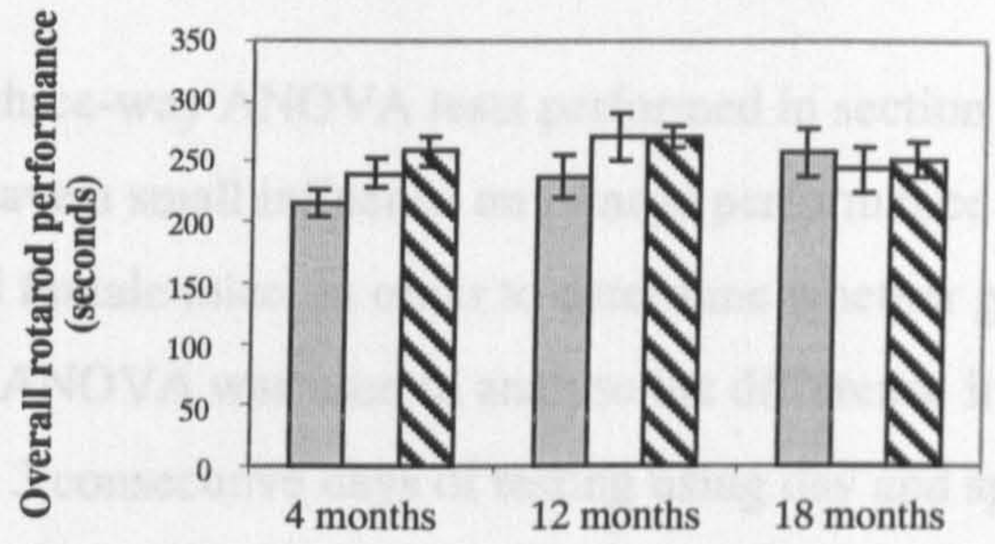

b) Female HD mice

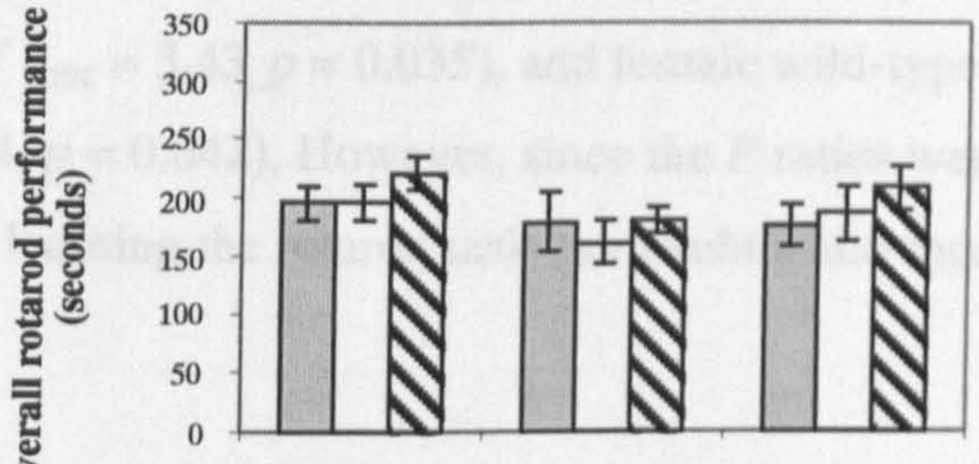

c) Male wild-type littermates

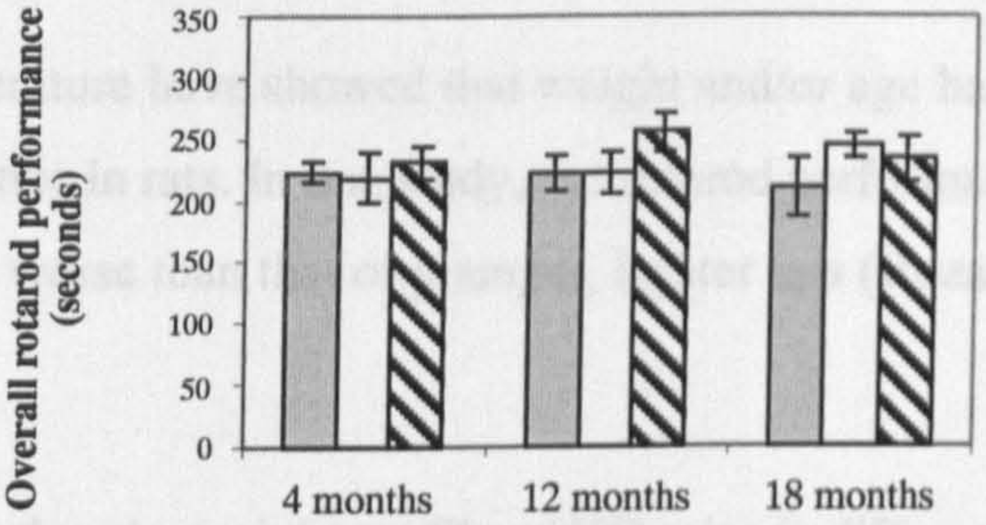

d) Male HD mice

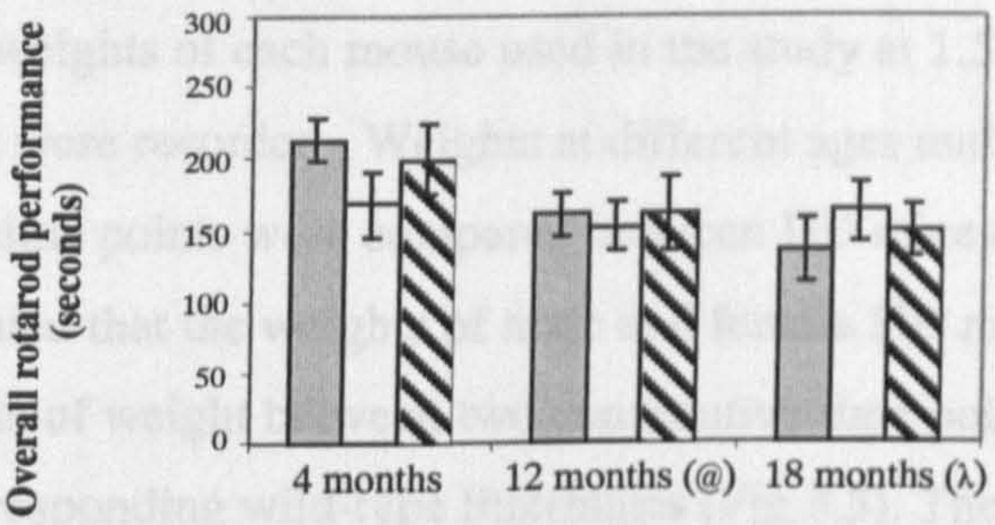

Figure 3.4 Comparisons of overall rotarod performance obtained from day 1 (grey column), day 2 (open column) and day 3 (striped column) assessments on 8 female wild-type littermates (a), 8 female HD mice (b), 8 male wild-type littermates (c) and 8 male HD mice (d) at 3 time points. Data are expressed as mean ± S.E. @ indicates 7 animals were tested. λ indicates 6 animals were tested. One-way ANOVA and post-hoc Tukey test were used to compare the performances of each group of mice on three consecutive days at each time point. No significant differences are shown between day 1, day 2, and day 3 performances for any group of mice at any time point.

In contrast, the three-way ANOVA tests performed in section 3.2.3 suggested that the day of testing may have a small influence on rotarod performance in 18 month-old male mice and 4 month-old female mice. In order to determine whether genotype contributes to this effect, two-way ANOVA was used to analyse the difference in performance of each group of mice over the 3 consecutive days of testing using day and speed as 2 factors. The results showed significantly different performances across the 3 consecutive days of testing in male HD mice at 4 months of age ($F_{2,191} = 3.49, p = 0.033$), male wild-type littermates at 12 months of age ($F_{2,191} = 3.43, p = 0.035$), and female wild-type littermates at 4 months of age ($F_{2,191} = 3.24, p = 0.042$). However, since the F ratios were not very high, it is possible that the effect of learning the rotarod task has a subtle and inconsistent influence on the results obtained.

3.2.4.2 Comparisons of the body weight profiles of HD mice and wild-type littermates

Studies in the literature have showed that weight and/or age has a significant effect on rotarod performance in rats. In one study, the rotarod performance of older, heavier rats was significantly worse than that of younger, lighter rats (Rozas and Labandeira Garcia, 1997).

To determine whether the weight profile of HD mice is different from that of wild-type littermates, a comparison of the weight profiles of HD mice and wild-type littermates was performed. The weights of each mouse used in the study at 1.5, 2.5, 3.5, 4.5, 5.5, 7, 8 and 18 months of age were recorded. Weights at different ages and the gain of weight between two consecutive time points were compared between HD mice and wild-type littermates. The results indicated that the weights of male and female HD mouse cohorts at all time points and the gain of weight between two consecutive time points were not different from those of their corresponding wild-type littermates (Fig 3.5). The results therefore suggest that the differences in the rotarod performance of male and female HD mice (compared to wild-type) cannot be attributed to weight differences.

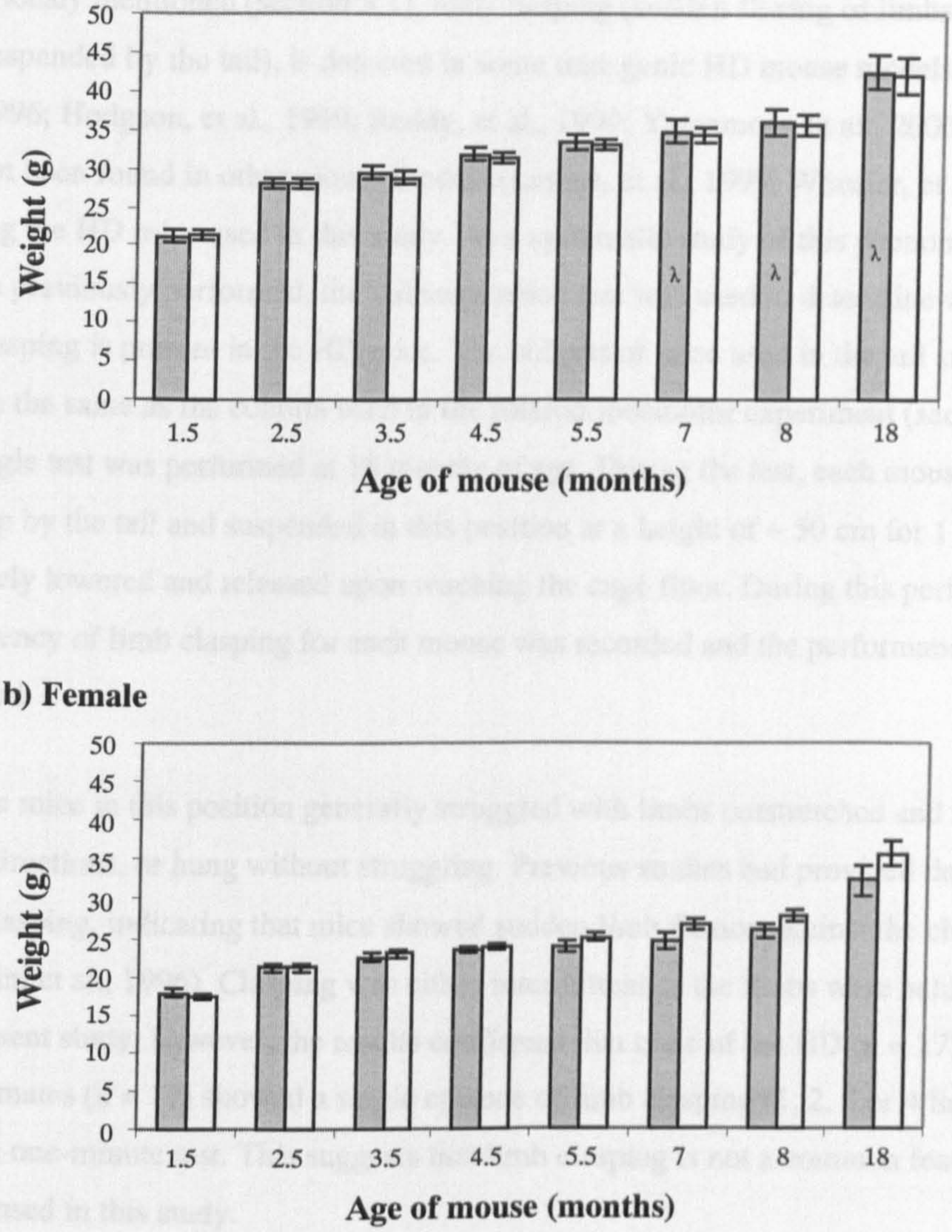

Figure 3.5 Comparisons of the weight profile of 8 male HD mice to 8 male wild-type littermates (a) and 8 female HD mice to 8 female wild-type littermates (b), at 8 different time points. Both male and female HD mice show no differences in weight at all time points, when compared to their wild type-littermates. Data are expressed as mean ± S.E. HD mice (grey column) and wild-type littermates (open column) were compared using the Student's *t* test (two-tailed). λ indicates only 6 mice were included.

3.3 Investigating general neurological deficits in HD mice using the tail suspension test

As previously mentioned (section 3.1), limb clasping (sudden flexing of limbs to the chest when suspended by the tail), is detected in some transgenic HD mouse models (Mangiarini, et al., 1996; Hodgson, et al., 1999; Reddy, et al., 1999; Yamamoto, et al., 2000). However it has not been found in other mouse models (Levine, et al., 1999; Wheeler, et al., 2000) including the HD mice used in this study. As a systematic study of this phenomenon had not been previously performed, the tail suspension test was used to determine whether and when clasping is present in the HD mice. The cohorts of mice used in the tail suspension test were the same as the cohorts used in the rotarod locomotor experiment (section 3.2), but a single test was performed at 18 months of age. During the test, each mouse was picked up by the tail and suspended in this position at a height of ~ 50 cm for 1 minute, then slowly lowered and released upon reaching the cage floor. During this period of time, the frequency of limb clasping for each mouse was recorded and the performance videotaped.

Wild-type mice in this position generally struggled with limbs outstretched and moving in random directions, or hung without struggling. Previous studies had provided descriptions of limb clasping, indicating that mice showed sudden limb flexion against the chest (Mangiarini et al., 1996). Clasping was either intermittent or the limbs were held stationary. In the present study, however, the results confirmed that none of the HD (n = 17) or wild-type littermates (n = 17) showed a single episode of limb clasping (1, 2, 3 or 4 limbs) during the one-minute test. This suggests that limb clasping is not a common feature of the HD mice used in this study.

4 Investigating the integrity of mtDNA in HD mouse brain as an indicator of early molecular pathology

4.1 Background

The aetiology of selective neuronal death in HD is still not clear. There could be a complex interplay between impaired energy metabolism, excitotoxicity, oxidative stress and apoptosis, all of which have been shown to play an important role in the pathogenesis of HD (section 1.2.4). Slow excitotoxicity may occur as a consequence of a defect in energy production (Beal, 1995; Beal, 1996) and excitotoxicity can lead to superoxide generation (Beal, 1995; Beal, 1996). As increased oxidative stress may further compromise energy metabolism in neurons, a vicious cycle may be initiated that finally results in cell death. Given that mitochondria could play a central role in these processes, studies of mitochondrial function in HD mice may shed light on the mechanism and molecular pathology of HD.

Because of its proximity to the respiratory chain (the most important source of free radicals), limited repair mechanisms, few non-coding sequences and absence of histones, mitochondrial DNA (mtDNA) is particularly susceptible to oxidative damage. Mitochondrial DNA damage, after exposure to high levels of reactive oxygen species, is mediated predominantly by intramitochondrial accumulation of 8-hydroxydeoxyguanosine (8-OHdG) (Richter et al., 1988). Incorporation of 8-OHdG into mtDNA causes base mispairing, point mutations and deletions. Many studies have demonstrated that mtDNA deletions increase with age and oxidative stress in many human and mouse tissues (Brossas et al., 1994; Hayakawa et al., 1991; Liu et al., 1998; Tanhauser and Laipis, 1995). Decreased levels of total mtDNA have been shown in affected tissues of Friedreich's ataxia (Bradley et al., 2000) and Alzheimer's patients (de la Monte et al., 1988; Rodriguez-Santiago et al., 2001), conditions associated with increased oxidative stress. Furthermore, increased levels of mtDNA deletions have been shown in the cortex of individuals affected by HD (Horton et al., 1995). Therefore, the levels of deleted mtDNA and total mtDNA content were investigated in HD mouse brain.

Different types of deleted mtDNA species occur in aged mice (Tanhauser and Laipis, 1995). All the deletions are flanked by perfect or imperfect direct repeats. While many deleted mtDNA species are present in aged mice, they are uncommon, and any one deletion generally constitutes less than 0.00006 % of total mtDNA in mouse brain (Tanhauser and Laipis, 1995). Based on this finding it is anticipated that most deletions, other than the commonest type, will be difficult to detect and quantify by PCR. Therefore, the commonest deletion type was investigated in this study (Fig. 4.1).

The HD mice used in this study are probably modelling early stages of HD, as there is no evidence of acute neurodegeneration in the brains of the mice (Shelbourne et al., 1999). The behavioural changes of these mice have been shown to occur at 3 months (Shelbourne et al., 1999) and as shown in Chapter 3, the locomotor abnormality is present at 4 months of age. However, the molecular/cellular pathology in HD mice has not been investigated. By investigating the integrity of mtDNA in the brains of HD mice at different time points, the aims of this study were: 1) to determine whether mitochondrial abnormalities occur specifically in the striatum, but not in other brain regions of HD mice, 2) to determine whether mitochondrial abnormalities in HD mice are progressive phenomena in nature.

4.2 Quantifying mtDNA levels using a competitive PCR approach

A competitive PCR assay modified from a previously published competitive RT-PCR assay (Siebert and Larrick, 1992; Tanhauser and Laipis, 1995) was employed to quantify the amounts of total mtDNA and deleted mtDNA in mouse tissue DNA. The use of a DNA competitor molecule (mimic) provides not only an internal control but also an opportunity for calculating the absolute level of target DNA, since the initial amount of competitor DNA in the PCR reaction is known (Siebert and Larrick, 1992). In competitive PCR, the mimic competes with the target template for primer binding and amplification. The mimic DNA shares the same primer sequences as the target DNA sequence but has a different intervening sequence (Fig. 4.2).

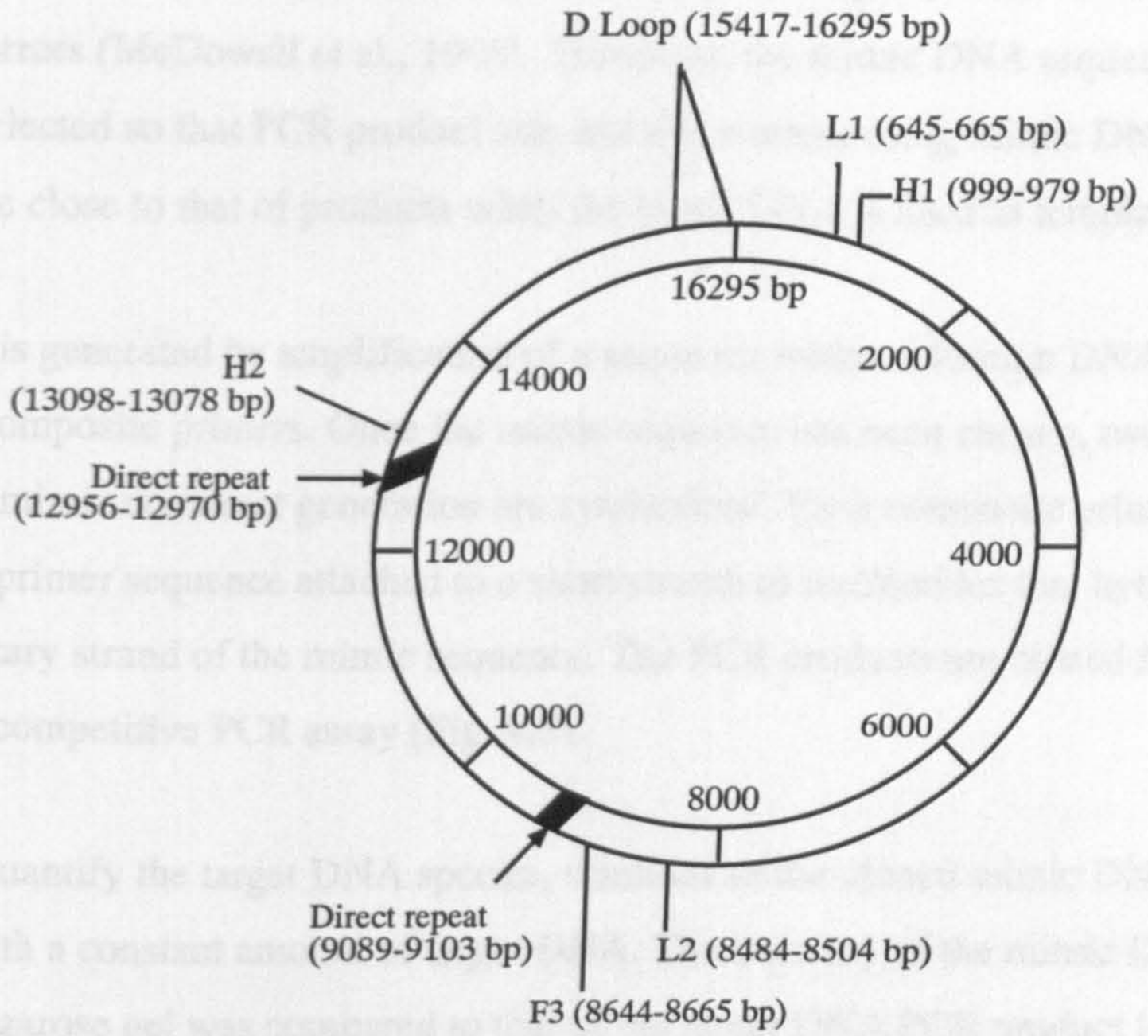

Figure. 4.1 Diagram of mouse mitochondrial DNA (16295 bp). Primers L1 and H1 (see sequence in section 2.1.7) were used to amplify intact mtDNA molecules. Primers L2 and H2 (see sequence in section 2.1.7) were used to amplify deleted mtDNA. A common large DNA deletion (3867 bp) occurs between a pair of direct repeats (indicated by arrows). An oligonucleotide (F3) (see sequence in section 2.1.7) was used to hybridize the product of deleted mtDNA amplification in a Southern blot analysis to confirm the identity of the deleted PCR product. Numbers inside the circle indicate the relative positions of mtDNA features in bp.

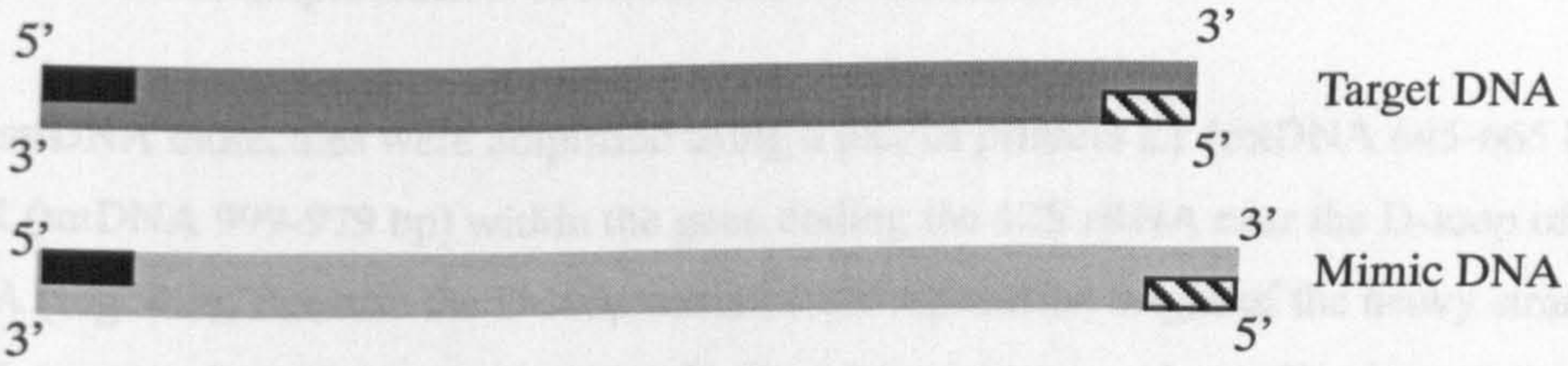

Figure 4.2 Schematic illustration of mimic and target DNA templates in a competitive PCR assay. The mimic template shares the same primer sequences but has a different intervening sequence to the target DNA.The mimic DNA sequence was selected so that the product size of PCR and the CG content of the mimic DNA template are close to those of the target DNA. PCR primers are indicated by the symbols ■ and ▨.

Differences in sequence length and content between the target and the mimic DNA may introduce errors (McDowell et al., 1998). Therefore, the mimic DNA sequence must be carefully selected so that PCR product size and GC content using mimic DNA as the template are close to that of products when the target DNA is used as template.

The mimic is generated by amplification of a sequence within a foreign DNA fragment using two composite primers. Once the mimic sequence has been chosen, two composite primers for mimic construct generation are synthesized. Each composite primer has the target gene primer sequence attached to a short stretch of nucleotides that hybridize to the complementary strand of the mimic sequence. The PCR products are cloned for the subsequent competitive PCR assay (Fig. 4.3).

In order to quantify the target DNA species, dilutions of the cloned mimic DNA are co-amplified with a constant amount of target DNA. The intensity of the mimic DNA PCR product on agarose gel was compared to that of the target DNA PCR product in the same reaction to determine the number of amplifiable target DNA molecules. This value is determined by calculating how much of the mimic DNA was required to achieve equal molar amounts of the respective PCR products.

4.3 Investigating mtDNA levels in HD mouse tissue

4.3.1 Amplification of mtDNA from mouse tissue

4.3.1.1 PCR amplification of intact mtDNA molecules

Intact mtDNA molecules were amplified using a pair of primers L1 (mtDNA 645-665 bp) and H1 (mtDNA 999-979 bp) within the gene coding the 12S rRNA near the D-loop of mtDNA (Fig. 4.1). Because the D-loop contains the replication origin of the heavy strand that is important for mtDNA replication, the flanking region near the replication origin of the heavy strand is unlikely to be deleted. The primers and amplification conditions have been previously reported (Tanhauser and Laipis, 1995). In this study, the amplification conditions were slightly modified (PCR cycles changed from 30 to 24 cycles and annealing temperature changed from 50 to 55°C) in order to optimize yield and specificity of PCR

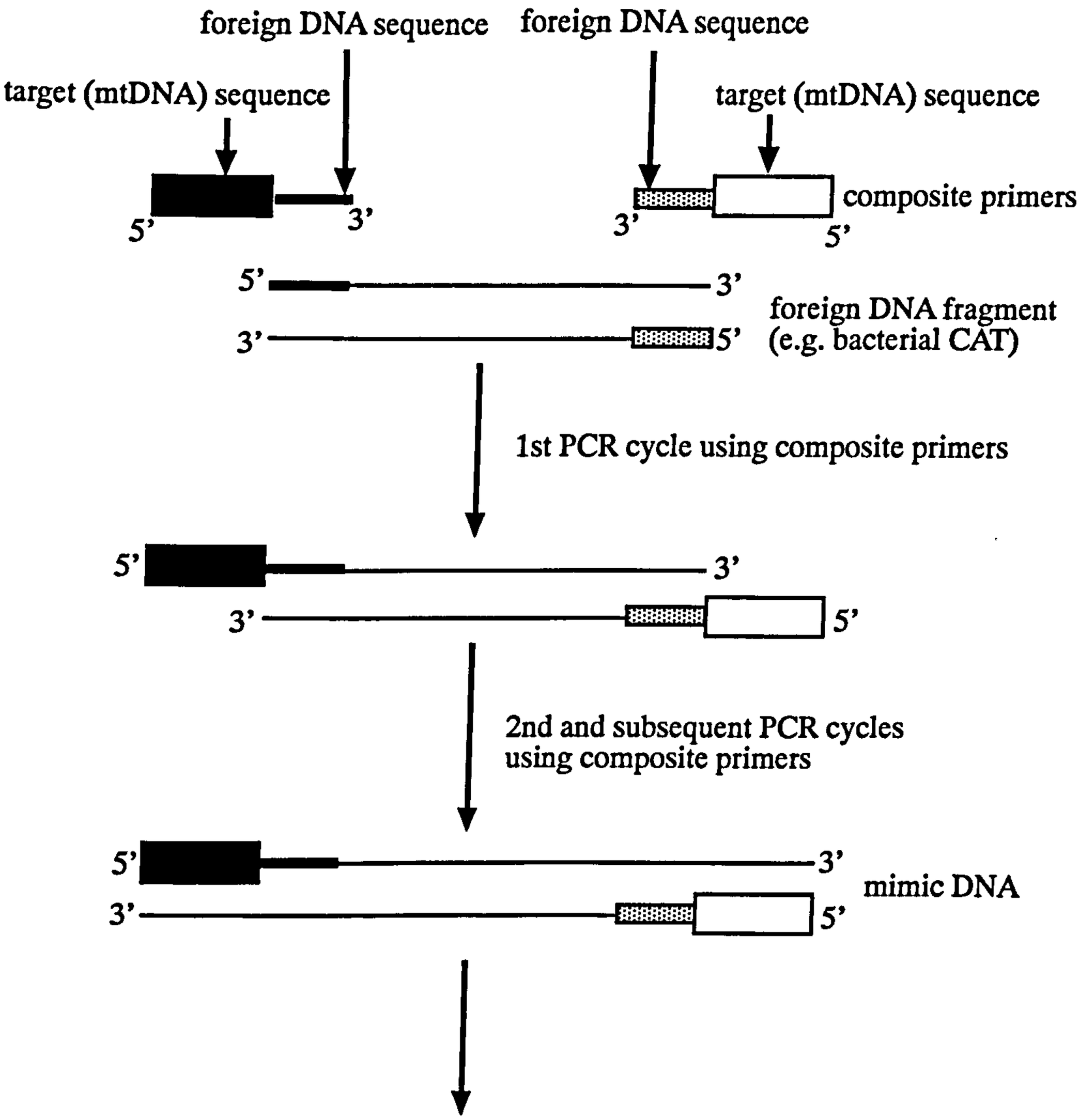

Figure 4.3 Generation of mimic constructs for use in competitive PCR assays. A composite primer is synthesized by attaching a target gene primer sequence to a short stretch of nucleotides that hybridize to complementary strand of a foreign DNA fragment [e.g. from bacterial chloramphenicol acetyltransferase (CAT) gene]. The composite primers are used to amplify the foreign DNA fragment for generation of the mimic DNA molecule.

products from the thermocycler in the laboratory (section 2.2.5.2). The size of PCR products using primers L1 and H1 was confirmed as 355 bp (Fig. 4.4a).

4.3.1.2 Optimising the PCR amplification of deleted mtDNA molecules

Deleted mtDNA species were amplified using a pair of primers (L2 and H2) that flank the most common deletion (3867 bp between a pair of direct repeats shown in Figure 4.1). Primers L2 (mtDNA 8484-8504 bp) and H2 (mtDNA 13098-13078 bp) could only amplify the deleted mtDNA species, because the fragment of undeleted mtDNA species flanked by L2 and H2 is too large (4.6 kb) to be amplified by PCR with a short extension time (20 s). The predicted size of the target PCR product was 748 bp. At first, multiple bands instead of a single band were obtained using previously published PCR conditions (Tanhauser and Laipis, 1995). Much effort was put into optimising the PCR conditions for amplification of the deleted mtDNA molecules from mouse brain and liver DNA. The optimisation was achieved by testing different annealing temperatures (50-55°C), adjusting the amount of DNA template added (from 75 ng to 2 μg), using different concentrations of $MgCl_2$ in the PCR reaction solution (1 to 4 mM) and testing *Taq* polymerase from different companies (Promega, Sigma, and Perkin Elmer). Finally, the predicted single band was obtained using the PCR conditions (55°C annealing temperature, 75-200 ng of DNA, 1.5 mM $MgCl_2$ and *Taq* polymerase from Perkin Elmer) detailed in section 2.2.5.2 (Fig. 4. 4b and c). The PCR products amplified using primers L2 and H2 were confirmed by Southern blot analysis (section 2.2.12.4), using a radio-labelled oligonucleotide probe termed F3 (mtDNA 8644-8665 bp) (Fig. 4.1) located between the L2 and H2 primers. This probe was predicted to hybridise to the correct PCR products (Fig. 4.5). The sequence of the PCR product was also confirmed by sequencing (section 2.2.10) as showing a 3867 bp deletion between a pair of direct repeats located in the mtDNA molecule (Fig. 4.6).

4.3.2 Generation of mimic constructs for quantifying mtDNA levels in mouse tissue

In this study, the programs Blast search (NCBI) and GeneJockey II (Biosoft, Cambridge, UK) were used to choose a mimic sequence from plasmid pBcxm [containing the gene encoding *E. coli* chloramphenicol acetyltransferase (CAT)].

a) Intact mtDNA amplification

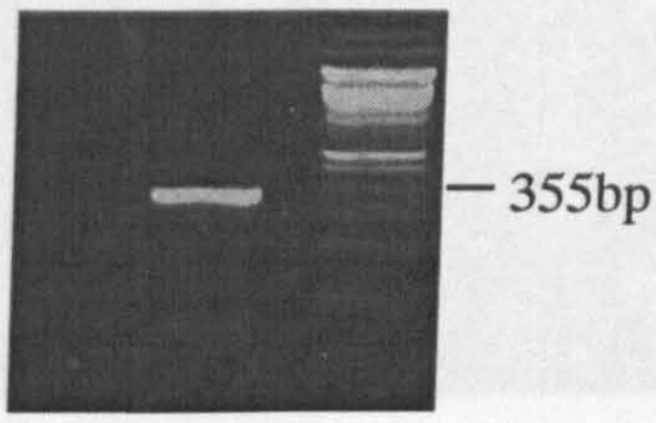

b) Deleted mtDNA amplification of liver DNA

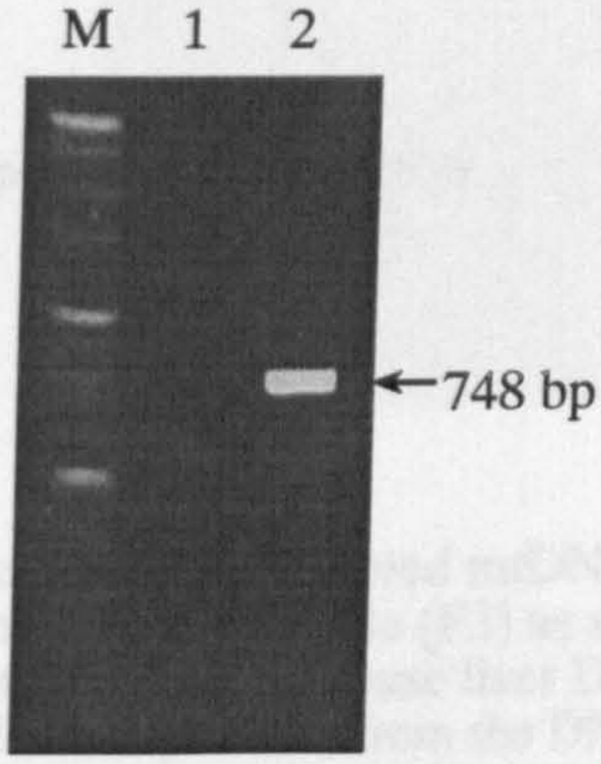

c) Deleted mtDNA amplification of brain DNA

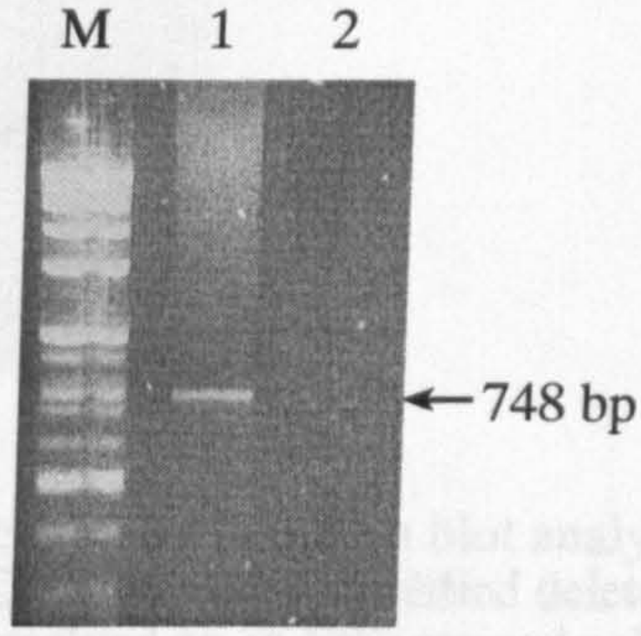

Figure 4.4 Images of PCR products of mtDNA molecules resolved on EtBr-agarose gels. Products of intact mtDNA molecules after amplification with L1 and H1 primers from 5 ng wild-type mouse brain DNA are shown in lane 1 (a). Products of deleted mtDNA molecules after amplification with L2 and H2 primers from 75 ng wild-type mouse liver DNA are shown in lane 2 (b) and from 300 ng wild-type mouse brain DNA are shown in lane 1 (c). Controls for DNA contamination of the PCR reagents, using water as a template, are shown in lanes 2 (a), 1 (b) and 2 (c). M indicates the 1Kb plus size ladder.

a) Deleted mtDNA amplification

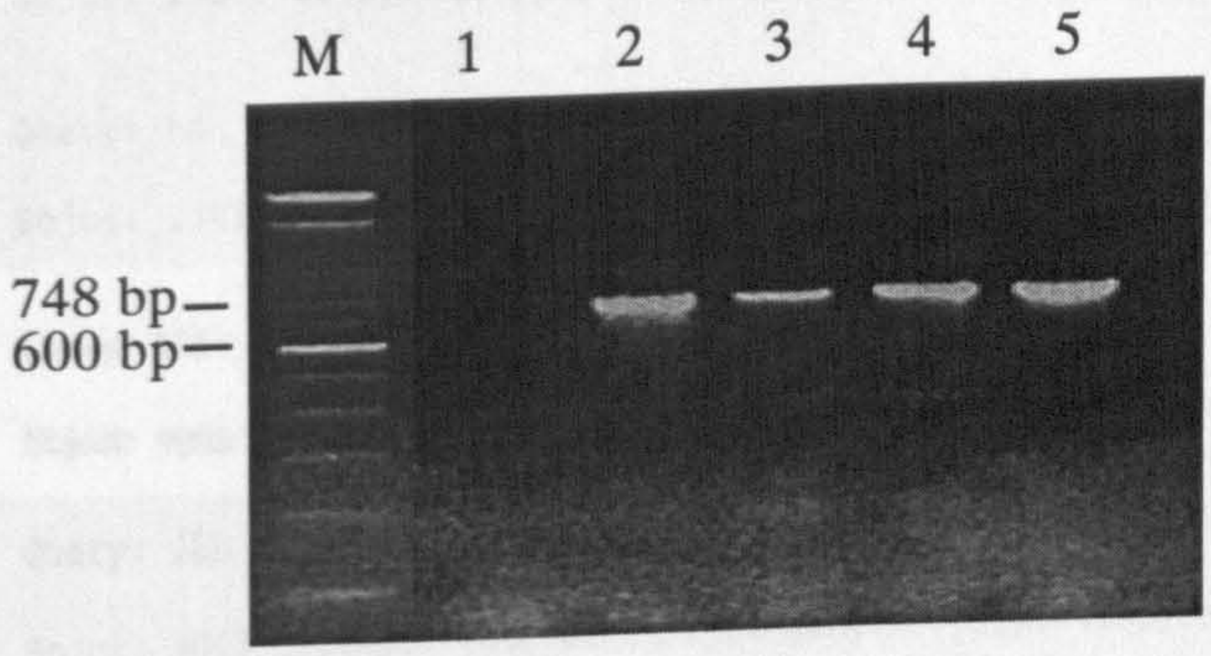

b) Southern blot

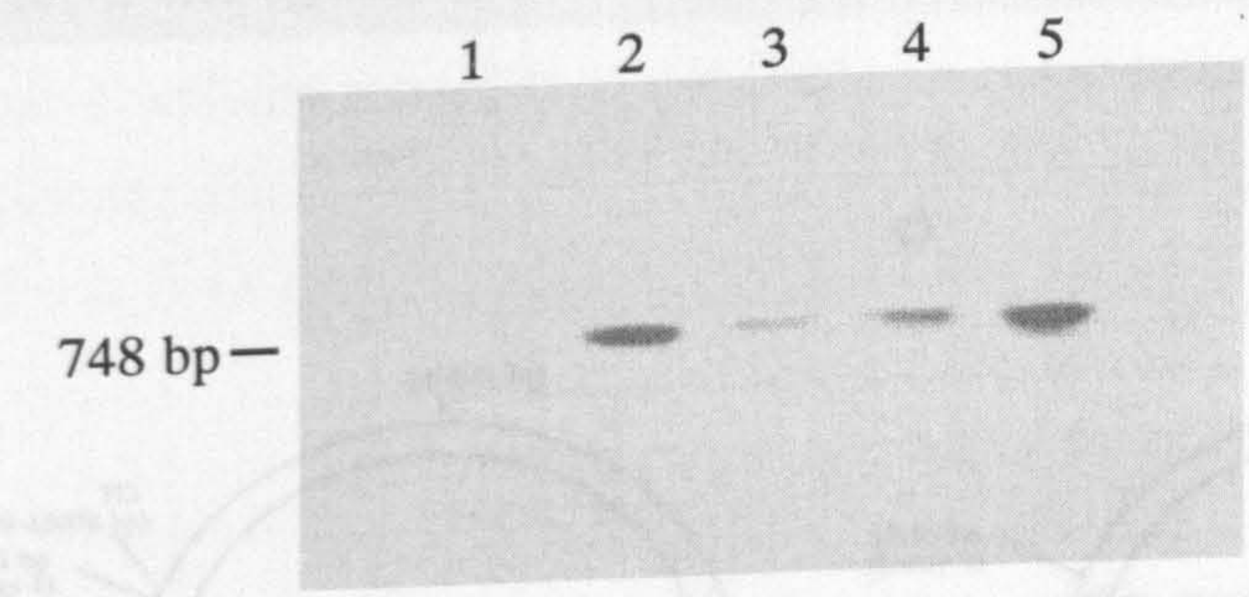

Figure 4.5 Confirmation of the deleted mtDNA amplification by Southern blot analysis using a radiolabelled oligonucleotide (F3) as a probe. PCR products of amplified deleted mtDNA molecules from 200 ng of mouse liver DNA were resolved on an EtBr-stained gel (a). Lanes 2 and 5 contain PCR products from the DNA of wild-type mice and lanes 3 and 4 from the DNA of HD mice. A control for DNA contamination of PCR reagents, using water as a template is shown in lane 1. M indicates the 100 bp size ladder. Southern blot analysis of the gel indicated in (a) probed with a radio-labelled oligonucleotide (F3) located between primers L2 and H2 (Figure 4.1) was performed (b) to confirm the correct amplification of the deleted mtDNA molecules.

a)

```
Query: 4      tttcgttaatggagattannnnnnnaaaacgcggttttgttattgttacgaaagtaaatg 63
              ||||||||||||||||||      ||||||||||||||||||||||||||||| |||||||
Sbjct: 13071 tttcgttaatggagattaggggggggaaaacgcggttttgttattgttacgaa-gtaaatg 13013


Query: 64    attcgtatgctgtacatagctgttatagaagtggcgattagtgtaattagtagggct 120
              ||||||||||||||||||||||||||||||||||||||||||||||||||||||||
Sbjct: 13012 attcgtatgctgtacatagctgttatagaagtggcgattagtgtaattagtagggct 12956


Query: 121   gatttatgtggtttcgtttaccttctataaggctatgatgagct 165
              |||||||||||||||||||||||||||||||||||||||||||
Sbject: 9088  gatttatgtggtttcgtttaccttctataaggctatgatgagct 9044


Query: 166   catgtaattgaaacacctgatgctacaagtactgaagtattaagtactgggacttctaca 225
              ||||||||||||||||||||||| |||||||||||||||||| |||||||||||| |
Sbjct: 9043  catgtaattgaaacacctgatgctagaagtactgaagtattaagtagtgggacttctaga 8984


Query: 226   gggttaattggtgaaatccctgttggaggtcgtcaccctcctatatcatgtgt 278
              ||||||| ||||||||| |||||||||||||  || ||||||| |||||||||
Sbjct: 8983  gggttaagtggtgaaattcctgttggaggtcagcagcctcctagatcatgtgt 8931
```

b)

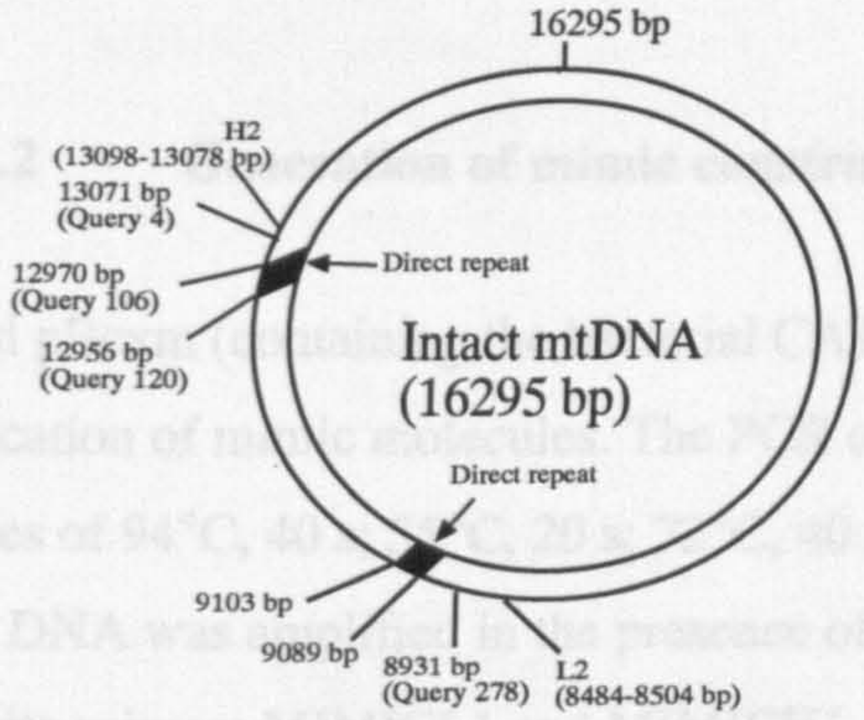

c)

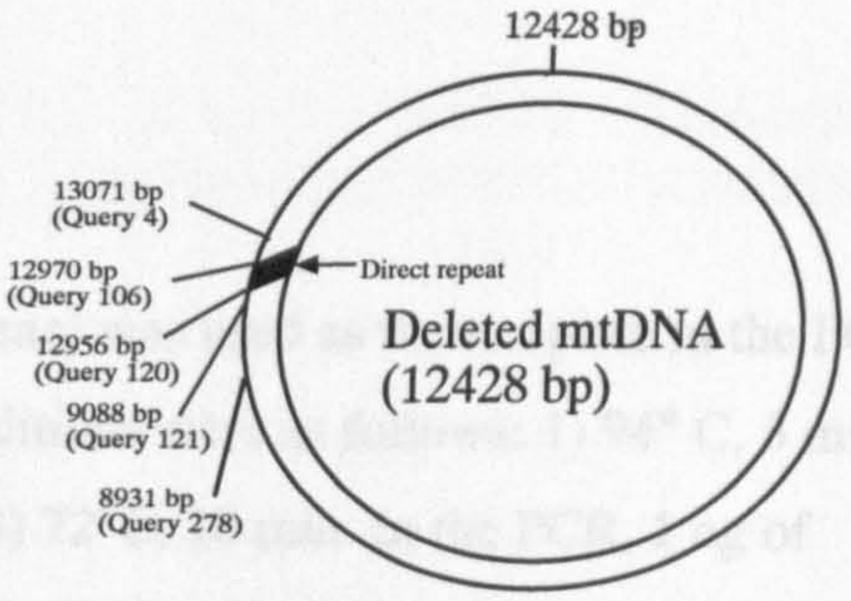

Figure 4.6 Sequencing of the PCR product amplified from deleted mtDNA. A PCR product of amplified deleted mtDNA using L2 and H2 primers was sequenced using primer H2. The sequence of a fragment [Query 4-278 nucleotides in (a)] of deleted mtDNA obtained from direct DNA sequencing was compared to the Genbank database [Sbjct 13071-8931bp in (a)] using the Blast programme (NCBI). The results show that a DNA fragment (3867 bp) including a repeat sequence is deleted between the pair of repeats (underlined) and 259 out of 278 query nucleotides were matched to the Genbank sequence. The unmatched nucleotides are probably due to the PCR errors. A schematic map of intact mtDNA (16295 bp) is shown in (b). A schematic map of deleted mtDNA (12428 bp) is shown in (c). A DNA fragment (3867 bp) including a repeat sequence is deleted between the pair of direct repeats.

4.3.2.1 Generation of mimic construct for quantifying total mtDNA content of mouse tissue

4.3.2.1.1 Selection of mimic DNA sequence and composite primers

As mitochondrial DNA sequence is AT rich, the DNA sequence of mimic p444 was chosen from the bacterial CAT gene (also AT rich) according to the principles described in section 4.2. The GC ratio of the mimic DNA sequence was 42 % and the GC ratio of the target mtDNA sequence flanked by primers L1 and H1 was 36 %. Primers were selected so that the predicted size of the mimic PCR product was 444 bp, which is close but distinguishable from the size of target mtDNA PCR product, 355 bp. The composite primers MIMICL1 and MIMICH1 were synthesized by attaching primer L1 to the CAT gene-specific oligonucleotide CAT1 and primer H1 to the CAT gene-specific oligonucleotide CAT2 (Fig. 4.7). The composite primers were used in a PCR reaction to amplify the bacterial CAT gene to generate mimic DNA molecules that were used subsequently for the p444 construction.

4.3.2.1.2 Generation of mimic construct

Plasmid pBcxm (containing the bacterial CAT gene) was used as the template in the PCR amplification of mimic molecules. The PCR conditions were as follows: 1) 94° C, 5 min; 2) 30 cycles of 94°C, 40 s; 55°C, 20 s; 72°C, 40 s; 3) 72°C, 10 min. In the PCR, 1 ng of pBcxm DNA was amplified in the presence of 1.5 mM $MgCl_2$ PCR buffer, 1.2 μM composite primers MIMICL1 and MIMICH1, 2.0 units *Taq* polymerase (Sigma), 200 μM dNTP, in a total reaction volume of 20 μl.

The PCR products were resolved on a 1.5 % EtBr-stained agarose gel (Fig. 4.8). These bands were gel purified using the QIAquick Gel extraction kit (section 2.2.7) and cloned using the TOPO™ TA cloning kit (section 2.2.9). Plasmid DNA was isolated by the miniprep isolation procedure (Qiagen). The plasmid DNA was digested with *Eco*RI to release the insert to ensure that the correct DNA fragment had been cloned (Fig. 4.9). Confirmation of a selected colony containing recombinant DNA was also achieved by

(a)

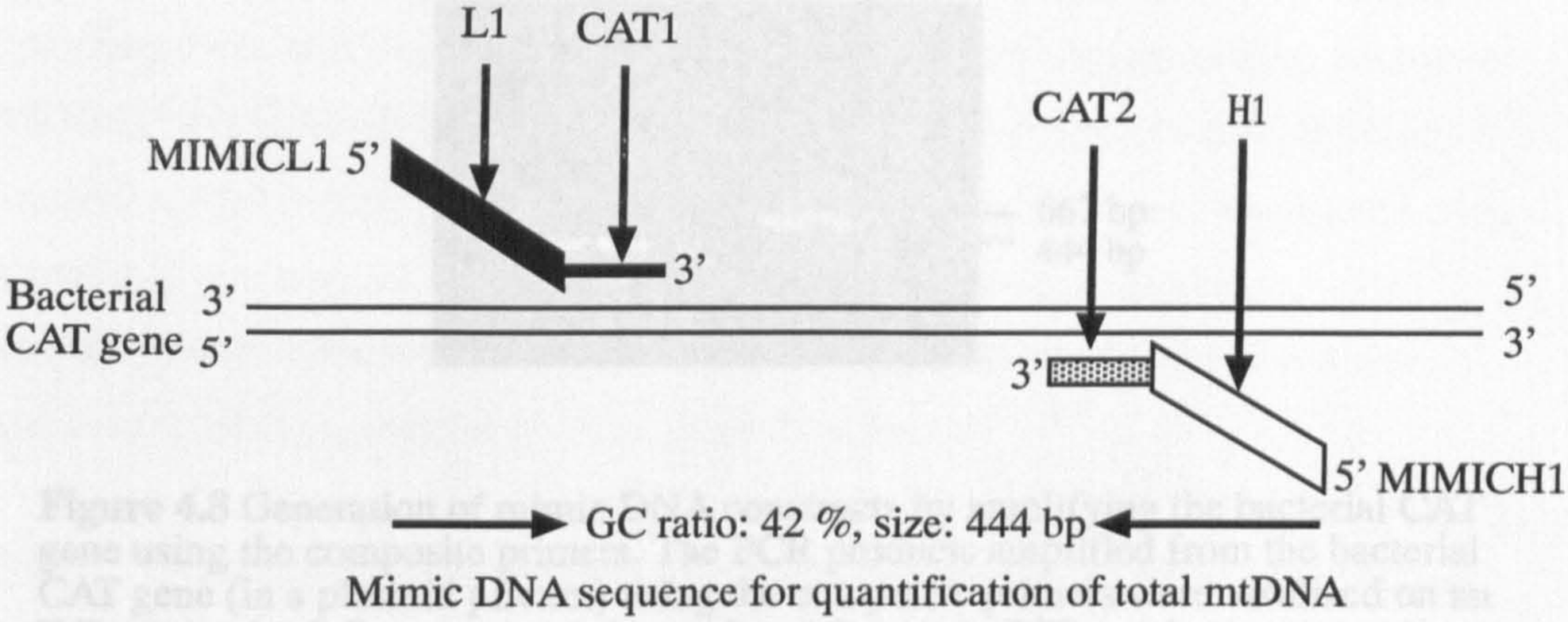

Mimic DNA sequence for quantification of total mtDNA

(b)

MIMICL1 primer sequence is:

5' CGCTCTACCTCACCATCTCTT AGAAGTTGTCCATATTGGCC 3'

L1 CAT1

MIMICH1 primer sequence is:

5' TGCTTACCTTGTTACGACTTA ATAACCAGACCGTTCAGCTG 3'

H1 CAT2

(c)

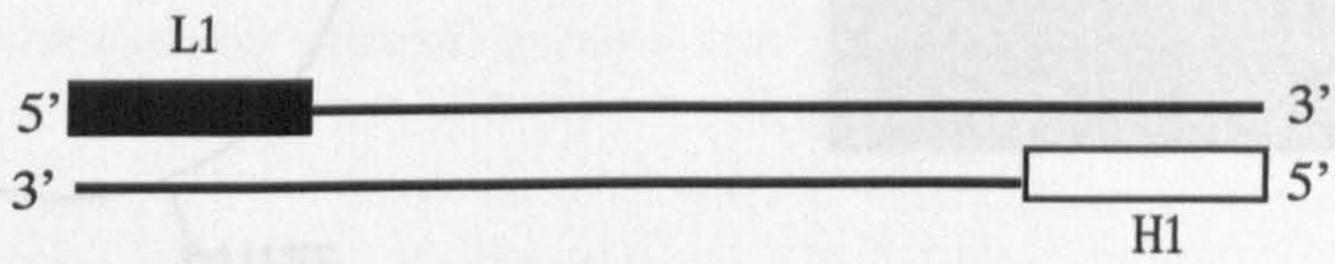

Intact mtDNA sequence amplified by L1 and H1 (GC ratio: 36 %, size:355 bp)

Figure 4.7 Selection of mimic DNA sequence and composite primers for quantifying total mtDNA content in mouse brain tissues. The composite primers (MIMICL1 and MIMICH1) were synthesized by attaching primer L1 to the CAT-gene specific oligonucleotide CAT1 and primer H1 to the CAT gene-specific oligonucleotide CAT2 (a and b). The GC ratio of the mimic DNA sequence is 42 % and the size is 444 bp (a). The GC ratio of the intact mtDNA sequence amplified by L1 and H1 is 36 % and the size is 355 bp (c).

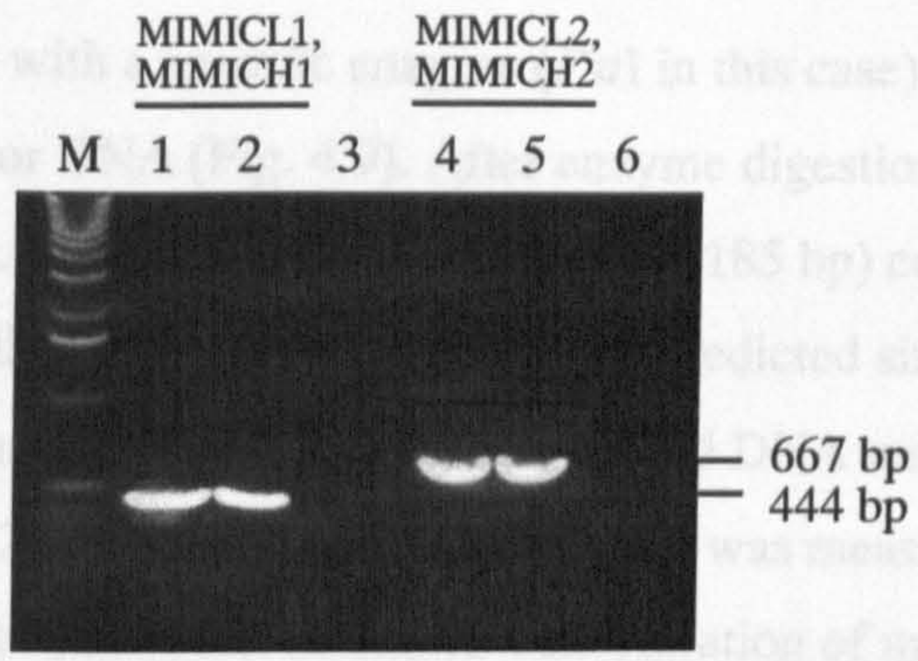

Figure 4.8 Generation of mimic DNA constructs by amplifying the bacterial CAT gene using the composite primers. The PCR products amplified from the bacterial CAT gene (in a plasmid pBcxm) using the composite primers were visulized on an EtBr-stained 1.5 % agarose gel. Lanes 1 and 2 contain PCR products using primers MIMICL1 and MIMICH1. Lanes 4 and 5 contain PCR products using primers MIMICL2 and MIMICH2. Lanes 3 and 6 are the controls for DNA contamination of PCR reagents using water as a template. The 1 Kb size ladder is indicated by M.

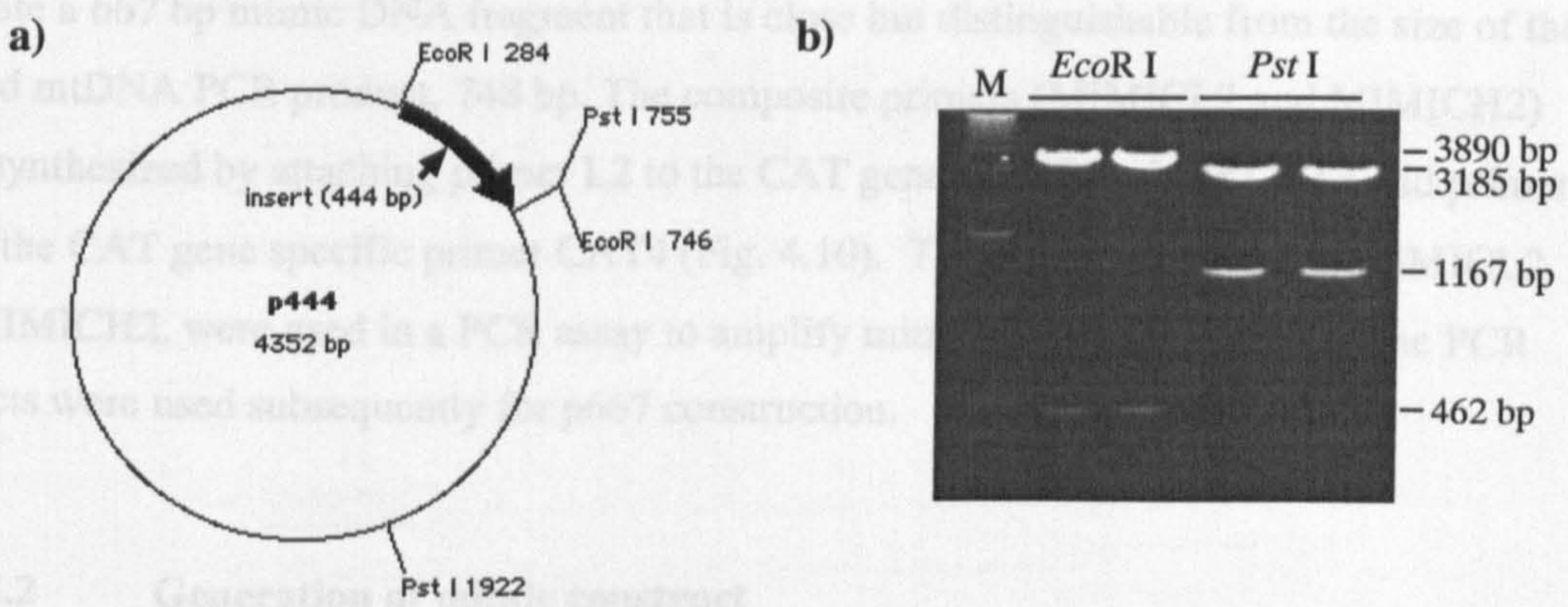

Figure 4.9 Confirmation of the recombinant plasmid p444. A restriction map of p444 shown in (a) illustrates the position of appropriate restriction enzyme recognition sites for *Eco*RI and *Pst*I. The thin line represents the vector Topo 2.1 (3808 bp). The thick line represents the 444 bp insert (arrow). *Eco*RI and *Pst*I-digested DNA from p444 DNA was resolved on an EtBr-stained agarose gel, shown in (b). The 462 bp DNA fragment, released from p444 digested with *Eco*RI is predicted to contain the 444 bp cloned insert. The 3185 bp DNA fragment, released from p444 DNA digested with *Pst*I, is predicted to contain the 444 bp cloned insert. The 1 Kb size ladder is indicated by M.

digesting the plasmid DNA with a specific enzyme (*Pst*I in this case) that has two recognition sites in the vector DNA (Fig. 4.9). After enzyme digestion, the DNA was cut into two fragments of DNA. The fragment (predicted size 3185 bp) containing the correct cloned insert will be larger than the equivalent fragment (predicted size 2641 bp) that comes from a non-recombinant plasmid (Fig. 4.9b). Plasmid DNA was midiprepped using a commercial kit (section 2.2.2.1) and its DNA concentration was measured by spectrophotometry. Thereafter, dilutions of known concentration of mimic DNA were prepared and used in the following competitive PCR assays.

4.3.2.2 Generation of mimic construct for quantifying levels of deleted mtDNA molecules in mouse tissue

4.3.2.2.1 Selection of mimic DNA sequence and composite primers

The DNA sequence of mimic p667 was chosen from the bacterial CAT gene according the principles described in section 4.2. The GC ratio of p667 was 44 % and the GC ratio of the target mtDNA sequence flanked by primers L2 and H2 was 39 %. Primers were selected to generate a 667 bp mimic DNA fragment that is close but distinguishable from the size of the deleted mtDNA PCR product, 748 bp. The composite primers (MIMICL2 and MIMICH2) were synthesized by attaching primer L2 to the CAT gene specific primer CAT3 and primer H2 to the CAT gene specific primer CAT4 (Fig. 4.10). The composite primers, MIMICL2 and MIMICH2, were used in a PCR assay to amplify mimic DNA molecules and the PCR products were used subsequently for p667 construction.

4.3.2.2.2 Generation of mimic construct

The PCR conditions for using primers MIMICL2 and MIMICH2 to amplify the mimic DNA sequence were the same as for using primers MIMICL1 and MIMICH1 (section 4.3.2.1.2). The PCR products were resolved on a 1.5 % EtBr-stained agarose gel and products of the expected sizes were observed (Fig. 4.8).

(a)

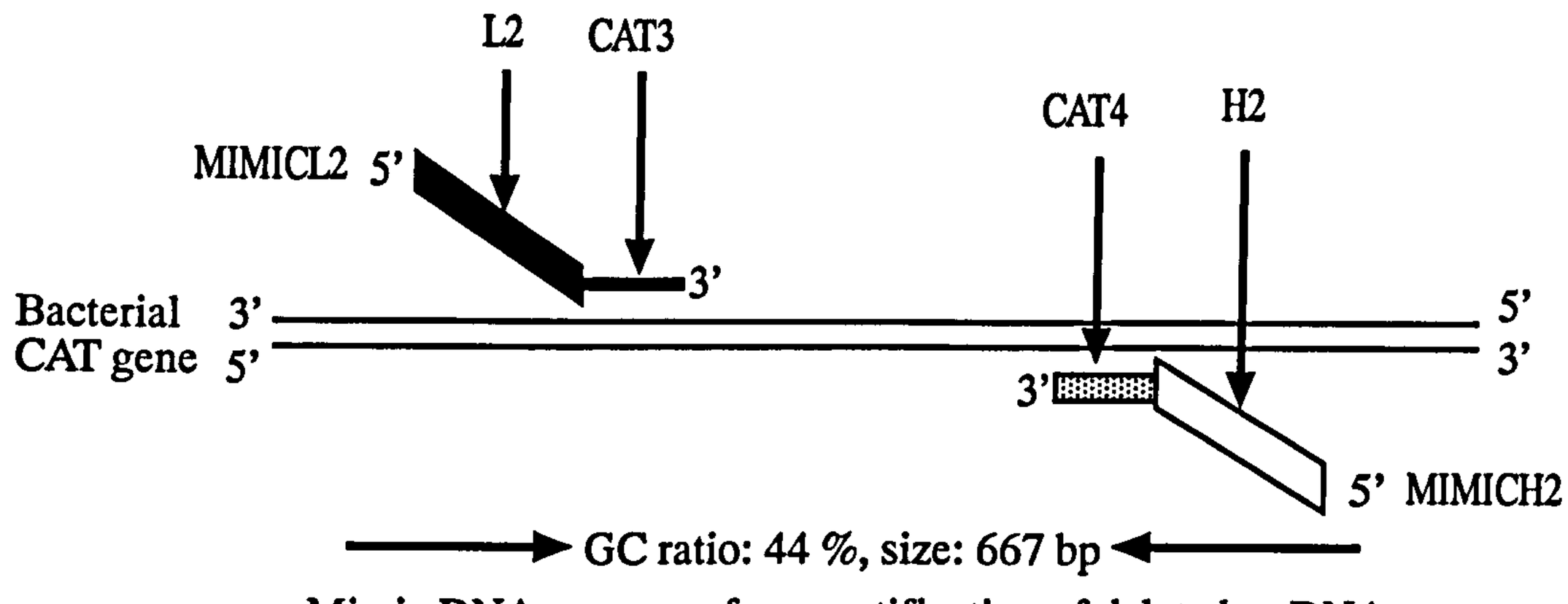

(b) MIMICL2 primer sequence is:

MIMICH2 primer sequence is:

(c)

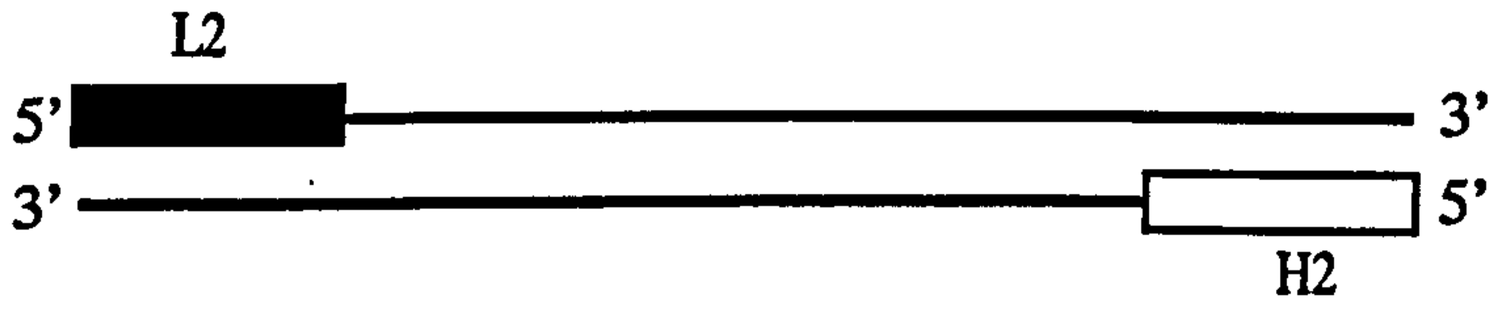

Deleted mtDNA sequence amplified by L2 and H2 (GC ratio: 39 %, size: 748 bp)

Figure 4.10 Selection of mimic DNA sequence and composite primers for quantifying deleted mtDNA molecules. The composite primers (MIMICL2) and MIMICH2) were synthesized by attaching primer L2 to the CAT-gene specific oligonucleotide CAT3 and primer H2 to the CAT-gene specific oligonucleotide CAT4 (a and b). The GC ratio of the mimic DNA sequence is 44 % and the size is 667bp (a). The GC ratio of the intact mtDNA sequence amplified by L2 and H2 is 39 % and the size is 748bp (c).

The procedures for generating mimic construct p667 were the same as for p444 (section 4.3.2.1.2) including the gel purification of PCR products, cloning, preparation of plasmid DNA, and confirmation of the correct insert in the plasmid clone (Fig. 4.11).

4.3.3 Optimising the quantitative competitive PCR assay for measuring mtDNA levels in mouse tissue

4.3.3.1 Determining the PCR conditions for measuring levels of total mtDNA molecules in mouse tissue

A prerequisite for obtaining quantitative data by competitive PCR is that both target and mimic DNA are co-amplified in the exponential phase of the amplification process and with similar amplification efficiencies. To ensure this, the kinetics of the competitive PCR amplification was determined. 10 ng of mouse liver DNA and 10 pg of p444 DNA template were amplified separately for up to 40 cycles using primers L1 and H1 that had been radio-labelled with [γ-^{32}P] ATP (section 2.2.11.2). 96 pmole of each radio-labelled primer was mixed with 504 pmole of non radio-labelled L1 and H1 and distributed evenly amongst 25 PCR tubes (12 tubes for p444 DNA amplification, 12 tubes for mouse liver DNA amplification and 1 tube for the control). The PCR conditions for amplification of mimic p444 were the same as for intact mtDNA amplification (section 2.2.5.2). Two of the PCR tubes (one from p444 amplification and one from liver DNA amplification) were removed every two cycles of the amplification process (between 18 to 40 cycles) and the products resolved on an EtBr-stained 2 % agarose gel (Fig. 4.12a). The radioactive gels were photographed, the appropriate bands excised and the radioactivity of each band quantified in a liquid scintillation counter (LS 5000 CE, Beckhman). The log of radioactivity for each band was plotted against the number of PCR cycles to show the exponential range of amplification efficiency for intact mtDNA and mimic p444 templates (Fig. 4.12b). The results showed that intact mtDNA and mimic p444 templates were co-amplified with a similar efficiency, within a linear range of between 18 and 24 cycles. According to these results, 24 cycles of PCR was chosen for subsequent competitive PCR assays to quantify total mtDNA levels in HD mice and wild type littermates.

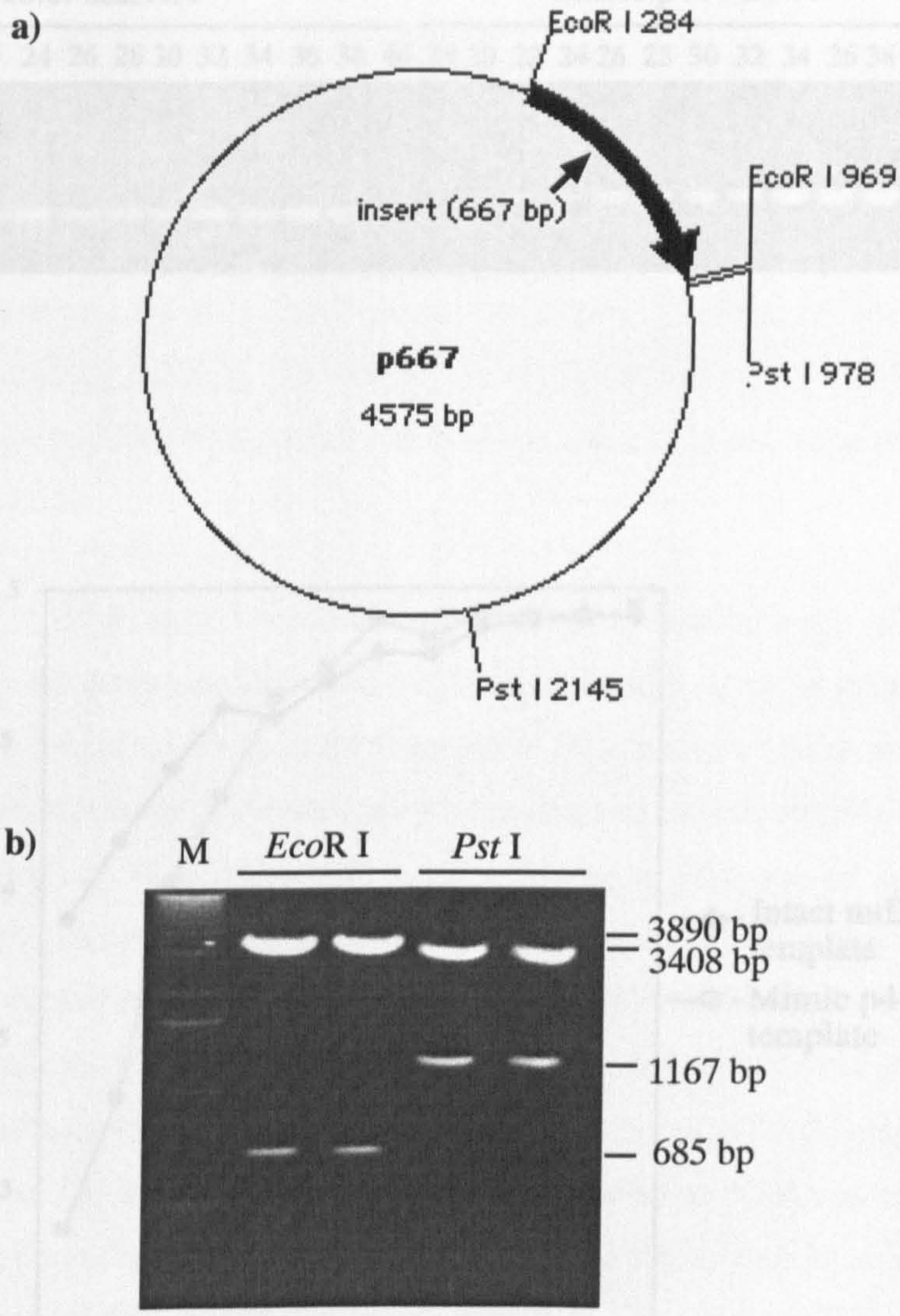

Figure 4.11 Confirmation of the recombinant plasmid p667. A restriction map of p667 shown in (a) illustrates the position of appropriate restriction enzyme recognition sites for *Eco*RI and *Pst*I. The thin line represents the vector Topo 2.1 (3808 bp). The thick line represents the 667 bp insert (arrow). *Eco*RI and *Pst*I-digested DNA from p667 DNA was resolved on an EtBr-stained agarose gel, shown in (b). The 685 bp DNA fragment, released from p667 digested with *Eco*RI is predicted to contain the 667 bp cloned insert. The 3408 bp DNA fragment, released from digesting p667 DNA with *Pst*I, is predicted to contain the 667 bp cloned insert. The 1 Kb size ladder is indicated by M.

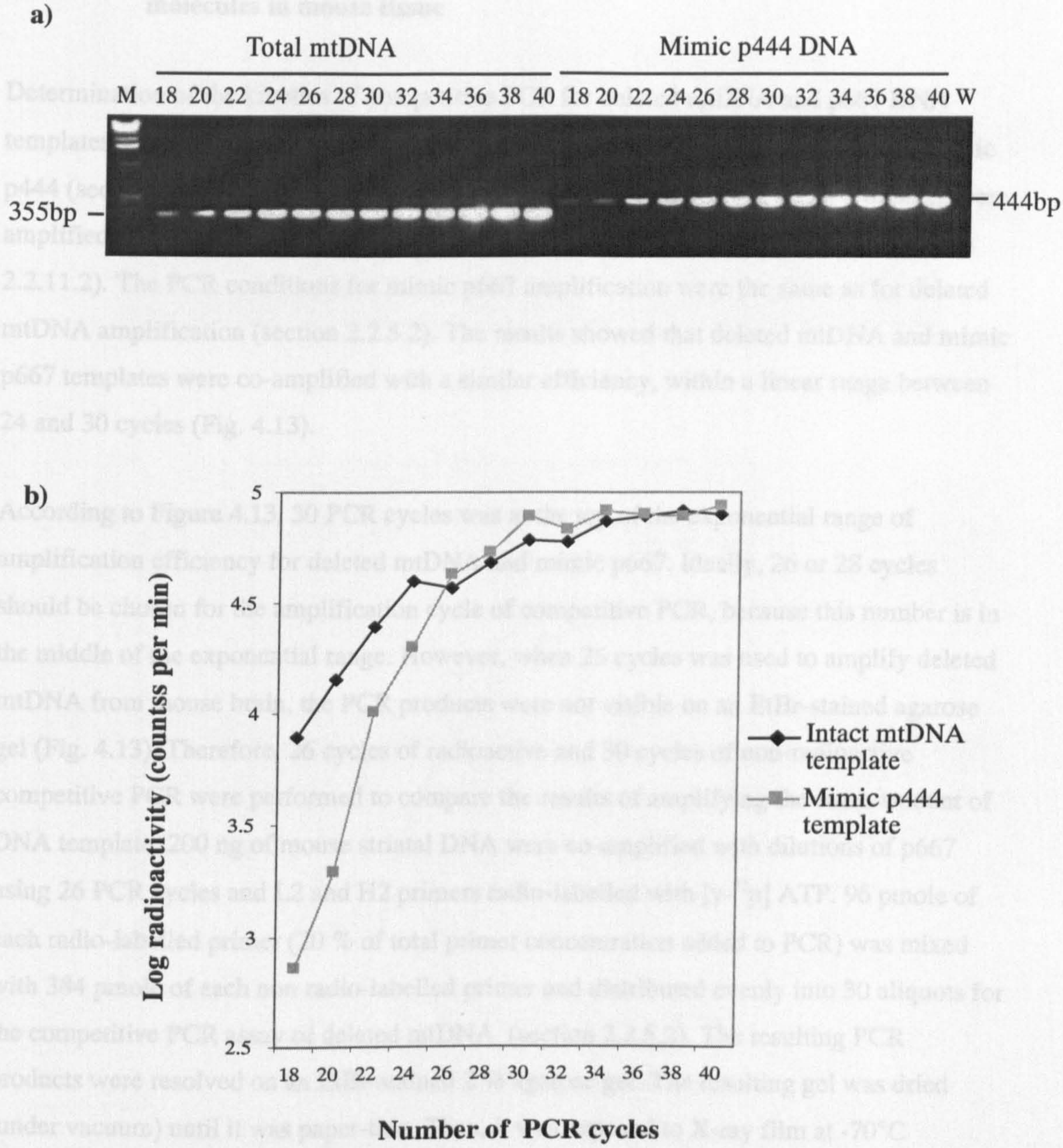

Figure 4.12 Kinetics of amplification of total mtDNA and mimic p444 molecules. Products of amplified total mtDNA and mimic p444 molecules after 18 to 40 cycles of PCR (numbers above the panel) were resolved on an EtBr-stained agarose gel shown in (a). W indicates the control for DNA contamination of PCR using water as a template. M indicates the 1 Kb size ladder. The plot (b) of log radioactivity of each band from the gel in (a) against number of PCR cycles shows that the linear range of PCR amplification for both total mtDNA and mimic p444 molecules is 18-24 cycles. 24 cycles was chosen in subsequent competitive PCR assays for quantification of total mtDNA levels.

4.3.3.2 Determining the PCR conditions for measuring levels of deleted mtDNA molecules in mouse tissue

Determination of the kinetics of competitive PCR for deleted mtDNA and p667 DNA templates was carried out using the same methods described for intact mtDNA and mimic p444 (section 4.3.3.1). 75 ng of mouse liver DNA and 150 fg of p667 DNA templates were amplified separately for up to 40 cycles using radio-labelled L2 and H2 primers (section 2.2.11.2). The PCR conditions for mimic p667 amplification were the same as for deleted mtDNA amplification (section 2.2.5.2). The results showed that deleted mtDNA and mimic p667 templates were co-amplified with a similar efficiency, within a linear range between 24 and 30 cycles (Fig. 4.13).

According to Figure 4.13, 30 PCR cycles was at the top of the exponential range of amplification efficiency for deleted mtDNA and mimic p667. Ideally, 26 or 28 cycles should be chosen for the amplification cycle of competitive PCR, because this number is in the middle of the exponential range. However, when 26 cycles was used to amplify deleted mtDNA from mouse brain, the PCR products were not visible on an EtBr-stained agarose gel (Fig. 4.13). Therefore, 26 cycles of radioactive and 30 cycles of non-radioactive competitive PCR were performed to compare the results of amplifying the same amount of DNA template. 200 ng of mouse striatal DNA were co-amplified with dilutions of p667 using 26 PCR cycles and L2 and H2 primers radio-labelled with [γ-^{32}p] ATP. 96 pmole of each radio-labelled primer (20 % of total primer concentration added to PCR) was mixed with 384 pmole of each non radio-labelled primer and distributed evenly into 30 aliquots for the competitive PCR assay of deleted mtDNA (section 2.2.5.2). The resulting PCR products were resolved on an EtBr-stained 2 % agarose gel. The resulting gel was dried (under vacuum) until it was paper-thin. Then, it was exposed to X-ray film at -70°C overnight in the presence of intensifying screens. The resulting autoradiograph was scanned and analysed (Fig. 4.14a). 30 cycles of non-radioactive competitive PCR assays were performed and the PCR products were resolved on an EtBr- stained gel (Fig. 4.14b). The results showed that the amount of deleted mtDNA quantified using the 30 cycles of competitive PCR reaction was similar to those using 26 cycles of competitive PCR. Based on this result, 30 cycles of PCR was subsequently used to quantify the amount of deleted

a)

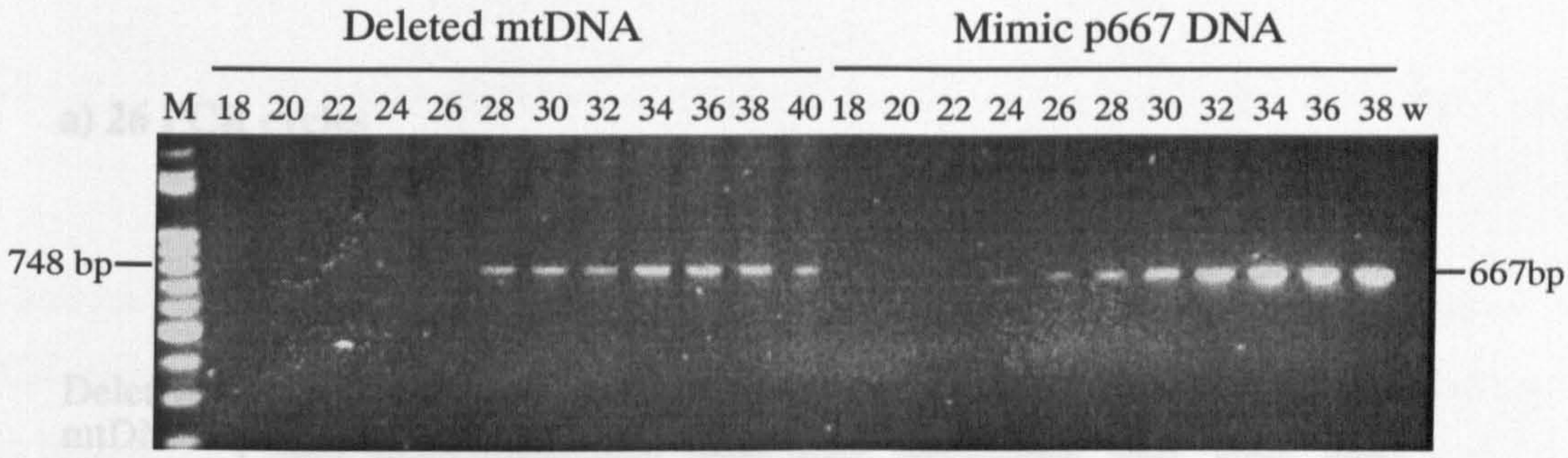

b)

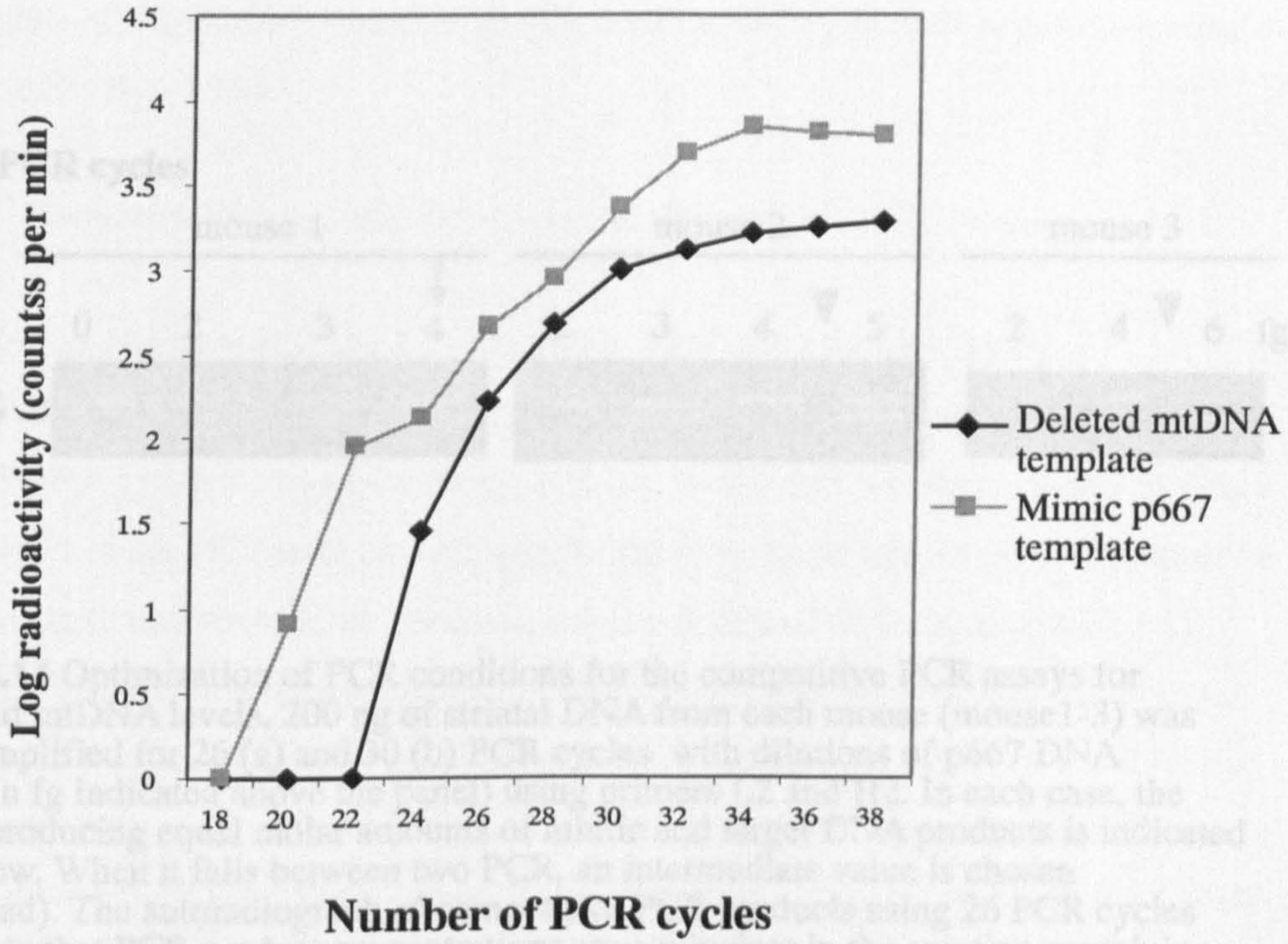

Figure 4.13 Kinetics of amplification of deleted mtDNA and mimic p667 molecules. Products of amplified deleted mtDNA and mimic p667 molecules after 18 to 40 cycles of PCR (numbers above the panel) were resolved on an EtBr-stained agarose gel shown in (a). W indicates the control for DNA contamination of PCR using water as a template. M indicates the 1 Kb size ladder. The plot (b) of the log radioactivity of each band from the gel in (a) against number of PCR cycles shows that the linear range of PCR amplification for both deleted mtDNA and mimic p667 molecules is 24-30 cycles.

a) 26 PCR cycles

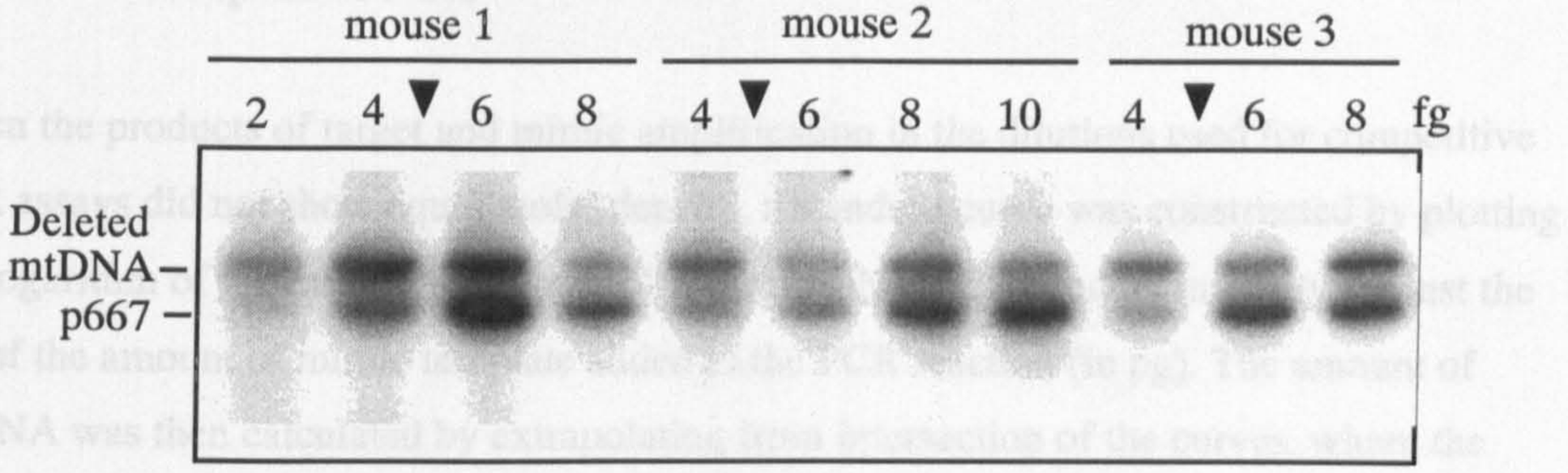

b) 30 PCR cycles

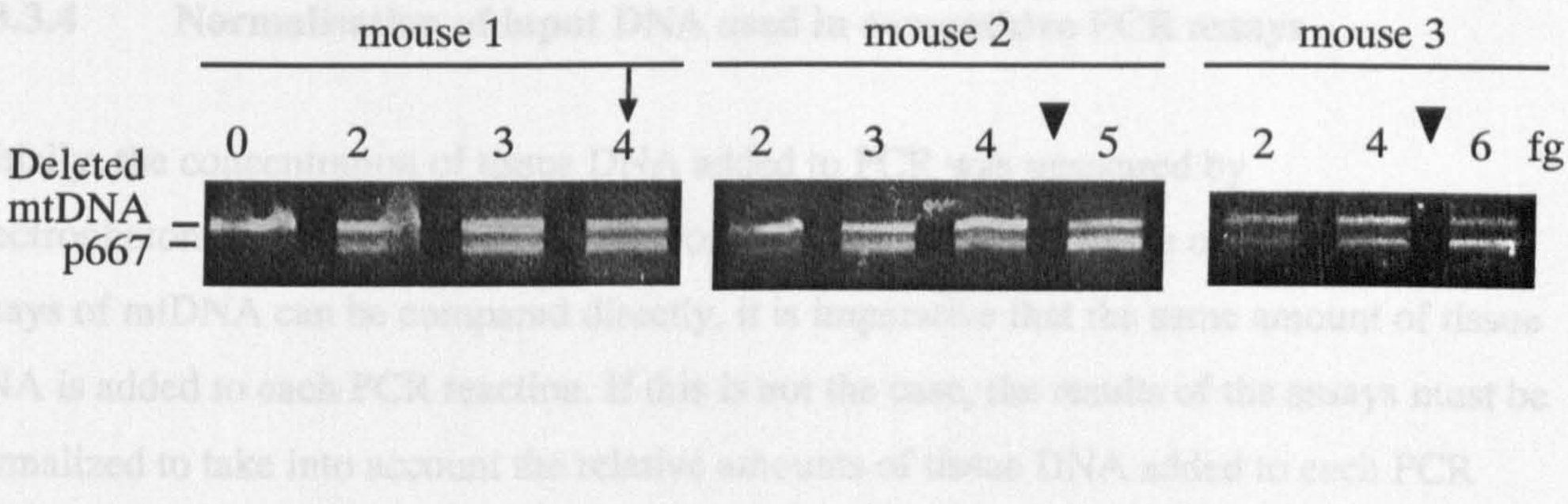

Figure. 4.14 Optimization of PCR conditions for the competitive PCR assays for the deleted mtDNA levels. 200 ng of striatal DNA from each mouse (mouse1-3) was was co-amplified for 26 (a) and 30 (b) PCR cycles with dilutions of p667 DNA (amount in fg indicated above the panel) using primers L2 and H2. In each case, the reaction producing equal molar amounts of mimic and target DNA products is indicated by an arrow. When it falls between two PCR, an intermediate value is chosen (arrow head). The autoradiograph of competitive PCR products using 26 PCR cycles (a) suggests that PCR product concentrations are equivalent in the reaction containing 5 fg of p667 in each case. The gel image of competitive PCR products using 30 PCR cycles (b) suggests that PCR product concentrations are equivalent in the reactions containing 4 (mouse1), 4.5 (mouse 2), and 5 (mouse 3) fg of p667 respectively. The amount of deleted mtDNA molecules in each mouse striatum obtained using 26 cycles of radioactive PCR and 30 cycles of non-radioactive PCR shows no significant difference and so 30 cycles of non-radioactive competitive PCR was used in subsequent competitive PCR assays so that products can be visualized on agarose gels.

mtDNA to enable visualization of the PCR products on agarose gels, thus avoiding the use of radioactivity.

4.3.3.3 Generating a standard curve for determining the levels of mtDNA by competitive PCR

When the products of target and mimic amplification in the dilutions used for competitive PCR assays did not show equal molar density, a standard curve was constructed by plotting the logarithm of the ratio of target mtDNA/mimic DNA PCR product intensity against the log of the amount of mimic template added to the PCR reaction (in pg). The amount of mtDNA was then calculated by extrapolating from intersection of the curves, where the molar amounts of target and competitor products are equal (log ratio of target/competitor = 0), to the x-axis (Fig. 4.15).

4.3.3.4 Normalisation of input DNA used in competitive PCR assays

Initially, the concentration of tissue DNA added to PCR was measured by spectrophotometry. In order that results from samples subjected to the competitive PCR assays of mtDNA can be compared directly, it is imperative that the same amount of tissue DNA is added to each PCR reaction. If this is not the case, the results of the assays must be normalized to take into account the relative amounts of tissue DNA added to each PCR tube. Therefore input DNA concentration was checked by Southern blot analysis of tissue DNA from each sample used in the study. Two single copy nuclear probes, 1.7 and N1.6, were used separately. Probe 1.7 is a 1.7 kb *Hin*dIII/*Sca*I fragment from upstream of the mouse *Hdh* gene (probe a in Figure 1 B of Shelbourne et al., 1999). Probe N1.6 is a 1.6 kb *Bss*HII fragment from a plasmid pmNN (a gift from Rosalind John, Wellcome/CRC institute, Cambridge, UK), which contains a 9 kb insert from the mouse neuronatin gene locus (Fig. 4.16).

All DNA samples subjected to competitive PCR assays in the study were digested with *Hin*dIII, transferred to a nylon membrane which was probed with N1.6 using methods described in section 2.2.12. The Southern blot analysis identified two fragments (3.7 kb and 2.3 kb) on autoradiographs (Fig. 4.17). Only the 3.7 kb fragment was used in subsequent

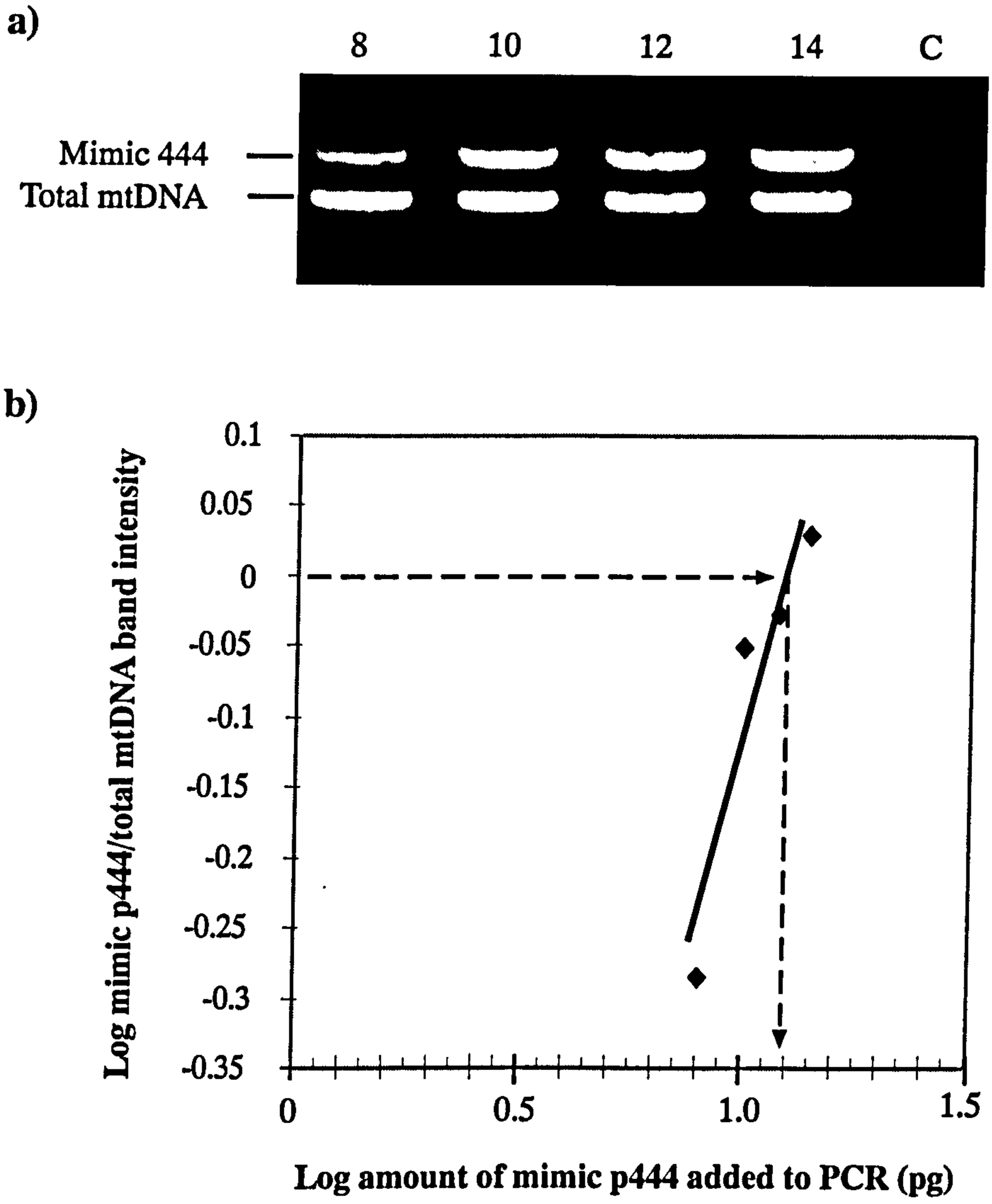

Figure 4.15 Determining mtDNA levels by competitive PCR from the constuction of a standard curve. PCR products of 5 ng tissue DNA co-amplified with dilutions of mimic p444 construct were resolved on an EtBr-stained agarose gel shown in (a). The concentration of mimic template added to each PCR tube is indicated by the numbers above the image (in pg). C indicates the control using water as a template for DNA contamination of PCR reagents. A standard curve (b) was generated from the data shown in (a) plotting log p444/total mtDNA band intensity of PCR products in each lane against log amount of p444 construct added to the PCR tube. In this case, the value extrapolating from the intersection of the curves where the molar amounts of target and competitor products are equal (log ratio of target/competitor = 0), to the x-axis is 1.1 (indicated by arrows). Therefore, the amount of p444 template added in the competitive PCR assay, where the PCR product amounts from p444 and from total mtDNA are equal, is 12.6 pg. Since 1 pg of p444 contains 4.24×10^5 molecules, the amount of total mtDNA present in this PCRtube is 5.34×10^6 molecules.

a)

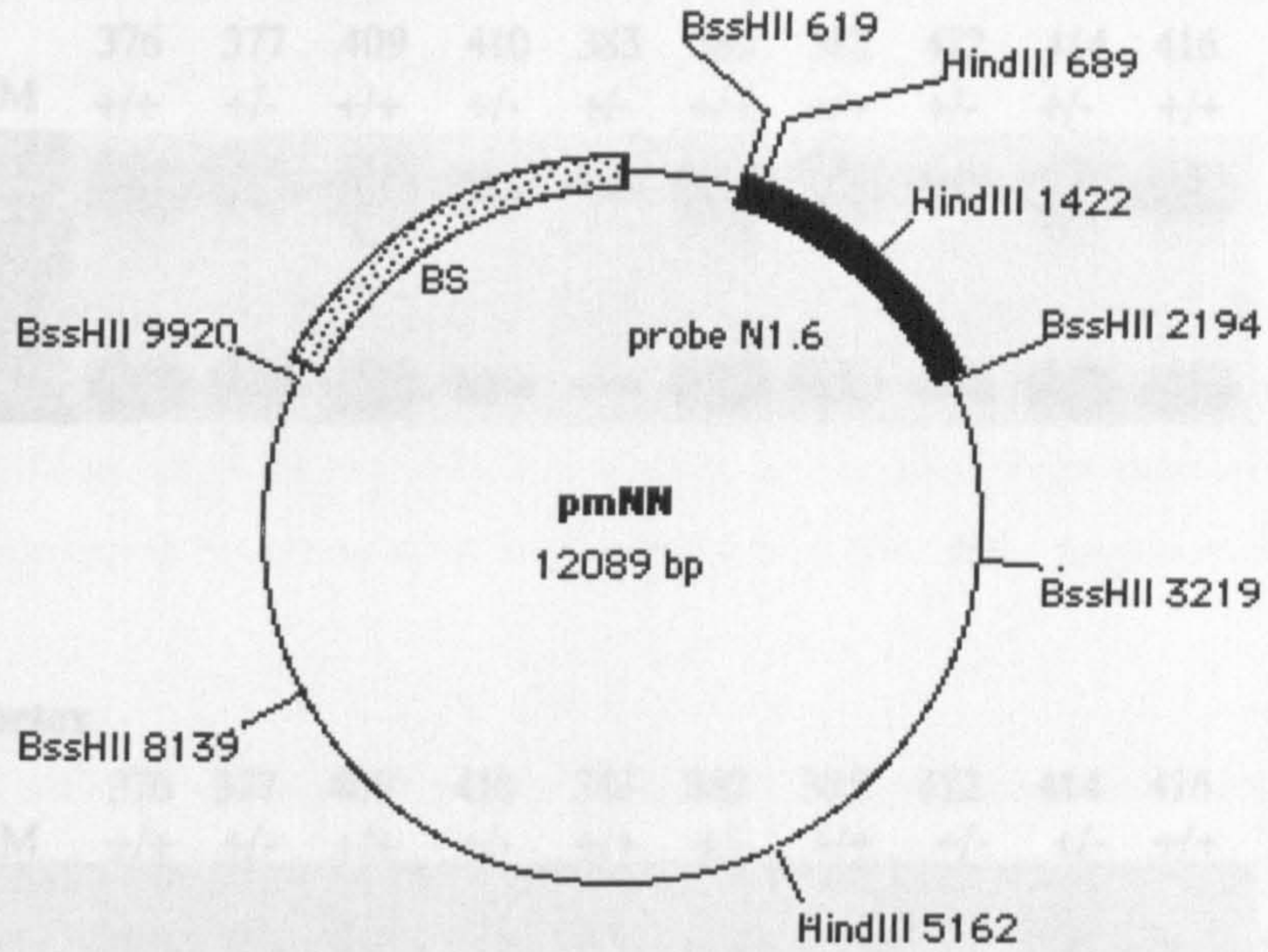

b)

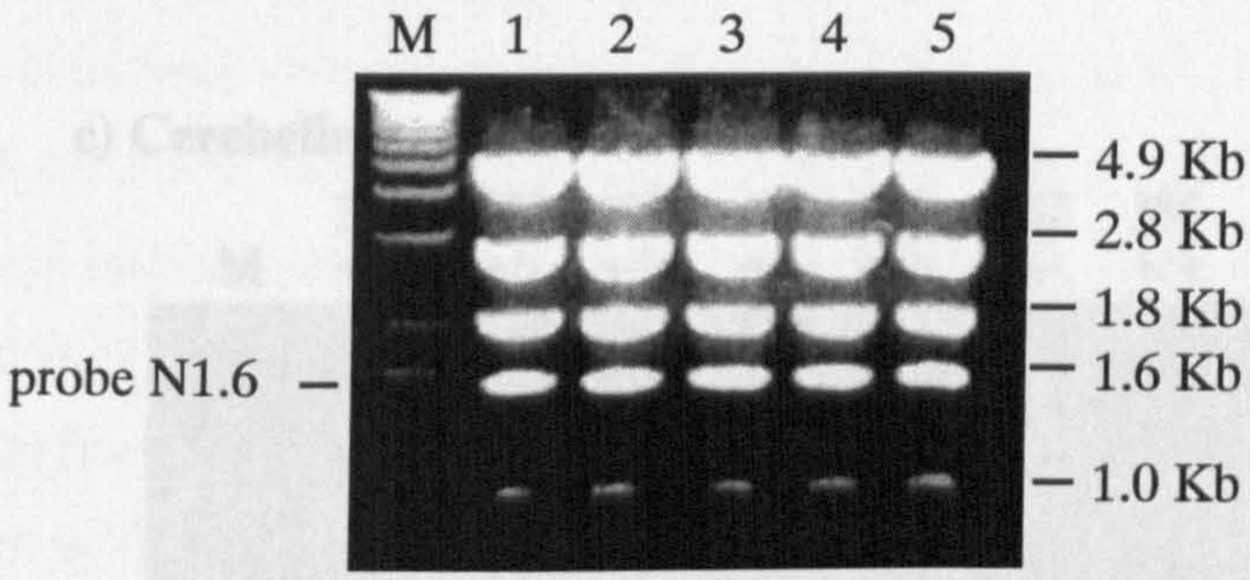

c)

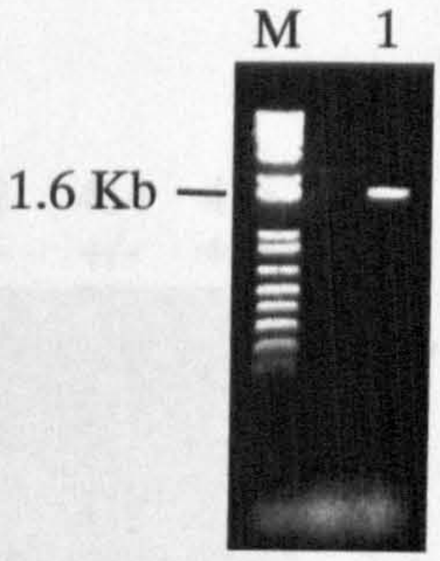

Figure 4.16 Generation of probe N1.6 for normalising input DNA in competitive PCR assays. The plasmid pmNN shown in (a) contains 9128 bp of mouse genomic DNA from the neuronatin locus (represented by thin line) cloned into vector pBluescript (represented by ▭). Probe N1.6 is a 1575 bp fragment (▬) released by digesting the plasmid DNA with *Bss*HII. The predicted DNA fragments generated from digestion of plasmid mNN with *Bss*HII were visualized on an EtBr-stained agarose gel in (b). Lanes 1-5 contain digested DNA from 5 reactions. The 1.6 Kb DNA bands were excised, gel purified and 4 µl (~25 ng) of gel purified N1.6 resolved on an EtBr-stained agarose gel in (lane 1, c). 4 µl of N1.6 was used in the Southern blot analysis for normalisation of input DNA. The 1 Kb plus size ladder is indicated by M.

a) Striatum

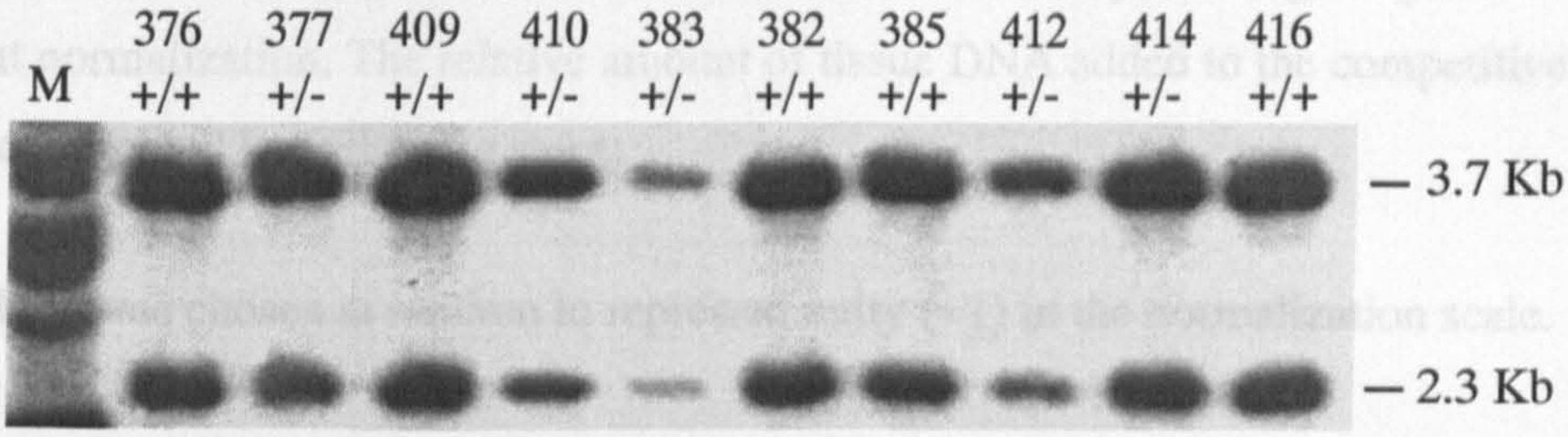

b) Cortex

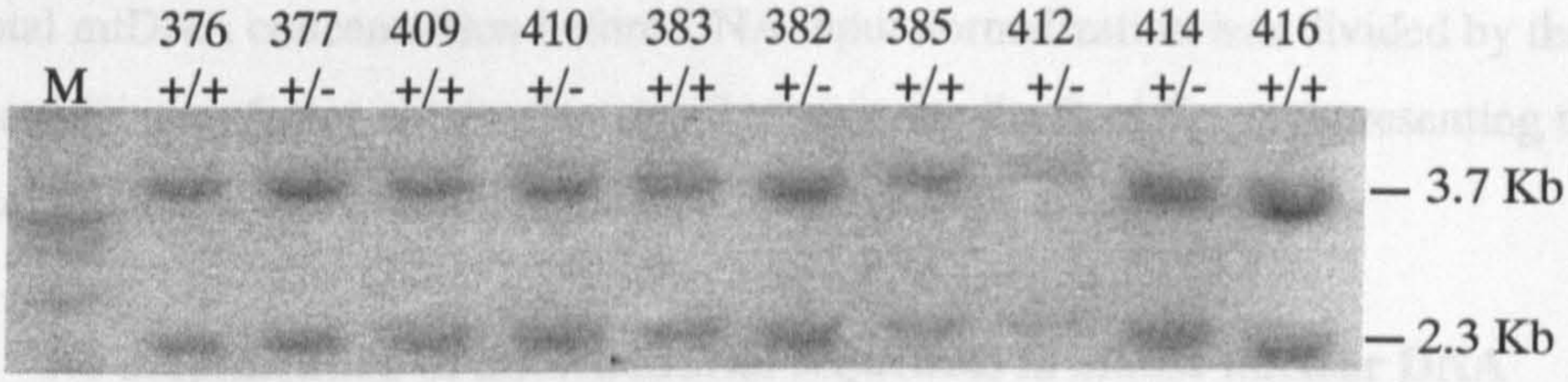

c) Cerebellum

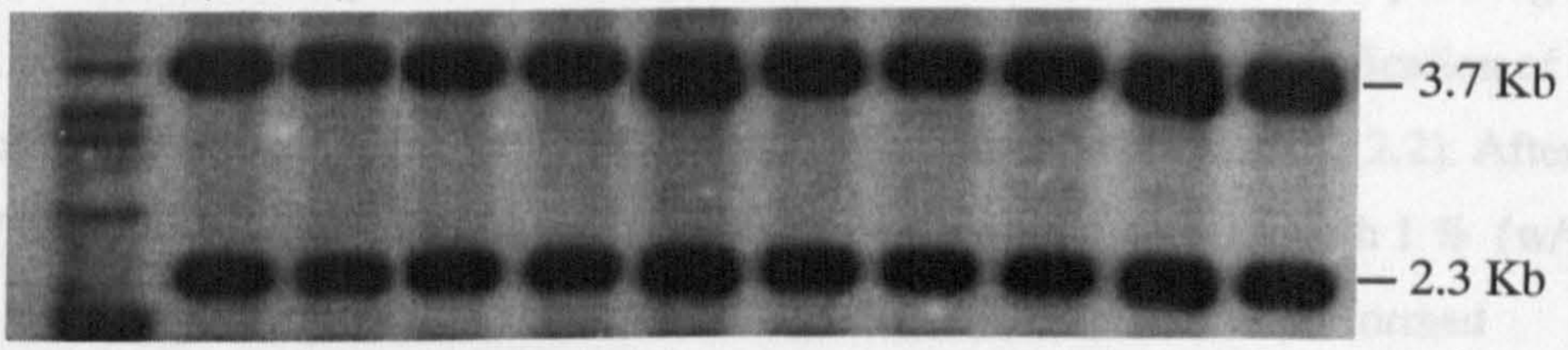

Figure 4.17 Normalization of input DNA added to competitive PCR assays. Images of autoradiographs from the Southern blot analysis (probed with N1.6) of striatal DNA (a), cortical DNA (b) and cerebellar DNA (c) from 5 HD (+/-) and 5 wild-type littermates (+/+). Each lane contains 5 μg of tissue DNA measured by spectrophotometry except from striata of mouse 382, 385, 412, 414, 416 (12.5 μg was loaded into each lane). Numbers above the image indicate animal ID. The 1 Kb plus size ladder is indicated by M.

normalization of input DNA. The resulting blot of all DNA samples from striatum, cortex and cerebellum of mice used in the study is shown in Figure 4.17. The same DNA samples from striatum were also subjected to a second Southern blot analysis using the probe 1.7 for DNA input normalization. The relative amount of tissue DNA added to the competitive PCR was determined by following steps:

1) A lane was chosen at random to represent unity (=1) in the normalization scale.

2) Normalization factors for all other samples on the same membrane were determined by comparing the intensity of the fragment with that of the fragment chosen in step 1.

3) Total mtDNA concentration before DNA input normalization was divided by the normalization factor obtained in step 2 to generate the final figure representing the total mtDNA concentration in each competitive PCR assay sample.

4.3.3.5 No amplification of mitochondrial sequences in mouse nuclear DNA

The presence of nuclear pseudogenes corresponding to the mtDNA fragments in rho zero (ρ°) cells have been reported previously (Michikawa et al., 1999). If mtDNA pseudogenes were present in the nucleus and varied between samples, this could affect the quantification of total mtDNA in this study. Therefore it was important to determine whether pseudogenes yield PCR products with the mtDNA-specific primers used in this study. Purification of cell nuclei from mouse brain was performed using methods described (section 2.2.2.2). After the absence of contaminating cytoplasm was confirmed by staining the nuclei with 1 % (w/v) methylene blue (Fig. 4.18), DNA extraction from purified cell nuclei was performed (section 2.2.2.2). Dilutions of purified nuclear DNA from mouse brain were amplified with *Hdh* specific primers MHD 16 and MHD 18 (section 2.2.5.3) to demonstrate the presence of nuclear DNA. The resulting amplification products were visible on an EtBr-stained agarose gel (Fig 4.19). In contrast, when the same amount of purified nuclear DNA was amplified with the mtDNA specific primers L1 and H1 (section 2.2.5.2), no products were visible on the EtBr-stained agarose gel (Fig. 4.19). The amplification of similar amounts of total DNA with L1 and H1 primers (section 2.2.5.2) were also included as positive controls (Fig. 4.19).

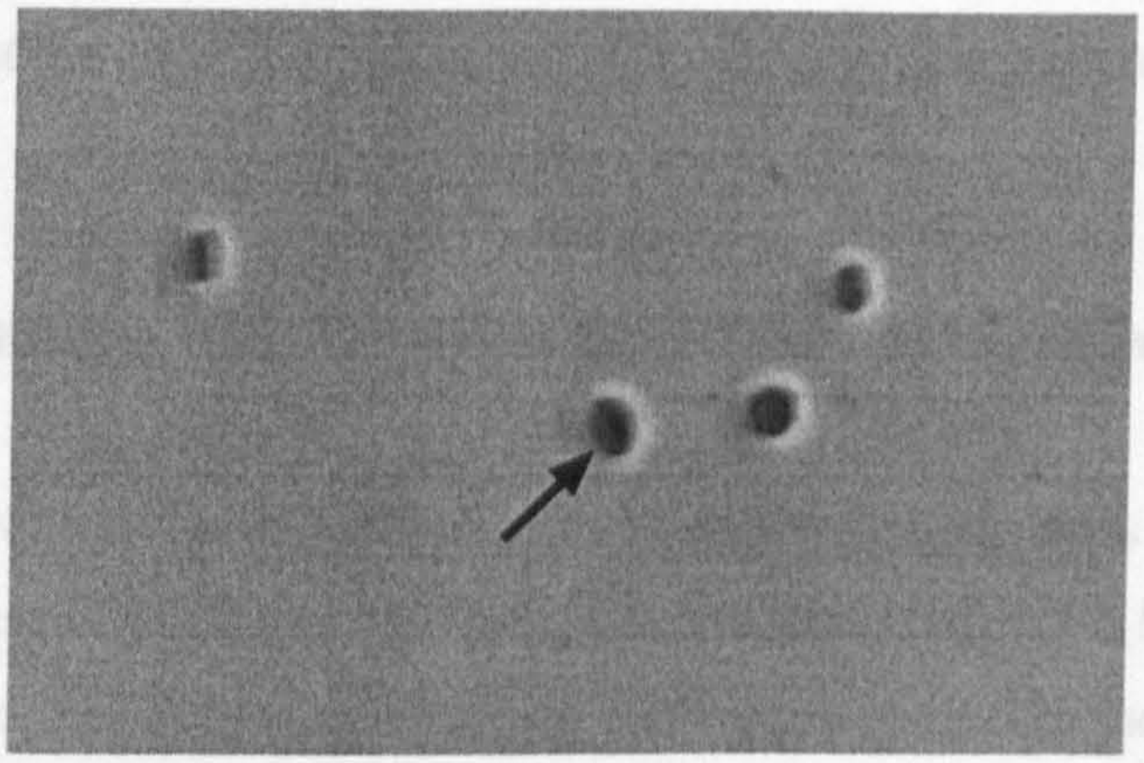

Figure. 4.18 Obtaining nuclear DNA to check for the presence of mtDNA pseudogenes. Purified mouse neuronal nuclei were stained with 1 % methylene blue. No cytoplasmic membrane adhering to the outside of the nucleus (arrow) was visible, indicating that the purified nuclei are free of contaminating cytoplasm and, by inference, mitochondria. Magnification: x400.

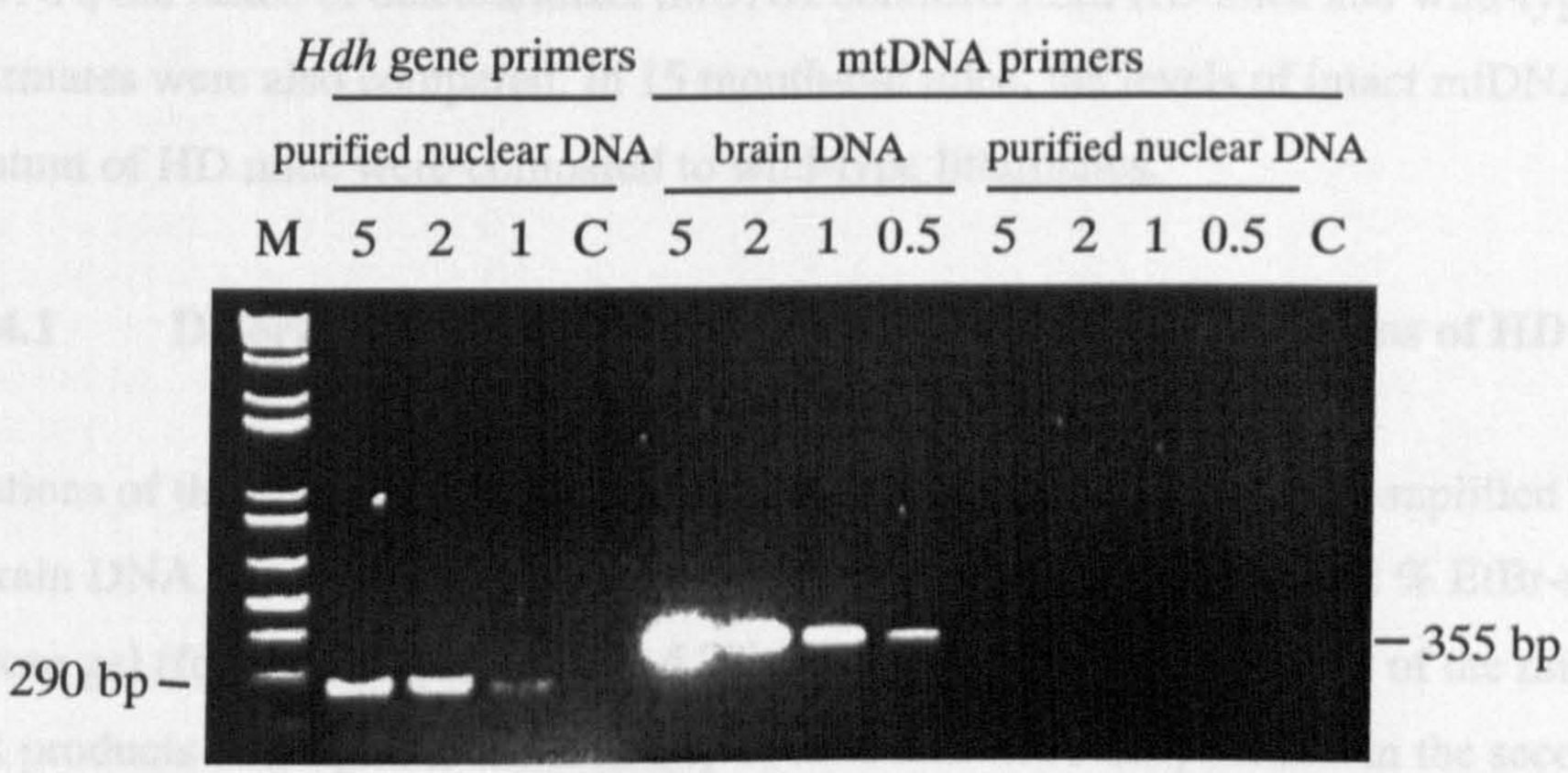

Figure 4.19 Lack of visible products after amplification of purified nuclear DNA with mtDNA specific primers. Different amounts of purified nuclear DNA were amplified with mouse *Hdh* gene-specific primers (MHD 16 and MHD18) and PCR products are visible. In contrast, when purified nuclear DNA is amplified with mtDNA specific primers (L1 and H1), PCR products are not visible. However, when brain DNA is amplified with primers L1 and H1, PCR products are very abundant. The 1 Kb plus size ladder is indicated by M. C indicates the control for DNA contamination of PCR reagents, using water as a template. The numbers above the image represent the amount of DNA (in ng) added to each PCR tube.

The results revealed that if present, nuclear mtDNA pseudogenes in mouse brain were unlikely to affect the quantification of mtDNA using the competitive PCR assay described in this study.

4.3.4 Determining mtDNA levels in HD mouse brain regions

Mitochondrial DNA levels in 6 HD mice and 6 wild-type littermates (section 2.1.18) at 24-28 months of age and 4 HD and 4 wild-type littermates (section 2.1.18) at 15 months of age were investigated. The cortex, striatum and cerebellum from each mouse brain were harvested and DNA purified using phenol/chloroform extraction (section 2.2.1). Quantification of mtDNA species in all samples was performed in duplicate and the mean value of the duplicate was used in subsequent statistical analyses using the Student's *t* test (two-tailed, paired). In 24 month-old mice the following comparisons were performed: 1) The levels of intact mtDNA in striatum, cortex and cerebellum of HD mice compared to wild-type littermates; 2) The levels of deleted mtDNA in striatum of HD mice compared to wild-type littermates; 3) As total mtDNA may influence the absolute levels of deleted mtDNA, the ratios of deleted/intact mtDNA obtained from HD mice and wild-type littermates were also compared. In 15 month-old mice, the levels of intact mtDNA in the striatum of HD mice were compared to wild-type littermates.

4.3.4.1 Determining total mtDNA levels in different brain regions of HD mice

Dilutions of the mimic p444 construct (5, 7.5, 10, 12.5, 15 pg) were co-amplified with 5 ng of brain DNA from each mouse, and PCR products were resolved on a 2 % EtBr-stained agarose gel (for an example see Fig. 4.20). In this example, the intensity of the mimic p444 PCR products was equal to the intensity of total mtDNA PCR products in the second lane. Since the concentration of mimic p444 added to this PCR assay was 7.5 pg and 1 pg of p444 contains 4.24×10^5 molecules, the amount of total mtDNA in this PCR was 3.18×10^6 molecules. If a series of dilutions failed to produce a lane where both bands were of equal intensity, the amount of mtDNA present was calculated as described in section 4.3.3.3.

The level of total mtDNA in striatum from 6 HD mice and 6 littermates at 24 months of age

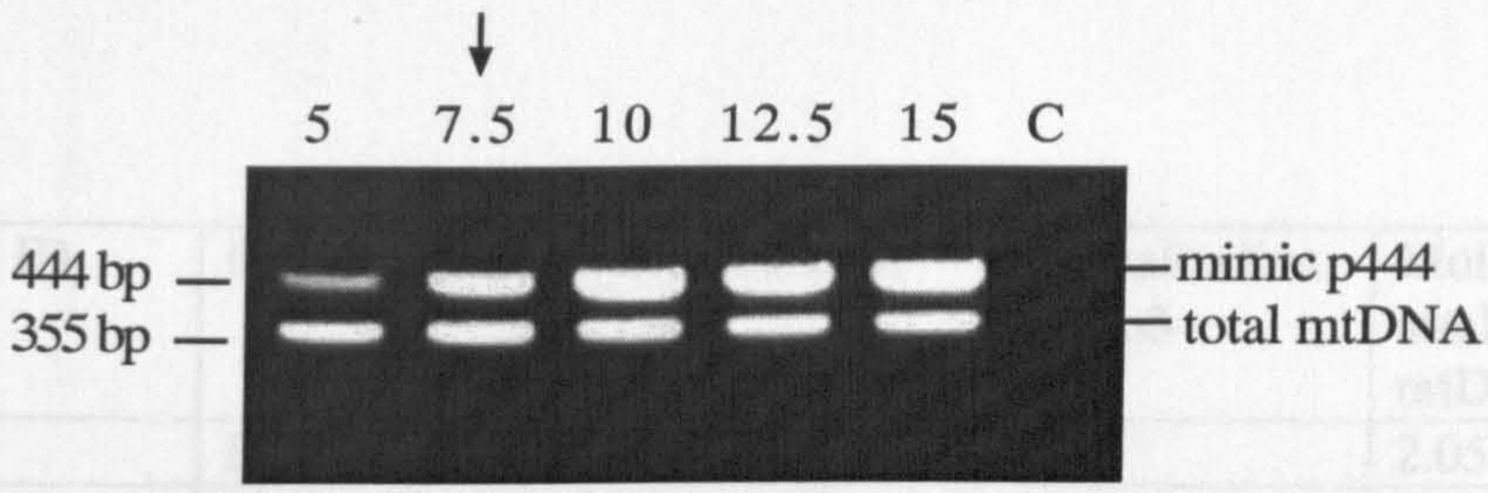

Figure 4.20 An example of amplifying total mtDNA levels in mouse brain tissue. A constant amount of cerebellar DNA (5 ng) was co-amplified with dilutions of p444 DNA [amount (in pg) added to each reaction indicated by the numbers above the panel]. and the products visualized on an EtBr stained agarose gel. The gel shows the intensity of the two bands, representing the products of mimic p444 and total mtDNA, are equal in the second lane. The number of total mtDNA templates is approximately equal to the number of p444 templates added to this PCR tube ie 7.5 pg (arrow). 1 pg of mimic p444 contains 4.24×10^5 molecules. Therefore, the amount of tortal mtDNA present in this PCR is 3.18×10^6 molecules. C indicates the control for DNA contamination of the PCR reagents, using water as a template.

before and after normalization of input tissue DNA (see section 4.3.3.4) is shown in Table 4.1 and Figure 4.21. The results of statistical analysis using data before normalization of input tissue DNA show that total mtDNA in the striatum of HD mice at 24 months of age is significantly decreased when compared to wild-type littermates. After normalization of input DNA using probes N1.6 and 1.7, total mtDNA in the striatum of HD mice at 24 months of age still showed a significant reduction when compared to wild-type littermates. The ~ 30 % reduction of total mtDNA was confined to striatum, since it was not detected in the cortex or cerebellum of HD mice (Table 4.2).

Animal ID	Genotype	Molecules of total mtDNA/5ng◗	Normalisation factor♣	Molecules of total mtDNA/5ng¶
383	HD	1.27×10^6	0.62	2.05×10^6
377	HD	2.54×10^6	2.36	1.08×10^6
410	HD	2.54×10^6	1.8	1.41×10^6
412	HD	0.85×10^6	0.59	1.44×10^6
414	HD	2.12×10^6	1.13	1.88×10^6
376	Wild-type	4.67×10^6	2.65	1.76×10^6
382	Wild-type	2.97×10^6	1	2.97×10^6
385	Wild-type	2.33×10^6	0.91	2.56×10^6
409	Wild-type	5.51×10^6	2.57	2.14×10^6
416	Wild-type	2.54×10^6	1.01	2.53×10^6

Table 4.1 Levels of total mtDNA in striatum of mice at 24 months of age.
◗ indicates that 5 ng of input tissue DNA was determined by spectrophotometry. ¶ indicates 5 ng of input tissue DNA after normalization by Southern blot analysis. Normalization factors for input tissue DNA as determined by Southern blot analysis (section 4.3.3.4) are indicated in column labelled ♣.

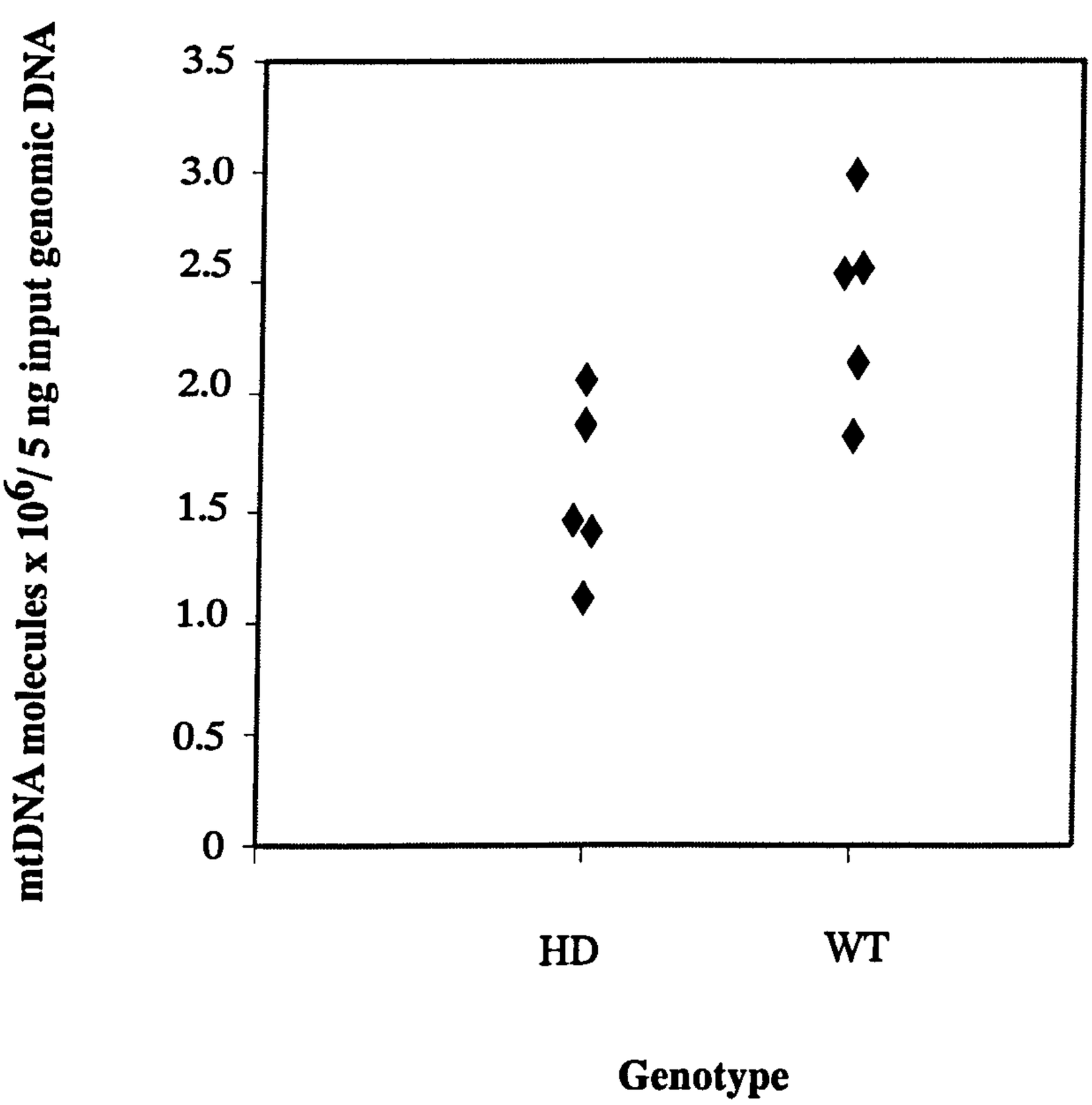

Figure 4.21 Scatter plot of total mtDNA levels (normalised for input tissue DNA) in the striatum of 24-month old HD mice (HD) and wild-type littermates (WT).

a) Striatum

	Wild-type (n=5)	HD (n=5)	*p* value
Total mtDNA molecules × 10^6/5 ng input tissue DNA	2.39 ± 0.2	1.57 ± 0.17	**0.016**

b) Cortex

	Wild-type (n=5)	HD (n=5)	*p* value
Total mtDNA molecules × 10^6/5 ng input tissue DNA	4.76 ± 0.45	3.67 ± 0.5	0.15

c) Cerebellum

	Wild-type (n=5)	HD (n=5)	*p* value
Total mtDNA molecules × 10^6/5 ng input tissue DNA	4.88 ± 0.5	4.85 ± 0.09	0.95

Table 4.2 Levels of mtDNA in striatum (a), cortex (b) and cerebellum (c) of 24 month-old mice (corrected for amount of tissue DNA added to the PCR tube).
Total mtDNA in the striatum of HD mice at 24 months of age is significantly decreased compared to wild-type littermates ($p < 0.02$). The reduction of total mtDNA is detected in the striatum but not cortex or cerebellum of HD mice. Comparisons were made using Student's *t*-test (two tailed). All values of total mtDNA are stated as mean ± SE.

In order to ascertain whether the striatal depletion of mtDNA is a progressive phenomenon, levels of total mtDNA in the striatum of HD mice at 15 months of age were investigated. Levels of total mtDNA in the striatum of 4 HD mice and 4 wild-type littermates at 15 months of age, before and after normalization of input DNA are shown in Table 4.3 and Figure 4.22. The results show that HD mice at 15 months of age do not have detectable differences in total mtDNA in the striatum when compared to wild-type littermates (Table 4.4). Total mtDNA levels in the striatum of HD mice and littermates at 24 months of age are significantly reduced when compared to the corresponding groups of mice at 15 months of age (Fig. 4.23). However, the DNA extraction from 15 and 24 month-old mice were not performed at the same time, which might introduce error to the differences in the total mtDNA in mouse striatum between these two time points. Therefore, further experiment is needed to confirm the result.

Animal ID	Genotype	Molecules of total mtDNA/5ng◗	Normalisation factor♣	Molecules of total mtDNA/5ng¶
788	HD	6.57	1.16	5.66
793	HD	4.24	0.93	4.56
795	HD	2.97	0.7	4.24
7104	HD	2.33	0.48	4.86
791	Wild-type	6.36	1.15	5.53
794	Wild-type	4.67	1	4.66
796	Wild-type	5.51	1.1	5.00
7101	Wild-type	4.03	1.07	3.77

Table 4.3 Levels of total mtDNA in striatum of mice at 15 months of age.
◗ indicates that 5 ng of input tissue DNA was determined by spectrophotometry. ¶ indicates 5 ng of input tissue DNA after normalization by Southern blot analysis. Normalization factors for input tissue DNA as determined by Southern blot analysis (section 4.3.3.4) are indicated in column labelled ♣.

	Wild-type (n=4)	HD (n=4)	*p* value
Total mtDNA molecules (striatum) × 10^6/5 ng input tissue DNA	4.74 ± 0.37	4.83 ± 0.31	0.86

Table 4.4 Comparison of total mtDNA levels in the striatum of 15 month-old HD mice and wild-type littermates (corrected for amount of tissue DNA added to the PCR tube).
No significant difference was found in total mtDNA levels in the striatum of HD mice when compare to their wild-type littermates. Comparisons were made using Student's *t*-test (two tailed). All values of total mtDNA are stated as mean ± SE.

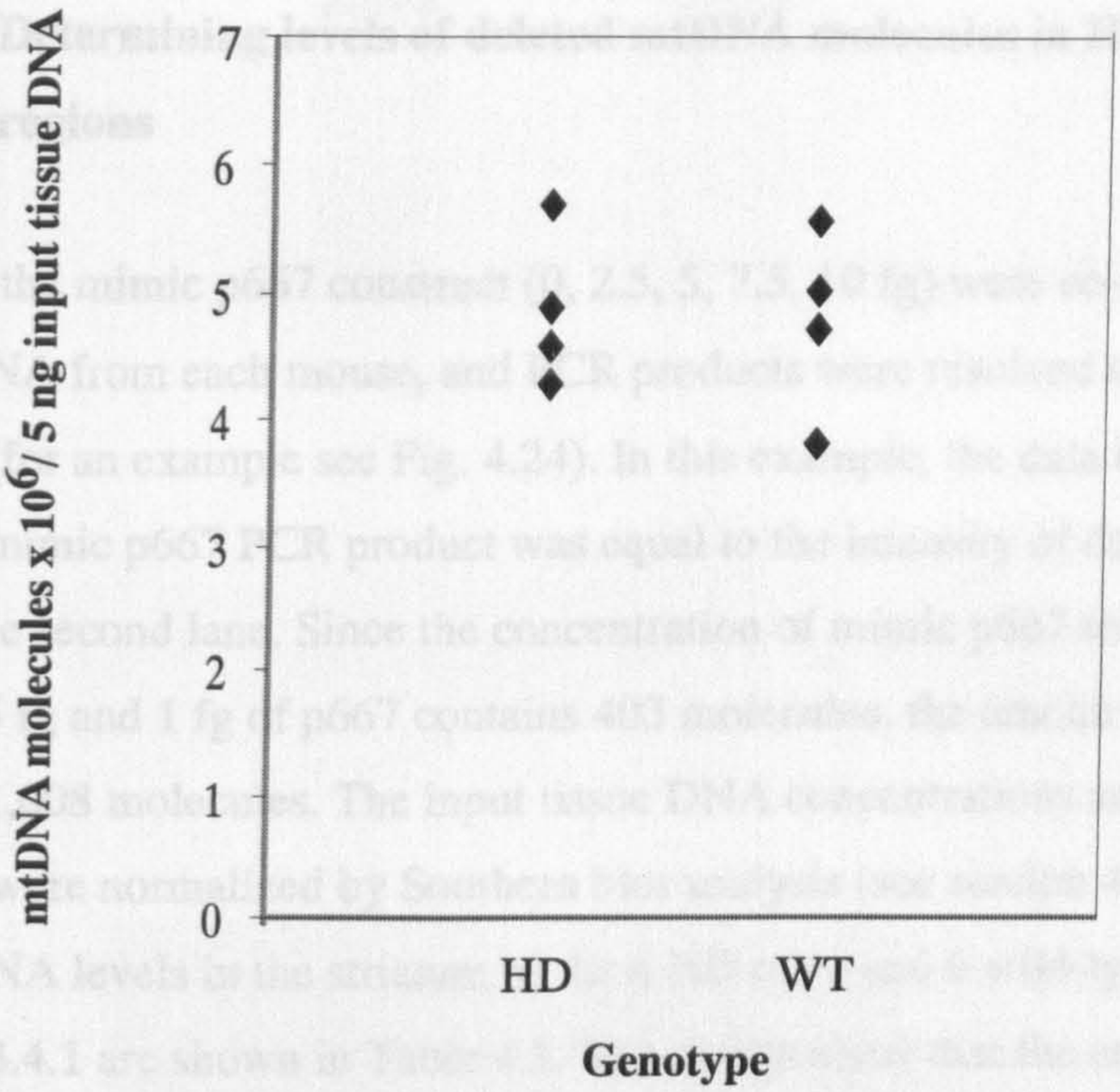

Figure 4.22 Scatter plot of total mtDNA levels (normalised for input tissue DNA) in the striatum of 15 month-old HD mice (HD) and wild-type littermates (WT).

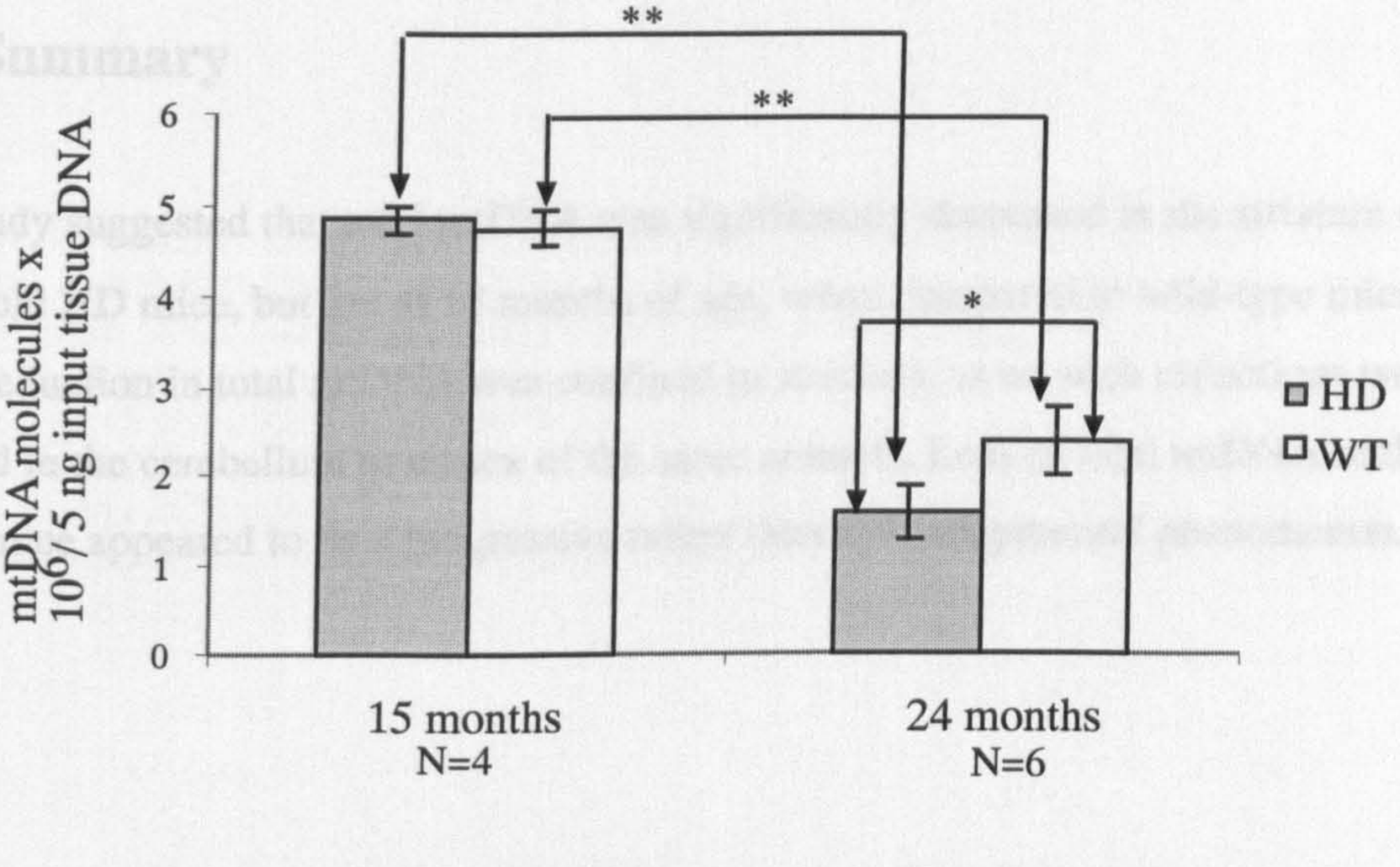

Figure 4.23 Comparisons of total mtDNA levels in the striatum of mice at 15 and 24 months of age. Total mtDNA levels in the striatum of HD mice and wild-type littermates at 24 months of age are significantly reduced when compared to the corresponding groups of mice at 15 months of age (**$p < 0.001$). Total mtDNA is significantly decreased in the striatum of HD mice at 24 months of age compared to the wild-type littermates (*$p < 0.05$). The Student's *t* test is used for statistical analysis. Data are expressed as mean ± S.E.

4.3.4.2 Determining levels of deleted mtDNA molecules in HD mouse brain regions

Dilutions of the mimic p667 construct (0, 2.5, 5, 7.5, 10 fg) were co-amplified with 200 ng of striatal DNA from each mouse, and PCR products were resolved on an EtBr-stained 2 % agarose gel (for an example see Fig. 4.24). In this example, the data indicated that the intensity of mimic p667 PCR product was equal to the intensity of deleted mtDNA PCR product in the second lane. Since the concentration of mimic p667 template added to this PCR was 2.5 fg and 1 fg of p667 contains 403 molecules, the amount of deleted mtDNA in this PCR is 1,008 molecules. The input tissue DNA concentrations added to competitive PCR assays were normalized by Southern blot analysis (see section 4.3.3.4). The resulting deleted mtDNA levels in the striatum of the 6 HD mice and 6 wild-type littermates studied in section 4.3.4.1 are shown in Table 4.5. The results show that the amount of deleted DNA in the striatum of HD mice at 24 months of age is not significantly different from that of wild-type littermates, and the ratio of deleted mtDNA/total mtDNA in the striatum of HD mice is not significantly different from that of wild-type littermates (Table 4.6).

4.4 Summary

This study suggested that total mtDNA was significantly decreased in the striatum of 24-month old HD mice, but not at 15 months of age, when compared to wild-type mice. This ~30% reduction in total mtDNA was confined to striatum, as no such reductions were detected in the cerebellum or cortex of the same animals. Loss of total mtDNA in the striata of HD mice appeared to be a progressive rather than a developmental phenomenon.

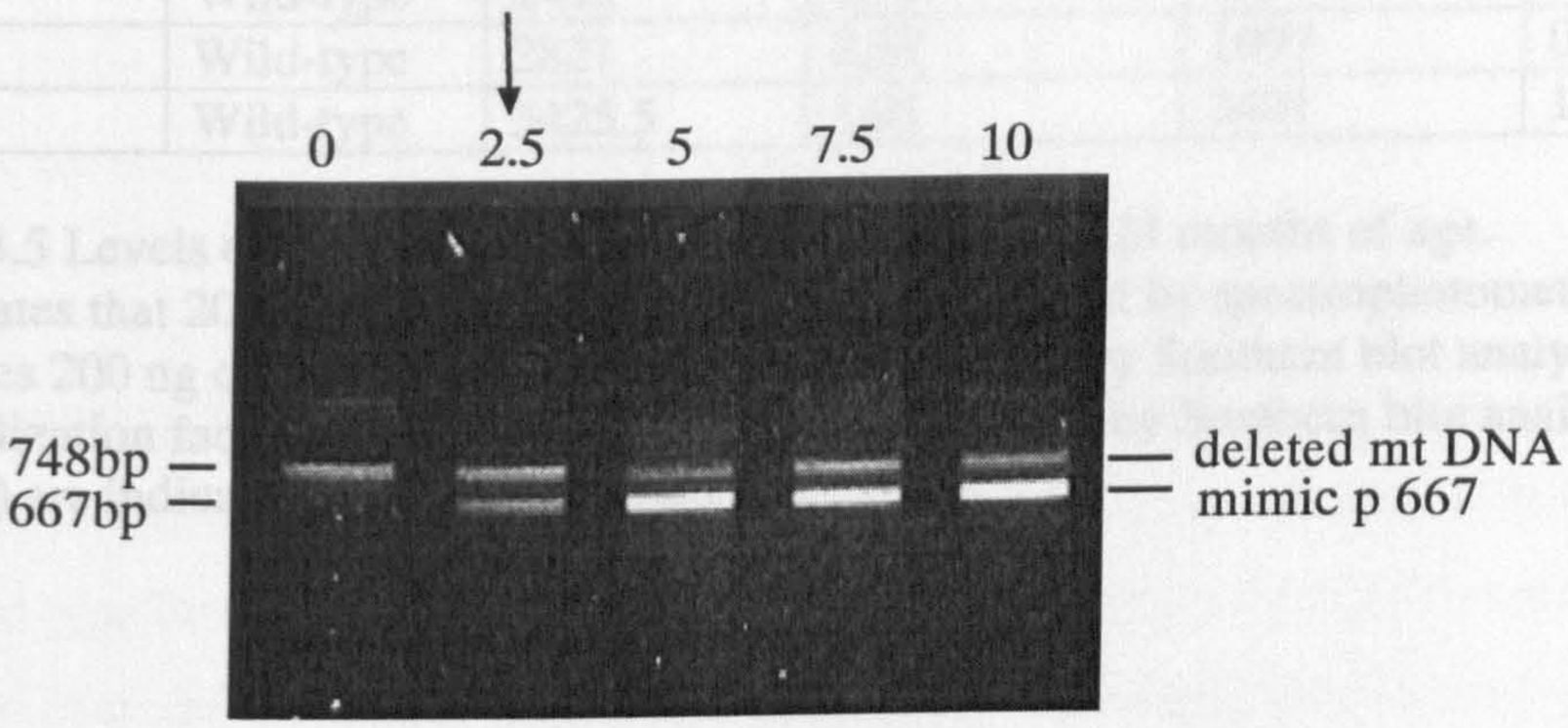

Figure 4.24 Determining levels of the common deleted mtDNA species in mouse brain regions. A constant amount (200 ng) of striatal DNA was co-amplified with dilutions of p667 mimic DNA and the products resolved on an EtBr-stained agarose gel. Numbers above the image represent the amount of mimic p667 added to each PCR tube (in fg). The image of the resulting gel shows equal intensity of the two bands representing deleted mtDNA and p667 DNA in the second lane (arrow). 2.5 fg of p667 DNA was added to this PCR tube. As 1 fg of p667 DNA contains 403 molecules, there are 1008 molecules of deleted mtDNA in this PCR assay.

Animal ID	Genotype	Molecules of deleted mtDNA /200ng◗	Normalisation factor♣	Molecules of deleted mtDNA /200ng¶	Ratio of deleted/total mtDNA
383	HD	2216.5	0.62	3574	1.74×10^{-3}
377	HD	2418	2.36	1109	1.03×10^{-3}
410	HD	2821	1.8	1567	1.1×10^{-3}
412	HD	1621	0.59	2732	1.9×10^{-3}
414	HD	2418	1.13	2139	1.14×10^{-3}
376	Wild-type	2619.5	2.65	988	0.56×10^{-3}
382	Wild-type	3425.5	1	3426	1.15×10^{-3}
385	Wild-type	2418	0.91	2657	1.04×10^{-3}
409	Wild-type	2821	2.57	1097	0.51×10^{-3}
416	Wild-type	3425.5	1.01	3401	1.35×10^{-3}

Table 4.5 Levels of deleted mtDNA in striatum of mice at 24 months of age.
◗ indicates that 200 ng of input tissue DNA was determined by spectrophotometry. ¶ indicates 200 ng of input tissue DNA after normalization by Southern blot analysis. Normalization factors for input tissue DNA as determined by Southern blot analysis (section 4.3.3.4) are indicated in column labelled ♣.

	Wild-type (n=5)	HD (n=5)	*p* value
Deleted mtDNA molecules (D) /200 ng input tissue DNA	2313 ± 537	2224 ± 433	0.9
Total mtDNA molecules $\times 10^6$ (T)/ 5 ng input tissue DNA	2.39 ± 0.2	1.57 ± 0.17	**0.016***
Ratio of D/T	$2.30 \times 10^{-5} \pm 4.12 \times 10^{-6}$	$3.46 \times 10^{-5} \pm 4.53 \times 10^{-6}$	0.096

Table 4.6 Levels of deleted mtDNA and ratios of deleted mtDNA/total mtDNA in the striatum of 24 month-old mice (corrected for amount of tissue DNA added to the PCR tube).
Comparisons were made using Student's *t*-test (two tailed). All data are expressed as mean ± SE. * indicates $p < 0.05$.

5 Investigating the cause of reduced levels of mtDNA in 24-month old HD mouse striatum

5.1 Introduction

The results shown in section 4.3.4.1 indicate that 24-month old HD mice had a significant reduction (~ 30 %) of total mtDNA in the striatum. It is notable that increased oxidative stress can either cause loss of mitochondria (Hirai et al., 2001) or decreased total mtDNA content (Mansouri et al., 1999; Mansouri et al., 2001). Therefore, it is important to clarify whether the reduction of total mtDNA is due to a decreased number of mitochondria, or a decreased number of mtDNA molecules per mitochondrion.

Western blot analyses (section 2.2.14) of the mitochondrial structural protein porin were performed to determine the mitochondrial mass in the striatum of 24 month-old HD mice and wild-type littermates. If the mitochondrial mass in the striatum of HD mice is not different from that of their wild-type littermates, the reduction of mtDNA may be due to the decreased number of mtDNA molecules per mitochondrion.

Mitochondrial transcription factor A (mtTFA) has been demonstrated to regulate mtDNA copy number *in vivo* and is essential for mitochondrial biogenesis (Larsson et al., 1998). Consistent with a role in regulating mtDNA copy number, the level of human mtTFA varies concomitantly with the level of mtDNA in human cell (Larsson et al., 1994). Mitochondrial transcription factor A plays an important role in the maintenance of mtDNA (Lee and Clayton, 1997) and studies have shown that mRNA of human mitochondrial transcription factor A gene (*TFAM*) is decreased in patients with myopathy associated with depletion of mtDNA (Poulton et al., 1994). Since a ~ 30 % reduction of mtDNA was found in the striatum of HD mice, the hypothesis that decreased mtTFA expression levels might be the cause of the mtDNA depletion is conceivable. Also, the 30 % reduction of mtDNA might have a positive feed back effect on the expression of mtTFA and therefore, mtTFA expression level increases as a compensatory response. Therefore, the expression levels of mtTFA in HD mouse brain regions including striatum, cortex, and cerebellum were

investigated. The aims of this study were to determine whether the change of mtTFA expression level is related to the depletion of mtDNA in the striatum of HD mice.

5.2 Determining levels of the mitochondrial structural protein, porin (representing mitochondrial mass), in 24 month-old HD mouse striatum

The outer membrane of the mitochondrion contains many copies of a transport protein called porin (VDAC, voltage dependent anion channel), which forms large aqueous channels through the lipid bilayer. The membrane thus resembles a sieve that is permeable to all molecules of 5000 daltons or less, including all small proteins. Porin, a 31 KiloDalton (kDa) protein, was investigated using western blot analysis to determine the mitochondrial mass present in the striatum of HD mice. Levels of β-tubulin III (50 kDa) were also investigated to provide an internal control for normalizing levels of protein loading.

Initially, a study to determine the intra-experimental error was conducted. Five equal amounts (12 μg) of the same protein lysate from one animal was loaded on a Bis-Tris SDS gel, and the ratios of porin intensity/β-tubulin III intensity were determined by western blot analysis for each lane (Fig. 5.1). The coefficient of variation (CV) that represents the precision of the experiment was 6 %. The result also suggested that western blot analysis could detect at least ~ 13 % difference in mean value between 2 groups, if the variances of 2 groups are similar to that of this experiment.

The next experiment was to compare porin levels in the striatum of 6 HD and 6 wild-type littermates. Animals of the same age and same genetic background as those used in section 4.3.4 were used for the analysis. The ratio of porin intensity/β-tubulin III intensity for each animal was determined in duplicate by western blot analyses (Fig. 5.2). The results showed that the ratio of porin/β-tubulin III in the striatum of HD mice at 24 months of age did not differ from that of wild-type littermates (Table 5.1). This indicates that the striatal mitochondrial mass in HD mice does not differ from that in wild-type littermates.

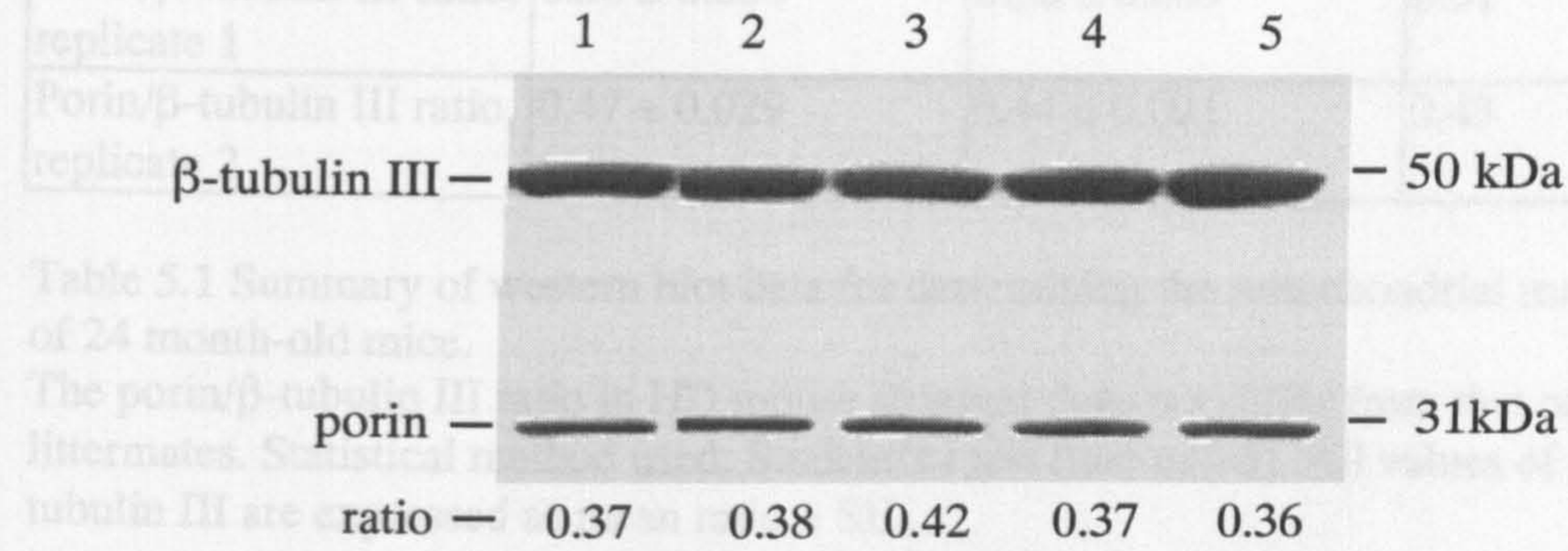

Figure 5.1 Determining intra-experimental error associated with the determination of porin levels by western blot analysis. 5 samples of the same brain protein lysate were loaded onto a Bis-Tris SDS gel (12 μg in each of lanes 1-5). The proteins were transferred onto a membrane and immunodetected with anti-porin and anti-β–tubulin III antibodies. The ratios of porin/β–tubulin III (measured by intensity of resulting bands) are stated below the panel. The coefficient of variation (CV) that represents the precision of the experiment is 6 %.

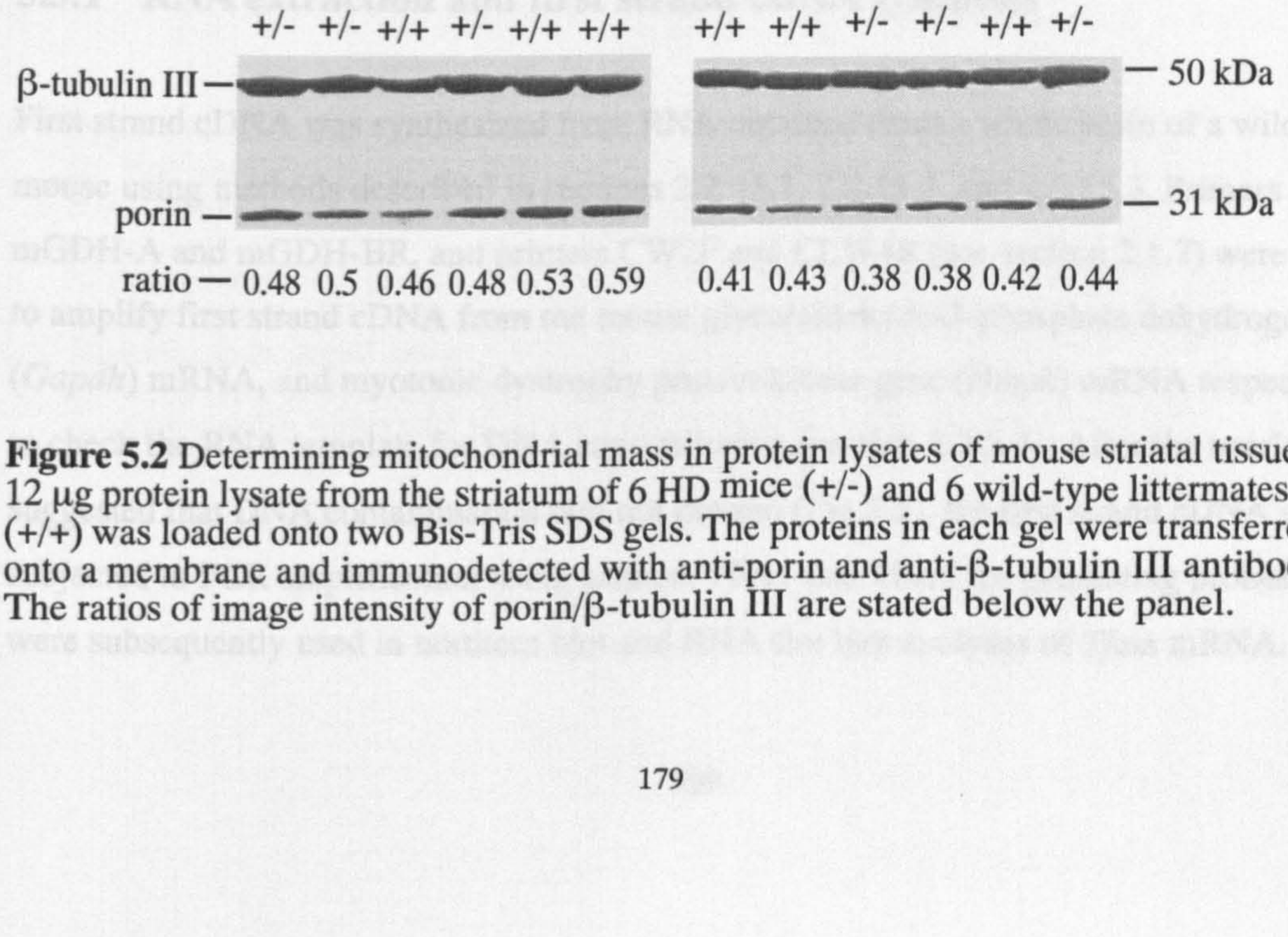

Figure 5.2 Determining mitochondrial mass in protein lysates of mouse striatal tissue. 12 μg protein lysate from the striatum of 6 HD mice (+/-) and 6 wild-type littermates (+/+) was loaded onto two Bis-Tris SDS gels. The proteins in each gel were transferred onto a membrane and immunodetected with anti-porin and anti-β-tubulin III antibodies. The ratios of image intensity of porin/β-tubulin III are stated below the panel.

	Wild-type (n=6)	HD (n=6)	*p* value
Porin/β-tubulin III ratio, replicate 1	0.56 ± 0.039	0.52 ± 0.039	0.51
Porin/β-tubulin III ratio, replicate 2	0.47 ± 0.029	0.44 ± 0.021	0.43

Table 5.1 Summary of western blot data for determining the mitochondrial mass in striatum of 24 month-old mice.
The porin/β-tubulin III ratio in HD mouse striatum does not differ from that of wild-type littermates. Statistical method used: Student's *t* test (two tailed). All values of porin/β-tubulin III are expressed as mean ratio ± SE.

5.3 Investigating the expression levels of mitochondrial transcription factor A (*Tfam*) mRNA in HD mouse brain regions

The mitochondrial transcription factor A (*Tfam*) mRNA expression levels in HD mice were investigated using northern blot and RNA slot blot analyses. The prerequisites of northern blot analysis are the good quality RNA, good probes, an internal control for RNA loading and adequate exposure times of X-ray film to radiolabelled northern blot membranes. Therefore, optimisations for those requirements were performed.

5.3.1 RNA extraction and first strand cDNA synthesis

First strand cDNA was synthesized from RNA obtained from a whole brain of a wild type mouse using methods described in sections 2.2.15.1, 2.2.15.2, and 2.2.15.3. Primers mGDH-A and mGDH-BR, and primers CW2F and CLW4R (see section 2.1.7) were used to amplify first strand cDNA from the mouse glyceraldehyde-3-phosphate dehydrogenase (*Gapdh*) mRNA, and myotonic dystrophy protein kinase gene (*Dmpk*) mRNA respectively, to check the RNA template for DNA contamination (section 2.2.5.4). After the results suggested that DNA contamination was not present (Fig 5.3), the first strand cDNA was subjected to PCR amplification using primers TFA1 and TFA2 for generating probes which were subsequently used in northern blot and RNA slot blot analyses of *Tfam* mRNA.

a) RT-PCR of *Gapdh mRNA*

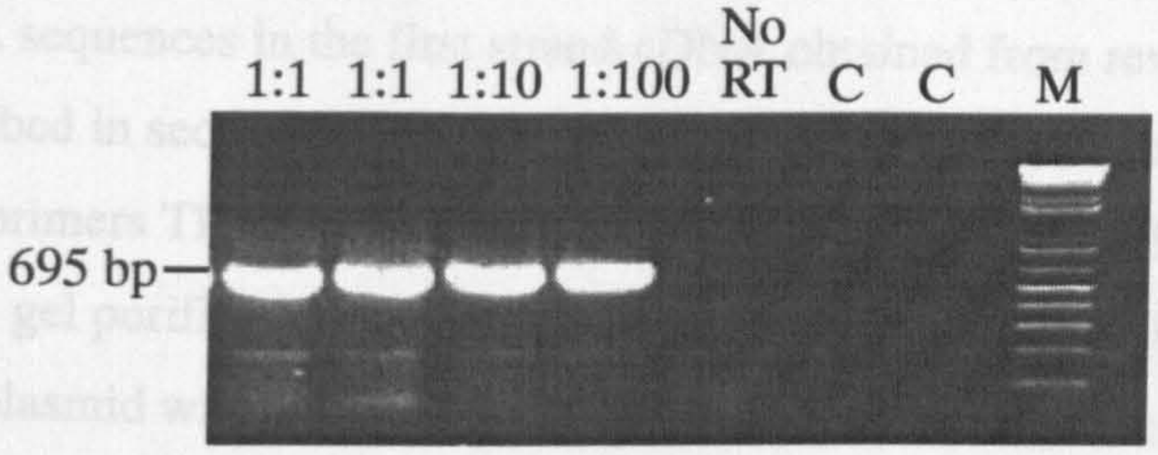

b) RT-PCR of *Dmpk mRNA*

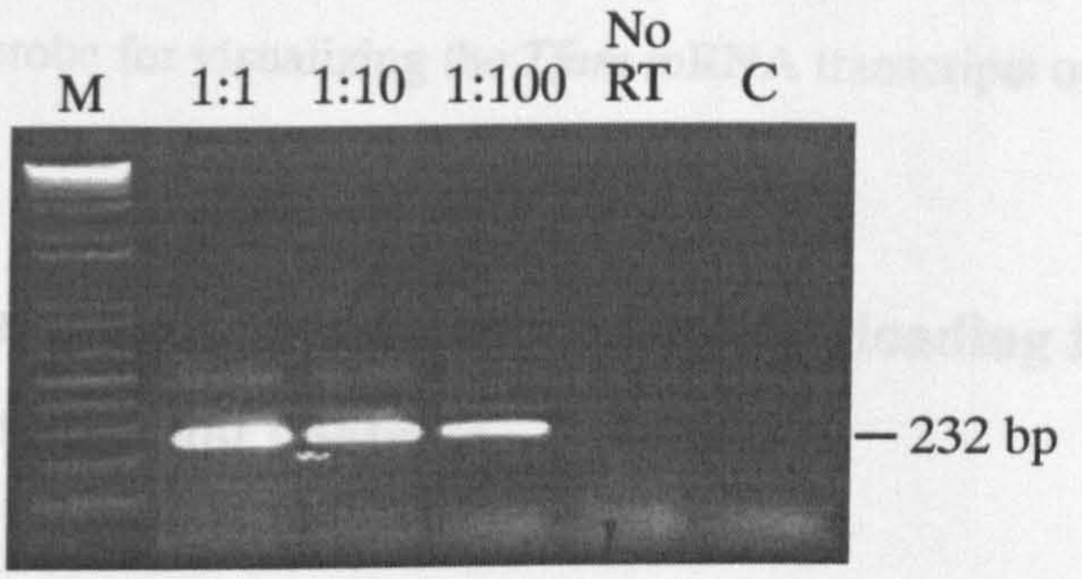

Figure 5.3 Confirmation that no DNA is present in a mouse brain RNA sample for first strand cDNA synthesis. Amplification products of the mouse *Gapdh* gene transcript from different dilutions (1:1, 1:1, 1:10, 1:100) of the first strand cDNA are visualised on an EtBr-stained agarose gel (a). Amplification products of the mouse *Dmpk* gene transcript from different dilutions (1:1, 1:10, 1:100) of the first strand cDNA are visualised on a EtBr-stained agarose gel (b). NoRT indicates the control lanes containing the reactions where the RNA template had not been treated with reverse transcriptase. C indicates control lanes containing the reactions using water as a template. The 1 kb size ladder is indicated by M.

5.3.2 Cloning RT-PCR products as a probe for northern blot and RNA slot blot analyses

The primers TFA1 and TFA2 (section 2.1.7) were carefully chosen from mRNA sequences published in GenBank (NCBI) to amplify mouse mitochondrial transcription factor A (*Tfam*) cDNA sequences in the first strand cDNA obtained from reverse transcription of mRNA described in section 5.3.1. The size of the PCR product amplified from first strand cDNA using primers TFA1 and TFA2 was predicted to be 632 bp (Fig. 5.4a). The PCR products were gel purified and cloned using the methods described in 2.2.9. The resulting recombinant plasmid was designated pTFA. Plasmid DNA from the clone was isolated (section 2.2.2.1) and digested with *Eco*RI to release the insert to ensure that the correct DNA fragment had been cloned (Fig. 5.4b). The identity of the cloned fragment was confirmed by sequencing (Fig. 5.5). The PCR products of amplifying pTFA DNA using primers TFA1 and TFA2 were gel purified and ~25 ng of the purified DNA fragments (Fig. 5.4c) were used as the probe for visualizing the *Tfam* mRNA transcripts on northern blots or RNA slot blots.

5.3.3 Using β-actin as an internal control for RNA loading in northern blot and RNA slot blot analyses

β-actin was used as an internal control for RNA loading in northern blot and RNA slot blot analyses. Before β-actin hybridisation, the *Tfam* probe was stripped off the membranes (section 2.2.13). To verify that no radioactivity was left on the membrane, the stripped membrane was exposed to X-ray film at -70°C overnight. If radioactivity was detected after an overnight exposure, the membrane was subjected to further stripping until no radioactivity was detected.

The probe for β-actin hybridisation was a 1.3 kb fragment of mouse β-actin cDNA cloned into a plasmid (pMoBA-10, a gift from Rosalind John, Wellcome/CRC Institute, Cambridge, UK).

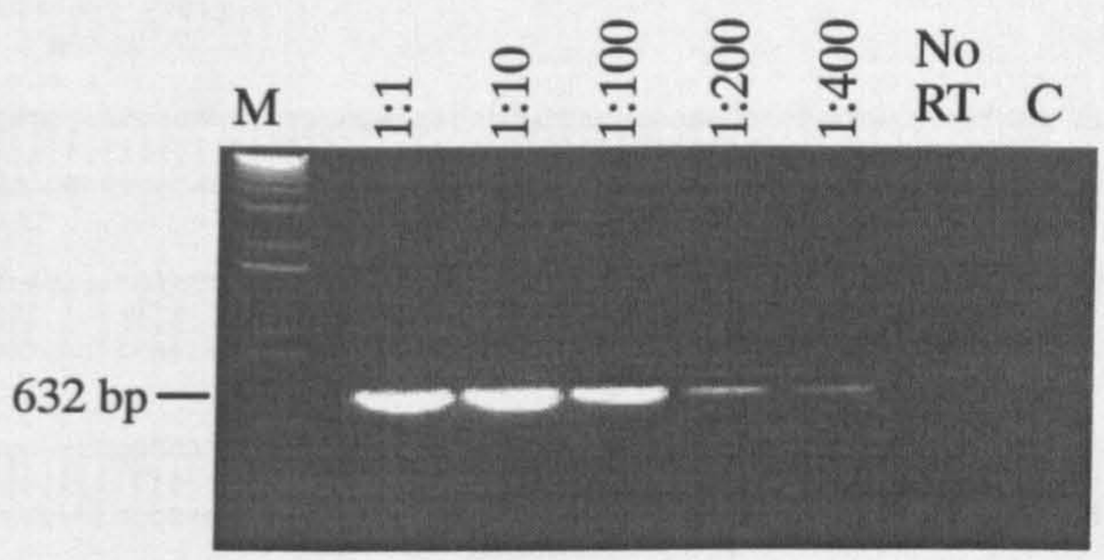

Figure 5.4 Generation of the probe for northern blot analysis of *Tfam* mRNA. Amplification products of amplifying *Tfam* gene transcript from different dilutions of first strand cDNA (1:1, 1:10, 1:100, 1:200, 1:400) are resolved on an EtBr-stained agarose gel (a). NoRT is the control lane containing the reaction where the RNA template had not been treated with reverse transcriptase. C is the control lane containing the reactions using water as a template. PCR products in gel (a) were purified and cloned to generate a recombinant plasmid called pTFA. *Eco*RI-digested DNA from pTFA (lane 1) was visualized on an EtBr-stained agarose gel (b). 4 μl of purified insert DNA from pTFA was loaded to an EtBr-stained agarose gel (lane 1, c). 2 μl (~ 30 ng) of the purified insert DNA was used as a probe in northern blot analyses. The 1 kb plus size ladder is indicated by M.

```
>gi|6678302|ref|NM_009360.1| Mus musculus transcription factor A, mitochondrial (Tfam), mRNA
          Length = 1449

 Score = 1197 bits (604), Expect = 0.0
 Identities = 623/632 (98%)
 Strand = Plus / Minus

Query: 1   cggatcgtttcacacttcgacggatgagatcacttcgtccaacttcagccatctgctctt 60
           ||||||||||||||||||||||||||||||||||||||||||||||||||||||||||||
Sbjct: 808 cggatcgtttcacacttcgacggatgagatcacttcgtccaacttcagccatctgctctt 749

Query: 61  cccaagacttcatttcattgtcgtaacgaatcctatcatctttagcaagctgaatatatg 120
           ||||||||||||||||||||||||||||||||||||||||||||||||||||||||||||
Sbjct: 748 cccaagacttcatttcattgtcgtaacgaatcctatcatctttagcaagctgaatatatg 689

Query: 121 cctgcttttcctcaggagacagattttccaagcctcatttacaagcttcaattttccct 180
           ||||||||||||||||||||||||||||||||||||||||||||||||||||||||||||
Sbjct: 688 cctgcttttcctcaggagacagattttccaagcctcatttacaagcttcaattttccct 629

Query: 181 gagccgaatcatcctttgcctcctggaagctttcagatacataaatgttatatgctgaac 240
           ||||||||||||||||||||||||||||||||||||||||||||||||||||||||||||
Sbjct: 628 gagccgaatcatcctttgcctcctggaagctttcagatacataaatgttatatgctgaac 569

Query: 241 gaggtctttttggttttccaagcaaaattaattctcttctctctaccagngctttctttt 300
           |||||||||||||||||||||||||||||||||||||||||| |||||| ||||||||||
Sbjct: 568 gaggtctttttggttttccaagcaaaattaattctcttctctttaccagtgctttctttt 509

Query: 301 ttaaccgtctctgccgggcctccttctccatacccatcagctgacttggagttagctgct 360
           ||||||||||||||||||||||||||||||||||||||||||||||||||||||||||||
Sbjct: 508 ttaaccgtctctgccgggcctccttctccatacccatcagctgacttggagttagctgct 449

Query: 361 ctttatacttgctcacagcttctttgtatgctttccactcagctttaaaatcagcttcat 420
           ||||||||||||||||||||||||||||||||||||||||||||||||||||||||||||
Sbjct: 448 ctttatacttgctcacagcttctttgtatgctttccactcagctttaaaatcagcttcat 389

Query: 421 aaaccnnnnnnnctgcttctggtagctcccctccacagggctgcaattttcctaaccaatt 480
           |||||      ||||||||||||||||||||||||||||||||||||||||||||||||
Sbjct: 388 aaacctttttttctgcttctggtagctcccctccacagggctgcaattttcctaaccaatt 329

Query: 481 ctgaaagttttgcatctgggtgtttagctttaaatttgggtagctgttctgtggaaaatc 540
           ||||||||||||||||||||||||||||||||||||||||||||||||||||||||||||
Sbjct: 328 ctgaaagttttgcatctgggtgtttagctttaaatttgggtagctgttctgtggaaaatc 269

Query: 541 gaaggtatgaactcataggtttctttggatagctacccatgctggaaaaacacttcggaa 600
           ||||||||||||||||||||||||||||||||||||||||||||||||||||||||||||
Sbjct: 268 gaaggtatgaactcataggtttctttggatagctacccatgctggaaaaacacttcggaa 209

Query: 601 tacagacaagactgatagacgaggggatgcga 632
           |||||||||||||||||||||||||||||||
Sbjct: 208 tacagacaagactgatagacgaggggatgcga 177
```

Figure 5.5 Identity of the pTFA plasmid insert was confirmed by DNA sequencing. The clone pTFA was sequenced and the resulting data (Query) was checked using the Blast program (NCBI) and a matched sequence from the mouse mtTFA mRNA (Sbjct) was retrieved from the Genbank database. The result shows that 623 bp out of 632 bp (98 %) are matched. Some of the unmatched sequence may be due to artifacts or errors of the DNA sequencing.

The resulting images of the autoradiographs from northern slot and RNA slot blot analyses were captured and the intensity of each hybridising band was measured using Kodak Digital Science ID software. The intensity value of each band representing the *Tfam* transcript level of each sample was obtained, and the ratio of the mRNA transcript level/β-actin mRNA transcript level was determined for quantifying levels of *Tfam* gene transcript.

5.3.4 Optimising the exposure time of X-ray film to radiolabelled northern and RNA slot blot membranes

It is notable that the linear range of signal response of X-ray film to radioactivity is narrower than that obtained by using a phosphoimager. However, the images generated using a phosphoimager in the laboratory provided less clear bands than autoradiography. Therefore, autoradiographs were used for visualizing the transcripts on northern and slot blot membranes. In order to ascertain that signal response of X-ray film to radiolabelled northern blot and RNA slot blot membranes generated in the study was within the linear range, the exposure times of X-ray film to radiolabelled membranes were optimised.

Generation of northern blot gels, membranes and hybridisation with probes were performed using the methods described in sections 2.2.15.5, and 2.2.16. The northern blot membranes probed for visualization of the β-actin mRNA transcript in HD and wild-type mouse tissue (section 2.2.15) were washed to a final stringency of 0.1 X SSC, 0.1 % (w/v) SDS at 68°C for at least 30-60 min and then exposed to X-ray film at -70°C in the presence of intensifying screens for 2, 4, 7, and 16 hours. The resulting images of the autoradiographs were captured and the intensity of each hybridizing band was measured. The linear range of signal response of X-ray film was determined by plotting the intensity of each band against exposure time. The linear range was between 2-7 hours, and therefore 4-6 hours of exposure time was chosen in the study (Fig. 5.6).

The expression level of *Tfam* mRNA in normal mouse brain regions is not abundant and 3-4 days of X-ray film exposure time were required to visualize the transcript on radiolabelled membranes. Therefore, 4 days of exposure time was chosen for visualization of the *Tfam* transcript by autoradiography.

a) Northern blot analysis of β-actin mRNA

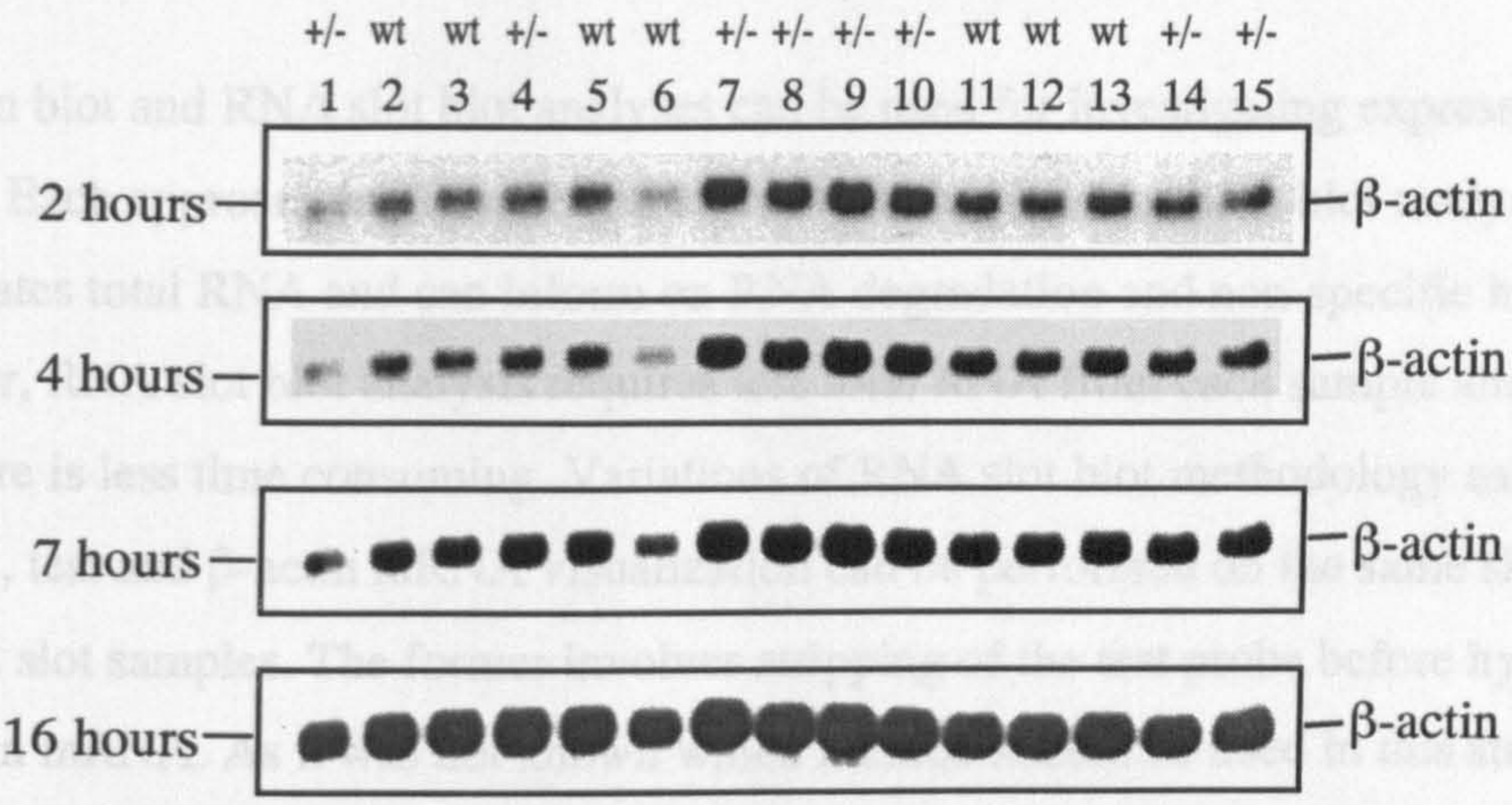

b) Linear range of signal response of X-ray film to radioactivity

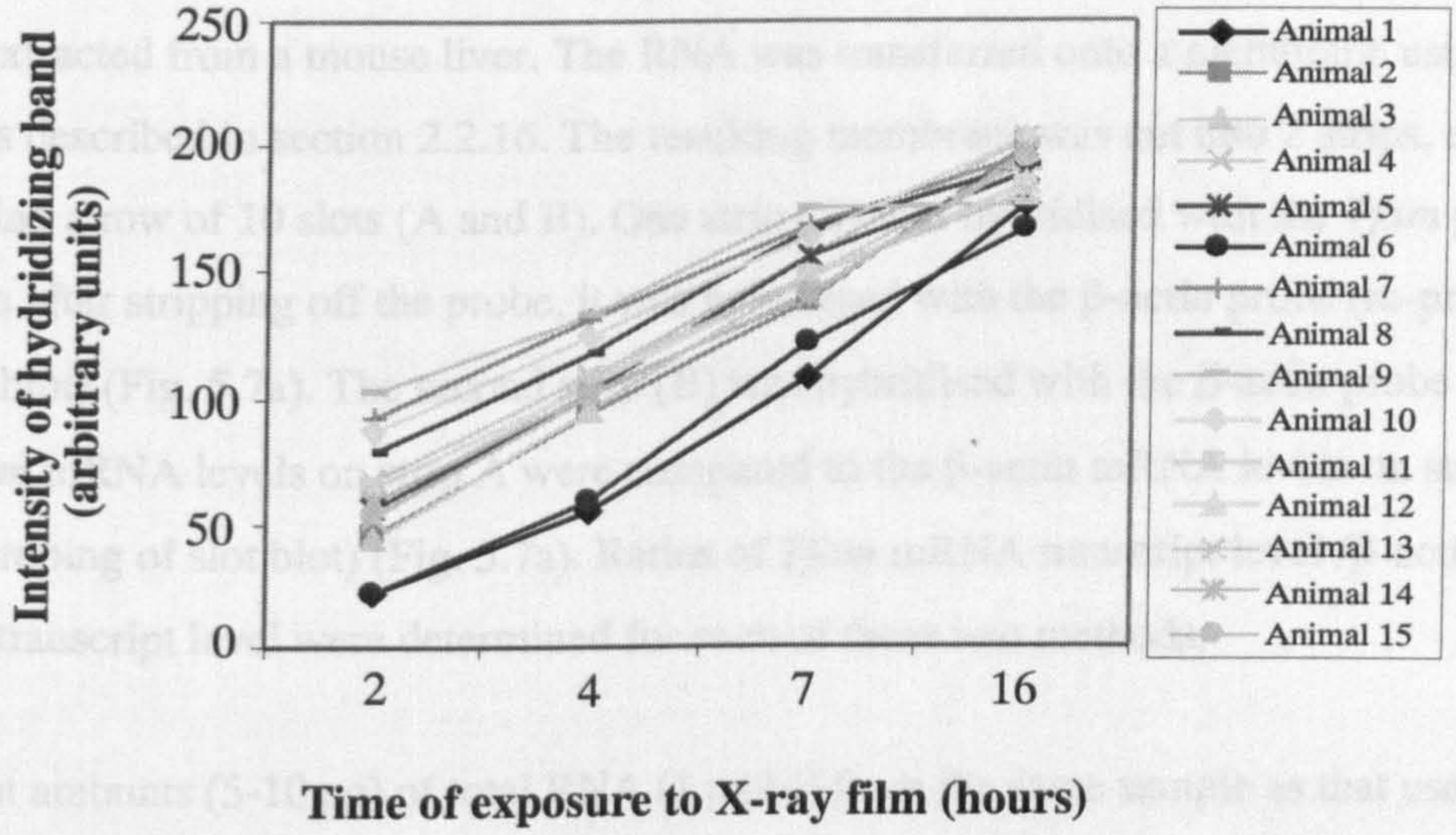

Figure 5.6 Determining the linear range of signal response of X-ray film to a radiolabelled membrane for northern blot analysis of β-actin mRNA. A northern blot membrane of RNA from 8 HD mice (+/-) and 7 wild-type littermates (wt) (lanes 1-15, a) was hybridised with a β-actin probe. After washing, it was exposed to X-ray film for different periods of time (2-16 hours). The resulting autoradigraphs are shown in (a). The intensity of each band in the autoradigraphs is plotted against exposure time (b). Each line represents the intensity of fragment from a different animal (a, 1-15). The linear range of response signal of X-ray film to radioactivity is 2-7 hours for northern blot analysis of β-actin mRNA.

5.3.5 Comparison of intra-experimental error of northern blot and slot blot analyses

Northern blot and RNA slot blot analyses can be used for investigating expression levels of mRNA. Each approach has advantages and disadvantages. Northern blot analysis fractionates total RNA and can inform on RNA degradation and non-specific hybridisation. However, RNA slot blot analysis requires less total RNA from each sample and the procedure is less time consuming. Variations of RNA slot blot methodology exist. For example, test and β-actin mRNA visualization can be performed on the same slot sample or different slot samples. The former involves stripping of the test probe before hybridisation of β-actin mRNA. As it was not known which method should be used in this study, a comparison of intra-experimental error associated with the northern blot and two slot blot methodologies was performed.

Two rows of 10 slots of the slot blot equipment were loaded with 5 µl of total RNA (1 µg/µl) extracted from a mouse liver. The RNA was transferred onto a membrane using the methods described in section 2.2.16. The resulting membrane was cut into 2 strips, each containing a row of 10 slots (A and B). One strip (A) was hybridised with the *Tfam* probe, and then after stripping off the probe, it was hybridised with the β-actin probe (re-probing the slot blot) (Fig. 5.7a). The second strip (B) was hybridised with the β-actin probe only. The *Tfam* mRNA levels on strip A were compared to the β-actin mRNA levels on strip B (no re-probing of slot blot) (Fig. 5.7a). Ratios of *Tfam* mRNA transcript level /β-actin mRNA transcript level were determined for each of these two methods.

Different amounts (5-10 µg) of total RNA (1 µg/µl) from the same sample as that used in the slot blot analysis were loaded onto a denaturing formaldehyde-agarose gel for northern blot analysis (section 2.2.15.4). The RNA was transferred and hybridised with *Tfam* probe (Fig. 5.7b). After stripping off the *Tfam* probe, the membrane was re-hydridized with the β-actin probe (Fig. 5.7b). Ratios of *Tfam* mRNA transcript level /β-actin mRNA transcript level were determined for northern blot analysis. A comparison of the results (Table 5.2) showed that the precision (Coefficient of Variation) of each method was around 5-6 %. Given that northern blot analysis has the benefit of checking for degraded RNA and

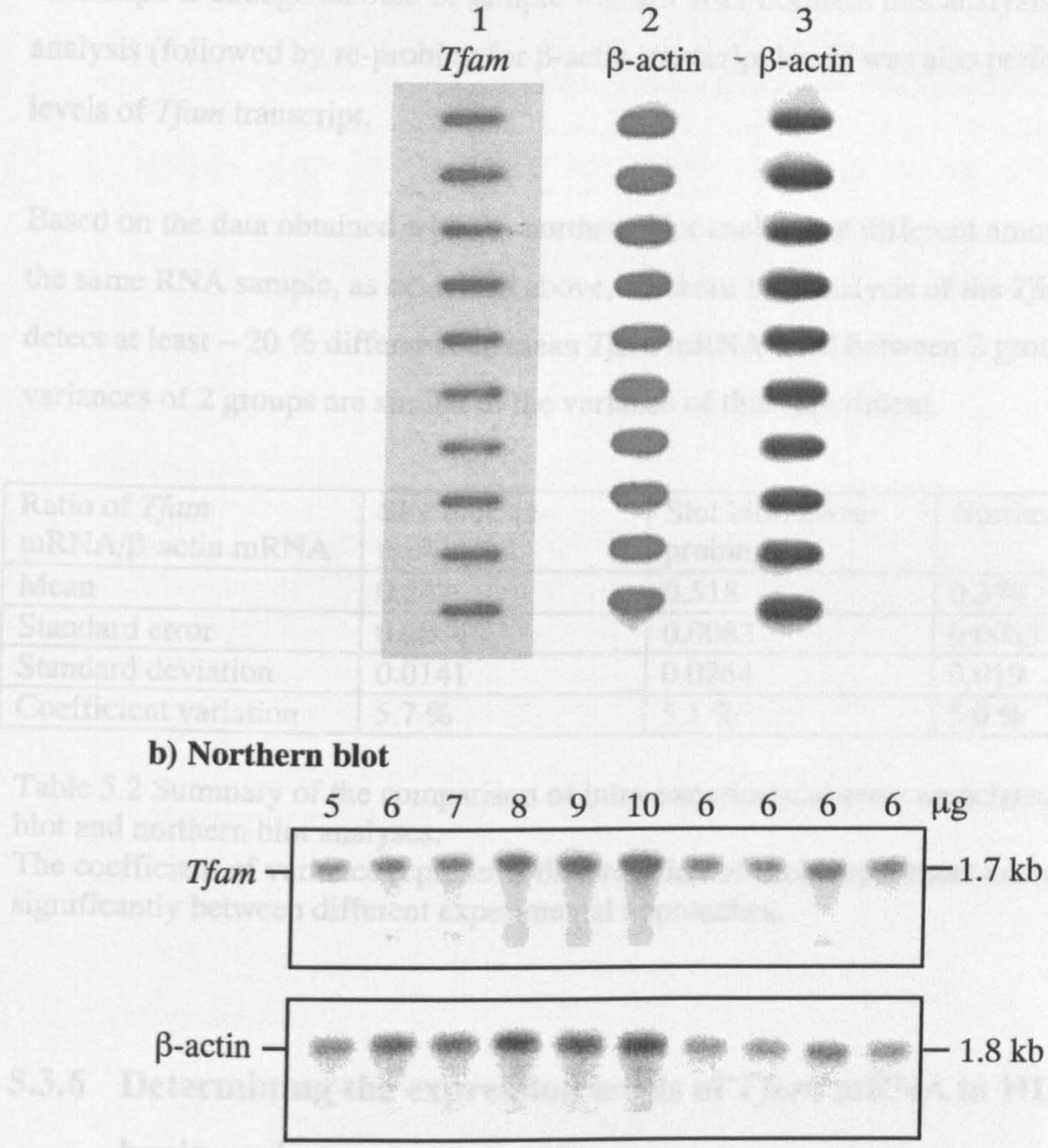

Figure 5.7 Comparison of intra-experimental error associated with RNA slot blot (a) and northern blot (b) analyses. 5 µg of total RNA extracted from a mouse liver was loaded into each of 20 slots. The resulting membrane was cut into 2 strips (so one strip contains 10 slots). One membrane was probed for visualization of *Tfam* mRNA (a, panel 1). The other membrane was probed for visualisation of β-actin mRNA (a, panel 3). The *Tfam* probe on panel1 was stripped off and the membrane re-probed with β-actin probe (panel 2). (b) Different amounts of total RNA (shown above panel) from the same sample as the slot blot were loaded onto a denaturing formaldehyde agarose gel. The RNA was transferred and hybridized with the *Tfam* probe. After stripping the *Tfam* probe, the membrane was reprobed with the β-actin probe. Ratios of *Tfam* mRNA level/β-actin mRNA level for each analysis were determined and presented in Table 5.2.

non-specific hybridisation, northern blot analysis was used to investigate levels of *Tfam* transcript. If enough amount of sample was left after northern blot analysis, RNA slot blot analysis (followed by re-probing for β-actin transcript level) was also performed to check levels of *Tfam* transcript.

Based on the data obtained with the northern blot analysis of different amounts (5-10 μg) of the same RNA sample, as described above, northern blot analysis of the *Tfam* mRNA could detect at least ~ 20 % difference in mean *Tfam* mRNA level between 2 groups, if the variances of 2 groups are similar to the variance of this experiment.

Ratio of *Tfam* mRNA/β-actin mRNA	Slot blot: re-probing	Slot blot: no re-probing	Northern blot
Mean	0.247	0.518	0.378
Standard error	0.0044	0.0083	0.0085
Standard deviation	0.0141	0.0264	0.019
Coefficient variation	5.7 %	5.1 %	5.0 %

Table 5.2 Summary of the comparison of intra-experimental error associated with RNA slot blot and northern blot analyses.
The coefficient of variance represents the precision of each experiment and does not vary significantly between different experimental approaches.

5.3.6 Determining the expression levels of *Tfam* mRNA in HD mouse brain regions

RNA was isolated from the striatum, cortex, and cerebellum of 7 HD mice and 7 wild-type littermates at 24 months of age (for details of mouse cohort used see section 2.1.18) for both northern and RNA slot blot analyses. RNA was extracted using the methods described in section 2.2.15.1. 15 μg of total RNA from the striatum, cortex and cerebellum of each mouse was fractionated on denaturing formaldehyde EtBr-stained agarose gels (section 2.2.15.4). Before proceeding with transfer process, the integrity of the separated RNA was checked by visualising the RNA under UV light. The intensity of the 28S and 18S ribosomal RNA bands indicated intact total RNA (Fig. 5.8). Since RNA is not fractionated

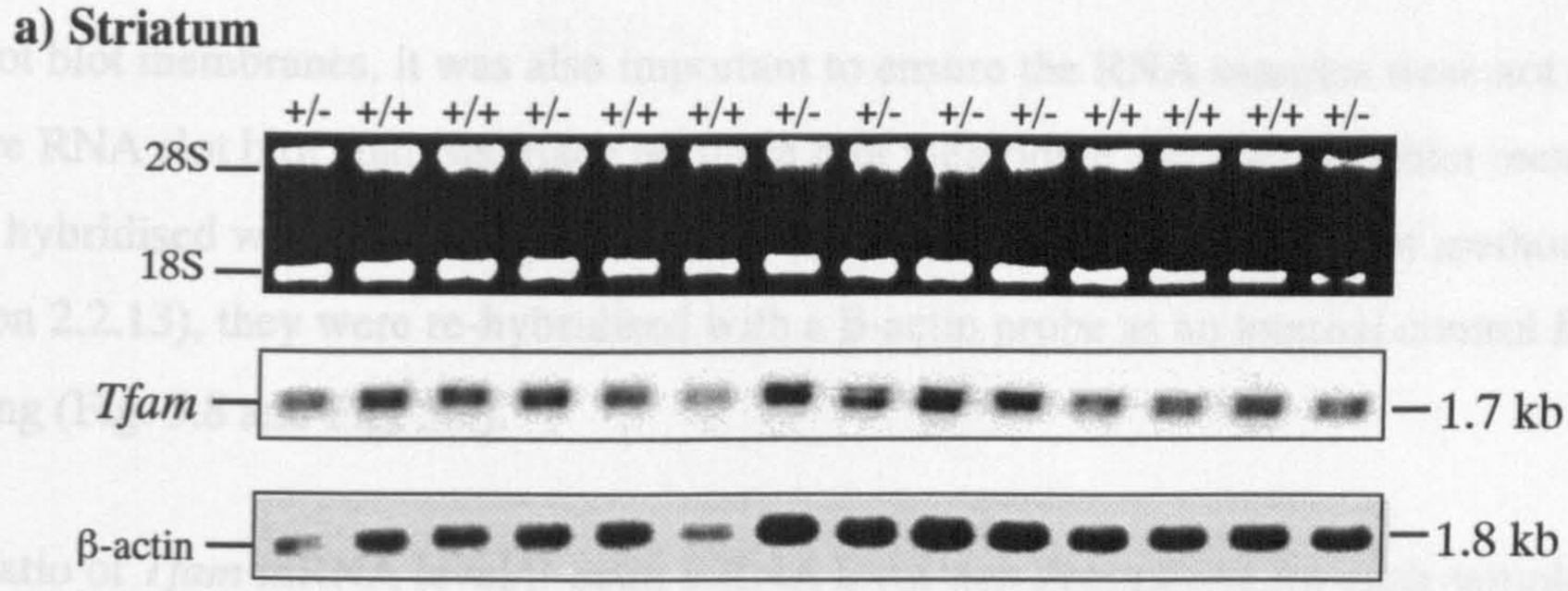

Figure 5.8 Northern blot analyses of *Tfam* mRNA in the striatum (a), cortex (b) and cerebellum (c) of 24 month-old mice. 15 μg of total RNA from 7 HD mice (+/-) and 7 wild-type littermates (+/+) was loaded onto a formaldehyde EtBr-stained gel (top panels in a,b and c). The clear and abundant 18S and 28S rRNA bands indicate good quality RNA. Total RNA in the gel was transferred to a nylon membrane which was probed for visualization of *Tfam* and β-actin mRNA transcripts (middle and bottom panels in a, b and c). The level of β-actin mRNA transcripts was used as an internal control for RNA loading.

on slot blot membranes, it was also important to ensure the RNA samples were not degraded before RNA slot blot analysis. Each northern blot membrane and each slot blot membrane were hybridised with the *Tfam* probe and after stripping the *Tfam* probe (see method in section 2.2.13), they were re-hybridised with a β-actin probe as an internal control for RNA loading (Fig. 5.8 and Fig. 5.9).

The ratio of *Tfam* mRNA level/β-actin mRNA level was determined for each sample and the results were summarised in Table 5.3 and Table 5.4 respectively. The results reveal that HD mice at 24 months of age showed no significant differences in mRNA levels of *Tfam* in any brain region studied when compared to normal littermates.

5.4 Western blot analysis of mitochondrial transcription factor A (mtTFA) protein in the striatum of HD mice

Results in the previous section (section 5.3.6) indicated that expression levels of *Tfam* mRNA in HD mouse brain regions were not significantly different from that in wild-type littermates. However, human mitochondrial transcription factor A (mtTFA) deficiency in patients associated with depletion of mtDNA due to reduced production or stability of the human mtTFA (h-mtTFA) protein has been reported (Poulton et al., 1994). It is therefore possible that changes of mtTFA may occur in the translation rate or the stability level of mtTFA protein in HD mice despite normal transcription levels. Therefore, steady-state levels of mtTFA protein in the striatum of HD mice were investigated using western blot analyses.

5.4.1 Western blot analysis

Western blot analyses were performed on protein lysates from the striatum of 6 HD mice and 6 wild-type littermates at 24 months of age (for details of mouse cohort and western blot methodology see section 2.1.18 and 2.2.14). mtTFA (25 kDa) and β-tubulin III (50 kDa) proteins, providing an internal control for normalizing levels of protein loading, were immunodetected using anti-mtTFA and anti-β-tubulin III antibodies respectively (section 2.2.14). The mtTFA antibody detected multiple bands as well as the previously reported

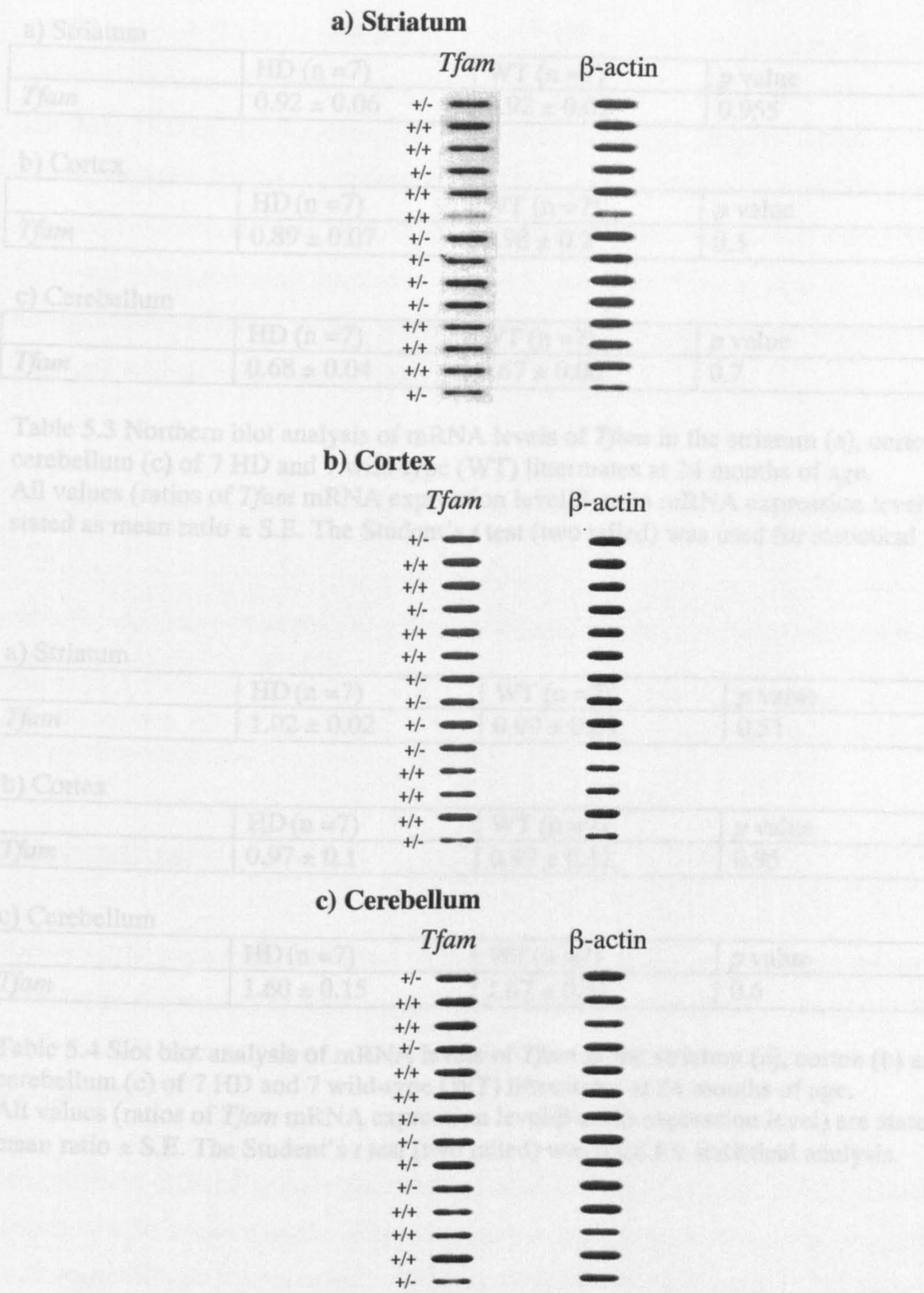

Figure 5.9 RNA slot blot analyses of *Tfam* mRNA in the striatum (a), cortex (b) and cerebellum (c) of 24 month-old mice. 5 μg of total RNA from striatum, cortex and cerebellum of 7 HD mice (+/-) and 7 wild-type littermates (+/+) was loaded into each slot and transferred to a nylon membrane. Each membrane was probed for visualization of *Tfam* and β-actin mRNA transcripts. The level of β-actin mRNA transcripts was used as an internal control for RNA loading.

a) Striatum

	HD (n =7)	WT (n =7)	*p* value
Tfam	0.92 ± 0.06	0.92 ± 0.05	0.955

b) Cortex

	HD (n =7)	WT (n =7)	*p* value
Tfam	0.89 ± 0.07	0.98 ± 0.2	0.3

c) Cerebellum

	HD (n =7)	WT (n =7)	*p* value
Tfam	0.68 ± 0.04	0.67 ± 0.06	0.7

Table 5.3 Northern blot analysis of mRNA levels of *Tfam* in the striatum (a), cortex (b) and cerebellum (c) of 7 HD and 7 wild-type (WT) littermates at 24 months of age.
All values (ratios of *Tfam* mRNA expression level/β-actin mRNA expression level) are stated as mean ratio ± S.E. The Student's *t* test (two tailed) was used for statistical analysis.

a) Striatum

	HD (n =7)	WT (n =7)	*p* value
Tfam	1.02 ± 0.02	0.99 ± 0.04	0.51

b) Cortex

	HD (n =7)	WT (n =7)	*p* value
Tfam	0.97 ± 0.1	0.97 ± 0.11	0.95

c) Cerebellum

	HD (n =7)	WT (n =7)	*p* value
Tfam	1.60 ± 0.15	1.67 ± 0.31	0.6

Table 5.4 Slot blot analysis of mRNA levels of *Tfam* in the striatum (a), cortex (b) and cerebellum (c) of 7 HD and 7 wild-type (WT) littermates at 24 months of age.
All values (ratios of *Tfam* mRNA expression level/β-actin expression level) are stated as mean ratio ± S.E. The Student's *t* test (two tailed) was used for statistical analysis.

mtTFA band of 25 kDa (Larsson et al., 1996). This band pattern persisted despite trying different dilutions of primary (from 1:10000 to 200000) and secondary antibodies (from 1:1000 to 1:6000). The band corresponding to the previously reported 25 kDa band, was therefore chosen for the quantification of mtTFA protein. The ratio of mtTFA band intensity/β-tubulin III band intensity for the striatum of each animal was determined (Fig. 5.10) and compared using the Student's *t* test (two-tailed). The results showed that there was no significant difference in the observed levels of mtTFA protein in the striatum of HD mice and wild-type littermates (Table 5.5).

	Wild-type (n=6)	HD (n=6)	*p* value
mtTFA/β-tubulin III ratio	0.51± 0.07	0.53 ± 0.03	0.77

Table 5.5 Summary of western blot data for determining the mtTFA protein levels in the striatum of 24 month-old mice.
The mtTFA/β-tubulin III ratio in the HD mouse striatum does not differ from that of wild-type littermates. All values of mtTFA/β-tubulin III ratios are stated as mean ratio ± SE. Statistical method used: Student's *t* test (two tailed).

5.5 Summary

Mitochondrial mass in the striatum of 24 month-old HD mice was not decreased compared to wild-type littermates, which suggested that mtDNA depletion in the striatum of 24 month-old HD mice was due to a decrease in the number of mtDNA molecules per mitochondrion.

No significant differences were observed in the levels of mtTFA protein and *Tfam* mRNA transcript in the striatum of HD mice and wild-type littermates at 24 months of age. This result suggested that the reduction of mtDNA molecules in the striatum of HD mice might not be related to the *Tfam* mRNA or mtTFA protein levels.

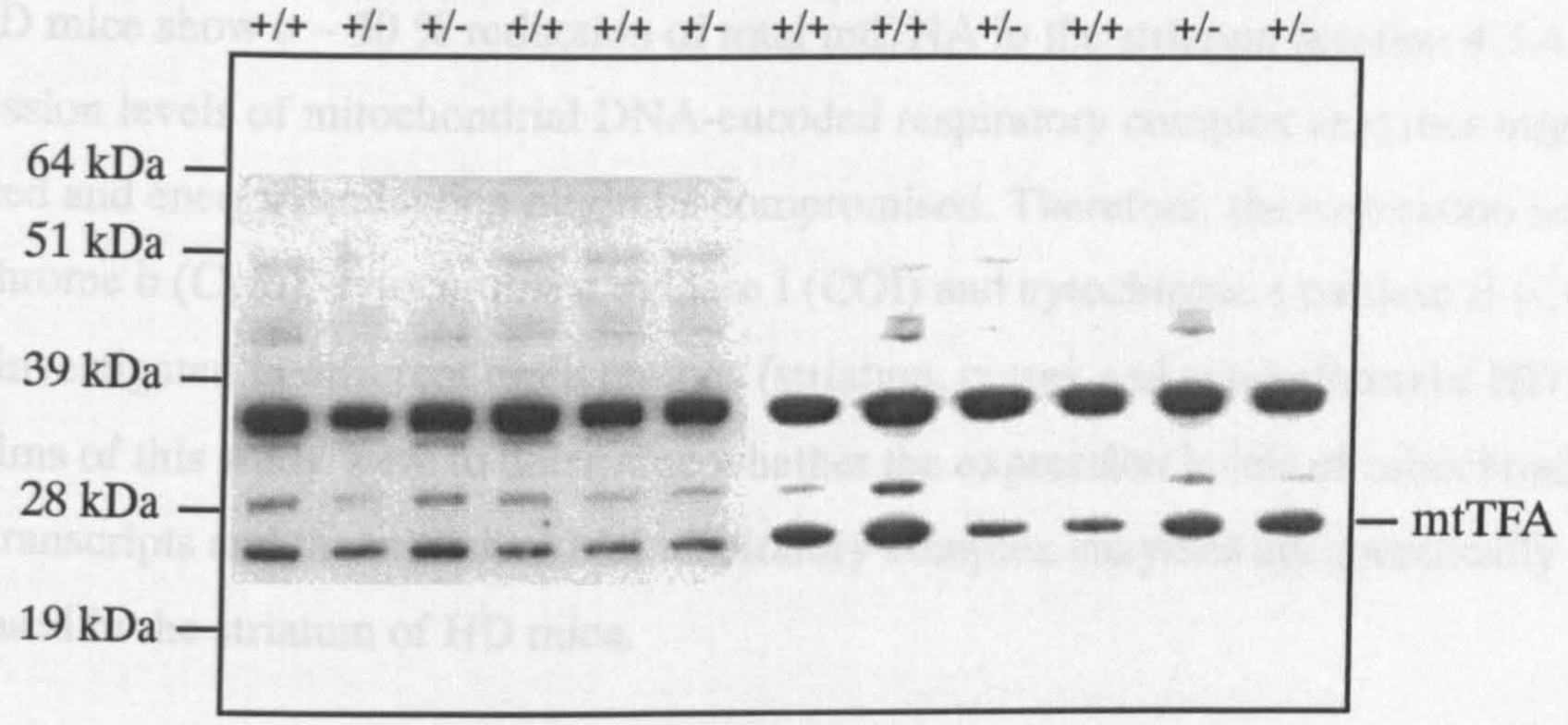

Figure 5.10 Determining mitochondrial factor A (mtTFA) levels in protein lysates of mouse striatal tissue. 20 μg protein lysate from the striatum of 6 HD mice (+/-) and 6 wild-type littermates (+/+) at 24 months of age were separated and transferred onto a membrane. Immunodetection with anti-mtTFA and anti-β-tubulin III antibodies was performed. The ratios of image intensity of mtTFA/β-tubulin III are stated below the panels.

6 Investigating the effect of depleted mitochondrial DNA levels on mitochondrial gene expression in HD mouse striatum

6.1 Introduction

As HD mice show a ~ 30 % reduction of total mtDNA in the striatum (section 4.3.4.1), the expression levels of mitochondrial DNA-encoded respiratory complex enzymes might be affected and energy production might be compromised. Therefore, the expression levels of cytochrome b (Cytb), cytochrome c oxidase I (COI) and cytochrome c oxidase II (COII) were investigated in different brain regions (striatum, cortex and cerebellum) of HD mice. The aims of this study were to determine whether the expression levels of mitochondrial gene transcripts and the mitochondrial respiratory complex enzymes are specifically decreased in the striatum of HD mice.

6.2 Investigating the expression levels of cytochrome b (*Cytb*), cytochrome c oxidase I (*CoI*), and cytochrome c oxidase II (*CoII*) mRNA in HD mouse brain regions

The expression levels of cytochrome b (*Cytb*), cytochrome c oxidase I (*CoI*), and cytochrome c oxidase II (*CoII*) mRNA in HD mice were investigated using northern blot and RNA slot blot analyses. Prerequisites for successful northern blot analyses are good quality RNA, specific probes, an internal control for RNA loading and adequate exposure times of X-ray film to radiolabelled northern blot membranes. Therefore, optimisation of these requirements were performed using the methods described in section 5.3

6.2.1 RNA extraction and first strand cDNA synthesis

RNA extraction and first strand cDNA synthesis were performed using the materials and methods described in section 5.3.1.

6.2.2 Cloning RT-PCR products as probes for northern blot and RNA slot blot analyses

The primers COIF, COIR, COIIF, COIIF, CytbF and CytbR (section 2.1.7) were carefully chosen from mRNA sequences published in GenBank (NCBI) to amplify fragment from mouse mitochondrial cytochrome b (*Cytb*), cytochrome c oxidase I (*CoI*), and cytochrome c oxidase (*CoII*) cDNA respectively. The size of the PCR products amplified from first strand cDNA using these primers were as predicted: 841 bp using primers COIF and COIR, 610 bp using primers COIIF and COIIF, 711 bp using primers CytbF and CytbR (Fig. 6.1a). The PCR products were gel purified and cloned using the methods described in section 2.2.9. The resulting recombinant plasmids were designated pCOI, pCOII, and pCytb respectively. Plasmid DNA from these clones was isolated using the isolation procedure described in section 2.2.2.1 and digested with *Eco*RI to release the insert to ensure that the correct DNA fragment had been cloned (Fig. 6.1b). The identity of the cloned fragment was confirmed by sequencing each of the 3 clones. The PCR products of amplifying pCOI, pCOII, and pcytb DNA with the corresponding primers were gel purified and ~ 25 ng of the purified DNA fragments (Fig. 6.1c) were used as the probes for visualizing *CoI*, *COII*, and *Cytb* mRNA transcripts on northern blots or RNA slot blots.

6.2.3 Optimising the exposure time of X-ray film to radiolabelled northern blot membranes

In order to obtain the linear range of signal response of X-ray film to radiolabelled membranes, the exposure times of X-ray film for northern blot analyses of *CoI*, *CoII* and *Cytb* mRNA were optimised using the methods described in section 5.3.4. Exposure times of 3-4, 7 and 8 hours were chosen for quantifying *CoI*, *CoII* and *Cytb* transcript levels respectively. The level of β-actin mRNA was used as an internal control for RNA loading and the exposure time for quantifying β-actin mRNA levels was 4-5 hours as described in section 5.3.4.

a) RT-PCR of *CoI, CoII and Cytb* mRNA

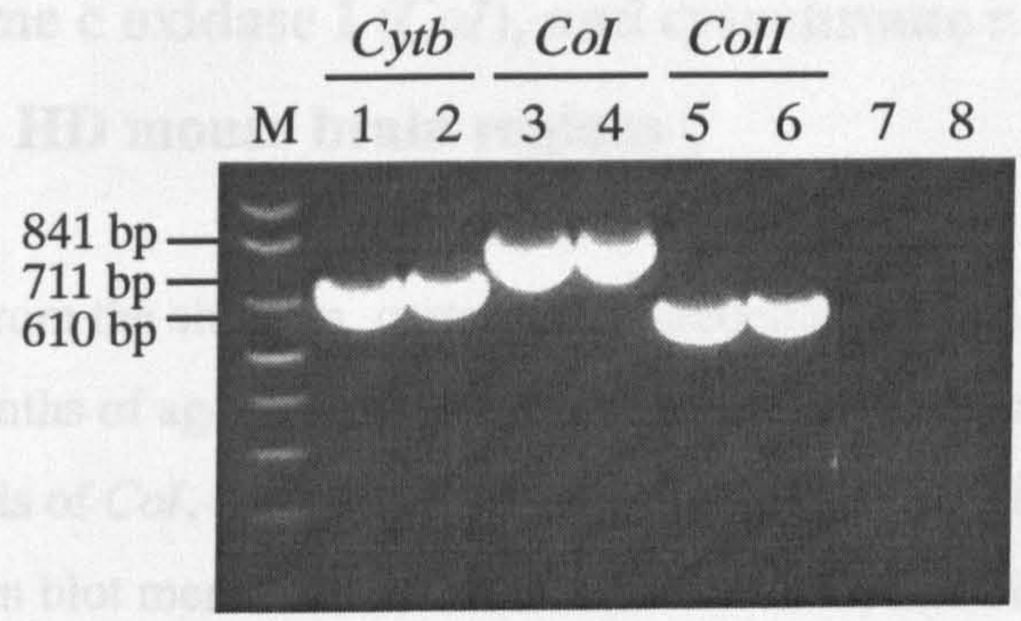

b) EcoRI-digested DNA from pCOI, pCOII and pCytb

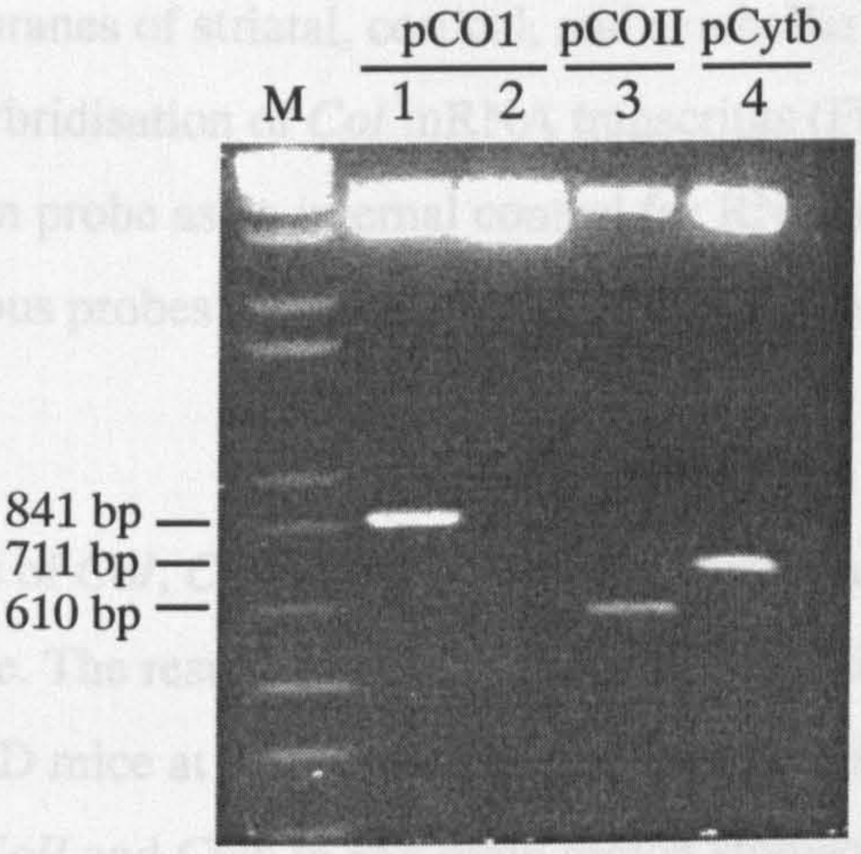

c) Purified insert DNA from pCytb, pCOI and pCOII

Figure 6.1 Generation of probes for northern blot analysis of *CoI, CoII and Cytb* mRNA. a) PCR products from amplifying first strand cDNA are resolved on an EtBr-stained agarose gel. Lanes 1 and 2 contain PCR products from *Cytb* mRNA using primers CytbF and CytbR. Lanes 3 and 4 contain PCR products from *CoI* mRNA using primers COIF and COIR. Lane 5 and 6 contain PCR products from *CoII* mRNA using primers COIIF and COIIR. Lane 7 is the control lane containing the reaction where COIF and COIR were used as primers and the RNA template had not been treated with reverse transcriptase. Lane 8 is the control lane containing the reaction using water as a template and using COIF and COIR as primers. PCR products in gel (a) were purified and cloned to generate recombinant plasmids called pCOI, pCOII and pCytb. b) *Eco*RI-digested DNA from pCOI, pCOII and pCytb (lane 1, 3, and 4 respectively) were visualized on an EtBr-stained agarose gel . Lane 2 contains digested DNA from a candidate bacterial colony containing a plasmid with no insert. c) 1.5 µl of purified insert DNA from pCytb, pCOI and pCOII was loaded onto an EtBr-stained agarose gel. 1 µl (~30 ng) of each of the purified insert DNAs was used as a probe in northern blot analyses. The 1 kb plus size ladder is indicated by M.

6.2.4 Determining the expression levels of cytochrome b (*Cytb*), cytochrome c oxidase I (*CoI*), and cytochrome c oxidase II (*CoII*) mRNA in HD mouse brain regions

RNA was isolated from the striatum, cortex, and cerebellum of 7 HD mice and 7 wild-type littermates at 24 months of age (for details of mouse cohort used see section 2.1.18) for northern blot analysis of *CoI*, *CoII* and *Cytb* mRNA and RNA slot blot analysis of *CoI* mRNA. The northern blot membranes of striatal, cortical and cerebellar RNA generated in section 5.3.6 were used for hybridisation of *CoII* and *Cytb* mRNA transcripts (Fig. 6.2). Other northern blot gels and membranes of striatal, cortical and cerebellar RNA were generated for the hybridisation of *CoII* mRNA transcripts (Fig. 6.3). The slot blot membranes of striatal, cortical, and cerebellar RNA generated in section 5.3.6 were used for the hybridisation of *CoI* mRNA transcripts (Fig. 6.4). Each membrane was hybridised with β-actin probe as an internal control for RNA loading. Before each membrane was re-probed, previous probes were stripped off the membrane using the method described in section 5.3.3.

Ratios of *CoI*, *CoII* and *Cytb* mRNA level/β-actin mRNA level were determined for each sample. The results are summarised in Table 6.1 and Table 6.2 respectively. They reveal that HD mice at 24 months of age showed no significant differences in mRNA levels of *CoI*, *CoII* and *Cytb* in any brain region studied when compared to normal littermates. However, the HD mice showed a trend toward decreased levels of *CoI* mRNA in the striatum in both slot blot ($p = 0.065$) and northern blot analyses ($p = 0.11$) when compared to wild-type littermates, although the difference did not reach statistical significance.

6.3 Immunohistochemical detection of cytochrome c oxidase I (COI) in HD mouse brain tissue

Results from the study described in the previous section (6.2.4) showed that mRNA levels of mitochondrial respiratory enzymes do not appear to be compromised in the striatum of HD mice despite mtDNA depletion. However, the striatum of HD mice showed a trend toward decreased cytochrome c oxidase I (*CoI*) mRNA levels in both RNA slot blot and

a) Striatum

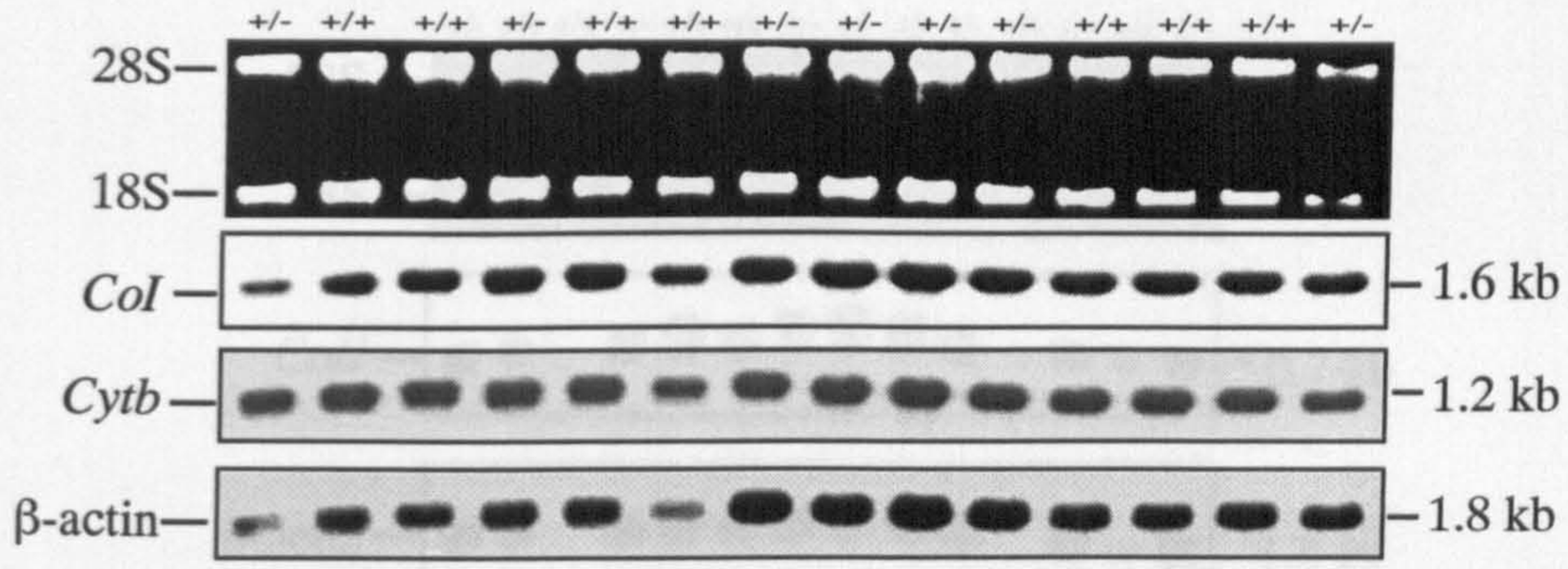

b) Cortex

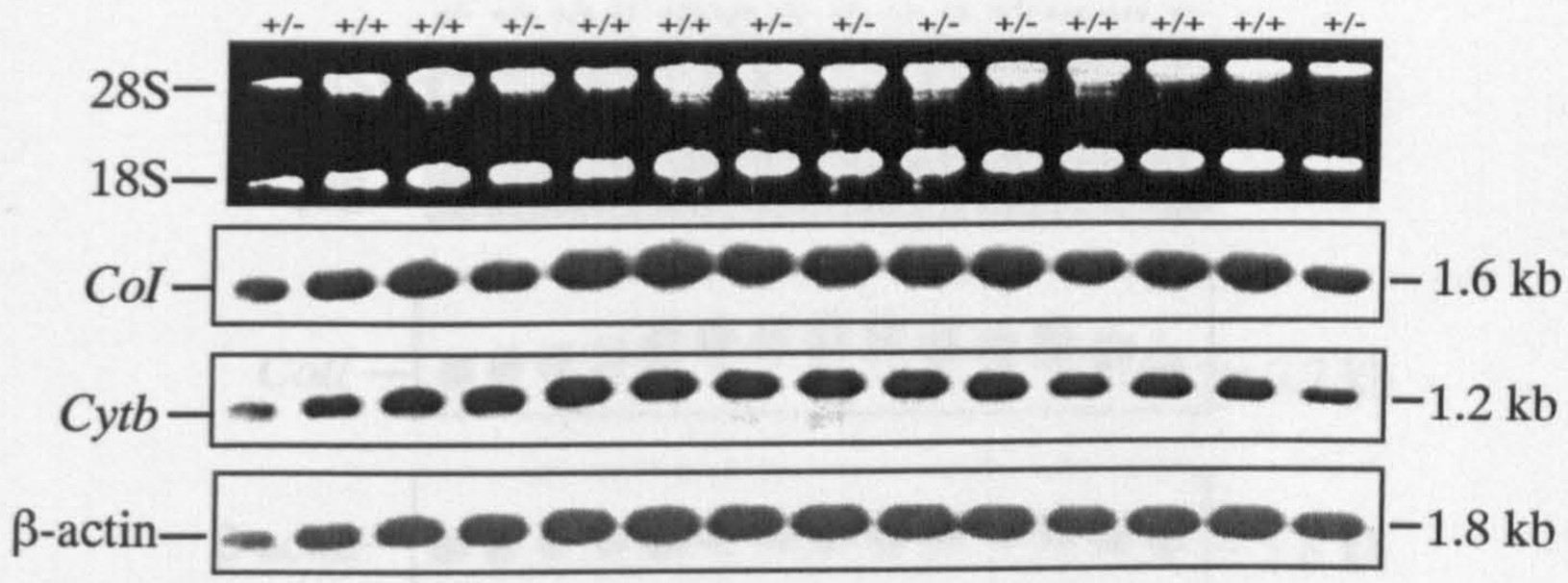

c) Cerebellum

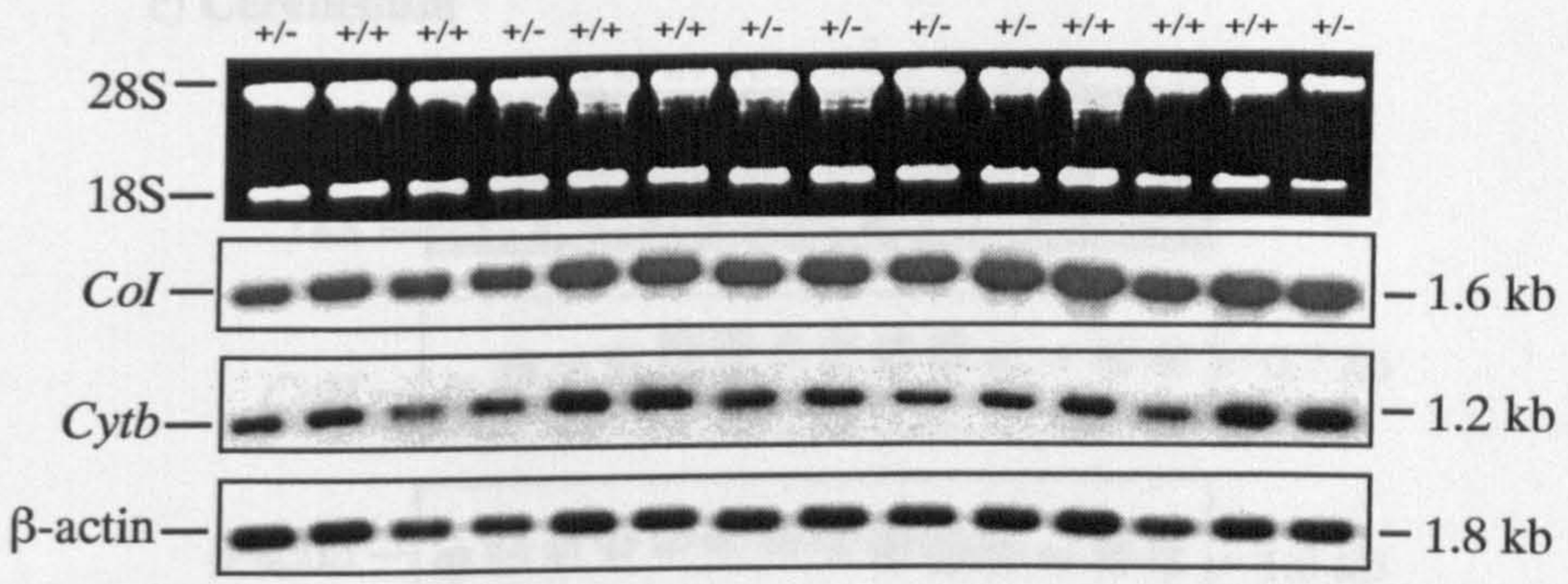

Figure 6.2 Northern blot analyses of *CoI* and *Cytb* mRNA in the striatum (a), cortex (b) and cerebellum (c) of 24 month-old mice. 15 μg of total RNA from 7 HD mice (+/-) and 7 wild-type littermates (+/+) was loaded onto a formaldehyde EtBr-stained gel (top panels in a,b,and c). Total RNA in gel was transferred to a nylon membrane which was probed for visualization of *CoI* , *Cytb* and β-actin mRNA transcripts (lower panels in a, b and c). The level of β-actin mRNA transcripts was used as an internal control for RNA loading.

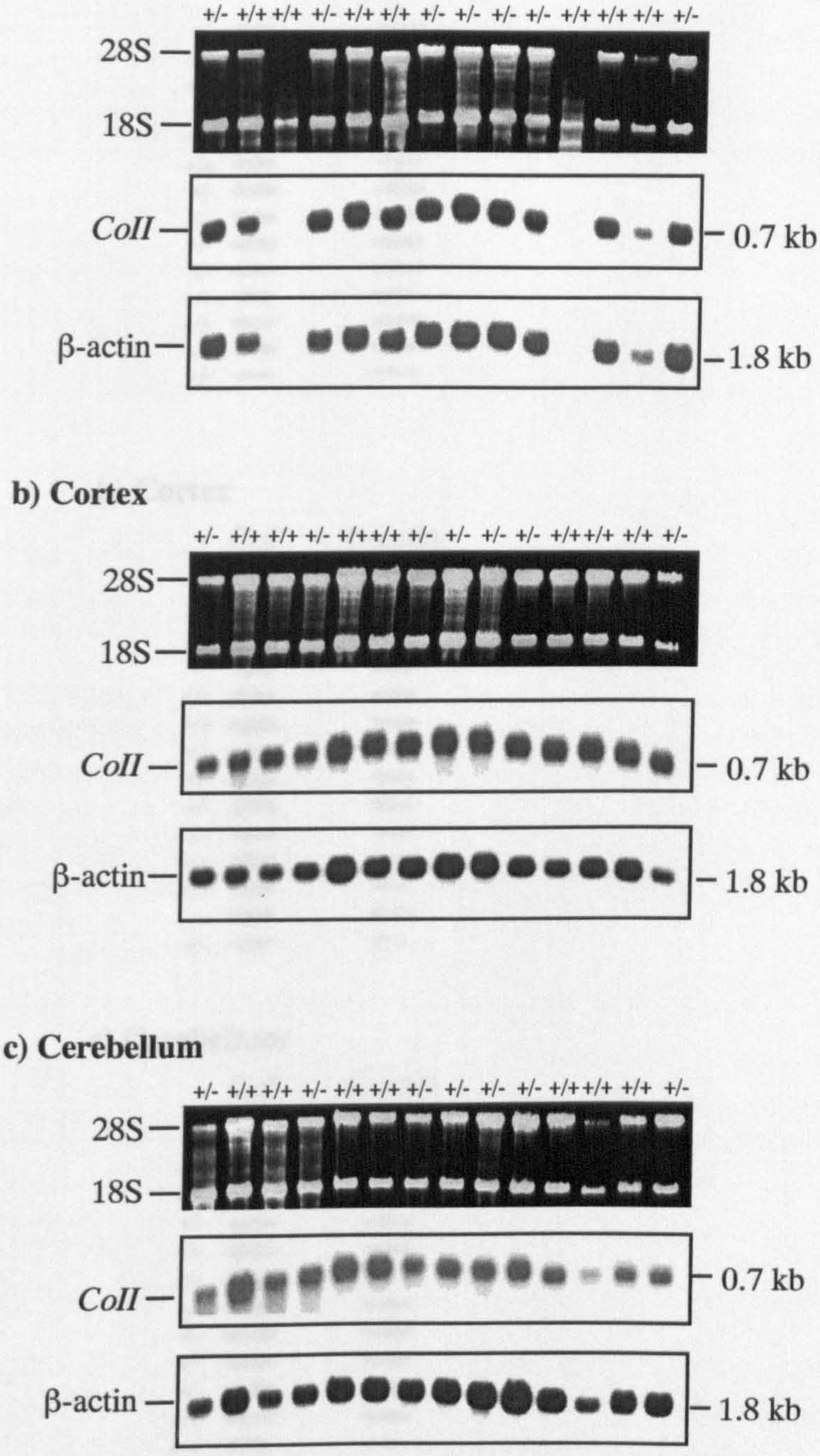

Figure 6.3 Northern blot analyses of *CoII* mRNA in the striatum, cortex and cerebellum of 24 month-old mice. 15 μg of total RNA from striatum (a), cortex (b) and cerebellum (c) of 7 HD mice (+/-) and 7 wild-type littermates (+/+) was loaded onto a formaldehyde EtBr-stained gel (top panel in a, b, and c). Total RNA in each gel was transferred, and probed for visualization of *CoII* and β-actin mRNA transcripts. β-actin mRNA transcripts was used as an internal control for RNA loading. Two RNA samples from 2 wild-type striatal tissues (a) were degraded. Therefore, the *CoII* and β-actin mRNA transcripts of these two samples are not visible on the appropriate autoradiographs.

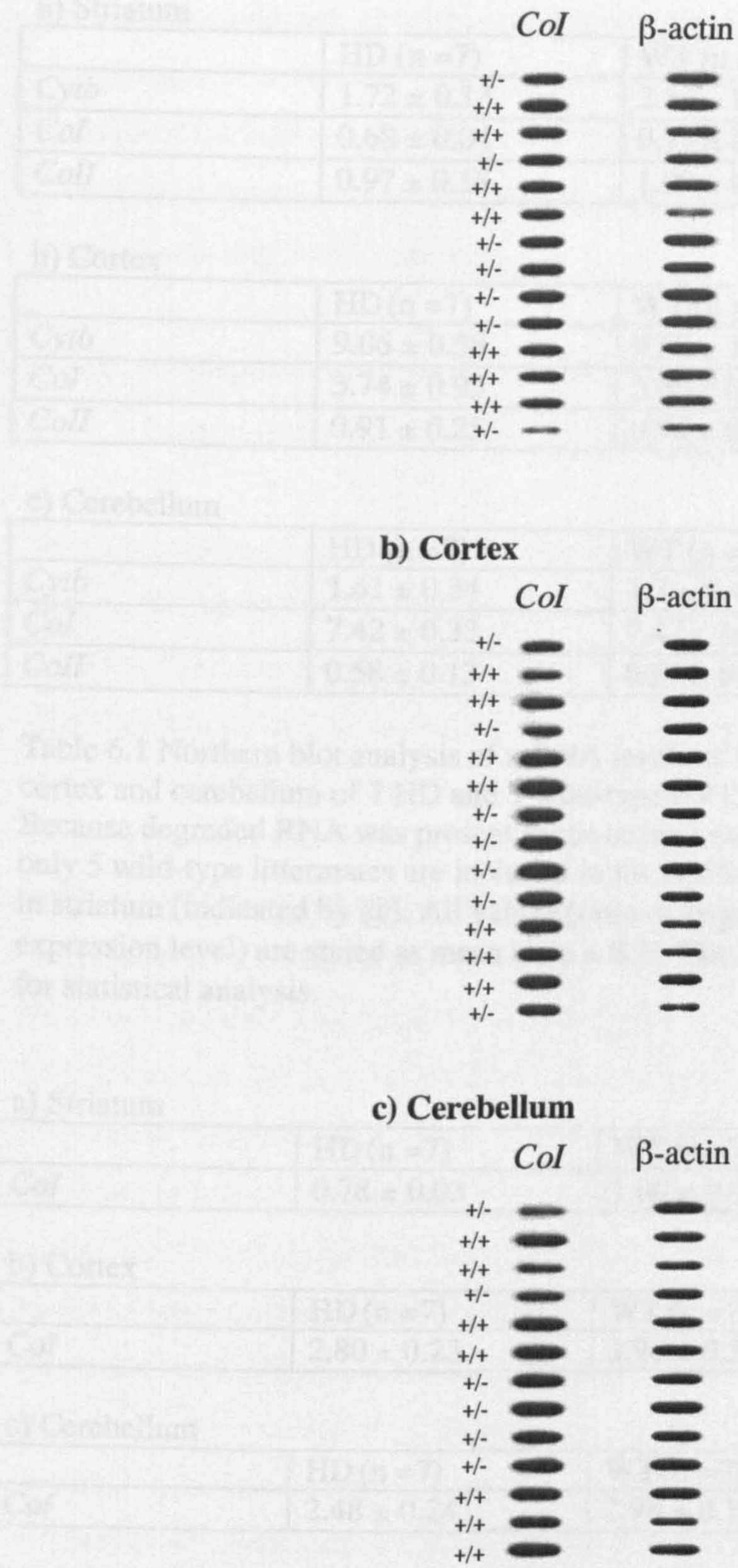

Figure 6.4 RNA slot blot analyses of *CoI* mRNA in the striatum (a), cortex (b) and cerebellum (c) of 24 month-old mice. 5 μg of total RNA from striatum, cortex and cerebellum of 7 HD mice (+/-) and 7 wild-type littermates (+/+) was loaded into each slot and transferred to a nylon membrane. Each membrane was probed for visualization of *CoI* and β-actin mRNA transcripts. The level of β-actin mRNA transcripts was used as an internal control for RNA loading.

a) Striatum

	HD (n =7)	WT (n =7)	*p* value
Cytb	1.72 ± 0.13	2.14 ± 0.24	0.17
CoI	0.68 ± 0.04	0.77 ± 0.04	0.11
CoII	0.97 ± 0.18	1.09 ± 0.11@	0.21

b) Cortex

	HD (n =7)	WT (n =7)	*p* value
Cytb	9.06 ± 0.58	9.58 ± 1.37	0.52
CoI	3.74 ± 0.93	3.86 ± 0.26	0.78
CoII	0.91 ± 0.25	0.96 ± 0.14	0.63

c) Cerebellum

	HD (n =7)	WT (n =7)	*p* value
Cytb	1.61 ± 0.34	1.7 ± 0.4	0.7
CoI	7.42 ± 0.33	7.47 ± 0.93	0.9
CoII	0.58 ± 0.13	0.63 ± 0.26	0.7

Table 6.1 Northern blot analysis of mRNA levels of C*ytb, CoI* and *CoII* in the striatum, cortex and cerebellum of 7 HD and 7 wild-type (WT) littermates at 24 months of age. Because degraded RNA was present in the striatal samples from 2 wild-type littermates, only 5 wild-type littermates are included in the northern blot analysis of *CoII* mRNA levels in striatum (indicated by @). All values (ratio of target gene expression level/β-actin expression level) are stated as mean ratio ± S.E. The Student's *t* test (two tailed) was used for statistical analysis.

a) Striatum

	HD (n =7)	WT (n =7)	*p* value
CoI	0.78 ± 0.03	1.00 ± 0.06	**0.065**

b) Cortex

	HD (n =7)	WT (n =7)	*p* value
CoI	2.80 ± 0.23	2.96 ± 0.32	0.7

c) Cerebellum

	HD (n =7)	WT (n =7)	*p* value
CoI	2.48 ± 0.24	2.94 ± 0.14	0.13

Table 6.2 Slot blot analysis of mRNA levels of *CoI* in the striatum (a), cortex (b) and cerebellum (c) of 7 HD and 7 wild-type (WT) littermates at 24 months of age.
HD mice show a trend toward reduction of *CoI* mRNA expression levels in the striatum when compared to normal littermates. All values (ratio of target gene expression level/β-actin expression level) are stated as mean ratio ± S.E. The Student's *t* test (two tailed) was used for statistical analysis.

northern blot analyses, although this failed to reach statistical significance. It is conceivable that changes in individual cells or localized to a small area of striatum may be masked by analysis of the bulk tissue homogenate used in northern blot and slot blot analyses. Therefore, immunohistochemical detection of COI was performed to investigate its expression at single cell resolution.

6.3.1 Comparison of free-floating and paraffin-embedded sections for immunohistochemical detection of COI

Several methods of preparing tissue sections have been employed in immunohistochemical studies, including free-floating (section 2.2.17.2) and paraffin-embedded (section 2.2.17.3) sections. There are advantages and disadvantages associated with both methods. Free-floating sections tend to show more non-specific staining than paraffin-embedded sections. However, free-floating sections can reveal more about the morphological relationship between different cell types in brain tissue than paraffin-embedded sections. In order to obtain good quality immunostaining, a pilot study comparing the two methods of tissue preparation for anti-COI antibody staining was conducted. Brains from two HD mice and two wild-type mice were fixed by transcardial perfusion (section 2.2.17.1). After fixation, brains from one HD and one wild-type mouse were subjected to paraffin-embedded section preparation (section 2.2.17.3) and the remaining HD and wild-type mouse brain tissue was subjected to free-floating section preparation (section 2.2.17.2). In this pilot study, positive control sections from rats that had received a cortical injection of α-amino-3-hydroxy-5-methyl-4-isoxazolepropionate (AMPA) (a gift from Jill Fowler, Wellcome Surgical Institute, Glasgow) were included in the immunostaining experiment of free-floating sections. Positive control sections from rats treated with cerebral artery occlusion were included in the immunostaining experiment of paraffin-embedded sections (a gift from Debbie Dewar, Wellcome Surgical Institute, Glasgow). Negative control sections, omitting the primary antibody, were also included in the study. Both paraffin-embedded and free-floating sections were subjected to immunohistochemical detection with different concentrations of primary antibody: 4, 2, 1, 0.4, 0.2 and 0.1 μg/ml. These sections were then treated with secondary antibodies, anti-mouse IgG (1:100) and ABC kits using methods described in sections 2.2.17.4 and 2.2.17.5. After examination using light microscopy, the

best free-floating sections stained with anti-COI antibody (2 μg/ml) were compared with the best paraffin-embedded sections stained with anti-COI antibody (4 μg/ml). The results indicated that paraffin-embedded sections provided better resolution and less background than free-floating sections (Fig. 6.5). Therefore, paraffin-embedded sections were used in subsequent immunodetection experiments.

6.3.2 Optimization of immunohistochemical assays

6.3.2.1 Positive control sections for assays

Immunostaining conditions for the anti-COI antibody were optimised in a pilot study where rat brain sections with an ischemic lesion were used as a positive control (section 7.3.1). However, HD is a slowly progressive degenerative disorder whilst acute pathological changes occur immediately after an ischemic insult. Therefore, the acute pathological changes observed in rat brain sections with an ischemic lesion may not provide an ideal positive control for investigating HD pathology. Reports in the literature have shown that systemic injection of 3-nitropropionic acid (3-NP) (an irreversible mitochondrial enzyme complex II inhibitor) in rodents and non-human primates is sufficient to replicate most of the clinical and pathophysiological hallmarks of HD (Borlongan et al., 1997; Guyot et al., 1997; Vis et al., 1999). Both 3-NP and malonate (a reversible mitochondrial enzyme complex II inhibitor) are mitochondrial enzyme complex II inhibitors. After malonate or 3-NP treatment, the striatum shows similar pathological changes, which include increased oxidative stress. However, since 3-NP generates symmetrical striatal lesions after systemic injection, the contrast between the damaged and the contralateral normal striatum is lost. A malonate injection into the striatum of mice allows the comparison of malonate-treated and contralateral normal striatum. Therefore, sections of brain from mice that had received injections of malonate into the striatum (a gift from Daniel Cuthill, Wellcome Surgical Institute, Glasgow) were used as positive controls for subsequent immunohistochemical assays.

a) Paraffin-embedded mouse brain section

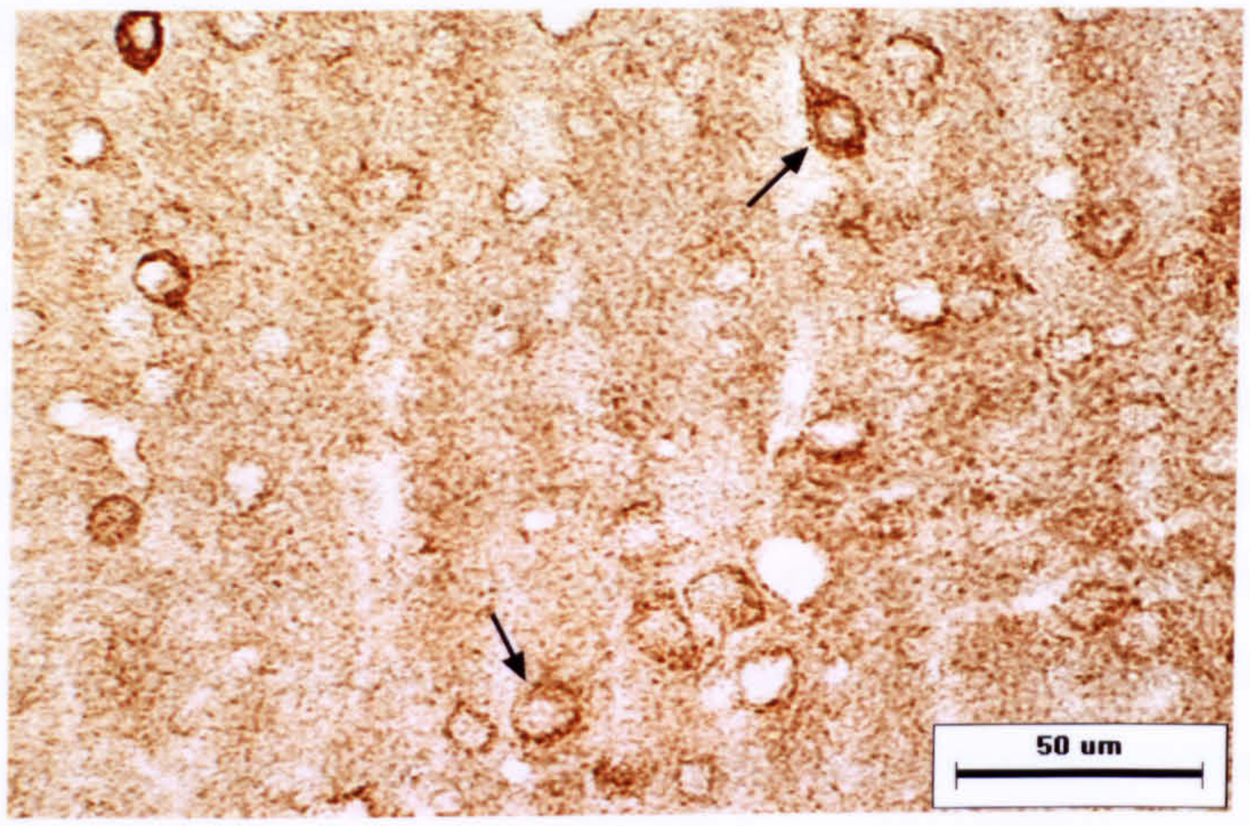

b) Free-floating mouse brain section

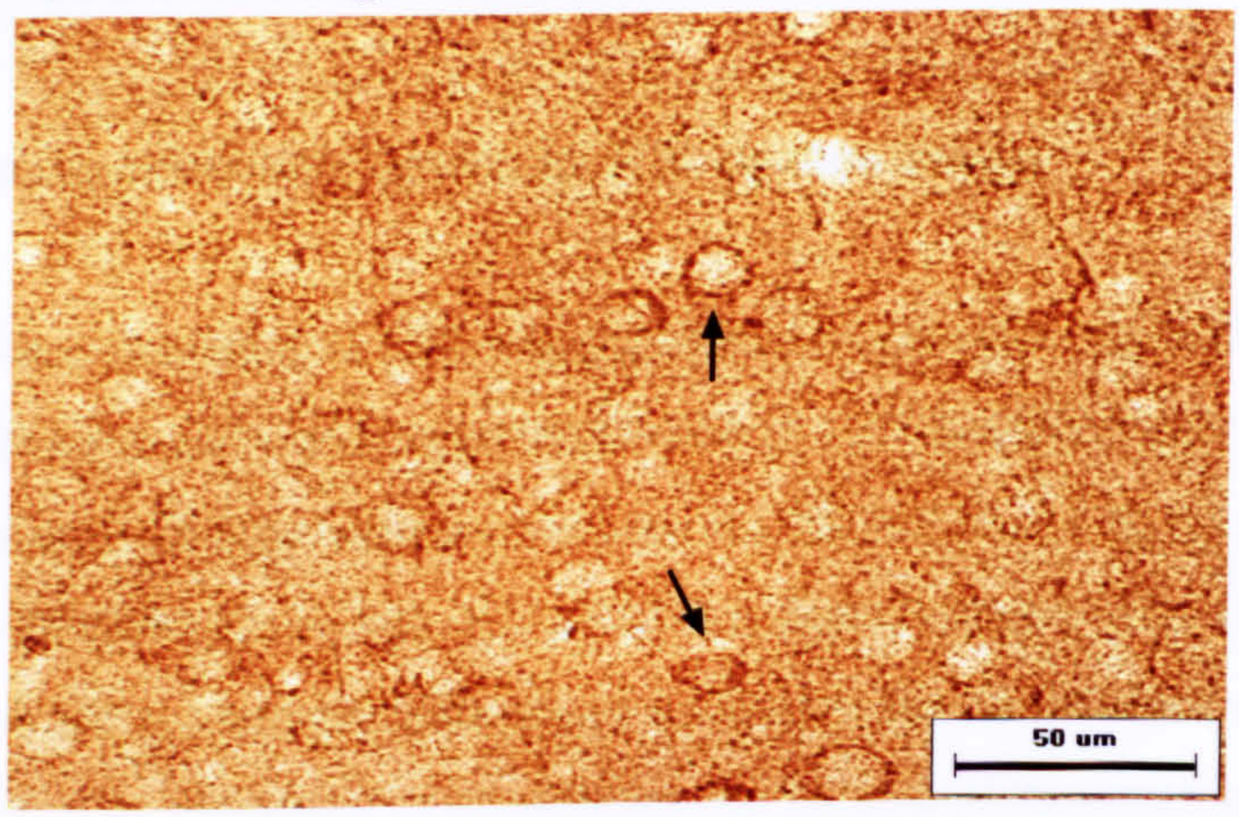

Figure 6.5 An example of the comparison between free-floating and paraffin-embedded sections stained with the anti-COI antibody. The paraffin-embedded section (a) from a normal mouse brain showed better staining resolution and less background than the free-floating section (b) from a normal mouse brain. Neurons with normal cytoplasmic staining are indicated by arrows. Scale bar = 50 μm

6.3.2.2 Optimization of immunohistochemical detection of COI

The positive control sections (with malonate injection) subjected to the conditions for anti-COI staining determined by the pilot study showed increased cytoplasmic staining around the lesion in the striatum (Fig 6.6a), when compared to the non-lesion striatum (Fig 6.6b). However, the negative control sections, omitting the primary monoclonal anti-COI antibody, subjected to the conditions for anti-COI staining determined by the pilot study, showed strong staining in the malonate-injected brain section (Fig 6.6c). The strong staining of the malonate lesion in these negative control sections was probably due to the non-specific binding of the secondary antibody to endogenous mouse IgG. To solve this problem, the dilution of secondary antibody used was changed from 1:100 to 1:500. In addition, the Mouse on Mouse Immunodetection kit (M.O.M) (Vector) for blocking non-specific binding to endogenous mouse IgG was applied when staining sections with the anti-COI antibody (Fig 6.6d). The staining intensity was also enhanced by using the *Elite* ABC kit instead of the standard ABC kit. The resulting optimized methods used for immunohistochemical detection of COI are described in section 2.2.17.5.

6.3.3 COI immunostaining levels in HD mouse brain

Immunohistochemical detection of COI was performed on paraffin-embedded brain sections from 4 HD mice and 4 wild-type littermates at ~ 25 months of age (for details of mouse cohorts and methodology used see sections 2.1.18, 2.2.17, 2.1.9, 2.1.10 and 2.2.17.5). A Leica DMRB microscope connected to a digital camera (Cool Snap-Pro, Media Cybernetics) and a computer with image analysis software (Image Pro Plus 4.5, Media Cybernetics) were employed to photograph the images of the resulting sections. Before analysing the results, all slides used were labelled with random numbers by another person so that the quantitative analysis was performed in a manner blind to genotype.

For semi-quantitative analysis of COI immunostaining, one caudal striatum (right striatum in a section), the most vulnerable region of HD brain, from each mouse was analysed. Each striatum was divided into 4 approximately equal parts, i.e. dorsomedial, dorsolateral, ventromedial and ventrolateral (Fig. 6.7). Two images from each striatal subarea were captured at x400 magnification. Care was taken to ensure these 2 images did not overlap.

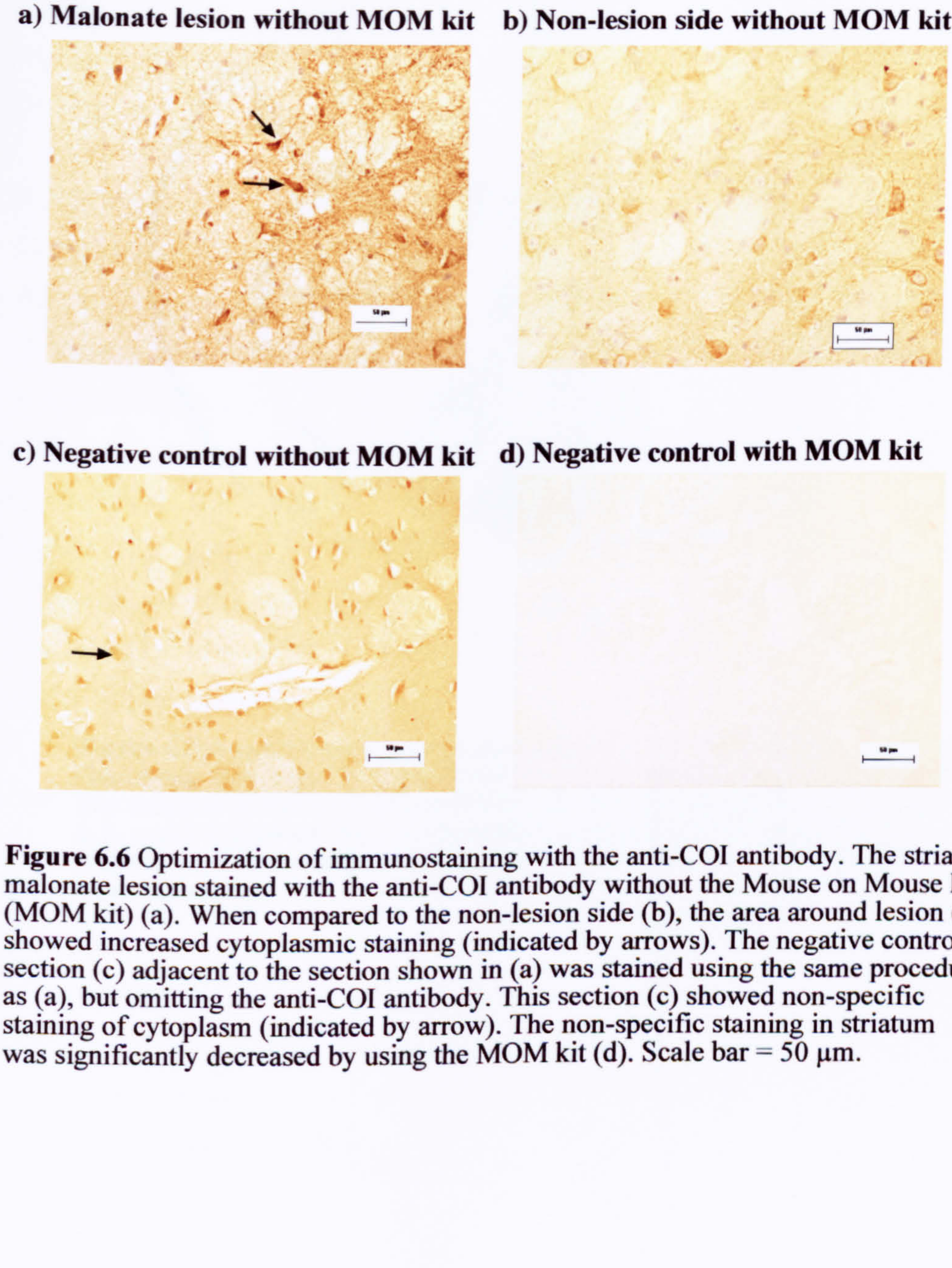

Figure 6.6 Optimization of immunostaining with the anti-COI antibody. The striatal malonate lesion stained with the anti-COI antibody without the Mouse on Mouse kit (MOM kit) (a). When compared to the non-lesion side (b), the area around lesion (a) showed increased cytoplasmic staining (indicated by arrows). The negative control section (c) adjacent to the section shown in (a) was stained using the same procedure as (a), but omitting the anti-COI antibody. This section (c) showed non-specific staining of cytoplasm (indicated by arrow). The non-specific staining in striatum was significantly decreased by using the MOM kit (d). Scale bar = 50 μm.

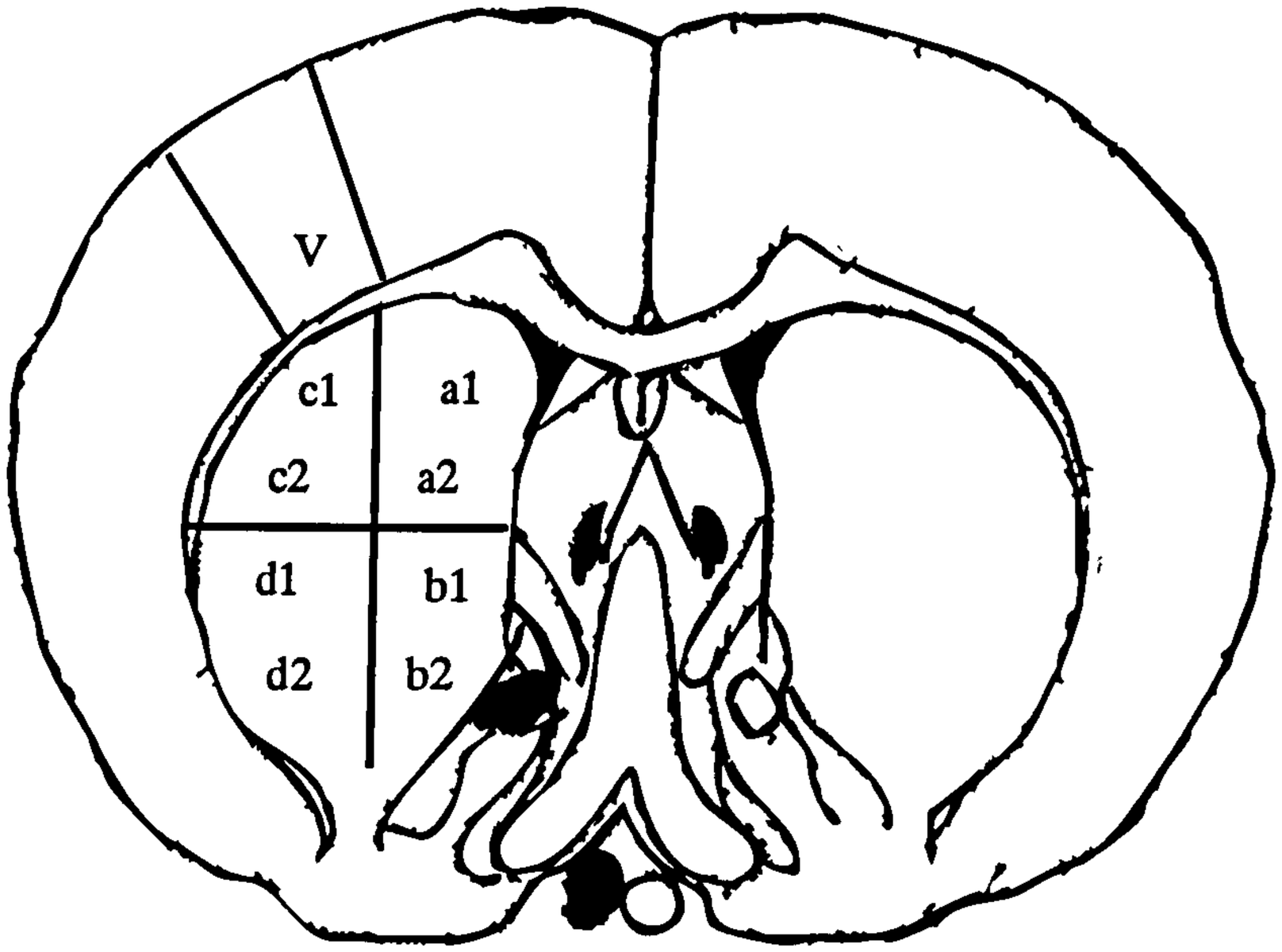

Figure 6.7 A mouse brain map for quantifying levels of COI immunostaining. One image from layer V of the cortex in each mouse brain section was captured. The striatum in one hemisphere of each mouse was divided into 4 equal parts, a, b, c and d (dorsomedial, ventromedial, dorsolateral, and ventrolateral respectively). Two images (e.g. a1 and a2) from each subarea of the striatum were captured.

The area of cortex showing greatest pathology in HD is layer III and V of the primary sensory cortex. Therefore, one image of the primary sensory cortex (containing layer V) was captured from one brain section per mouse at the level of caudal striatum (Fig. 6.7). COI immunostaining of cells was classified into one of three groups [weak staining (score 1), moderate staining (score 2) and intense staining (score 3)], according to the intensity of cytoplasmic immunostaining (Fig. 6.8). An area of 0.06 mm^2 from the centre of each image was selected and the number of cells with weak, moderate, or intense staining counted. From these results, a total score [(number of weakly staining cells x 1) + (number of moderately staining cells x 2) + (number of intensely staining cells x 3)] was calculated for each image.

The two staining scores from each striatal subarea of each mouse were averaged (Table 6.3). The score of each subarea from the striatum of HD mice was combined and compared to that of wild-type littermates using the Student's *t* test (two tailed). A *p* value of less than 0.05 was considered statistically significant. The results showed that COI immunostaining was significantly decreased in the dorsolateral striatum, but not in any other part of striatum of HD mice, when compared to wild-type littermates (Fig. 6.9a). However, it is notable that other parts of the striatum of HD mice also showed a trend toward decreased staining scores when compared to wild-type littermates. When the scores from the four parts of striatum were combined, the result also showed that the immunostaining of COI is significantly decreased in the striatum of HD mice when compared to wild-type littermates (Fig. 6.9a). Immunostaining in the cell soma, but not the axon, was quantified. The finding that COI immunostaining was decrease in the cell soma in HD striatum may be due to the re-distribution of mitochondria to the cell processes. However, when examing COI immunostaining in the axons of HD mice and wild-type littermates, decreased axonal staining intensity was observed in the HD striatum when compared to wild-type littermates (Fig. 6.10). This observation suggests that mitochondrial re-distribution is unlikely and COI immunostaining in both cell soma and processes is decreased in HD striatum. The staining score of cortex from each mouse was also calculated (Table 6.4). The results showed that no significant difference in COI staining scores of cortex was observed between HD and wild-type littermates (Fig. 6.9b).

Although the use of Student's *t*-test analysis is valid in this situation, it might inflate differences between mutant and wild-type sections. The raw data showed high variability between samples within each group. Therefore, the results of the statistical analysis should be considered preliminary and should be confirmed in further experiments using larger cohorts and multiple tissue sections for each animal.

Animal ID	Genotype	Dorsomedial	Ventromedial	Dorsolateral	Ventrolateral
7836	+/-	15	25	32	22
7783	+/-	19	21	21	27
7839	+/-	22	38	25	51
7778	+/-	11	11	19	14
7705	+/+	41	41	53	49
7689	+/+	33	53	44	66
7781	+/+	12	44	51	82
7777	+/+	42	25	26	28

Table 6.3 Cell staining scores in 4 subareas of striatum from 4 HD mice (+/-) and 4 wild-type littermates (+/+) subjected to immunostaining with the anti-COI antibody.
Each value is the mean of 2 staining scores from each striatal subarea of each mouse.

Animal ID	Genotype	Layer V
7836	+/-	54
7783	+/-	83
7839	+/-	77
7778	+/-	60
7705	+/+	79
7689	+/+	88
7781	+/+	55
7777	+/+	56

Table 6.4 Cell staining scores in layer V of cortex from 4 HD mice (+/-) and 4 wild-type littermates (+/+) subjected to immunostaining with the anti-COI antibody.

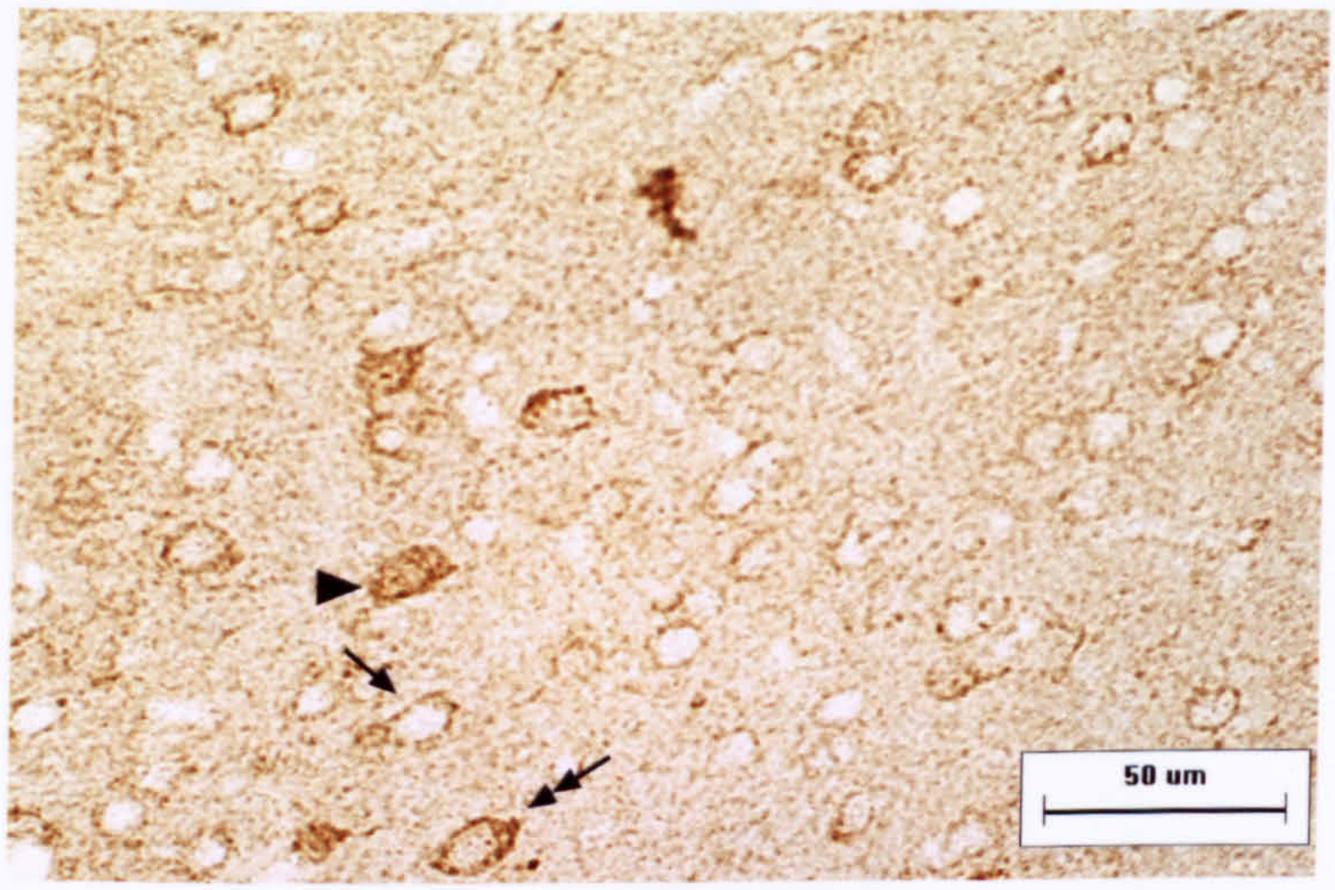

Figure 6.8 Scoring cytoplasmic staining with the anti-COI antibody. The cortical image from an HD mouse brain section shows weakly staining (score 1, arrow), moderately staining (score 2, double arrow), and intensely staining (score 3, arrow head) cells. Scale bar=50 μm

a)

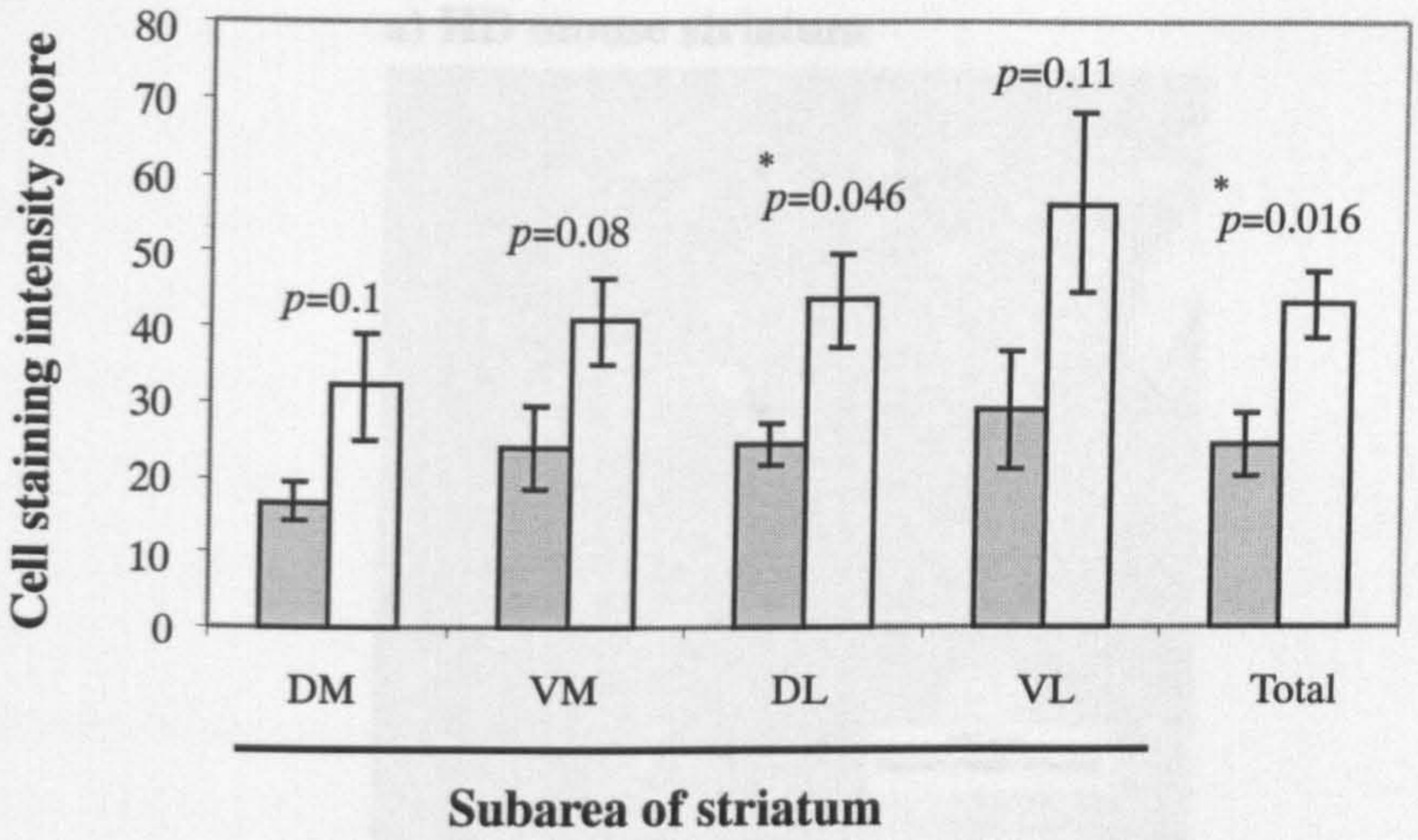

b)

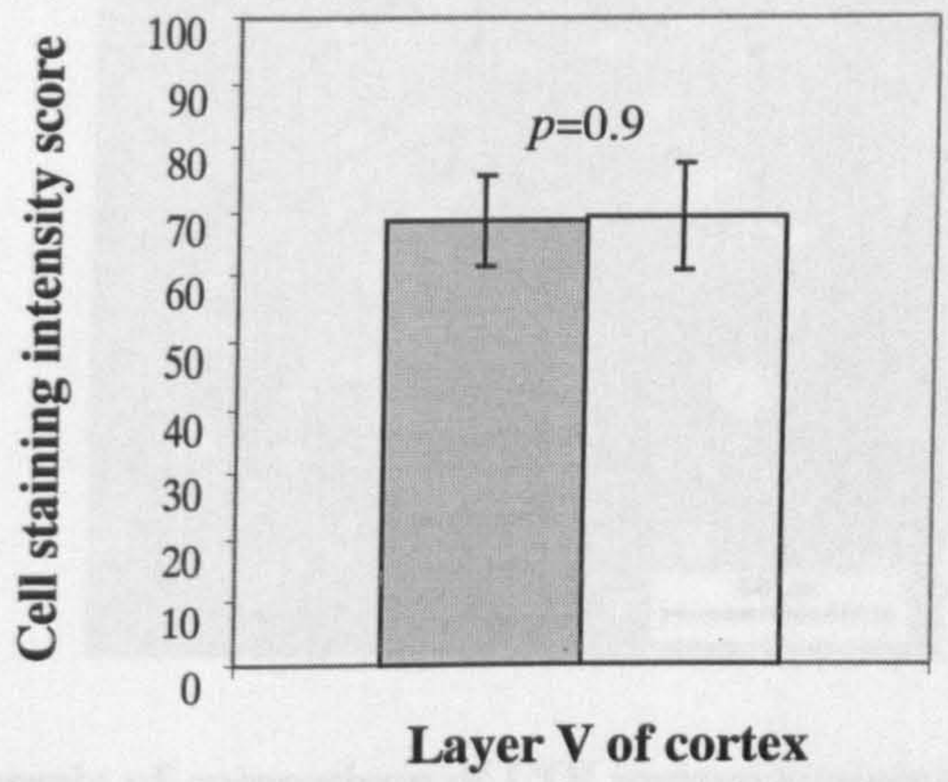

Figure 6.9 Immunostaining of COI in the striatum (a) and layer V of cortex (b) of 4 HD mice and 4 wild-type littermates at ~25 months of age. The column termed Total represents the combined results from four subareas of striatum: dorsomedial (DM), ventromedial (VM), dorsolateral (DL) and ventrolateral (VL). Stained cells were counted and a score for weak (1), moderate (2) and intense staining (3) assigned. The cell staining intensity score is the sum of the individual scores within an 0.06 mm^2 area. Data are expressed as mean ± S.E. The *p* values indicated are obtained from comparing the results obtained with HD mice (grey column) and wild-type littermates (open column) using the Student's *t* test (two-tailed) for statistical analysis. *indicates $p<0.05$.

a) HD mouse striatum

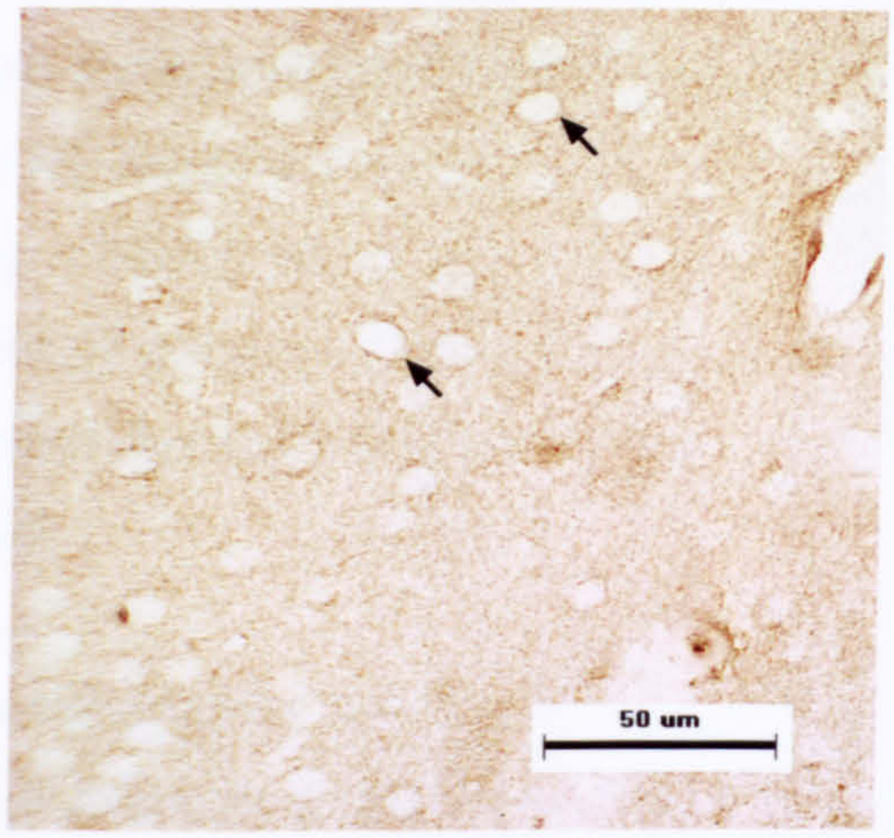

b) Wild-type littermate striatum

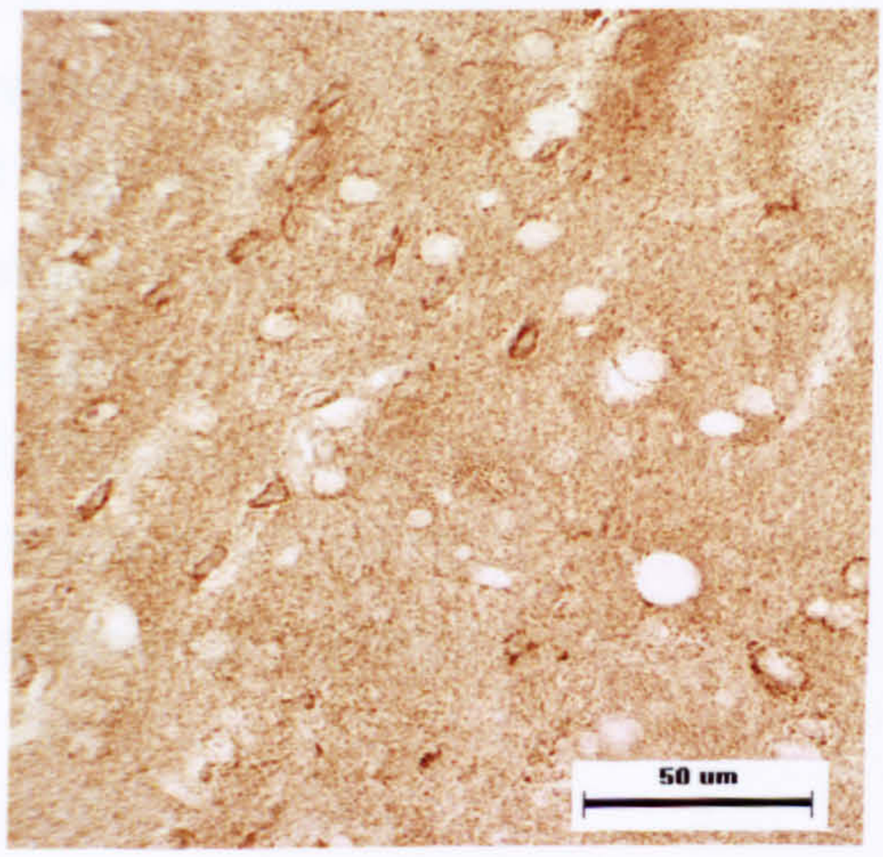

Figure 6.10 An example of comparison of COI immunostaining between HD mice and wild-type littermates. HD mouse striatum (a) shows decreased COI immunostaining in the cell soma (arrows) and the axon (fine granule staining between neurons) when compared to the wild-type littermate (b). Bar = 50 μm.

6.4 Summary

The results indicate that HD mice at ~ 25 months of age show no significant differences in mRNA levels of *CoI, CoII,* and *Cytb* in any brain region studied when compared to normal littermates. However, the HD mice show a trend toward decreased levels of *CoI* mRNA in the striatum in both slot ($p = 0.065$) and northern blot analyses ($p = 0.11$) when compared to wild-type littermates, although this does not reach statistical significance. This suggests that the mitochondrial gene expression levels may not be significantly compromised when mtDNA is ~ 30 % depleted.

COI immunostaining was significantly decreased in the dorsolateral striatum, but not in any other part of the striatum of 24 month-old HD mice when compared to wild-type littermates. However, when the results from all four parts of striatum were combined, it also showed that the immunostaining of COI was significantly decreased in the whole striatum of 24 month-old HD mice compared to wild-type littermates. The decreased staining was not found in the cortex of HD mice when compared to wild-type mice. The results suggest that immunohistochemical detection might be a better method in detecting pathological changes in HD mice where the changes can be detected at single cell level or localized to a small region. The results of CO-I immunostaining are consistent with a gradient of vulnerability within the striatum of HD, with the dorsal striatum more vulnerable and showing earlier pathological changes than other regions (Vonsattel and DiFiglia, 1998).

7 Investigating the direct evidence of increased oxidative stress in the striatum of HD mice

7.1 Background

The study in chapter 4 showed that mtDNA depletion is present in striata of 24 month-old HD mice. The striatal depletion of mtDNA in striatum is probably not caused by decreased expression levels of the *Tfam* mRNA, a key regulator of mtDNA replication (section 5.3 and 5.4). Several lines of evidence from the literature support the speculation that mtDNA depletion can occur as a consequence of increased oxidative damage of mtDNA possibly through DNA mispairing, point mutations, deletions, and fragmentation (Barazzoni et al., 2000; Bradley et al., 2000; de la Monte et al., 1988; Rodriguez-Santiago et al., 2001). Searching for direct evidence of increased oxidative stress in the HD mice is then imperative for trying to account for the finding of mtDNA depletion in the striata of HD mice.

Direct markers of increased oxidative stress can be categorized into the following three groups (Toyokuni, 1999). The first category includes those molecules that are generated in a reaction with reactive oxygen species (ROS), such as 8-hydroxydeoxyguanosine (8-OHdG), 4-hydroxy-2-nonenal (4-HNE), malondialdehyde and nitrotyrosine. These molecules are subjected to either cross-linking or covalent modification in reactions with ROS. Accordingly, the amount of these molecules will be increased when increased levels of ROS are generated. The second category consists of proteins associated with ROS metabolism, such as glutathione, glutathione peroxidase, superoxide dismutase, heat shock proteins and DNA repair enzymes. In most cases, the steady state levels and activity of these molecules are reduced immediately after exposure to ROS. However, levels tend to recover and may even show an overshooting response hours, days or even weeks after exposure. The third category is transcription factors, such as NF-kB, c-myc and c-fos. It has been shown that ROS modulate not only the expression of transcription factors but also their transcriptional activity via redox regulation (Sun and Oberley, 1996). When considering these different categories of molecules, modulation of transcription factors requires moderate levels of oxidative stress (Toyokuni, 1999) and difficulty in visualizing low-level effects in paraffin-

embedded tissues is anticipated. Levels of proteins in the second category are difficult to evaluate because of the differential response over time, as previously mentioned. Therefore, the first category molecules are pragmatically the most straightforward targets for visualizing ROS-induced damage. Furthermore, the first category molecules are proportionally responding to the dosage of oxidative stress and so the markers accumulate and will be detected precisely at the place where the free radical damage takes place (Toyokuni, 1999).

Among the first category of markers of increased oxidative stress, increased levels of 8-OHdG, a product of DNA oxidation, have been found in nuclear DNA and mtDNA in the striatum of HD patients (Browne et al., 1997; Polidori et al., 1999) and in R6/2 mice (Bogdanov et al., 2001) and also in aged human brain. Increased level of malondialdehyde, a product of lipid peroxidation, has been shown in the brains of HD patients (Browne et al., 1997). Increased level of 4-HNE modified protein, a toxic product of lipid peroxidation, has also been shown in the affected regions of Parkinson's disease (Yoritaka et al., 1996), Alzheimer's disease (Markesbery, 1997) and olivopontocerebellar atrophy (Yamashita et al., 2000); disorders that are associated with increased oxidative stress. The expression levels of 8-OHdG and 4-HNE in HD mouse brains were investigated using immunohistochemical detection. Among the second category of markers of increased oxidative stress, increased levels of heme oxygenase-1, which shows a compensatory response to oxidative stress, have been demonstrated in the striatum of HD patients (Browne et al., 1999) and the affected brain regions of Parkinson's disease (Castellani et al., 1996; Schipper et al., 1998) and other neurodegenerative disorders (Castellani et al., 1995). The expression level of heme oxygenase-1 in mouse brains was investigated using immunohistochemical detection and northern blot analysis. Alpha B-crystallin, a heat shock protein, has been shown to be increased in the brain regions of patients with some neurodegenerative disorders (Braak et al., 2001; Iwaki et al., 1992; Renkawek et al., 1999). Therefore, expression levels of αB-crystallin in mouse brains were also investigated using RNA slot blot analysis.

Previous studies of cytochrome c oxidase I expression in HD mouse brain tissues showed that changes in individual cells or localized to a small area of striatum were probably masked by analysis of the bulk tissue homogenate used in northern blot and slot blot

analyses. Striatum in HD mice showed a decreased expression level of COI when compared to littermates using immunohistochemical detection (section 6.3). For this reason, the expression levels of heme oxygenase-1, 8-OHdG and 4-HNE in HD mouse brain tissues were also investigated using immunohistochemical detection, to avoid a possible masking effect of bulk tissue analysis.

The experiments were conducted on striatum, cortex and cerebellum from HD mouse brains. These brain regions were chosen because mtDNA levels were significantly reduced in the striatum of 24-month old HD mice, but not in cortex or cerebellum, when compared to wild-type littermates (section 4.4). Therefore, cortex and cerebellum were included to ask whether any changes in the expression levels of oxidative stress markers were specific to HD mouse striatum.

7.2 Quantifying levels of heme oxygenase-1 (*Hmox1*) and αB-crystallin transcripts in mouse brain tissue

The heme oxygenase-1 (*Hmox1*) gene expression levels in HD mice were investigated using northern blot analysis and αB-crystallin gene expression levels were investigated using RNA slot blot analysis. The reason for using a slot blot approach to quantify αB-crystallin expression levels was that northern blot analysis revealed two αB-crystallin mRNA transcripts of similar sizes. These were not easily differentiated and therefore, measuring the intensity of each band was difficult (Fig. 7.1).

The primers HOF and HOR (section 2.1.7) were carefully chosen from the mouse *Hmox1* mRNA sequence published in GenBank (NCBI) to amplify specific products from first strand cDNA. The size of the PCR product amplified from first strand cDNA using HOF and HOR primers was 799 bp, as predicted from the Genbank sequence (Fig. 7.2a). The PCR product was gel purified and cloned using the methods described in section 2.2.9. The resulting clone was designated pHO. Plasmid DNA from pHO was isolated as described in section 2.2.2.1, and digested with *Eco*RI to release the insert to check that the correct DNA fragment had been cloned (Fig. 7.2b). The identity of the cloned fragment was confirmed by sequencing (Fig. 7.3). The PCR product after amplifying pHO DNA with HOF and HOR

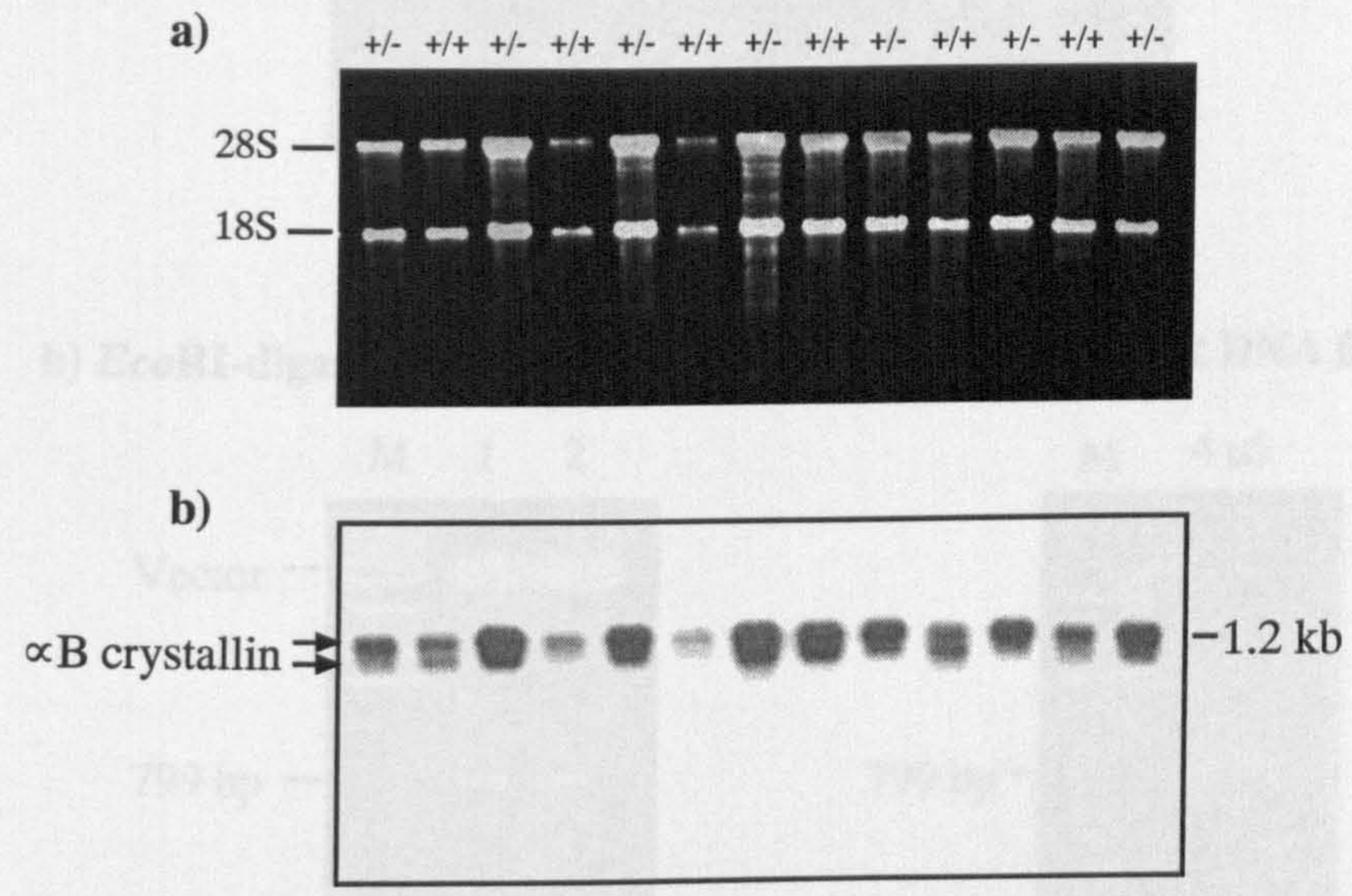

Figure 7.1 Northern blot analysis of ∝B crystallin mRNA in the striatum of 24 month-old mice. Total RNA from 6 HD mice (+/-) and 5 wild-type littermates (+/+) was resolved on a EtBr-stained formaldehyde gel (a). 10-15 μg total RNA was loaded into each lane. The clear and abundant 18S and 28S rRNA bands indicate good quality RNA. Total RNA in gel (a) was transferred to a membrane which was hybridized with the ∝B crystallin probe (b). Two mRNA transcripts of similar sizes were identified (arrows) and not easily differentiated. Therefore, the measurement of the intensity of each band was difficult.

a) RT-PCR of *Hmox1* mRNA

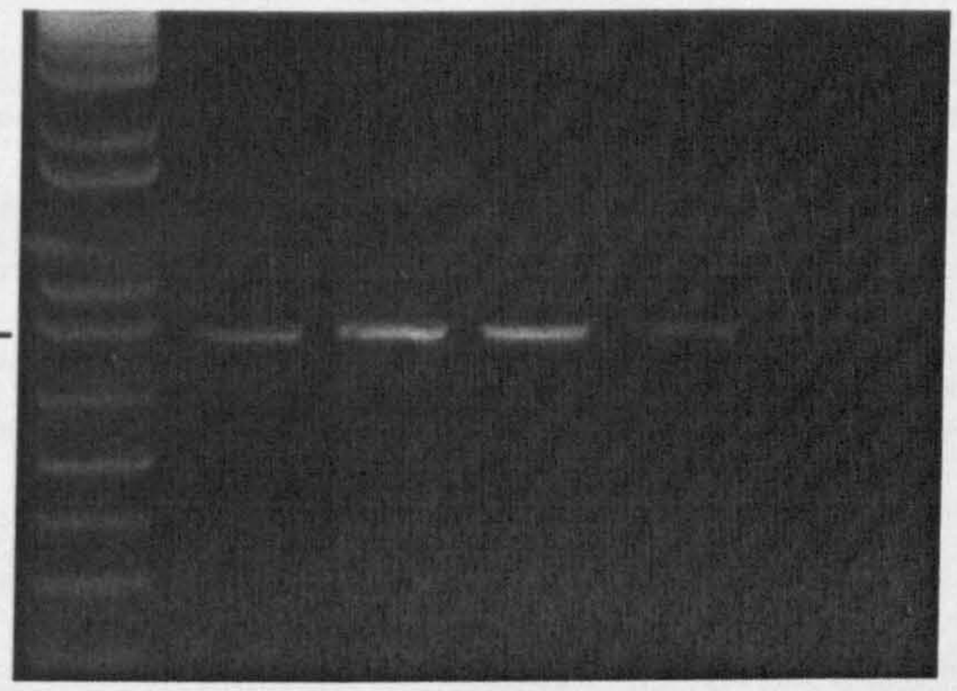

b) *Eco*RI-digested DNA from pHO

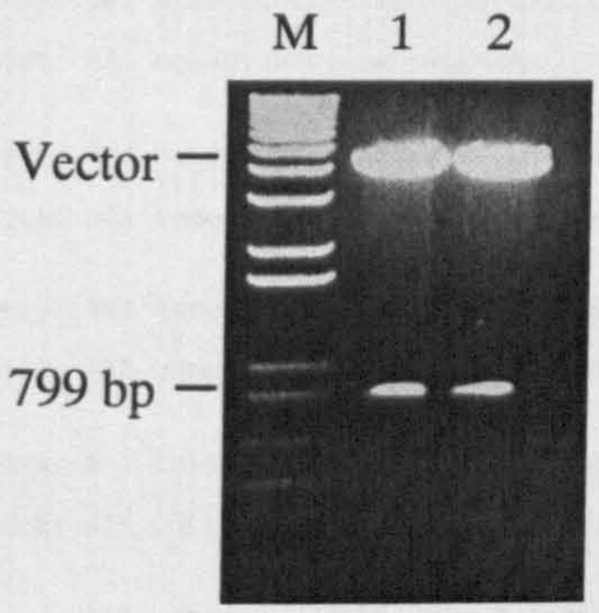

c) Purified insert DNA from pHO

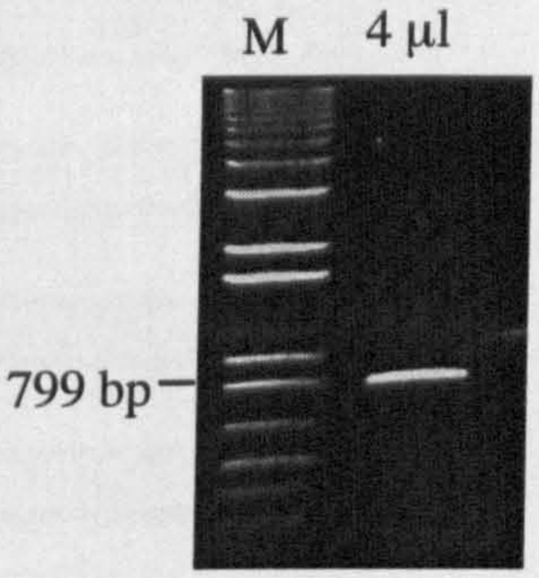

Figure 7.2 Generation of the probe for northern blot analysis of *Hmox1* mRNA. PCR products amplified from dilutions of first strand cDNA (1:1, 1:10, 1:10, 1:100) using primers HOF and HOR were visualized on an EtBr-stained agarose gel (a). NoRT indicates the control lane containing the reaction where the RNA template had not been treated with reverse transcriptase. *Eco*RI-digested DNA from pHO was visualized on an EtBr-stained agarose gel (b). Lanes 1 and 2 contain digested plasmid DNA derived from different colonies. 4 µl of purified 799 bp insert DNA from pHO was loaded onto an EtBr-stained agarose gel (c). 2 µl (~ 30ng) of purified insert DNA was used as a probe in the northern blot analysis. The 1 kb plus size ladder is indicated by M.

```
>gi|200186|gb|M33203.1|MUSP32A Mouse tumor-induced 32 kD protein (p32) mRNA, complete cds
          Length = 1510

 Score = 1419 bits (716), Expect = 0.0
 Identities = 760/772 (98%), Gaps = 4/772 (0%)
 Strand = Plus / Plus


Query: 1   cgtccacagcccgacagcatgccccaggatttgtctgaggccttgaaggaggccaccaag 60
            ||||||||||||||||||||||||||||||||||||||||||||||||||||||||||||
Sbjct: 81  cgtccacagcccgacagcatgccccaggatttgtctgaggccttgaaggaggccaccaag 140


Query: 61  gaggtacacatccaagccgagaatgctgagttcatgaagaactttcagaagggtcaggtg 120
            ||||||||||||||||||||||||||||||||||||||||||||||||||||||||||||
Sbjct: 141 gaggtacacatccaagccgagaatgctgagttcatgaagaactttcagaagggtcaggtg 200


Query: 121 tccagagaaggctttaagctggtgatggcttccttgtaccatatctacacggccctggaa 180
            ||||||||||||||||||||||||||||||||||||||||||||||||||||||||||||
Sbjct: 201 tccagagaaggctttaagctggtgatggcttccttgtaccatatctacacggccctggaa 260


Query: 181 gaggagatagagcgcaacaagcagaacccagtctatgccccactctacttccctgaggag 240
            ||||||||||||||||||||||||||||||||||||||||||||||||||||||||||||
Sbjct: 261 gaggagatagagcgcaacaagcagaacccagtctatgccccactctacttccctgaggag 320


Query: 241 ctgcaccgaagggctgccctggagcaggacatggccttctggtatgggcctcactggcag 300
            ||||||||||||||||||||||||||||||||||||||||||||||||||||||||||||
Sbjct: 321 ctgcaccgaagggctgccctggagcaggacatggccttctggtatgggcctcactggcag 380


Query: 301 gaaatcatcccttgcacgccagccacacagcactatgtaaagcgtctccacgaggtgggg 360
            ||||||||||||||||||||||||||||||||||||||||||||||||||||||||||||
Sbjct: 381 gaaatcatcccttgcacgccagccacacagcactatgtaaagcgtctccacgaggtgggg 440


Query: 361 cgcactcaccctgagctgctggtggcccacgcatatacccgctacctgggtgacctctca 420
            ||||||||||||||||||||||||||||||||||||||||||||||||||||||||||||
Sbjct: 441 cgcactcaccctgagctgctggtggcccacgcatatacccgctacctgggtgacctctca 500


Query: 421 gggggtcaggtcctgaagaagattgcacagaaggccatggccttgcccagctctggggag 480
            ||||||||||||||||||||||||||||||||||||||||||||||||||||||||||||
Sbjct: 501 gggggtcaggtcctgaagaagattgcacagaaggccatggccttgcccagctctggggag 560


Query: 481 ggcctggcnnnnnnnnaccttcccgaacatcgacagccccaccaagttcaaacagctctat 540
            ||||||||        ||||||||||||||||||||||||||||||||||||||||||||
Sbjct: 561 ggcctggctttttttaccttcccgaacatcgacagccccaccaagttcaaacagctctat 620


Query: 541 cgtgctcgaatgaacactctggagatgacacctgaggtcaagcacagggtgacagaagag 600
            ||||||||||||||||||||||||||||||||||||||||||||||||||||||||||||
Sbjct: 621 cgtgctcgaatgaacactctggagatgacacctgaggtcaagcacagggtgacagaagag 680


Query: 601 gctaagaccg-cttcctgctcaacattgagctgtttgaggagcttgcaggtgatgctgac 659
            |||||||||| |||||||||||||||||||||||||||| ||||||||||||||||||
Sbjct: 681 gctaagaccgccttcctgctcaacattgagctgtttgaggagc-tgcaggtgatgctgac 739


Query: 660 agaggaacacaaagaccaagagtccctcacagatggcgtcacttcgtcagangcctgcta 719
            |||||||||||||||| ||||||||||||||||||||||||||||| |||||||||
Sbjct: 740 agaggaacacaaagacc-agagtccctcacagatggcgtcacttcgtcagaggcctgcta 798


Query: 720 gcctggtgcaaagatactgcccctgcagagacaccccgagggaaaccccaga 771
            |||||||||| ||||||||||||||||||||||||||||||||||||||
Sbjct: 799 gcctggtgc-aagatactgcccctgcagagacaccccgagggaaaccccaga 849
```

Figure 7.3 Identity of the cloned insert of pHO plasmid was confirmed by DNA sequencing. The clone pHO was sequenced and the resulting data (Query) was checked using the Blast program (NCBI) and a matched sequence from the mouse HO-1 gene (Sbjct) was retrieved from the database search (Genbank). The result shows that 760 bp out of 772 bp (98%) are matched. Some of the unmatched sequence may be due to the genetic background differences of the mice used in query and sbjct, or due to sequencing artifacts or errors.

primers was gel purified and ~25 ng of the purified DNA fragment (Fig. 7.2c) was used as the probe for visualization of *Hmox1* mRNA on northern blot membranes.

The probe for hybridisation of αB-crystallin mRNA was obtained from amplifying plasmid DNA containing part of the αB-crystallin cDNA, pαB-CRO (previously constructed by Peggy Shelbourne). The size of the PCR product amplified using CROF and CROR2 primers (section 2.1.7) was 610 bp and the purified PCR product was used as the probe for RNA slot blot analysis (Fig. 7.4).

7.2.1 Northern blot and RNA slot blot analyses of heme oxygenase-1 (*Hmox1*) and αB-crystallin expression levels

In this study, RNA from the striata of 6 HD mice and 6 wild-type littermates at 24 months of age (section 2.1.18) was investigated for expression levels of *Hmox1* mRNA from the striata, cerebellum and cortex of 6 HD mice and 6 wild-type littermates at 24 months of age was investigated for αB-crystallin mRNA expression levels.

The level of β-actin mRNA was used as an internal control for RNA loading (section 5.3.3). The intensity value of each band representing the mRNA transcript level (αB-crystallin, *Hmox1*, or β-actin) of each animal was obtained, and the ratio of the test mRNA transcript level/β-actin mRNA transcript level was determined. Statistical analysis of the data was performed using the Student's *t* test (two tailed).

7.2.1.1 Northern blot analysis of *Hmox1* mRNA expression levels

Northern blot analysis was performed using the methods described in sections 2.2.15.4, 2.2.15.5 and 2.2.16. The northern blot membranes, probed for visualization of *Hmox1* mRNA transcripts, were washed to a final stringency of 0.1 X SSC, 0.1 % (w/v) SDS at 65°C for 10 min and exposed to X-ray film at -70°C in the presence of intensifying screens for about 4 days to ensure that only the *Hmox1* mRNA transcripts, and no non-specific hybridization, were detected (Fig. 7.5). The northern blot analysis of *Hmox1* mRNA transcript levels was performed in duplicate using 2 different northern gels. The results

a) Amplification of pαB-CRO insert DNA using primers CROF and CROR2

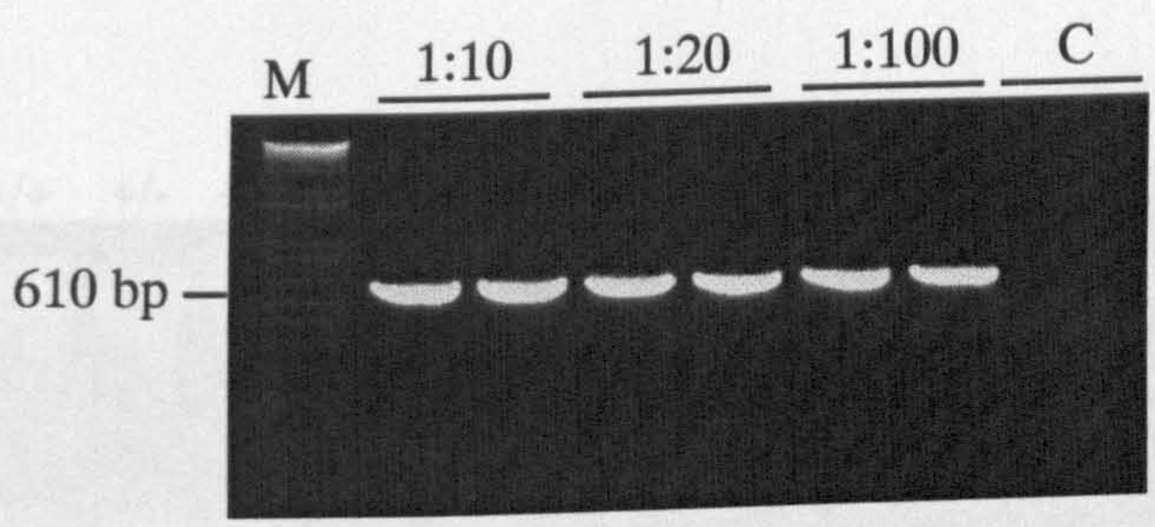

b) Purified insert DNA from pαB-CRO

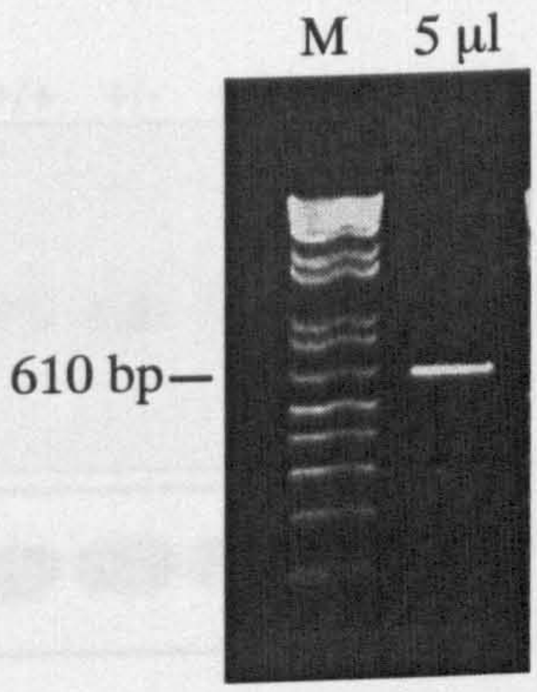

Figure 7.4 Generation of the hybridization probe for slot blot analysis of αB-crystallin mRNA**.** PCR products amplified from dilutions of pαB-CRO DNA (1:10, 1:10, 1:20, 1:20, 1:100, 1:100) using primers CROF and CROR2 were resolved on an EtBr-stained agarose gel (a). C indicates the negative control using water as a template to check for DNA contamination of PCR reagents. 5 µl of purified PCR products from (a) was loaded onto an EtBr-stained agarose gel (b). 2.5 µl (~30 ng) of purified PCR products from (a) was used as a probe in the RNA slot blot analysis. The 1 kb plus marker is indicated by M.

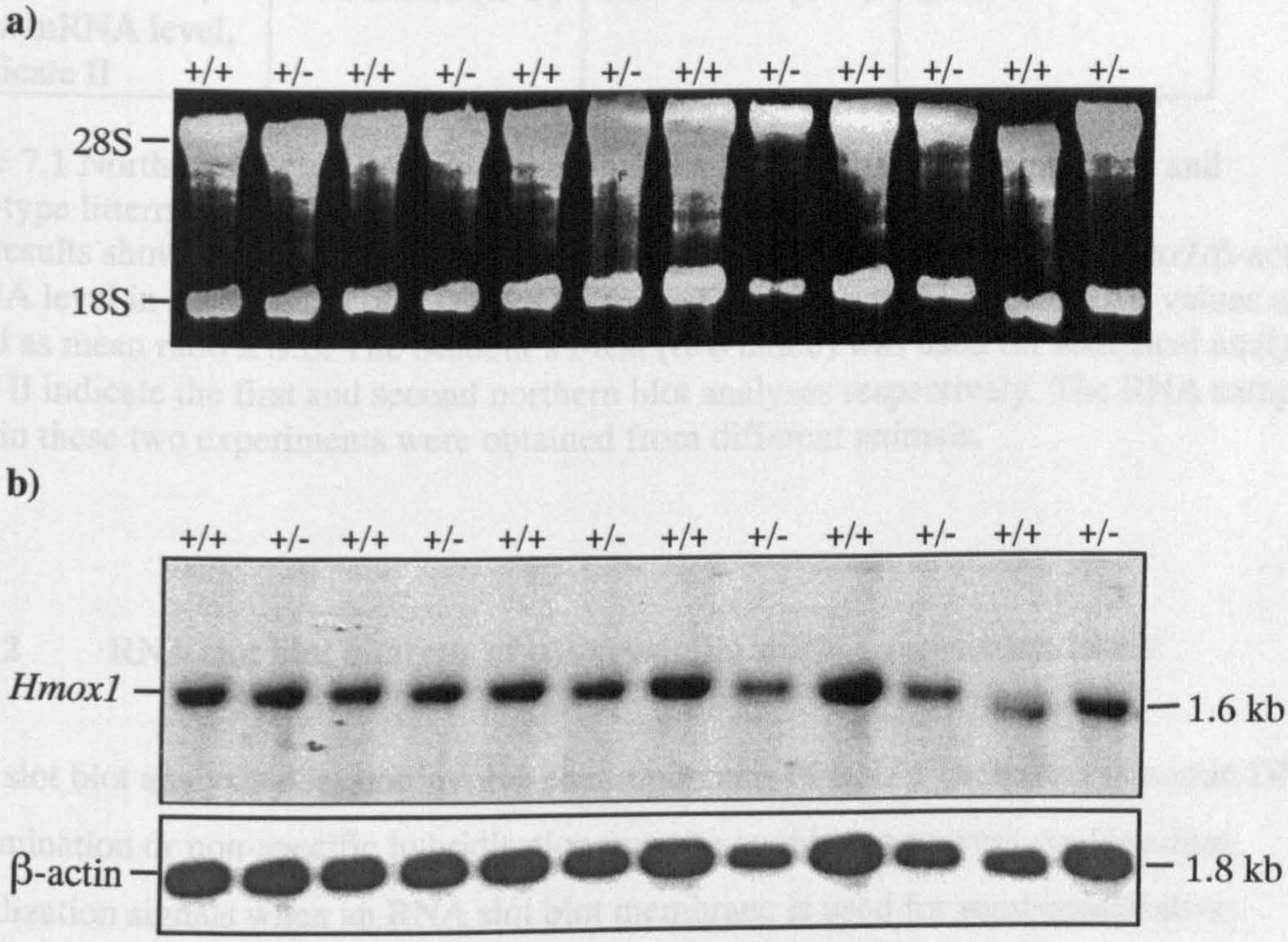

Figure 7.5 Northern blot analysis of *Hmox1* mRNA in the striatum of 24 month-old mice. Total RNA from 6 HD mice (+/-) and 6 wild-type littermates (+/-) was resolved on an EtBr-stained formaldehyde gel (a). 15 μg total RNA was loaded into each lane. The clear and abundant 18S and 28S rRNA bands indicate good quality RNA. Total RNA in the gel (a) was transferred onto a membrane, and probed for visualization of *Hmox1* and β-actin mRNA transcripts (b). The levels of β-actin mRNA transcript were used as an internal control for RNA loading.

revealed that 24 month-old HD mice showed no significant differences in the *Hmox1* mRNA level in the striatum, when compared with wild-type littermates (Table 7.1).

	HD	WT	*p* value
Ratio of *Hmox1*/β-actin mRNA level, replicate I	0.62 ± 0.04 (n=6)	0.7 ± 0.04 (n=6)	0.14
Ratio of *Hmox1*/β-actin mRNA level, replicate II	0.50 ± 0.06 (n=5)	0.54 ± 0.03 (n=5)	0.52

Table 7.1 Northern blot analysis of *Hmox1* mRNA levels in the striatum of HD and wild-type littermates (WT) at 24 months of age.
The results show that no significant differences were found in the ratios of *Hmox1*/β-actin mRNA level in the striatum of HD mice compared to wild-type littermates. All values are stated as mean ratio ± S.E. The Student's *t*-test (two tailed) was used for statistical analysis. I and II indicate the first and second northern blot analyses respectively. The RNA samples used in these two experiments were obtained from different animals.

7.2.1.2 RNA slot blot analysis of αB-crystallin mRNA expression levels

RNA slot blot analysis does not involve electrophoresis of RNA. Therefore, genomic DNA contamination or non-specific hybridisation must be avoided to prevent confounding hybridization signals when an RNA slot blot membrane is used for semi-quantitative analysis. To ensure this, northern blot analysis of αB-crystallin mRNA was optimised to avoid non-specific hybridisation (Fig. 7.1). After this, RNA slot blot analyses were performed using the methods described in section 2.2.16. The resulting slot blot membranes, probed for visualization of αB-crystallin mRNA transcripts, were washed to a final stringency of 0.1 X SSC, 0.1 % (w/v) SDS at 65°C for 30 min and exposed to X-ray film at -70°C in the presence of intensifying screens for about 2 days (Fig. 7.6).

The results (Table 7.2) revealed that 24 month-old HD mice showed no significant differences in the levels of αB-crystallin mRNA in the striatum, cerebellum and cortex, when compared with wild-type littermates.

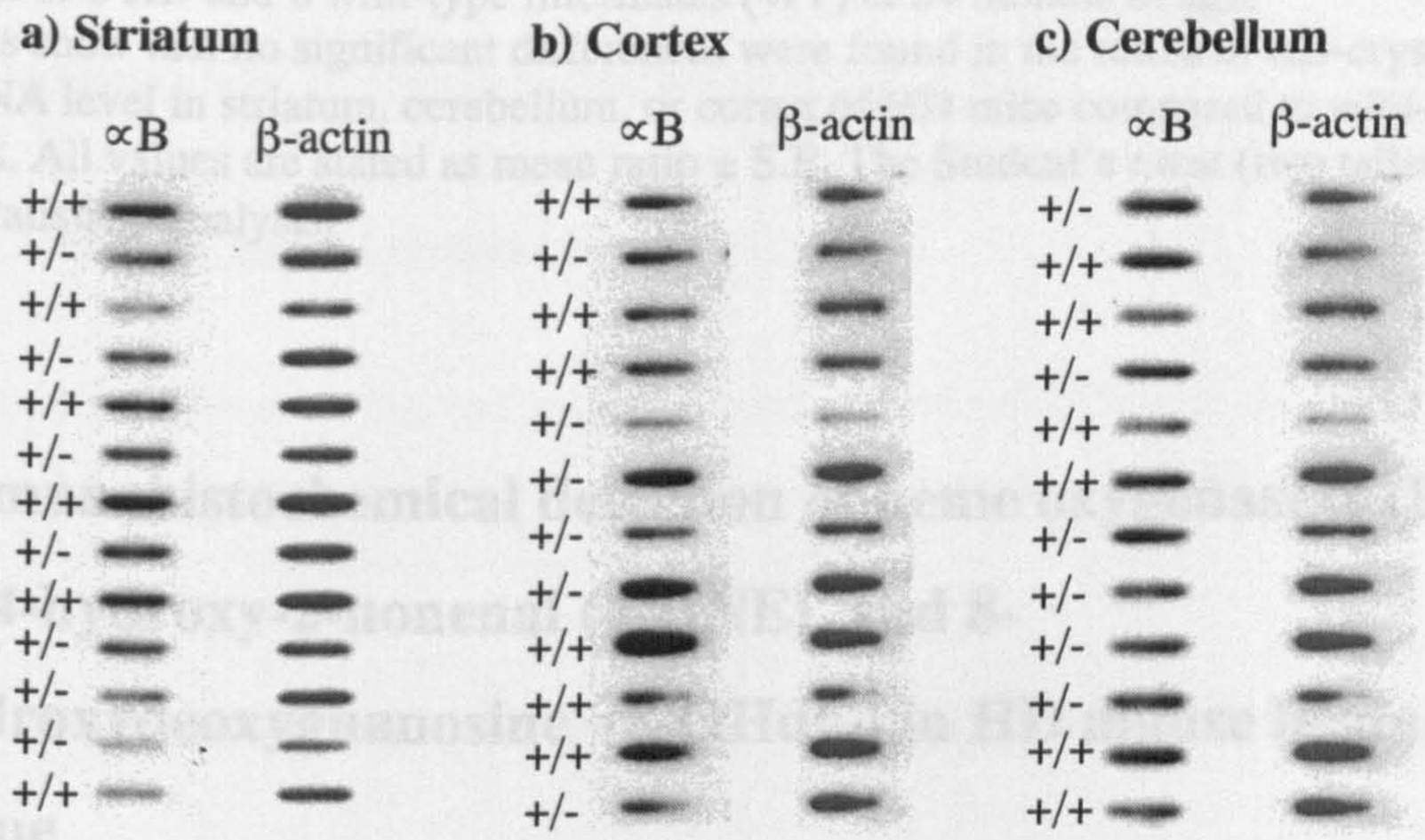

Figure 7.6 Slot blot analysis of ∝B-crystallin mRNA in stratum (a), cortex (b) and cerebellum (c) of HD mice (+/-) and wild-type-littermates (+/+) at 24 months of age. 5 μg of total RNA from was added to each slot. The visualization of β-actin mRNA transcripts was used as an internal control for RNA loading. ∝B indicates ∝B crystallin data.

	HD (n =6)	WT (n =6)	*p* value
Ratio of αB-crystallin/β-actin mRNA level in the striatum	0.78 ± 0.09	0.78 ± 0.1	1.0
Ratio of αB-crystallin/β-actin mRNA level in the cortex	1.29 ± 0.12	1.31 ± 0.1	0.9
Ratio of αB-crystallin/β-actin mRNA level in the cerebellum	1.15 ± 0.12	1.17 ± 0.14	0.9

Table 7.2 Slot blot analysis of αB-crystallin mRNA levels in the striatum, cortex and cerebellum of 6 HD and 6 wild-type littermates (WT) at 24 months of age.
The results show that no significant differences were found in the ratios of αB-crystallin/β-actin mRNA level in striatum, cerebellum, or cortex of HD mice compared to wild-type littermates. All values are stated as mean ratio ± S.E. The Student's *t*-test (two tailed) was used for statistical analysis.

7.3 Immunohistochemical detection of heme oxygenase-1 (HO-I), 4-hydroxy-2-nonenal (4-HNE), and 8-hydroxydeoxyguanosine (8-OHdG) in HD mouse brain tissue

7.3.1 Comparison of free-floating and paraffin-embedded sections for immunohistochemical detection of HO-I and 4-HNE

In the literature both free-floating and paraffin-embedded sections have been used for staining 4-HNE and HO-1. In order to obtain good quality immunostaining, a pilot study comparing these two section preparations for anti-4-HNE and HO-1 antibody staining was conducted using the methods described in section 6.3.1. The pilot study did not include 8-OHdG immunostaining as only paraffin-embedded sections were used in previous research studies. Both paraffin-embedded and free-floating sections were subjected to immunohistochemical detection with serial dilutions of primary antibody; anti-4-HNE (1:500, 1:1000, 1:2000, 1:3000 and 1: 4000), and anti-HO-1 (1:500, 1:1000, 1:2000, 1:3000

and 1:4000). These sections were then treated with secondary antibodies, anti-rabbit IgG (1:100) and ABC kits using methods described in sections 2.2.17.4 and 2.2.17.5. After examination using the light microscope, the best free-floating sections [anti-4-HNE (1:2000), and anti-HO-1 (1:2000)] were compared with the best paraffin-embedded sections [anti-4-HNE (1:2000), and anti-HO-1 (1:2000)] for each primary antibody. The results revealed that paraffin-embedded sections for each primary antibody used in the study provide better resolution and less background than free-floating sections (Fig. 7.7). Therefore, paraffin-embedded sections were used in subsequent immunodetection experiments.

7.3.2 Optimization of immunohistochemical assays

7.3.2.1 Positive control sections for assays

Sections of brain from mice that had received injections of malonate into the striatum (section 6.3.2.1) were used as positive controls for the detection of 4-HNE, HO-1 and 8-OHdG.

7.3.2.2 Optimization of immunohistochemical detection of 4-HNE and HO-1

Although conditions for anti-4-HNE and anti-HO-1 immunostaining used in the pilot study differentiated ischemic lesions from normal tissue, they were unable to stain the malonate lesion clearly. The refinement of immunostaining conditions for both test and malonate-treated positive control sections was performed. Faint staining with anti-4-HNE and anti-HO-1 antibodies within the malonate lesion section was enhanced by using the *Elite* ABC kit instead of a standard ABC kit (Vector) and by increasing the concentration of the anti-HO-1 antibody used (using a dilution of 1:1500 instead of 1:2000) (Fig. 7.8). The resulting optimised methods used for immunohistochemical detection of 4-HNE and HO-1 are more comprehensively detailed in section 2.2.17.5.

a) Paraffin-embedded mouse brain section

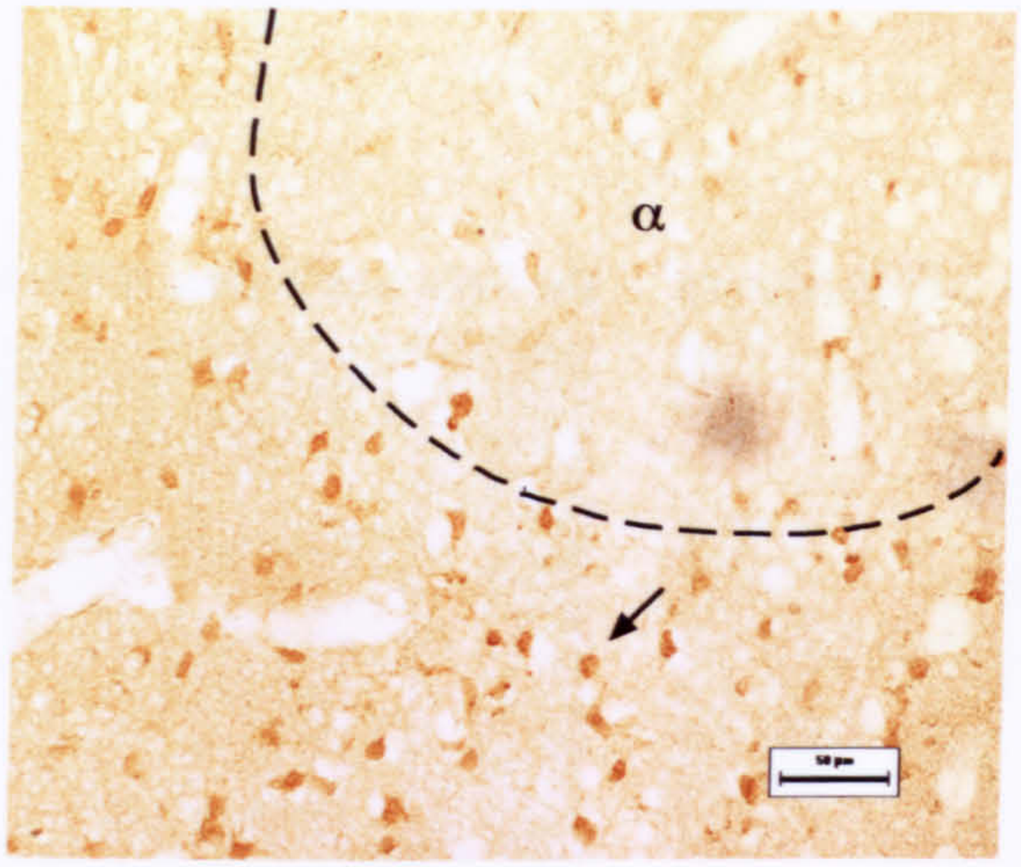

b) Free-floating mouse brain section

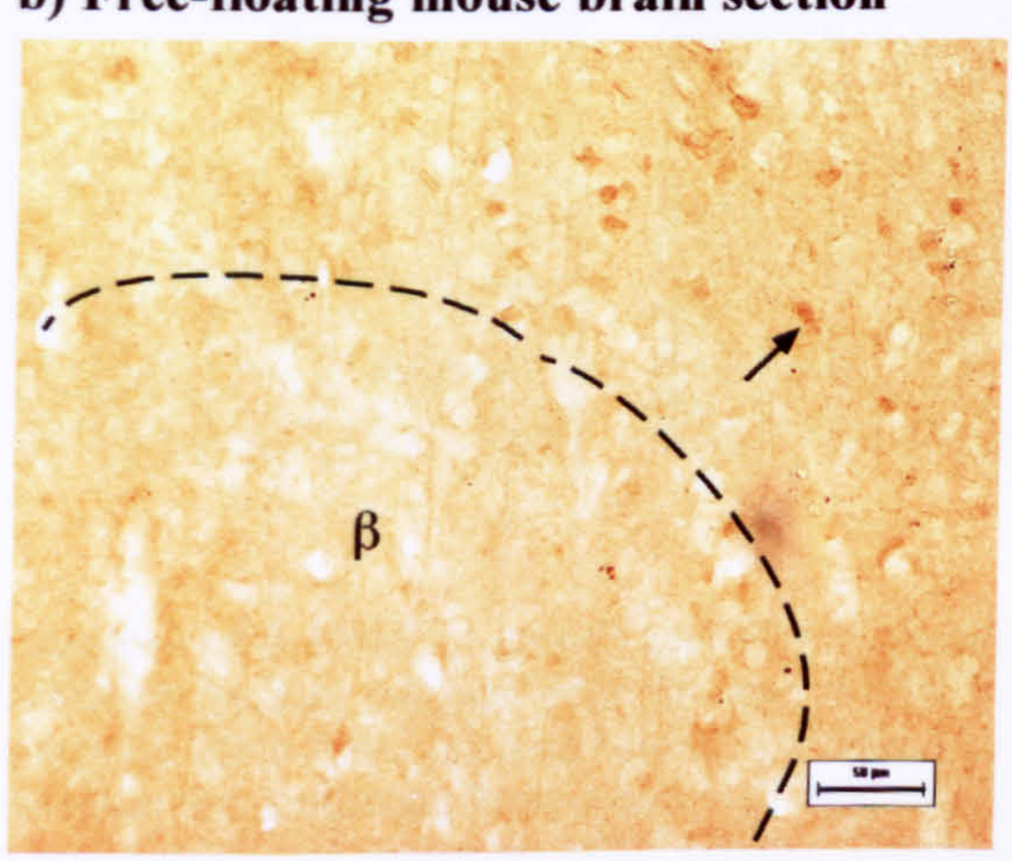

Figure 7.7 An example of a comparison between a free-floating section and a paraffin-embedded section stained with the anti-4-HNE antibody. The paraffin-embedded brain section (a) from a mouse with an ischemic lesion showed better staining resolution and less background than free-floating brain section (b) from a mouse that received a cortical AMPA injection. Neurons with increased staining are indicated by arrows. α indicates the ischemic lesion and β indicates the lesion generated by an AMPA injection. Scale bar = 50 μm

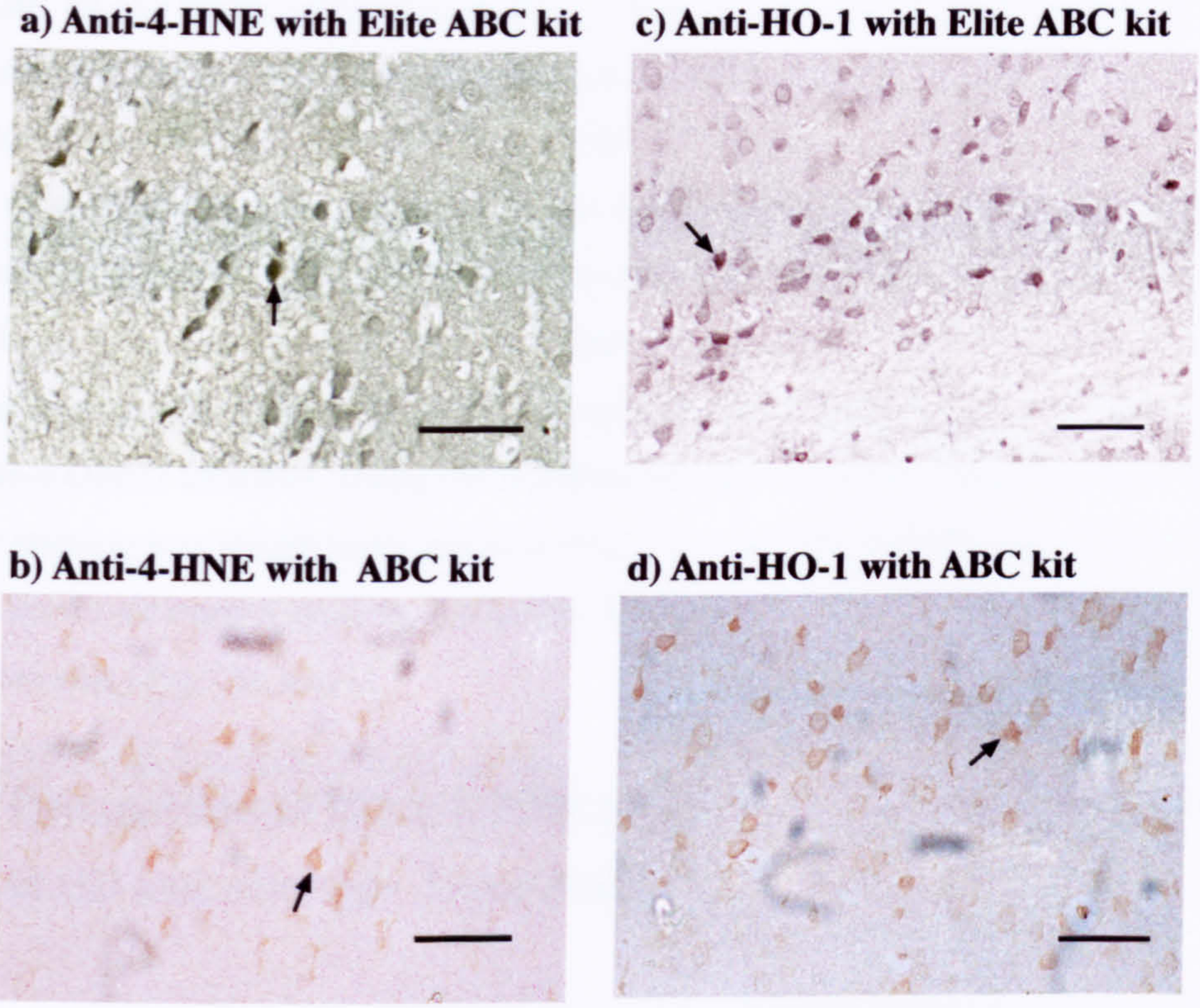

Figure 7.8 Optimization of 4-HNE (a and b) and HO-1 immunostaining (c and d) in mouse brain. A malonate lesion, stained with the anti-4-HNE antibody (1:2000 dilution) and visualized using the Elite ABC kit and Nickel enhancement (a) showed better staining resolution than the malonate lesion stained with the anti-4-HNE antibody (1:2000 dilution) and visualized using an ABC kit (b). The malonate lesion, stained with the anti-HO-1 antibody (1:1500 dilution) and visualized using the Elite ABC kit and Nickel enhancement (c) showed better staining resolution than the malonate lesion, stained with the anti HO-1antibody (1:1500 dilution) and visualized using the ABC kit (d). Increased neuronal cytoplasmic staining is indicated by arrows. Scale bar = 60 μm

7.3.2.3 Optimization of immunohistochemical detection of 8-OHdG

Test, positive control and negative control sections were subjected to serial dilutions of anti-8-OHdG antibody (0.25, 0.5, 1, and 2 μg/ml). The test and positive control sections stained with anti-8-OHdG antibody showed best staining at the concentration of 1 μg/ml with the *Elite* ABC kit and Nickel enhancement (Fig. 7.9a). However, as previously described for COI staining (section 6.3.2.1), the negative control sections, omitting the primary monoclonal anti-8-OHdG antibody, showed strong staining in the malonate-injected brain section (Fig. 7.9b). To solve this problem, the dilution of the secondary antibody used was changed from 1:100 to 1:500, and the primary antibody concentration was increased to 2 μg/ml. In addition, the Mouse on Mouse Immunodetection kit (the MOM kit, Vector) for blocking non-specific binding to mouse endogenous IgG was applied when staining sections with anti-8-OHdG antibody. Using the resulting optimized methods (section 2.2.17.5), non-specific staining was significantly reduced (Fig. 7.9c), and the positive control sections showed increased nuclear staining around the lesion of the striatum when compared to the non-lesion side (Fig.7.9d and e).

7.3.3 Comparisons of HO-I, 4-HNE and 8-OHdG immunostaining levels in HD and wild-type mouse brain

The mice except for one wild-type mouse, the equipment for capturing images, and the statistical method used for comparing levels of HO-I, 4-HNE and 8-OHdG immunostaining were the same as those used in the investigation of COI immunostaining levels in HD mouse brain (section 6.3.3). Quantitative analyses of the HO-I, 4-HNE and 8-OHdG immunostaining were also performed in a manner blind to genotype.

7.3.3.1 Analysis of HO-I immunostaining levels in mouse brain

Images of mouse brain sections stained with anti-HO-1 antibody were captured at a magnification of x200 for semi-quantitative analysis. Two brain sections from each mouse at the level of caudal striatum (the most vulnerable part of HD brain) were analysed. The striatum in each hemisphere was divided into 4 approximately equal subareas - dorsomedial, dorsolateral, ventromedial and ventrolateral (Fig. 7.10). The cortex in each

a) Malonate lesion without MOM kit

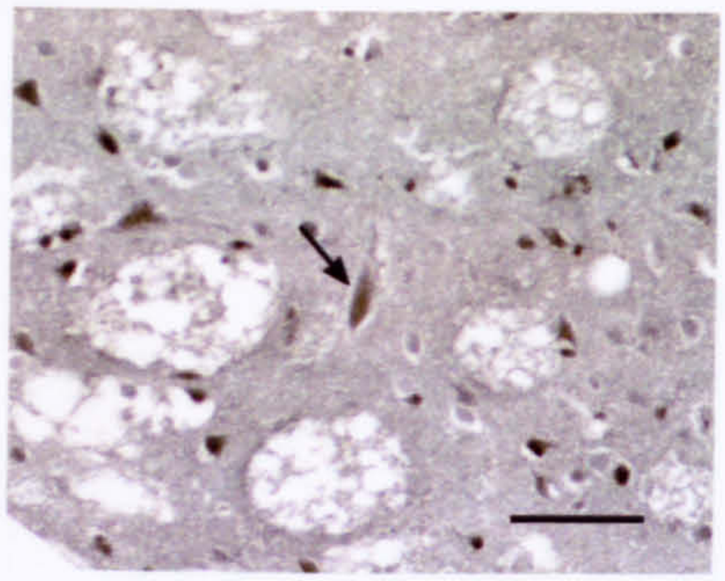

b) Negative control without MOM kit

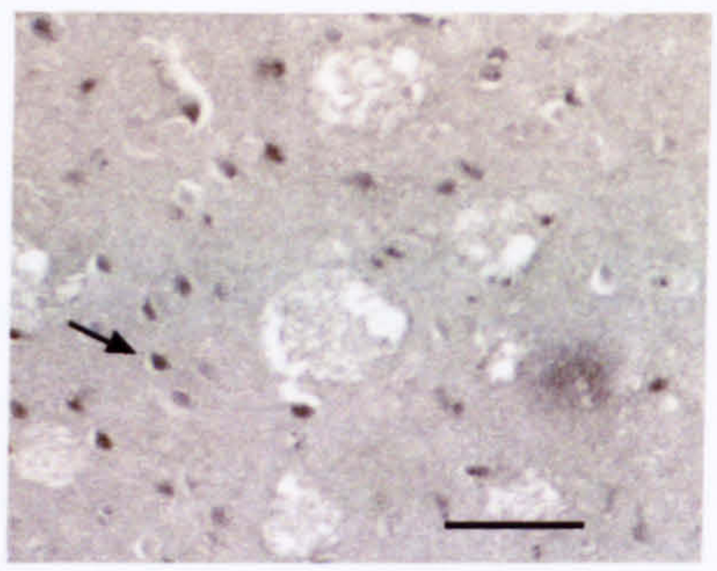

c) Negative control with MOM kit

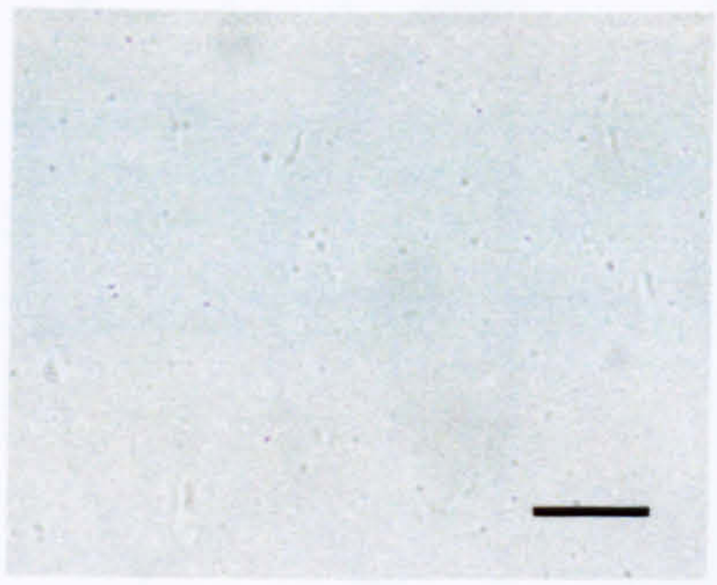

d) Malonate lesion with MOM kit

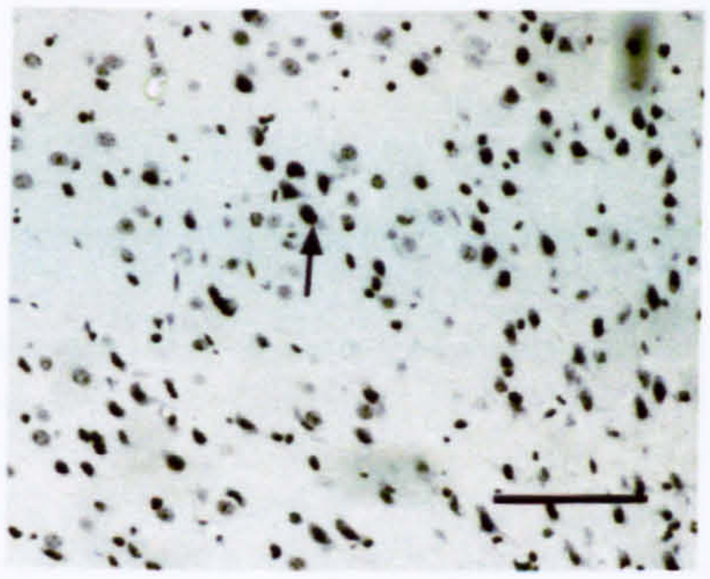

e) Non-lesion side with MOM kit

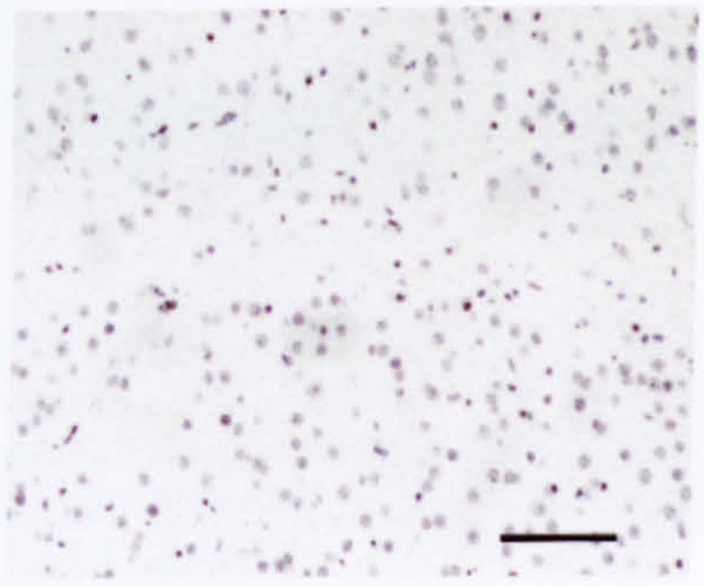

Figure 7.9 Optimization of immunostaining with the anti-8-OHdG antibody. The striatal malonate lesion stained with the anti-8-OHdG (1μg/ml) without the Mouse on Mouse kit (MOM kit) (a). The negative control section (b) adjacent to (a) was stained using the same procedure as (a), but omitting anti-8-OHdG. This section (b) showed non-specific staining of nuclei. The non-specific nuclear staining in striatum was significantly decreased by using the MOM kit (c). The striatum around the malonate lesion stained with anti-8-OHdG (2 μg/ml) and the MOM kit (d). When compared to the non-lesion side (e), the lesion side (d) showed increased nuclear staining (indicated by arrows). Scale bar=60 μm.

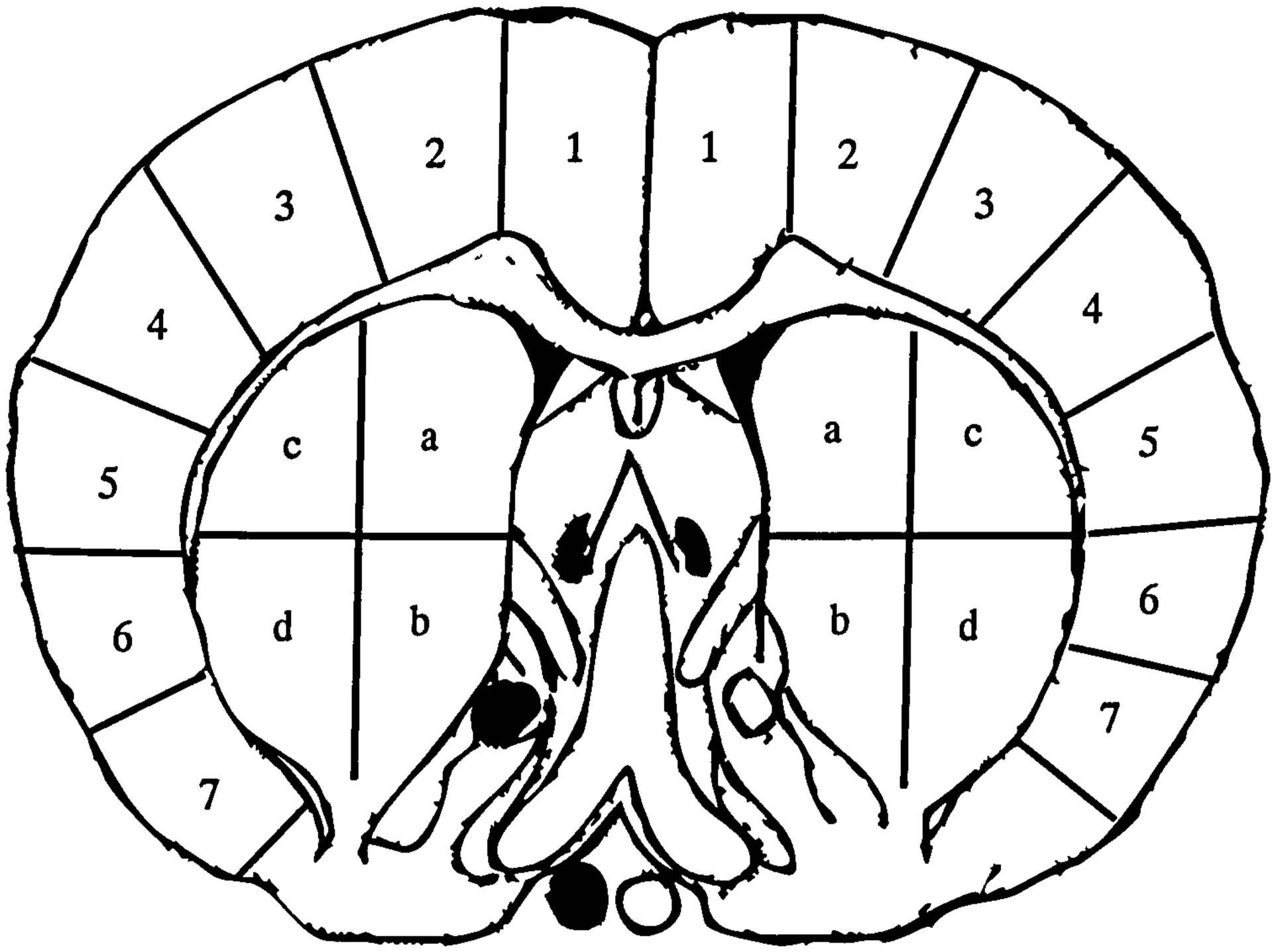

Figure 7.10 A mouse brain map for quantification of neurons with increased HO-1 and 4-HNE staining. The cortex in each hemisphere was divided into 7 equal parts indicated by numbers 1-7. The striatum in each hemisphere was divided into 4 equal parts, a, b, c and d (dorsomedial, ventromedial, dorsolateral, and ventrolateral respectively). One image from each subarea was captured.

hemisphere was divided into 7 approximately equal subareas (Fig. 7.10). The cells were classified into one of two groups (weak staining or intense staining) according to the intensity of cytoplasmic immunostaining. When cytoplasmic staining masked nuclear staining and blurred the nuclear boundary, the cell was classified in the intense staining group (Fig. 7.11). The brain sections from normal mice showed a basal staining level [(faint staining) (Fig. 7.11)] in most cells and the brain sections from malonate-treated mice (positive control) showed intense staining in the cells around the lesion (Fig. 7.11). An area of 0.2 mm^2 was chosen from the centre of each of the 8 striatal subareas and 14 cortical subareas per mouse brain section. The cells showing intense staining within this area were counted. The mean cell count of the four striatal subareas of each mouse (e.g. 4 dorsolateral regions from right and left striatum of 2 brain sections) was determined (Table 7.3). The data from 4 HD and 4 wild-type littermates were combined and a comparison between each striatal subarea of HD mice and corresponding subarea of wild-type littermates was performed. None of these comparisons showed significant differences between HD mice and littermates (Fig. 7.12a). When the scores from all four subareas (dorsomedial, dorsolateral, ventromedial and ventrolateral) of the striatum of each mouse in the cohort were combined, the result also showed that the HO-I immunostaining in HD striatum was not significantly different from that in wild-type littermates (Fig. 7.12a). The mean cell count of the 4 cortical subareas of each mouse (e.g. subarea 1 from right and left cortex of 2 brain sections) was determined (Table 7.4). Comparisons between each cortical subarea of 4 HD mice and corresponding subarea of 4 wild-type littermates were performed. None of these comparisons showed significant differences between HD mice and littermates (Fig. 7.12b). When the mean scores from all 7 subareas of the cortex from each mouse in the cohort were combined, the result also showed that levels of HO-I immunostaining in HD cortex did not significantly differ from wild-type littermates (Fig. 7.12b). In summary, these results suggest that HO-I immunostaining in the cortex and striatum of HD mice is not increased compared to wild-type mice.

7.3.3.2 Analysis of 4-HNE immunostaining levels in mouse brain

The level of 4-HNE immunostaining in tissue sections was analysed using the same procedures as for HO-1 immunostaining levels (section 7.3.3.1). The mice used were the same as those in the HO-1 immunostaining study except for one animal. The cells showing

a) Normal striatum section

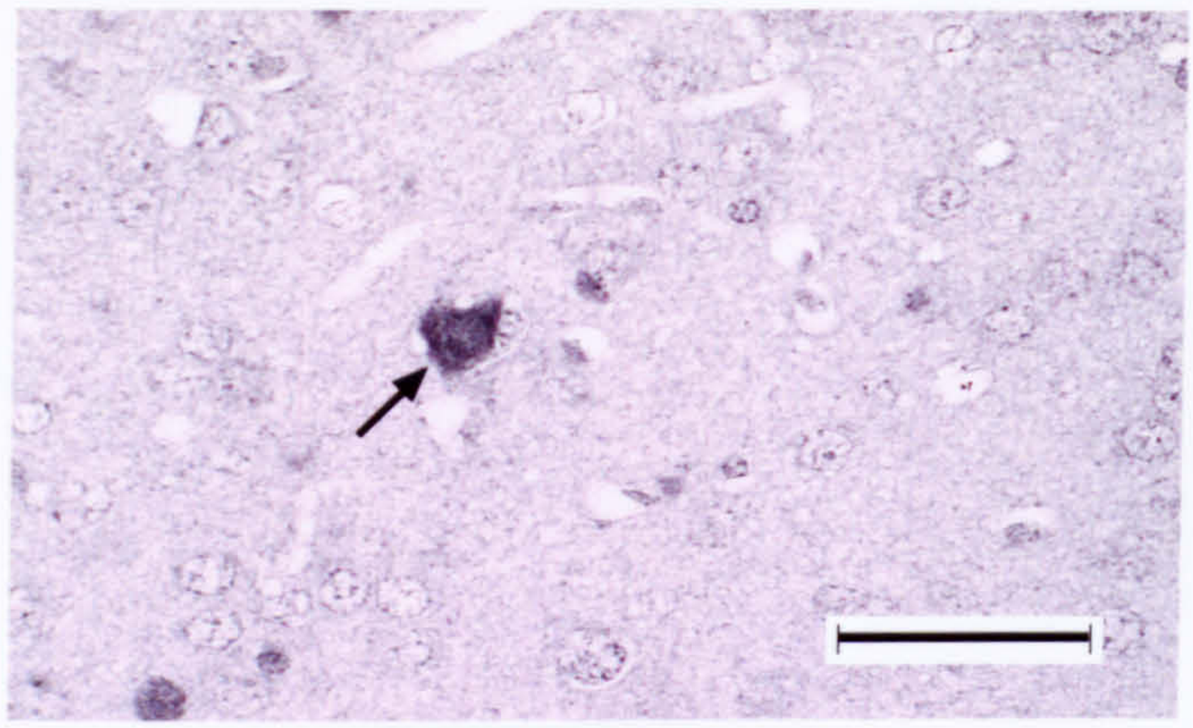

b) Malonate injected striatum section

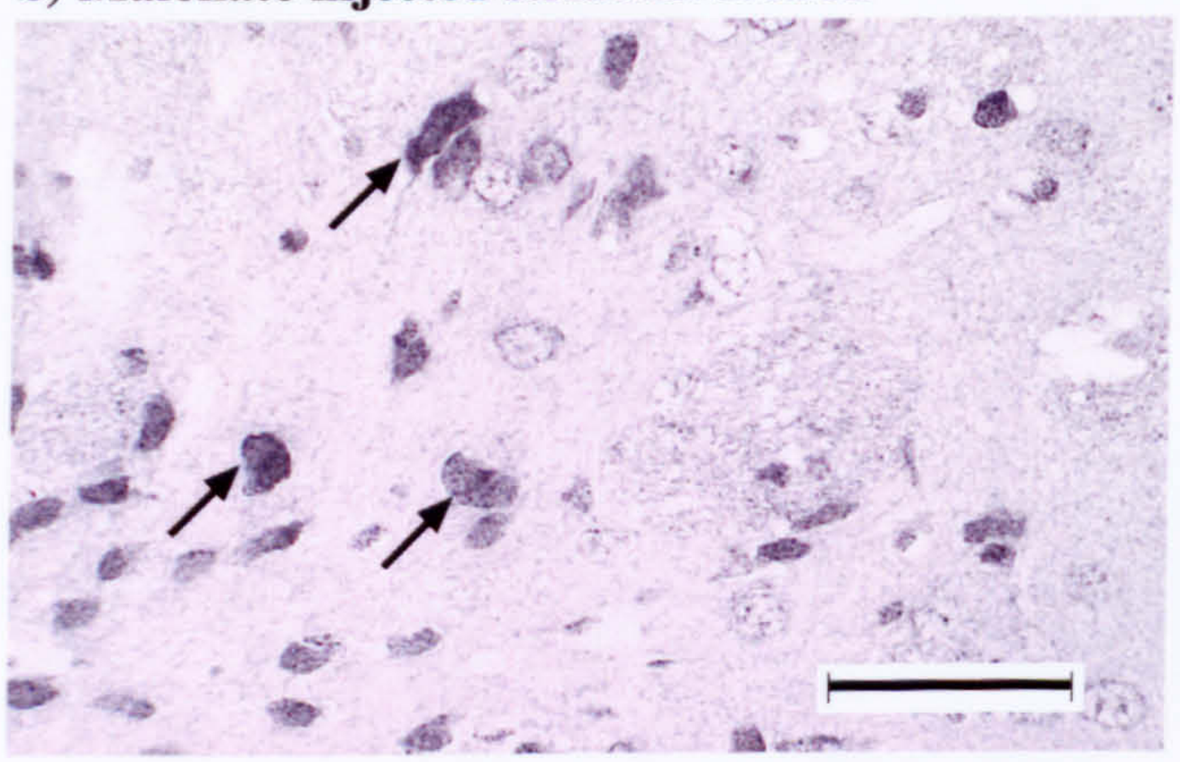

Figure 7.11 Classification of cell immunostaining with the anti-HO-1 antibody. a) The striatum in a brain section from a normal mouse shows a basal staining level in most cells, which is classified as faint staining (except the cell indicated by an arrow). b) The striatum in a brain section from a mouse treated with a malonate injection shows an increased number of cells with intense staining indicated by arrows. Scale bar = 50 μm.

a)

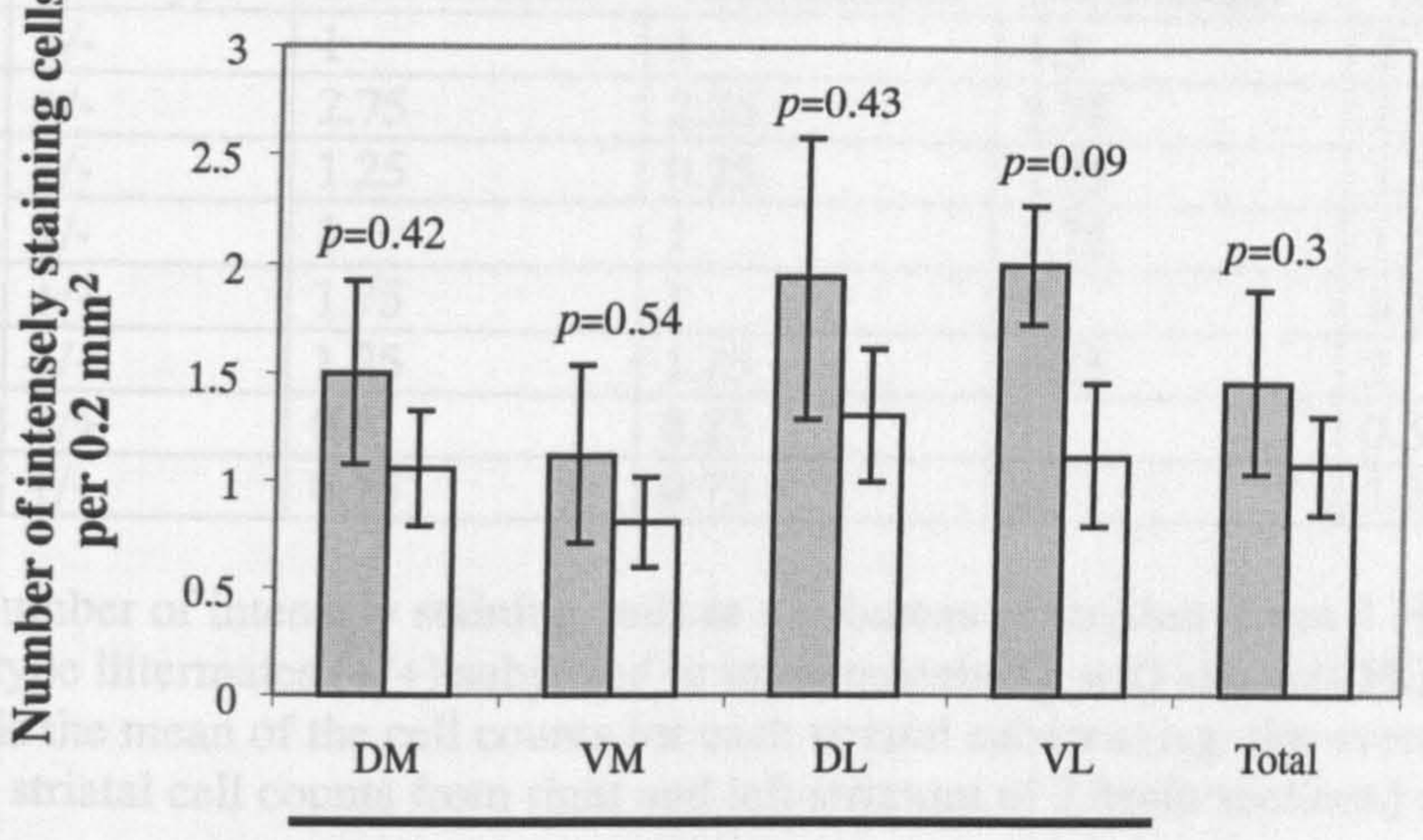

b)

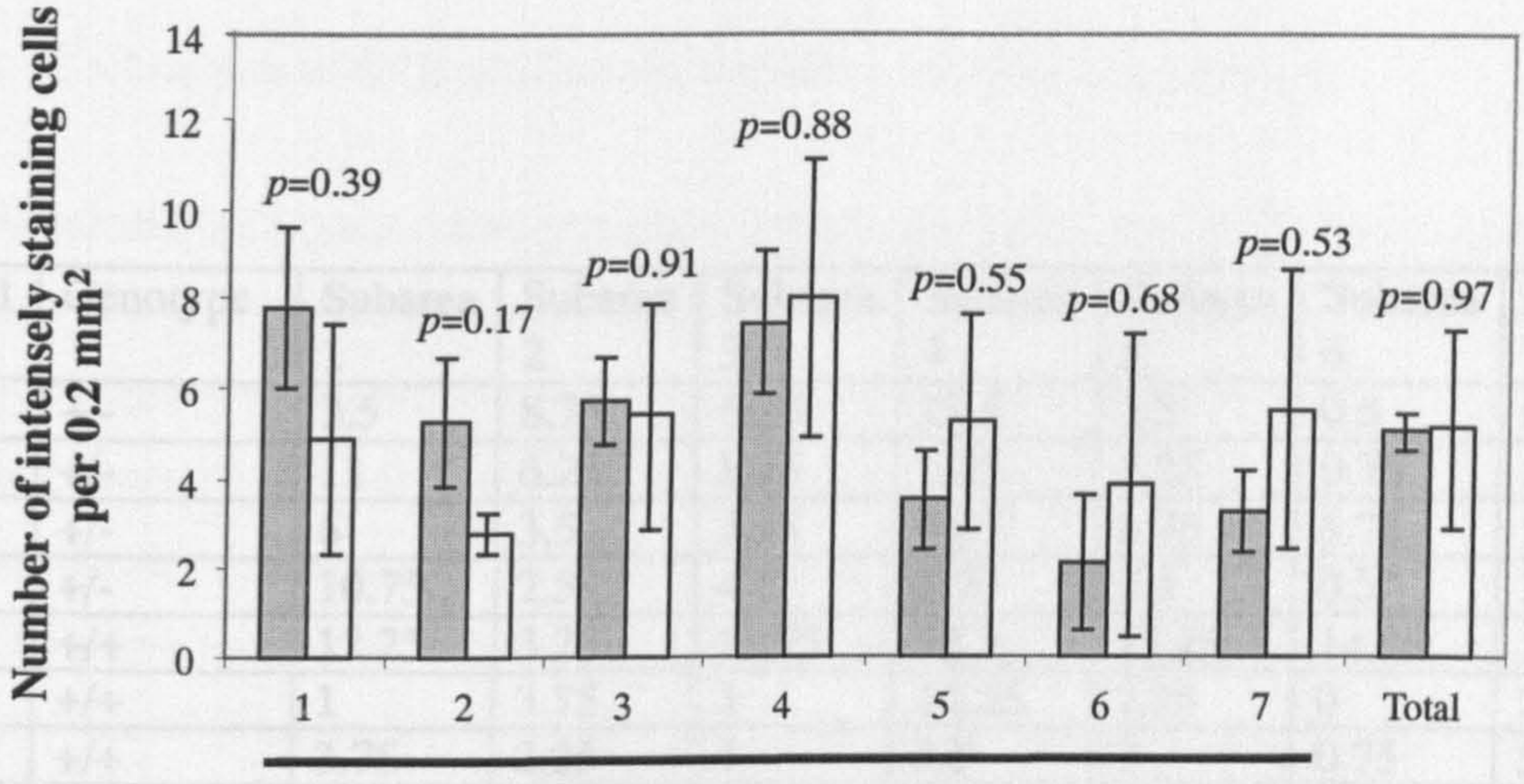

Figure 7.12 Immunostaining levels of HO-I in the striatum (a) and cortex (b) of 4 HD mice and 4 wild-type littermates at ~25 months of age**.** The column termed Total in (a) represents the combined results from the four subareas of striatum: dorsomedial (DM), ventromedial (VM), dorsolateral (DL) and ventrolateral (VL). The column termed Total in (b) represents the combined results from 7 subareas of cortex. Thedata are expressed as mean ± S.E. The *p* values indicated were obtained from comparing the results obtained with HD mice (grey column) and wild-type littermates (open column) using the Student's *t* test (two-tailed) for statistical analysis.

Animal ID	Genotype	Dorsomedial	Ventromedial	Dorsolateral	Ventrolateral
7836	+/-	1	1	1.5	2
7783	+/-	2.75	2.25	3.75	2.75
7839	+/-	1.25	0.25	1.75	1.75
7778	+/-	1	1	0.75	1.5
7781	+/+	1.75	1	1	0.75
7689	+/+	1.25	1.25	2.25	2
7687	+/+	0.5	0.25	1	0.5
7777	+/+	0.75	0.75	1	1.25

Table 7.3 Number of intensely staining cells in 4 subareas of striatum from 4 HD (+/-) mice and 4 wild-type littermates (+/+) subjected to immunostaining with the anti-HO-1 antibody. Each value is the mean of the cell counts for each striatal subarea (e.g. the average of 4 dorsolateral striatal cell counts from right and left striatum of 2 brain sections) of each mouse.

Animal ID	Genotype	Subarea 1	Subarea 2	Subarea 3	Subarea 4	Subarea 5	Subarea 6	Subarea 7
7836	+/-	3.5	8.75	6.25	11.5	1.5	0.5	0.75
7783	+/-	11	6.25	8.25	6.25	3.25	0.75	3.75
7839	+/-	6	3.5	3.75	8.25	6.75	6.75	5.5
7778	+/-	10.75	2.5	4.5	3.75	2.5	0.5	3
7781	+/+	12.25	3.25	12.75	12.5	11.25	14.25	14.5
7689	+/+	1	3.75	3	14.25	7.25	0	2.5
7687	+/+	3.75	2.25	4	3.5	2	0.75	5
7777	+/+	2.5	1.75	1.75	1.75	0.5	0.25	0

Table 7.4 Number of intensely staining cells in 7 subareas of cortex from 4 HD mice (+/-) and 4 wild-type littermates (+/+) subjected to immunostaining with the anti-HO-1 antibody. Each value is the mean of the cell counts for each cortical subarea (e.g. the average of 4 cell counts obtained from right and left cortex of 2 brain sections) of each mouse.

intense staining within each subarea of striatum were counted (Table 7.5). The results revealed that HD mice showed no significant differences in the 4-HNE staining score of any striatal subarea, when compared to wild-type littermates (Fig. 7.13a). When the scores from the four subareas of the striatum of each mouse were combined, the levels of 4-HNE immunostaining within the entire striatum of HD mice were not significantly different from that in wild-type littermates (Fig. 7.13a). The cells showing intense staining within each cortical subarea were also counted (Table 7.6). Comparisons between each cortical subarea of HD mice and the corresponding subarea of wild-type littermates were performed. None of these comparisons showed significant differences between HD mice and wild-type littermates (Fig. 7.13b). When the scores from the 7 subareas of the cortex of each mouse were combined, 4-HNE immunostaining levels in the cortex of HD mice were not significantly different from that in wild-type littermates (Fig. 7.13b). In summary, the results suggested that 4-HNE immunostaining levels in the cortex and striatum of HD mice were not increased compared to wild-type littermates.

7.3.3.3 Analysis of 8-OHdG immunostaining levels in mouse brain

Four caudal striata [2 consecutive sections x 2 (right and left striatum)] from each mouse, the most vulnerable part in HD brain (Vonsattel et al., 1998), were analysed. Each striatum was divided into 4 approximately equal parts, i.e. dorsomedial, dorsolateral, ventromedial and ventrolateral (Fig. 7.14). Two images from each striatal subarea were captured at x400 magnification for semi-quantitative analysis of 8-OHdG immunostaining. Care was taken to ensure these two images did not overlap. Layer III and V of the primary sensory cortex is the most vulnerable area of cortex to HD pathology. Therefore, 2 images of the primary sensory cortex (one containing layer III and one containing layer V) were captured from one brain section per mouse at the level of caudal striatum (Fig. 7.14). 8-OHdG immunostaining of the cells was classified into one of two groups [weak staining (score 1) and intense staining (score 2)] according to the intensity of nuclear immunostaining. Staining of the nucleus that masked staining of the nucleoli and blurred the boundary of nucleoli was classified as intense staining (Fig. 7.15). Brain sections from normal mice showed a basal nuclear staining level [(faint staining) (Fig. 7.9e)] in most cell nuclei but brain sections from malonate-treated mice showed intense staining in the cell nuclei around the lesion (Fig.

Animal ID	Genotype	Dorsomedial	Ventromedial	Dorsolateral	Ventrolateral
7836	+/-	0	0.5	0.5	0.25
7783	+/-	2.25	0	1.5	0.25
7839	+/-	0.5	0.25	0	0.25
7778	+/-	0	0	0	0
7705	+/+	0.5	0.5	0.25	0.5
7689	+/+	0.5	0	1	0.5
7777	+/+	0.5	0	1.25	1.5
7781	+/+	0	0	0	0

Table 7.5 Number of intensely staining cells in 4 subareas of striatum from 4 HD mice (+/-) and 4 wild-type littermates (+/+) subjected to immunostaining with the anti-4-HNE antibody. Each value is the mean of the cell counts for each striatal subarea (e.g. the average of 4 cell counts-dorsolateral striata from right and left striatum of 2 brain sections) of each mouse.

Animal ID	Genotype	Subarea 1	Subarea 2	Subarea 3	Subarea 4	Subarea 5	Subarea 6	Subarea 7
7836	+/-	4.5	7.5	9.75	5.5	2.25	0	1
7783	+/-	18.75	19.75	14.5	36.25	2.75	3.25	5.5
7839	+/-	10.25	2	2.25	7.75	6.25	1.5	1.5
7778	+/-	18.25	10.25	10.25	5.25	5.75	8.75	7
7705	+/+	9.75	1.75	3	5.5	3.5	0.5	1.75
7689	+/+	3	2.25	3	13	4	0.75	1.25
7777	+/+	1	1.75	4.5	1	0.25	1	0.5
7781	+/+	7.5	1	8.25	21.25	17.25	21.75	24

Table 7.6 Number of intensely staining cells in 7 subareas of cortex from 4 HD mice (+/-) and 4 wild-type littermates (+/+) subjected to immunostaining with the anti-4-HNE antibody. Each value is the mean of 4 cell counts for each cortical subarea (e.g. the average of 4 cell counts from right and left cortex of 2 brain sections) of each mouse.

a)

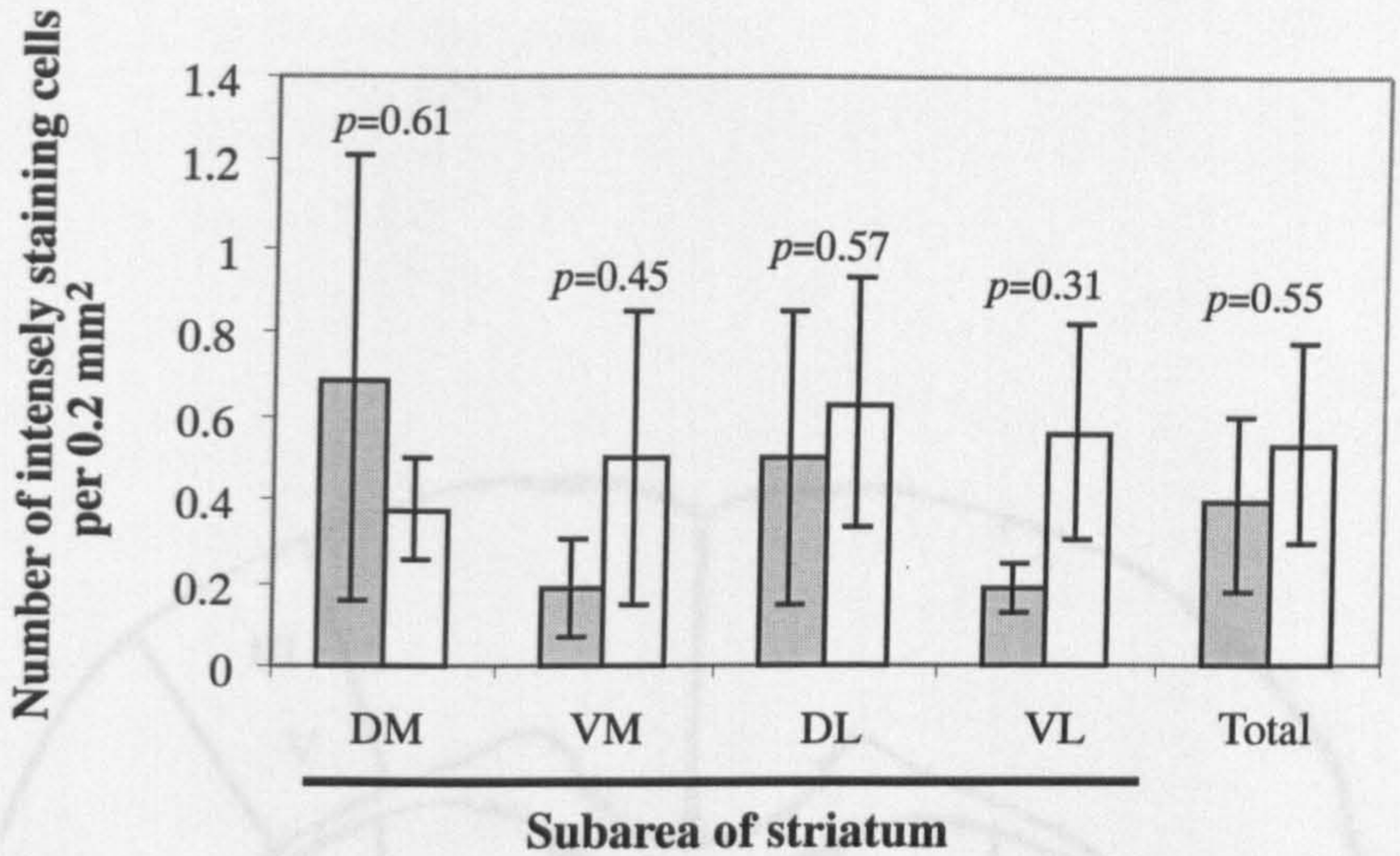

b)

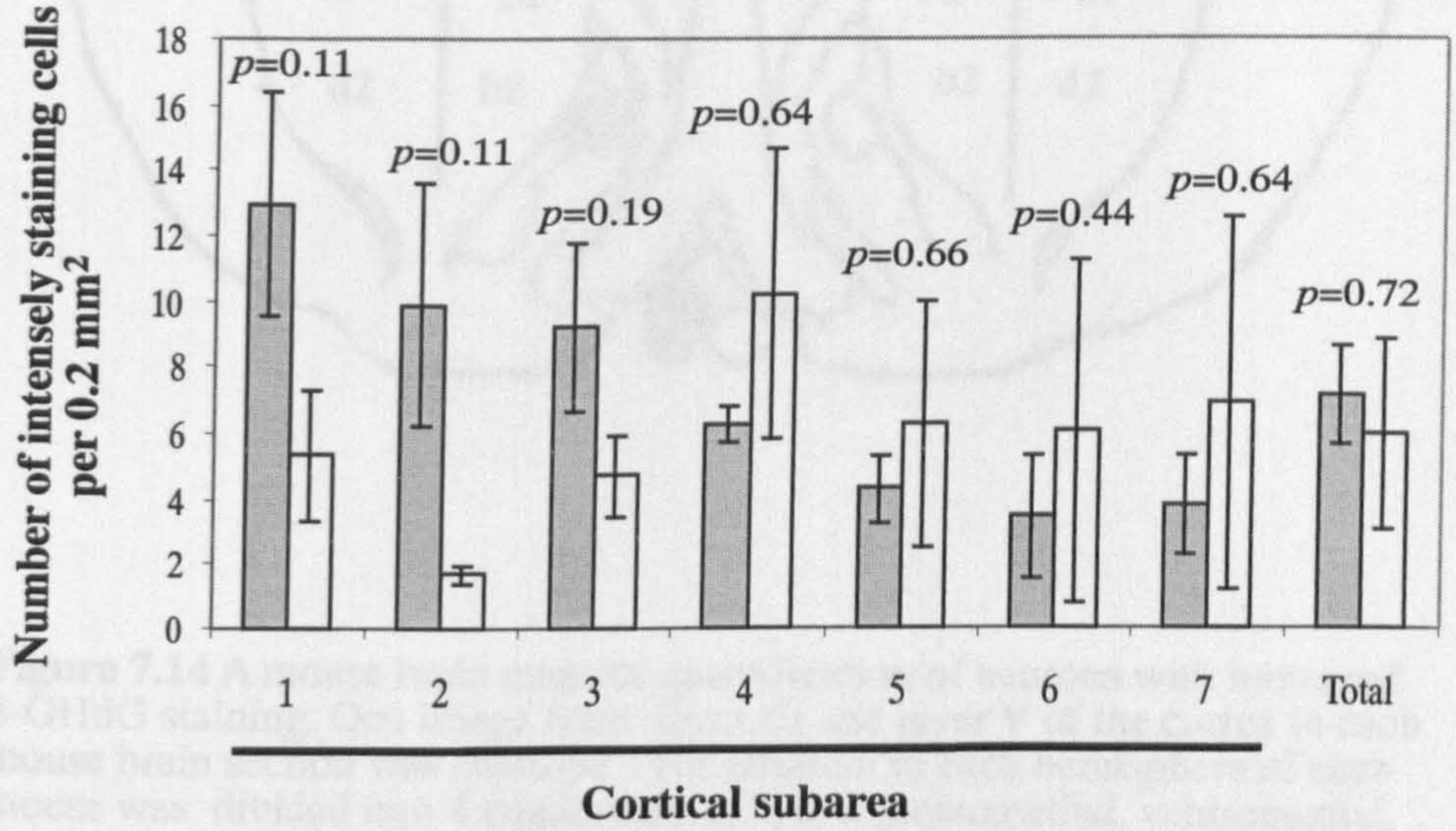

Figure 7.13 Immunostaining levels of 4-HNE in the striatum (a) and cortex (b) of 4 HD mice and 4 wild-type littermates at ~25 months of age. The column termed Total in (a) represents the combined results from the four subareas of striatum: dorsomedial (DM), ventromedial (VM), dorsolateral (DL) and ventrolateral (VL). The column termed Total in (b) represents the combined results from 7 subareas of cortex. The data are expressed as mean ± S.E. The *p* values indicated were obtained from comparing the results obtained with HD mice (grey column) and wild-type littermates (open column) using the Student's *t* test (two-tailed) for statistical analysis.

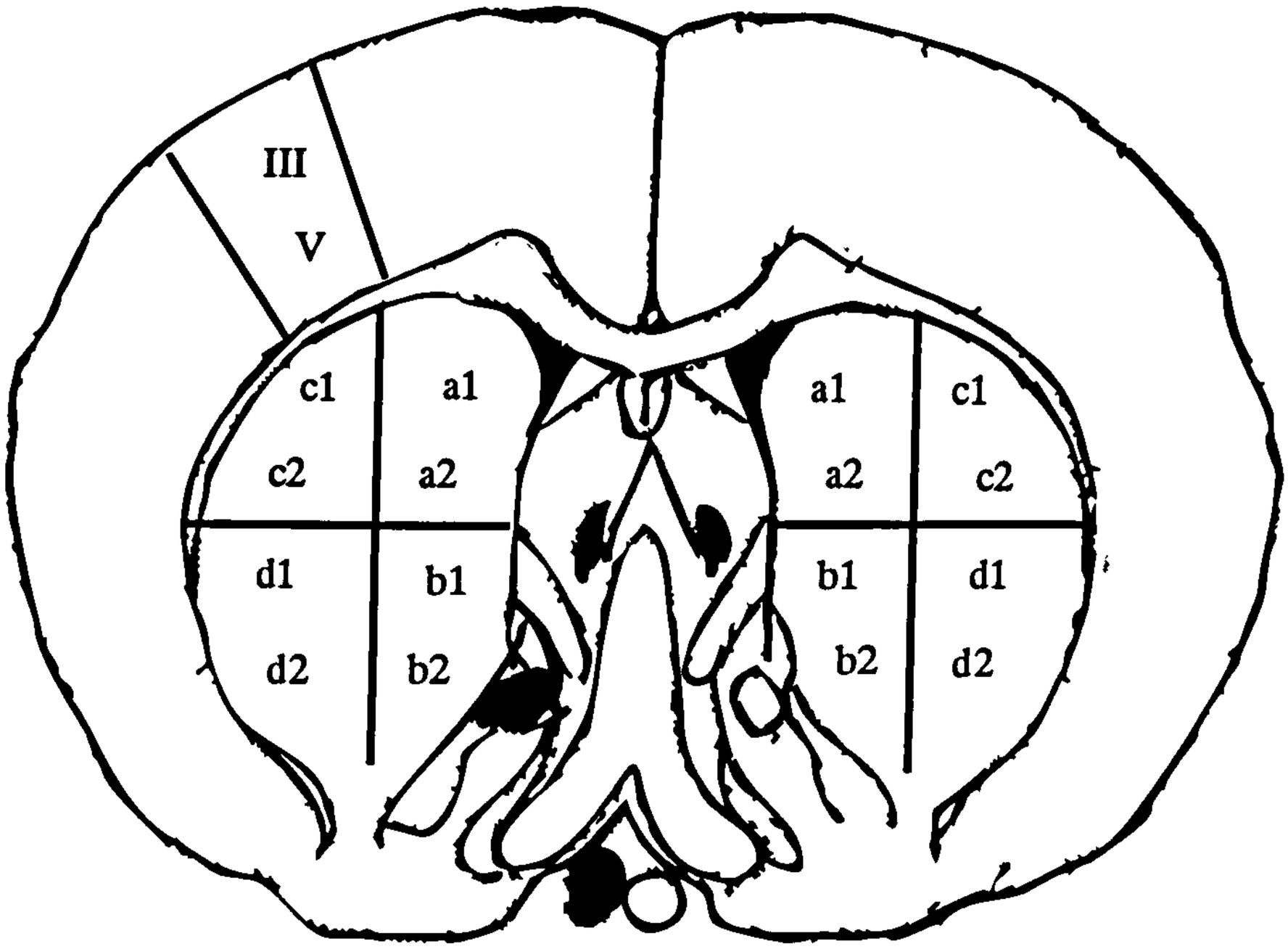

Figure 7.14 A mouse brain map for quantification of neurons with increased 8-OHdG staining. One image from layer III and layer V of the cortex in each mouse brain section was captured . The striatum in each hemisphere of each mouse was divided into 4 equal parts, a, b, c, d (dorsomedial, ventromedial, dorsolateral, and ventrolateral). Two images (e.g. a1 and a2) from each subarea of the striatum were captured.

a) HD mouse brain section

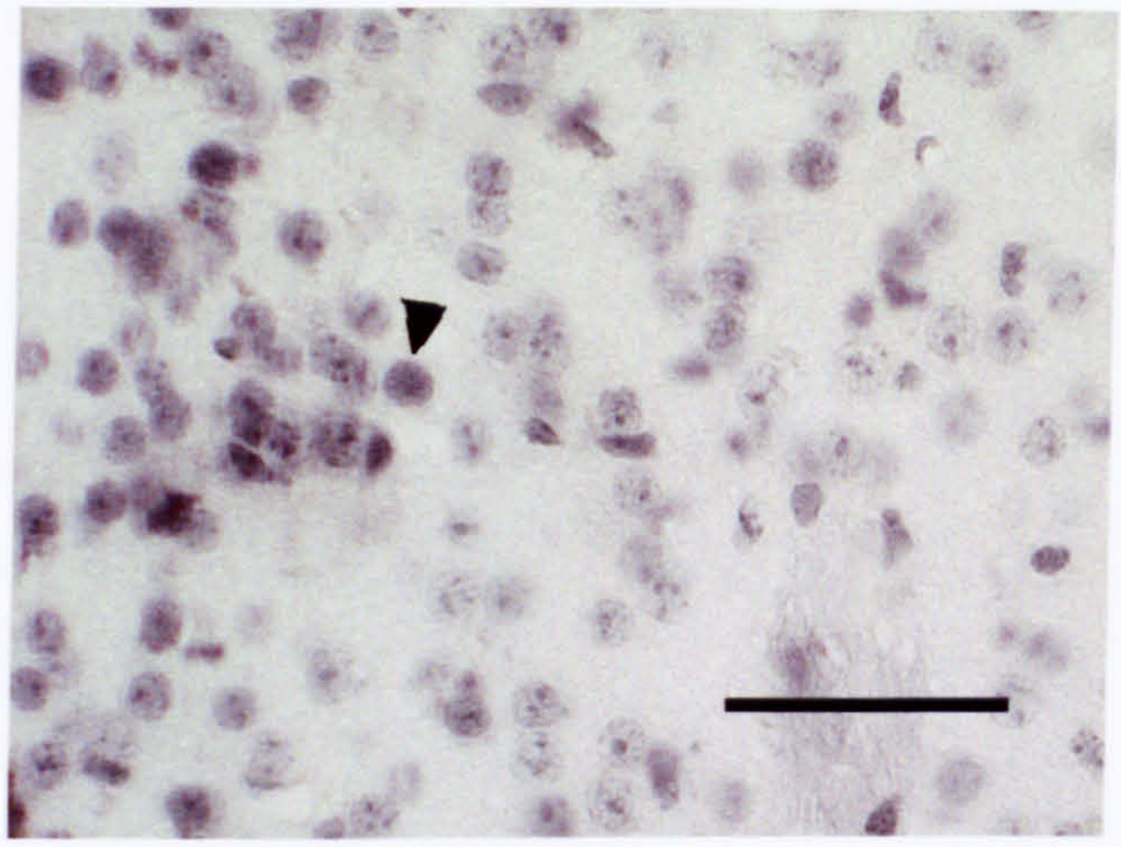

b) Wild-type littermate brain section

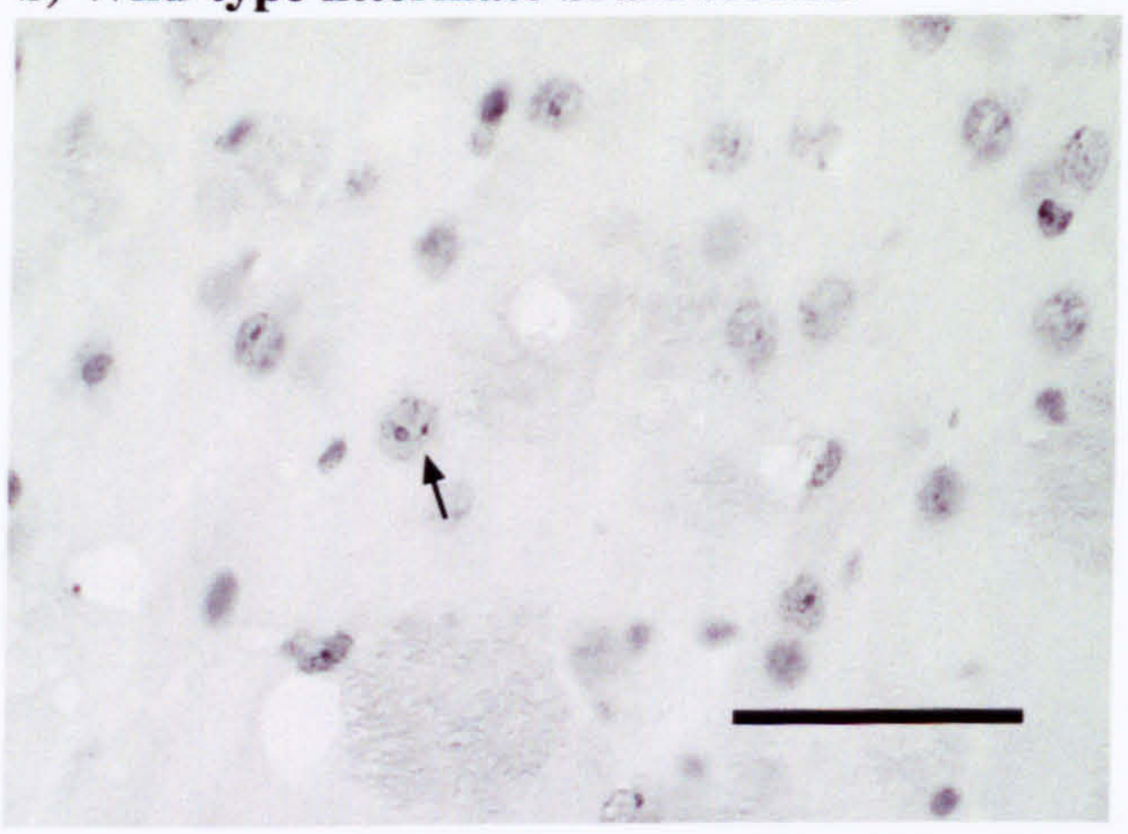

Figure 7.15 Scoring nuclear staining using the anti-8-OHdG antibody. The striatal image (a) from an HD mouse brain section shows increased cell numbers with intense nuclear staining (score 2, arrow head). The striatal image (b) from a wild-type littermate brain section shows faint staining in most nuclei (score 1, arrow). Scale bar = 50 μm.

7.9d). An area of 0.06 mm^2 from the centre of each image was selected and the number of cells with weak or intense staining counted. From the results, a total score [(number of weakly staining cells) x 1 + (number of intensely staining cells) x 2] was calculated for each image.

Eight staining scores for each of the four striatal subareas (e.g. 4 dorsolateral regions from right and left striata of 2 brain sections and 2 scores from each dorsolateral subarea) of each mouse were combined (Table 7.7). The results showed that 8-OHdG immunostaining was significantly increased in the dorsomedial, dorsolateral and ventromedial striatum, but not in the ventrolateral striatum of HD mice when compared to wild-type mice (Fig. 7.16a). When scores from all four parts of the striatum were combined, the results also showed that 8-OHdG immunostaining was significantly increased in the HD striatum as a whole when compared to wild-type littermates (Fig. 7.16a). The staining score of each cortical subarea was calculated (Table 7.8). The score of each subarea from the cortex of HD mice was compared to that of wild-type littermates. None of these comparisons showed significant differences between HD mice and littermates (Fig. 7.16b). When the scores from the 2 subareas of the cortex from each mouse were combined, the result also showed that the immunostaining of 8-OHdG in cortex of HD mice was not significantly different from that in wild-type littermates (Fig 7.16b). In summary, the results suggested that 8-OHdG immunostaining was significantly increased in the striatum, but not in the cortex of HD mice when compared to wild-type littermates.

As it is possible that assigning a score for nuclear staining intensity of cells might artificially inflate differences between mutant and wild-type sections, an alternative method was used to quantify the 8-OHdG immunostaining in HD mouse brain striatum. The ratio of number of intensely stained nuclei/total number of stained nuclei for each image was determined and comparisons were performed between HD and wild-type littermates using two-way ANOVA. Genotype and individual mouse within groups were used as the 2 factors. Every mouse has 8 repeated data points for each striatal subarea. The results showed that 8-OHdG immunostaining was significantly increased in all four parts of HD striatum when compared to wild-type littermates (DM subarea: $F_{1,63} = 18.66$, $p < 0.001$; VM subarea: $F_{1,63} = 11.66$, $p = 0.001$; DL subarea; $F_{1,63} = 14.26$, $p < 0.001$; VL subarea: $F_{1,63} = 23.14$, $p < 0.001$). This result supports the previous analysis using Student's *t* test and

Animal ID	Genotype	Dorsomedial	Ventromedial	Dorsolateral	Ventrolateral
7836	+/-	171	165.5	142.5	132.5
7783	+/-	161	158	153.5	134.5
7839	+/-	208	208.5	187.5	174.5
7778	+/-	199	198.5	161	164.5
7705	+/+	135	140	127	122.5
7689	+/+	136	143	127.5	129
7687	+/+	156	153.5	136.5	127
7777	+/+	135	128	118.5	114

Table 7.7 Score of cell staining in 4 subareas of striatum from 4 HD mice (+/-) and 4 wild type littermates (+/+) subjected to immunostaining with the anti-8-OHdG antibody. Each value is the mean of 8 staining scores for each striatal subarea (e.g. the average of 8 scores- dorsolateral regions from right and left striatum of 2 brain sections, and 2 scores from each dorsolateral region) of each mouse.

Animal ID	Genotype	Layer III	Layer V
7836	+/-	181	145
7783	+/-	247	180
7839	+/-	223	190
7778	+/-	222	154
7705	+/+	201	157
7689	+/+	224	177
7687	+/+	250	149
7777	+/+	216	173

Table 7.8 Score of cell staining in 2 subareas (layer III and layer V) of cortex from 4 HD mice mice (+/-) and 4 wild type littermates (+/+) subjected to immunostaining with the anti-8-OHdG antibody.

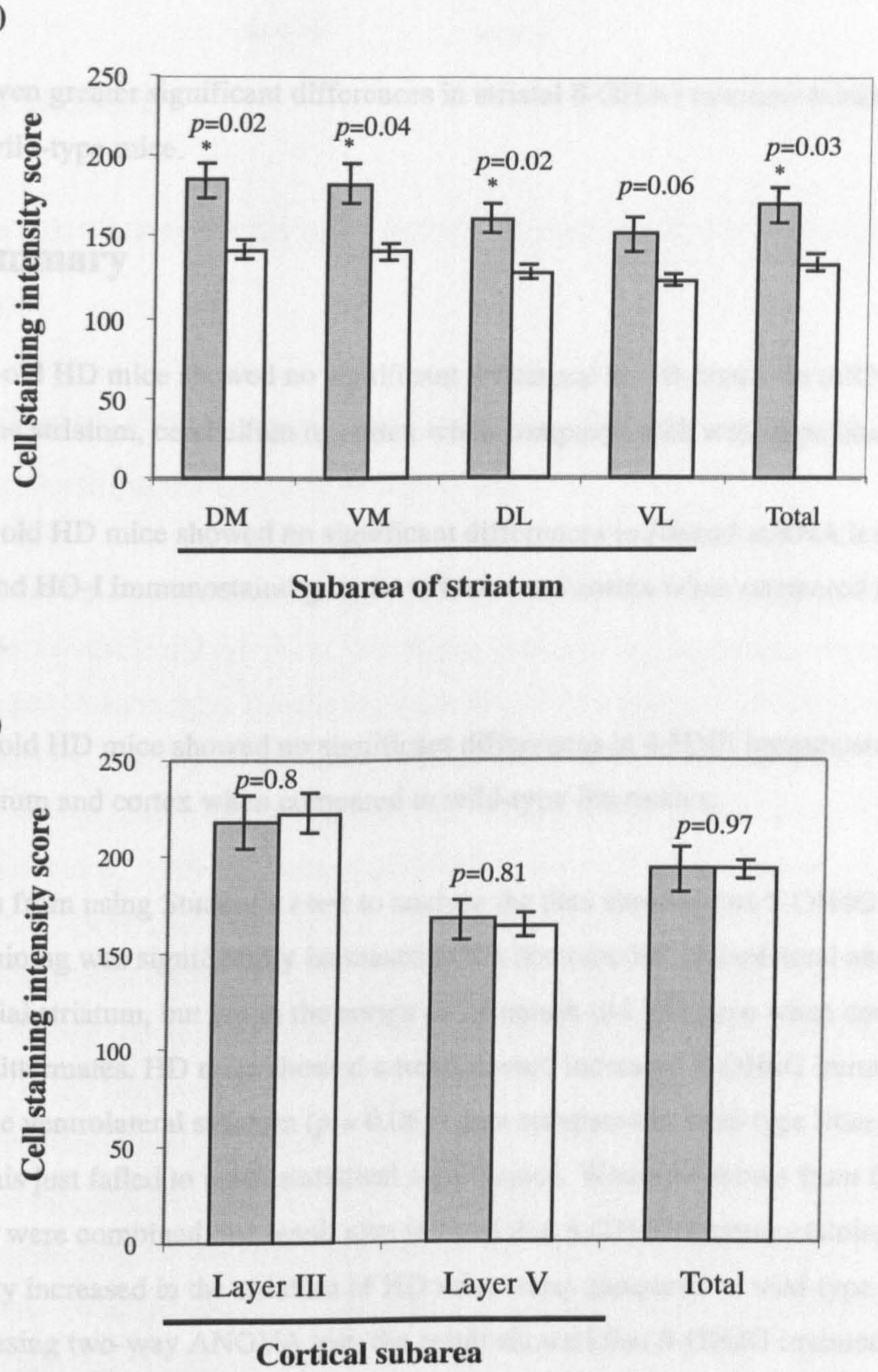

Figure 7.16 Immunostaining of 8-OHdG in the striatum (a) and cortex (b) of 4 HD mice and 4 wild-type littermates at ~ 25 months of age. The column termed Total in (a) represents the combined results from four subareas of striatum: dorsomedial (DM), ventromedial (VM), dorsolateral (DL) and ventrolateral (VL). The column termed Total in (b) represents the combined results from 2 subareas (layer III and V) of cortex. Stained cells were counted and a score for weak (1) and intense staining (2) was assigned. The cell staining intensity score is the sum of the individual scores within an 0.06 mm^2 area. Data are expressed as mean ± S.E. The *p* values indicated were obtained from comparing the results of HD mice (grey column) with wild-type littermates (open column) using the Student's *t* test (two-tailed) for statistical analysis. * indicates $p<0.05$.

showed even greater significant differences in striatal 8-OHdG immunostaining between HD and wild-type mice.

7.4 Summary

24 month-old HD mice showed no significant difference in αB-crystallin mRNA level either in the striatum, cerebellum or cortex when compared with wild-type littermates.

24 month-old HD mice showed no significant differences in *Hmox1* mRNA level in the striatum and HO-I immunostaining in the striatum and cortex when compared to wild-type littermates.

24 month-old HD mice showed no significant differences in 4-HNE immunostaining levels in the striatum and cortex when compared to wild-type littermates.

The results from using Student's *t* test to analyse the data showed that 8-OHdG immunostaining was significantly increased in the dorsomedial, dorsolateral and ventromedial striatum, but not in the cortex of 24 month-old HD mice when compared to wild-type littermates. HD mice showed a trend toward increased 8-OHdG immunostaining levels in the ventrolateral striatum ($p = 0.06$) when compared to wild-type littermates, although this just failed to reach statistical significance. When the scores from the four parts of striatum were combined, the result also showed that 8-OHdG immunostaining was significantly increased in the striatum of HD mice when compared to wild-type littermates. However, using two-way ANOVA test, the result showed that 8-OHdG immunostaining was significantly increased in all four parts of HD striatum when compared to wild-type littermates.

These results suggest that immunohistochemical detection might be a better method for detecting increased oxidative stress in HD mice where the increase in oxidative stress markers can be detected at the single cell level or localized to a small region. The results of 8-OHdG staining are consistent with a gradient of vulnerability within the striatum of HD, with the dorsomedial striatum more vulnerable and showing earlier pathological changes than other regions (Vonsattel and DiFiglia, 1998).

8 Discussion

8.1 Locomotor deficits and other phenotypic features in HD mice

8.1.1 HD mice show progressive locomotor deficits in rotarod performance from 4 months of age

Investigation of the psychomotor function of HD mice is important, since the aims of this study are to provide insights into the link between molecular/cellular pathology and phenotype and to investigate the use of progressive phenotypic abnormalities as a surrogate marker to test the efficacy of potential therapies in the future. Using different tools, early and progressive psychomotor abnormalities have been shown in most transgenic HD mouse models (Carter et al., 1999; Dunnett et al., 1998; Lione et al., 1999; Luesse et al., 2001; Hodgson et al., 1999; Laforet et al., 2001; Guidetti et al., 2001; Schilling et al., 1999). However, the present study uses a "knock-in" HD model and the phenotype of the mice is much more slowly progressive than that observed in transgenic HD mice and more reminiscent of the late onset, slowly, progressive disease course of human HD. One of current limitations of using "knock-in" HD mice as a tool to investigate HD is that robust protocols for measuring modest behavioural phenotypes are less well developed. Therefore, the development of more sensitive assays and more robust protocols is required for assessing these mice. Investigating the motor function of HD mice may maximize the information that HD "knock-in" mice can provide.

Despite previous efforts, studies of locomotor performance using beam walking and rope tests did not detect significant motor deficits in Glasgow knock-in HD mice (Peggy Shelbourne, unpublished data). Beam walking and rope tests are more passive tests, which depend very much on the motivation and attention of mice, and are therefore less sensitive. This prompts the need for developing more sensitive and appropriate analytic tools to detect motor abnormalities of these mice. A rotarod apparatus (Dunham et al., 1957) that gives the tested mice a more challenging task, thus providing a more sensitive measure of

locomotor performance was used to assess four limb motor coordination, balance, and muscle strength of HD mice.

In this longitudinal study, a rotarod apparatus was used to investigate the locomotor function of HD mice at 4, 12 and 18 months of age. The data obtained were analysed using different methods. All methods indicated differences in locomotor function between HD and wild-type cohorts at 12 and 18 months of age, but the results varied when the data obtained at 4 months of age were analysed. ANOVA tests detected performance deficits in both male and female HD mice at 4 months of age ($p = 0.001$and $p < 0.001$ for male and female respectively), but other analyses using summary measures such as the maximum overall rotarod performance, did not ($p = 0.3$ and $p = 0.07$ for male and female respectively). ANOVA tests detected progressive performance deficits in both male and female HD mice from 4 to 18 months of age ($p < 0.001$ and $p = 0.004$ for males and females respectively), whilst other analyses using summary measures such as the maximum overall rotarod performance, only detected progressive performance deficits in both male and female HD mice from 4 to 12 months of age ($p = 0.008$ and $p = 0.008$ for males and females respectively), but not from 12 to 18 months of age ($p = 0.76$ and $p = 0.1$ for male and female respectively). All methods show that male and female cohorts of HD mice did not differ with respect to the onset and progression of performance deficits. It could be argued that ANOVA is probably a more powerful data analysis approach because it uses all raw data points and takes into account different factors such as different speeds, days, individual mice and their interactions, which might influence the rotarod performance. Therefore, it is very likely that the rotarod performance deficits of HD mice at 4 months of age and the progressive performance deficits over time are robust findings.

The findings have implications for the design of future experiments, particularly, if this assay is used to test the efficacy of treatments. Firstly, male and female HD mice do not show significant differences in the onset and progression of performance deficits, suggesting that one gender of mice is enough to represent the HD cohort. However, this study indicates that the ability to stay on rotarod is different between male and female mice, suggesting that a single sex cohort should be used rather than mixed sex cohort. Secondly, mice used in this study were tested at 8 different speeds per trial, which is a tiring task for the mice and time-consuming for the experimenter. Further analyses using ANOVA were

carried out to determine whether fewer than eight tests were required to achieve a similar outcome. The results of the analysis indicated that mice should be tested at least at three speeds, and that maximum information was obtained at 15, 20 and 25 rpm, because HD mice did not significantly differ from wild-type littermates in rotarod performance at low speeds and high speeds. Thirdly, a significant variability in performance was present among individual mice within all cohorts tested (male and female HD mice, and male and female wild-type littermates). It was noted that some mice showed a more prominent deterioration in performance with age, whilst others did not show any sign of decline. This variability in performance suggests that a longitudinal study testing the same mice at different ages is probably more powerful than using different mice of different ages to investigate the effects of age on rotarod performance.

Previously published studies have suggested that motor deficits in knock-in HD mice were difficult to detect using a rotarod apparatus (Wheeler et al., 2000; Lin et al., 2001). However, deficits in Glasgow HD mice were detected at an early age (~ 4 month of age). This discrepancy might be explained by aspects of the protocol and the experimental plan utilized in this study. Firstly, after 8 rounds of backcrossing onto the C57BL/6 background, the cohort of mice tested had a reasonably homogeneous background (statistically 99.7 % C57BL/6, 0.3 % 129/Sv), which would theoretically reduce the effects of potential genetic modifiers on rotarod performance. Secondly, all mice were subjected to handling twice a week from 5 weeks of age by the experimenter until the rotarod assessments began. It was felt that this would decrease the handling stress imposed on mice prior to performing the rotarod task. Thirdly, it is known that the rotarod task can be influenced by several factors such as weight, sex, learning ability of test, motivation and perseverance. Learning effects may have been reduced by subjecting each mouse to a training course that included trials at 0 to 20 rpm for 1 day and 3 trials at speed 20 rpm per day for three consecutive days. The lack of influence of learning effects is supported by the observation that performances did not differ over 3 days for any group of mice at any age tested when the data was analysed using summary measures (overall rotarod performance). However, three-way ANOVA tests suggest that the day of testing may have a small influence on rotarod performance of 18 month-old male mice ($F_{2,335} = 3.32, p = 0.037$) and 4 month-old female mice ($F_{2,383} = 4.52, p = 0.012$). Since the F ratios were not very high and the day of testing has influences on both wild-type and HD mice, it is probable that the effect of learning the rotarod task had,

at most, a subtle influence on the results obtained. Weight effects were also investigated. The results showed that differences in the rotarod performance of both male and female HD mice (compared to wild-type) could not be attributed to weight differences. The motivation and perseverance of mice is difficult to measure. However, it was observed that during the training course one wild-type littermate and two HD mice showed no effort to stay on the rod and fell off the rod immediately. These three mice were excluded from further testing.

How do these data compare with studies using other HD mice? Rotarod tests have shown early (from 5 weeks to 3 months of age) and progressive motor deficits in other transgenic HD models. R6/2 mice showed motor deficits in rotarod performance at 5 weeks of age with progressive deterioration (Carter et al., 1999). HD100 transgenic mice demonstrate progressive motor deficits in rotarod performance from 3 months of age until 12-15 months of age, after which the deterioration of motor function appears to plateau (Laforet et al., 2001). Progressive motor deficits in rotarod performance have been shown in N171-Q82 mice progression from 3 to 5 months of age (Schilling et al., 1999). HD89 mice demonstrate motor deficits in rotarod performance at ~13 months of age (Guidetti et al., 2001). It is not known whether HD 89 mice have earlier onset and progression of motor deficits in rotarod performance, since HD mice were tested only at ~13 months of age.

Are there any molecular/cellular correlates of functional deficits that can be drawn from the studies of the Glasgow HD mice and the transgenic HD mice? Inclusions have been postulated to be candidates for the pathological agent in HD. Glasgow HD mice show motor deficits prior to the appearance of neuronal inclusions (11 months of age), as do HD 100 and N171-Q82 mice, suggesting neuronal inclusions may not be responsible for initiating the motor deficits. However, these observations do not exclude the possibility that microaggregates or soluble nuclear mutant huntingtin may be involved in the pathogenesis. Although R6/2 mice show motor deficits in rotarod performance just after the presence of neuronal inclusions, hyperactivity in spontaneous locomotor behaviour at 3 weeks of age has been detected by a modified open field test, suggesting that some other molecular pathological changes may contribute to the motor dysfunction (Lüesse et al., 2001). Motor deficits are present in Glasgow HD mice at the earliest age (4 months) tested in this study. The finding that motor deficits are detected early (often at the first time point tested) in most of other studies of transgenic HD mice raises the question of whether developmental

deficits contribute to the motor deficits. If a developmental deficit is involved, what is the cause? Increasing evidence suggests that loss of normal huntingtin function may contribute to the phenotypes of HD (Dragatsis et al., 2000; Zuccato et al., 2001; Leavitt et al., 2001; Sun et al., 2001; Cattaneo et al 2001) and hypomorphic alleles might cause defects in neurogenesis (Auerbach et al., 2001; Nasir et al., 1995; White et al., 1997). Since most models express a very long expanded polyglutamine tract (> 80 residues, in excess of the size generally associated with juvenile HD patients) during early development, the toxic effect of the long polyglutamine might already exist during the early embryonic development. Despite these possible developmental effects, the motor deficits are progressive in most models, suggesting that an additional ongoing pathological process might be involved. Further studies to determine when the motor deficits start to occur in these mice may be informative to help clarify the developmental effects on motor deficits.

How do the results of the present study compare to the reported motor deficits in other "knock-in" HD mouse models? Motor deficits have been found in HdhQ111 mice at 24 months of age by using gait analysis (Wheeler et al., 2002), but were not detected at 2-17 months of age by using an accelerating rotarod apparatus (Wheeler et al., 2000). As details of the rotarod protocol were not described in the paper, it is difficult to know what might account for the discrepancy between this and the present study. $Hdh^{(CAG)150}$ mice at mixed age (15-40 weeks) did not show significant deficits in rotarod performance (5 rpm only), whilst mice at other ages were not tested with rotarod apparatus (Lin et al.,2001). The results obtained with the Glasgow HD mice demonstrate no significant differences from wild-type littermates at 5 rpm at any age tested. It is conceivable that the use of the 5 rpm test could not detect subtle deficits and that applying the protocol used in this study to test the rotarod performance of $Hdh^{(CAG)150}$ mice might allow the detection of earlier motor deficits in these mice. In summary, the present study may provide a robust rotarod test protocol that can be used as a reliable tool to assess the efficacy of potential treatments on HD mice in the future.

8.1.2 The body weight profiles of HD mice and wild-type littermates

Several lines of evidence suggest that weight loss is a clinical feature of HD, despite an adequate diet and feeding (Morales et al., 1989; Pratley et al., 2000). A characteristic

feature of the R6/2 mice is progressive weight loss despite increased caloric intake (Mangiarini et al., 1996). N171-82Q mice also exhibit a progressive loss of weight (Schilling et al., 1999). However, there is no evidence that either male or female HD mice showed progressive weight loss in the present study. Also, male and female HD mice did not show significant differences in the weight profile when compared to the corresponding group of wild-type littermates. Weight loss has not been observed in some "knock-in" HD mouse lines (Wheeler et al., 2000; Levine et al., 1999), but after 25 weeks of age, 1 in 10 $Hdh^{(CAG)150}$ mice appeared to be noticeably smaller than its wild-type littermates (Lin et al., 2001). These findings suggest that weight loss is probable not a common feature in "knock-in" HD mice, modelling early disease stages of HD, but may be influenced by very long (~ 150 CAG) repeat lengths. As HD mice with more aggressive phenotypes tend to show weight loss, it is probable that weight loss is a feature of the later stages of the disease process, possibly as a secondary consequence to the pathological process.

8.1.3 Absence of limb clasping phenotype in the HD mice

Limb clasping is detected in some transgenic HD mouse models (Mangiarini, et al., 1996; Schilling et al., 1999; Hodgson, et al., 1999; Reddy, et al., 1999; Yamamoto, et al., 2000), but not others (Levine, et al., 1999; Wheeler, et al., 2000). The result of a tail suspension test in the present study indicates that limb clasping is not a common feature of the Glasgow HD mice. The clasping phenomenon has also been observed in mouse models for other neurological disorders (for example, "weaver" and "staggerer" mice) (Lalonde, 1987a; Lalonde, 1987b), and thus appears not to be a specific phenotype in HD mouse models. As "weaver" and "staggerer" mice show pathological changes specifically in the cerebellum, the clasping phenomenon detected in transgenic mouse HD models might reflect cerebral lesions other than the striatal lesion. Indeed, HD mice with limb clasping tend to show a diffuse distribution of neuronal inclusions in the brain, suggesting that clasping may be related to the CAG repeat length, mutant huntingtin expression level and the genomic context of mutation, and may be a consequence of the later stages of disease process.

8.2 Mitochondrial abnormalities and oxidative stress in HD mouse brain

Several lines of evidence suggest that mitochondria play a central role in excitotoxicity, energy failure and oxidative stress, all of which may be involved in HD pathogenesis. Investigating the mitochondrial integrity in HD mice may shed light on the mechanism and molecular pathology of HD and thus provide a basis for developing potential treatments. As mentioned in the previous section (section 4.1), mitochondrial DNA (mtDNA) is particularly susceptible to oxidative damage. mitochondrial DNA deletions increase with age and oxidative stress in many human and mouse tissues (Hayakawa et al., 1991; Liu et al., 1998; Brossas et al., 1994; Tanhauser et al., 1995). Furthermore, increased mtDNA deletions have been shown in the cortex of individuals affected by HD (Horton et al., 1995). Decreased levels of total mtDNA have been shown in affected tissues of Friedreich's ataxia (Bradley et al., 2000) and Alzheimer's patients (de la Monte et al., 2000; Rodriguez-Santiago et al., 2001), conditions associated with increased oxidative stress. Therefore, the levels of deleted mtDNA and total mtDNA content were investigated in Glasgow HD mice.

8.2.1 Depletion of mtDNA in HD mouse striatum

A competitive PCR strategy was used to quantify total and deleted mitochondrial DNA species. The reasons for using competitive PCR assays have been stated in section 4.2. Briefly, They provide an internal control (mimic DNA) and an opportunity for calculating the absolute level of target DNA, since the initial amount of mimic DNA in the PCR reaction is known. The results have shown that total mtDNA is significantly decreased in the striatum of 24-month old HD mice, when compared to wild-type mice. This ~30% reduction in total mtDNA is specific to striatum, as no such reductions were detected in the cerebellum or cortex of the same animals. However, the level of deleted mtDNA species is not increased in HD mice. By using western blotting analysis to quantify the mitochondrial porin protein (representing mitochondrial mass), the study shows that the striatal mitochondrial mass in HD mice does not significantly differ from that in wild-type littermates. Therefore, the reduction of total mtDNA in striatum is most likely due to a

decrease in the number of mtDNA molecules per mitochondrion, rather than a decrease in the number of mitochondria in the striatum.

In order to ascertain whether the striatal depletion of mtDNA is a progressive phenomenon, levels of total mtDNA in the striatum of HD mice at 15 months of age were investigated. The results show that HD mice at 15 months of age do not have detectable differences in total mtDNA in the striatum when compared to wild-type littermates, suggesting mtDNA depletion is a late-onset and progressive, rather than a developmental, phenomenon.

Recently a study has reported that proper specimen storage is a critical issue in quantitative mtDNA analysis and that poor handling and storage of tissue, such as thawing tissues at room temperature over 4 hours, may mimic a severe mtDNA reduction (Berger et al., 2001). Such artefacts have been avoided in the present study, since the brain was immediately removed from the animal after sacrifice, dissected and quenched on dry ice or stored at -80°C. When brain tissues were removed from -80°C, they were immediately subjected to DNA extraction. Moreover, if other artifacts influenced our technical approach, the reduction of mtDNA might also be observed in brain regions other than striatum. Other efforts deployed to increase the likelihood of the correct results included duplicate competitive PCR assays for each sample and using two different methods (spectrophotometry and Southern blot analysis) to determine the amount of DNA template added to competitive PCR assays.

Many mitochondrial abnormalities including decreased activity of complex enzymes II/III (Brennan et al., 1985; Gu et al., 1996; Browne et al., 1997; Tabrizi et al., 1999) and IV (Tabrizi et al., 1999), decreased aconitase activity (Tabrizi et al., 1999), increased levels of mtDNA deletion (Horton et al., 1995) and increased 8-hydroxydeoxyguanosine (8-OHdG) mtDNA (Polidori et al., 1999) have been found in brains of HD patients. A significant reduction in aconitase and mitochondrial complex IV activities in the striatum has been shown in R6/2 mice (Tabrizi et al., 2000) and increased cyanide (complex IV enzyme inhibitor)-induced mitochondrial depolarization has been demonstrated in the lymphoblasts of HD89 mice (Sawa et al., 1999). However, depletion of mtDNA has never been reported in HD patients or other HD mouse models. One possible explanation is that depletion of mtDNA was only recently recognized as a heritable infantile mitochondrial disease

(Poulton et al., 1994) and its role in the pathogenesis of neurodegenerative disorders (de la Monte et al., 2000; Rodriguez-Santiago et al., 2001) was not fully appreciated until recently it was also found in other diseases such as chronic liver hepatitis and liver cirrhosis (Barbaro et al., 1999; Pesce et al., 2002), and in patients with antiviral drug-induced toxicity (Lewis et al., 2001). The present results draw attention to the fact that mtDNA depletion may play a role in HD molecular pathology.

8.2.2 Decreased mitochondrial complex enzyme IV subunit I (cytochrome c oxidase I) in HD mice

What are the consequences of ~30 % reduction of total mtDNA in the striatum of HD mice? Following the mtDNA depletion, the expression levels of mitochondrial DNA-encoded respiratory complex enzymes might be affected and energy production might be compromised. Northern blot and RNA slot blot analyses of cytochrome b (*Cytb*), cytochrome c oxidase I (*CoI*) and cytochrome c oxidase II (*CoII*) mRNA demonstrate that HD mice at ~25 months of age show no significant differences in mRNA levels of *CoI*, *CoII*, and *Cytb* in any brain region (striatum, cortex and cerebellum) studied when compared to normal littermates. However, HD mice showed a trend toward decreased levels of *CoI* mRNA in the striatum in both slot blot (p= 0.065) and northern blot analyses (p= 0.11) when compared to wild-type littermates, although the difference did not reach statistical significance.

COI immunostaining was significantly decreased in the dorsolateral striatum, but not in any other part of the striatum of 24 month-old HD mice when compared to wild-type littermates. The significantly decreased CO-I immunostaining with marginally decreased *CoI* mRNA levels in striatum may suggest that when levels of mtDNA are reduced, mtDNA transcription might increase as a compensatory response, but the stability of the resulting mitochondrial enzyme is decreased, perhaps due to increased oxidative damage (Morel et al., 1995). Depletion of mtDNA with compensated mitochondrial mRNA expression has been reported in aged rats (Barazzoni et al., 2000) and in skeletal muscle of diabetes mellitus patients (Antonetti et al., 1995). An alternative explanation for these findings may be that changes in individual cells or a small area of the striatum might be masked by analysis of the bulk tissue homogenate used in northern blot and slot blot

analyses. Therefore, immunohistochemical detection might be a better method than northern blot and slot blot analyses to detect pathological changes in HD mice where changes occur at the single cell level or localized to a small region. Interestingly, the results of CO-I immunostaining are also consistent with a gradient of neuropathological vulnerability within the striatum of HD, where the dorsal striatum is more vulnerable and shows earlier pathological changes than other regions (Vonsattel et al., 1998).

The decreased CO-I immuostaining in the striatum of the Glasgow HD mice is reminiscent of decreased expression levels of *CoI* mRNA in the striatum, external globus pallidus and putamen of HD brains (Gourfinkel-An et al., 2002) and the decreased complex enzyme IV activity in the striatum of HD patients (Tabrizi et al., 1999). How do the results of the present study compare to the reported mitochondrial enzyme abnormalities in other HD mouse models? Decreased complex enzyme IV activity has been shown in the striatum and cortex of end-stage R6/2 mice at ~ 12 weeks of age (Tabrizi et al., 2000). In contrast, activity of mitochondrial complex enzymes I-IV did not show significant changes in the brain regions of HD89 mice at 13-15 months of age (Guidetti et al., 2001), suggesting that HD89 mice examined were at the age when onset of mitochondrial abnormalities had not commenced. This supports the present study, which suggests that mitochondrial abnormalities are a relatively late pathological event.

8.2.3 Are mitochondrial abnormalities primarily responsible for motor deficits in HD mice

Total mtDNA is decreased in the striatum of 24-month old HD mice, but not at 15 months of age, when compared to wild-type mice. This suggests that the reduction of total mtDNA in the striatum of HD mice appears to be a progressive rather than a developmental phenomenon. Locomotor deficits appeared (4 months of age) before the detection of mtDNA depletion in our HD mouse model. This suggests that mitochondrial abnormalities may follow the pathological events responsible for the motor dysfunction. Measurements of mitochondrial complex enzymes I-IV did not reveal changes in the striatum and cerebral cortex in HD89 mice at 13-15 months of age, despite evidence of motor deficits, suggesting that mitochondrial energy impairment might follow early neuropathological changes responsible for motor deficits (Guidetti et al., 2001). This study also demonstrated that no

significant changes of mitochondrial enzymes were found in brains of pre-symptomatic HD patients. Furthermore, most mitochondrial abnormalities detected todate have occurred in brain tissue from end-stage HD patients (Brennan et al., 1985; Browne et al., 1997; Gu et al., 1996; Tabrizi et al., 1999). Taken together, these findings support the notion that mitochondrial abnormalities may occur in later stages of the disease and may be a consequence, rather than a cause, of early pathological changes in HD mice.

8.2.4 Increased oxidative stress in HD mice

Reduction of mtDNA could be due to decreased replication of mtDNA or increased oxidative damage of mtDNA and/or insufficient mtDNA repair activities. Indeed, reduced levels of mtDNA have been shown in brains of several diseases associated with increased oxidative stress such as Friedreich's ataxia (Bradley et al., 2000) and Alzheimer's disease (de la Monte et al., 2000; Rodriguez-Santiago et al., 2001). Increased levels of 8-hydroxydeoxyguanosine (8-OHdG) have also been shown in brains of Alzheimer's disease (de la Monte et al., 2000) and increased levels of plasma malondialdehyde in Friedreich's ataxia (Emond et al., 2000). These findings suggest mtDNA depletion is strongly associated with increased oxidative stress. Further supportive studies have demonstrated that massive reduction of mitochondrial DNA was found in liver, brain, heart and skeletal muscle of mice with alcohol-induced oxidative stress (Mansouri et al., 1999; Mansouri et al., 2001). Reduction of mtDNA can occur as a consequence of increased oxidative damage of mtDNA through DNA mispairing, point mutations, deletions, and fragmentation (Barazzoni et al. 1999). Mutation of the mtDNA replication control region may affect the replication of mtDNA by interfering with transcription factor binding to mtDNA promoter sites, or by reducing the stable structure of RNA-DNA hybrid structure thereby resulting in reduced mtDNA content (Michikawa et al., 1999). Insufficient mtDNA repair activities (Shadel et al., 1997) may aggravate increased oxidative damage and lead to mtDNA depletion. Cell-specific differences in mtDNA repair capacity have been shown (Ledoux et al., 1998), although cell-specific differences in mtDNA repair between different neuronal populations have not been previously reported. Given that striatum has diminished antioxidant defences than other brain regions (Cardozo-Pelaez et al., 1999), it is conceivable that the mtDNA repair ability of medium spiny neurons may be selectively decreased, which makes their mtDNA more vulnerable to increased oxidative damage.

Speculation that mtDNA depletion possibly results from increased oxidative stress prompts the necessity to search for direct evidence of increased oxidative stress in the HD mice. By using northern blot analysis of heme oxygenase-1 (*Hmox1*) mRNA and RNA slot blot analysis of αB-crystallin mRNA in mouse brain tissues, the present study reveals that 24 month-old HD mice showed no significant differences in the levels of *Hmox1*and αB-crystallin mRNA in the striatum when compared with wild-type littermates. These results and negative results from a previous study that determined levels of malondialdehyde in the brain regions of the Glasgow HD mice (Shelbourne, unpublished data), did not provide evidence of increased oxidative stress in the brains of HD mice. However, both experiments used bulk tissue homogenates for analysis. Changes in individual cells or small areas of the striatum might be masked by analysis of the bulk tissue homogenates and so immunochemical detection of heme oxygenase-1 (HO-I), 4-hydroxy-2-nonenal (4-HNE) and 8-hydroxydeoxyguanosine (8-OHdG) in HD mouse brain tissue was performed. The reasons for using these markers as an indicator of increased oxidative stress have been described in section 7.1. Importantly, increases in the levels of these markers have been shown in the brains of HD patients (Brown et al. 1999; Polidori et al., 1999; Bogdanov et al., 2001).

The present study demonstrated that 24 month-old HD mice showed no significant differences in HO-1 and 4-HNE immunostaining levels in the striatum and cortex when compared to wild-type littermates. In contrast, 8-OHdG immunostaining was significantly increased in the dorsomedial, dorsolateral and ventromedial striatum, but not in the cortex of 24 month-old HD mice when compared to wild-type littermates. HD mice showed a trend toward increased 8-OHdG immunostaining levels in the ventrolateral striatum when compared to wild-type littermates, although this just failed to reach statistical significance (using Student's *t* test). The results of 8-OHdG staining are consistent with a gradient of vulnerability within the striatum of HD, with the dorsomedial striatum more vulnerable and showing earlier pathological changes than other regions (Vonsattel and DiFiglia, 1998). These results also suggest that immunohistochemical detection might be a better method for detecting increased oxidative stress in HD mice where levels of oxidative stress markers can be resolved at the single cell level or localized to a small region. The reason that 4-HNE and HO-1 immunostaining level is not increased in HD striatum may suggest that 8-OHdG is a more sensitive marker of increased oxidative stress than 4-HNE and HO-1. It

may also reflect a selective increase of oxidative damage of DNA, but less damage of lipids in HD striatum at the stage when mice were examined. The presumption of selective increased oxidative damage of DNA in HD striatum is supported by the finding that mtDNA is ~ 30 % depleted in HD striatum.

Increased 8-OHdG levels are also observed in the brains of end-stage R6/2 mice (Bogdanov et al., 2001) and in the striatum of HD patients (Browne et al., 1997). These findings and the demonstration that mutant huntingtin causes increased levels of reactive oxygen species in cell culture (Wyttenbach et al., 2002) support the notion that increased oxidative stress has a role in HD pathogenesis. It is interesting to note that increased 8-OHdG staining was not confined to the striatum, but present throughout the brain in both cortical and subcortical areas of R6/2 mice. In contrast, increased 8-OHdG level is confined to the striatum of Glasgow HD mice, suggesting a selective vulnerability to oxidative stress in Glasgow HD mice. Previous studies of mutation length variability in somatic tissue of the Glasgow HD mice have shown evidence that the largest mutations are observed in the striatum and that repeat instability may occur by mechanisms that are not replication-based (Kennedy and Shelbourne, 2000). The authors suggest normal age-related DNA damage due to increased oxyradical concentrations and diminished antioxidant defences in the striatum (Cardozo-Pelaez et al., 1999) could be exacerbated by the functional consequences of the HD mutation, thereby initiating a vicious cycle of mutation expansion and associated cellular pathology in vulnerable cells. The present study provides direct evidence of increased oxidative stress specifically in the striatum of HD mice, supporting the idea that the mutation instability may be caused by DNA repair in response to increased oxidative damage.

Increased oxidative stress in the striatum of HD mice could be the cause or the consequence of mtDNA depletion. Mitchondrial DNA depletion could result in decreased levels of respiratory enzyme complexes encoded by mtDNA, which then compromise energy production and lead to increased oxidative stress (Esposito et al., 1999). This study does not provide any direct evidence to distinguish the causal relationship of these two pathological changes. However, studies have shown that energy production by neurons is impaired only when COI activity is reduced to 30 % (Davey et al., 1998). In addition, myoblats showed no changes in energy production when 70 % of complex IV activity was inhibited (Leary et

al., 1998). In light of these findings, although mtDNA is ~ 30 % depleted and the COI immunostaining is about 50 % decreased in the striatum of Glasgow HD mice, the striatal neurons might still be able to maintain their ATP production. This suggests that it is less likely that the increased oxidative stress in HD mice is caused by energy failure through mtDNA depletion and decreased COI levels. Therefore, the mtDNA depletion and decreased COI levels in the striatum of HD mice may be the consequences of increased oxidative stress.

8.2.5 Maintenance of mitochondrial DNA (mtDNA) in HD mice

Reduced levels of mtDNA could be due to decreased replication of mtDNA or increased oxidative damage of mtDNA and/or insufficient mtDNA repair activities (Shadel and Clayton, 1997). Evidence of increased oxidative stress in the striatum of HD mice has been presented in the current study. However, does decreased replication also contribute to the depletion of mtDNA?

Mitochondrial transcription factor A (mtTFA) is a transcription factor that is involved in mtDNA transcription and mtDNA replication (section 1.5.5). mtTFA is essential for mtDNA replication and has been demonstrated to regulate mtDNA copy number *in vivo* . However, the present study has shown that the expression levels of mitochondrial transcription factor A (*Tfam*) mRNA and mtTFA protein in Glasgow HD mouse striatum do not appear to differ from those of wild-type littermates. Therefore, the reduction of mtDNA in the striatum of HD mice is probably not caused by decreased mtTFA levels.

As mentioned in chapter 1 (section 1.5.5), the replication of mtDNA requires mtTFA and other factors including mitochondrial RNA polymerase, mitochondrial RNA processing endoribonuclease (RNase MRP), polymerase γ (pol γ), single-stranded DNA-binding protein (SSB), and nuclear respiratory factors 1 and 2. In addition, deoxyguanosine kinase and thymidine kinase-2 have been recently reported to be essential for the mtDNA replication (Mandel et al., 2001; Saada et al., 2001). The reduction of mtDNA in the striatum of HD mice might be caused by a decrease in one or more of these factors, which have not been investigated in this study (because of limited time). Indeed, the mtDNA depletion caused by antiviral drugs such as zidovudine (AZT) in AIDS patients (Chariot et

al., 1999; Davison et al., 1996) appears to be due to the inhibition of pol γ activity by antiviral drugs (Benbrik et al., 1997). Furthermore, there have been reports of thymidine phosphorylase gene mutations in mitochondrial neurogastrointestinal encephalomyopathy (MNGIE), an autosomal recessive disorder associated with mtDNA depletion and multiple mtDNA deletions (Nishino et al., 1999), the mitochondrial deoxyguanosine kinase gene mutations in hepatocerebral mitochondrial diseases with mtDNA depletion (Mandel et al., 2001) and thymidine kinase mutations in mitochondrial DNA depletion myopathy (Saada et al., 2001).

When considering these mtDNA replication-related factors, it is interesting to note that pol γ contains a 10-polyglutamine tract. Recently, a study showed that expanded polyglutamine strethes particularly interferes with CBP-activated gene transcription, suggesting that mutant huntingtin may cause dysregulation of transcription (Nucifora et al., 2001). It has been postulated that CBP contains a polyglutamine tract that interacts with polyglutamine in mutant huntingtin and its activity is thus inhibited (section 1.2.3.8). It is possible that mutant huntingtin might interact with pol γ through their respective polyglutamine tracts and thus interfere with the activity of pol γ. Alternatively, the transcription levels of pol γ and other mtDNA replication-related proteins might be decreased due to the transcriptional dysregulation caused by the interaction of mutant huntingtin with CBP and other nuclear transcription factors. Although the microarray study in R6/2 mice did not show altered transcription levels of some of mtDNA replication-related proteins (Luthi-Carter et al., 2000), the possibility that transcription levels of the mtDNA replication-related proteins are decreased still cannot be excluded. Investigating thoroughly the expression levels and activity of the mtDNA replication-related factors in HD mice are necessary to determine whether depletion of mtDNA is attributable to decreased replication of mtDNA.

8.2.6 How might mutant huntingtin cause increased oxidative stress in HD?

This study has shown evidence of increased oxidative stress in the striatum of HD mice at 24 months of age. Possible mechanisms by which mutant huntingtin causes increased oxidative stress are discussed in the following section.

Striatal neurons in transgenic and "knock-in" HD mouse models display increased sensitivity to NMDA receptor-mediated excitotoxicity (Levine et al., 1999; Zeron et al., 2002). The possible links link between excitotoxicity and mutant huntingtin has been discussed in the literature and have been presented in sections 1.2.4.1 and 1.4.3.4. In addition, downregulated genes belonging to specific neuronal signalling systems including Ca^{2+} homeostasis system, have been shown in R6/2 mice (Luthi-Carter et al., 2000). An impaired Ca^{2+} homeostasis system will result in intracellular Ca^{2+} influx that will also increase sensitivity to excitotoxicity. One of the consequences of excitotoxicity is the generation of reactive oxygen species (ROS) and increased oxidative damage to neurons. It is thus postulated that glutamate-induced excitotoxicity and impaired Ca^{2+} homeostasis may contribute to the increased oxidative stress observed in the striatum of Glasgow HD mice.

Impairment of the ubiquitin-proteasome system can be caused by polyglutamine aggregation (Bence et al., 2001) and chaperone proteins (heat shock proteins) can be sequestrated into intracellular aggregates in cellular and mouse models of polyglutamine diseases (Cummings et al., 1998; Chai 1999 et al., Stenoien et al., 1999; Warrick et al., 1999; Jana et al., 2000). There is evidence that the proteasome is responsible for degrading oxidized proteins (Sitte et al., 2000) and heat shock proteins protect cells from oxidative damage (Ding and Keller, 2001). It has also been reported that inhibition of proteasome function results in increased oxidative damage, because inhibition of proteasome function can diminish the efficiency of degrading oxidized proteins (Lee et al., 2001). In addition, heat shock protein 27 can prevent cellular polyglutamine toxicity and suppress the increase of reactive oxygen species caused by mutant huntingtin in cell culture (Wyttenbach et al., 2002). Therefore, it is plausible that the inhibition of proteasome and heat shock proteins by intracellular huntingtin aggregates results in increased oxidative damage in HD mice.

Increased oxidative stress could, in turn, further inhibit proteasome function (Ding and Keller, 2001) and initiate a vicious cycle which results in more and more oxidative damage.

It has been suggested that transcriptional dysregulation caused by expanded polyglutamine is involved in HD pathogenesis (section1.2.3.8). Cell models have demonstrated that CREB-dependent transcriptional activation can be suppressed through the binding of $TAF_{II}130$ (a cofactor for CREB-dependent transcriptional activation) and CBP (CREB-binding protein) to expanded polyglutamine stretches (Shimohata et al., 2000; Steffan et al., 2000; Nucifora et al., 2001). When neurons are subjected to moderate oxidative stress, CREB-mediated transcription increases in response to a pro-survival signal mediated by the activation of extracellular signal-regulated kinase 1 and 2 (ERK1/2) (Bonni et al., 1999; Crossthwaite et al., 2002). The anti-apoptotic Bcl-2 gene is induced by hypoxia and produces a protective effect, which is dependent upon the cyclic AMP response element (CRE) in the Bcl-2 promoter (Freeland et al., 2001). The protective effect is generated through the enhanced phosphorylation of the CREB transcription factor and enhanced transcriptional activation by the CBP (Freeland et al., 2001). These studies suggest that CREB-dependent transcription may play a protective role in the event of oxidative stress and apoptosis. Mutant huntingtin binds strongly to specificity protein 1 (Sp1), a transcription factor, inhibiting the Sp1-dependent transcription activity has also been shown (Dunah et al., 2002; Li et al., 2002). Sp1 activates transcription of a variety of genes including the human *SOD1* and *SOD2* genes encoding respectively manganese superoxide dismutase 1 and 2, which have a protective role against increased oxidative stress (Porntadavity et al., 2001; Xu et al., 2002). Since mutant huntingtin inhibits Sp1-dependent transcription, the expression of *SOD1* and *SOD2* might be compromised, leading to increased oxidative stress. Therefore, it is conceivable that increased oxidative stress might occur due to decreased Sp1- and CREB-dependent transcription through the interaction of Sp1 or CBP with expanded polyglutamine in the Glasgow HD mice.

Defining how mitochondrial abnormalities and increased oxidative stress develop in HD mice and their possible relationship to mutant huntingtin expression may provide insights into HD pathogenesis (Fig. 8.1).

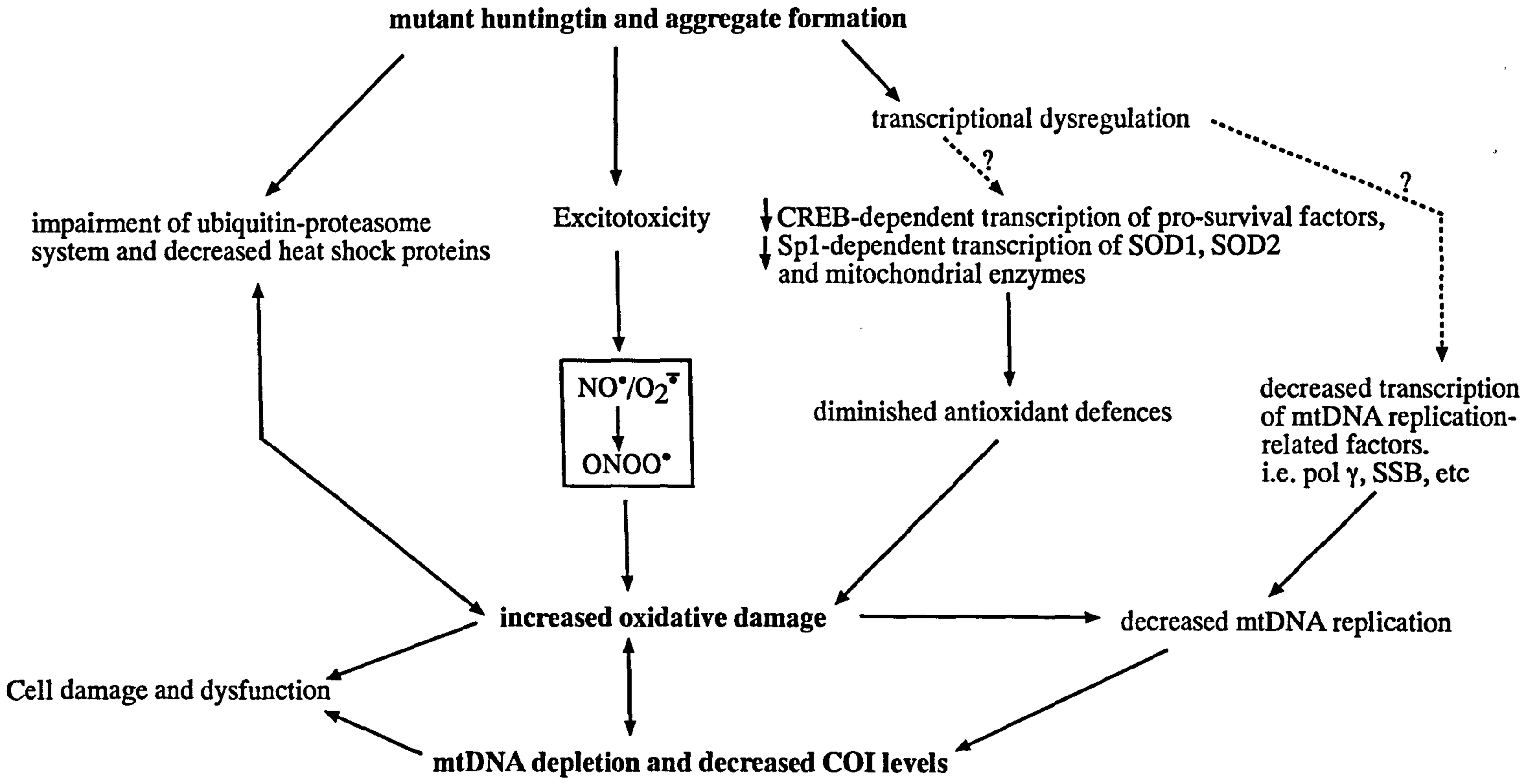

Figure 8.1 Putative causal mechanisms of mitochondrial abnormalities and increased oxidative stress in HD mice. $NO^{\bullet}$: nitric oxide. $O_2^{\bullet-}$: superoxide, $ONOO^{\bullet}$: peroxynitrite. pol γ: polymerase γ. SSB: single-stranded DNA-binding protein. Arrows indicate established association. Dashed arrows indicate putative association.

8.3 Prospects for potential therapies

As previously mentioned (section 1.2.5), there is increasing evidence that defective energy metabolism, oxidative stress, glutamate-mediated excitotoxicity, mitochondrial abnormalities and their interplay may contribute to the pathogenesis of Huntington's disease. This study provides evidence of mitochondrial abnormalities and increased oxidative stress in a "knock-in" HD mouse model, thus reinforcing this hypothesis. Strategies that reduce glutamate-mediated excitotoxicity, preventing generation of reactive oxygen species and/or augmenting mitochondrial energy production might have significant therapeutic benefits. Indeed, neuroprotective effects of creatine have been shown in R6/2 mice (Ferrante et al., 2000). Creatine may exert its effect by increasing phosphocreatine levels or by stabilizing the mitochondrial permeability transition. Remacemide hydrochloride, a non-competitive NMDA receptor antagonist, and Co-enzyme Q10 (CoQ10), an essential cofactor of the electron transport chain and a potent free radical scavenger, have been used to treat HD patients in a 5-year clinical trial study (HDCRG, 2001). CoQ10 showed a trend toward slowing the progression of disease, but statistical significance was not achieved. In contrast, remacemide appeared to be ineffective as did combination therapy in the clinical trial. However, in the HD-N171-82Q transgenic mice, remacemide and CoQ10 administration did appear to transiently improve motor performance on the rotarod, but did not prolong the survival or delay the appearance of inclusions (Schilling et al., 2001). These results suggest that further, more detailed studies of these compounds at different doses in other HD mouse models, and possibly in HD patients, are warranted.

8.4 Conclusions and future studies

Using a rotarod test, this study has been able to show, for the first time, progressive motor deficits in knock-in HD mice from 4 months of age. The progressive motor deficits can be used as a biomarker to test the efficacy of potential therapy strategies in the future. This study has also defined a robust rotarod protocol that may be useful in studies of other HD mouse models.

It is not known whether motor deficits occur in the Glasgow HD mice before 4 months of age. Further studies should include earlier time points to determine whether developmental defects also contribute to the motor deficits. Despite the presence of early-onset, progressive motor deficits, weight loss and limb clasping are not common features in Glasgow HD mice. Total mtDNA content is reduced in the striatum of Glasgow HD mice at 24 months of age, but not at 15 months of age, suggesting mtDNA depletion is a progressive rather than a developmental phenomenon. As motor deficits appear before mtDNA depletion, it is possible that mitochondrial abnormalities may follow the pathological events responsible for the motor dysfunction. If mtDNA depletion is the primary cause of mitochondrial dysfunction in *HD*, these findings raise the possibility that potential treatments to prevent mtDNA depletion or rescue mitochondrial function may not prevent the onset of motor deficits. Since the Glasgow HD mice model early stages of HD, it will be interesting and informative to determine whether mtDNA depletion is present in early stages of human HD and other polyglutamine diseases.

Depletion of mtDNA in the striatum could be the cause or the consequence of increased oxidative stress. Increased 8-OHdG immunostaining in the dorsomedial, dorsolateral and ventromedial striatum, but not in the cortex of 24 month-old HD mice provides direct evidence that increased oxidative stress specifically occurs in the striatum. COI immunostaining is also specifically decreased in the dorsolateral striatum, but not in any other part of the striatum of 24 month-old HD mice. The decreased levels of COI immunostaining in the striatum may be due to mtDNA depletion, or increased oxidative damage of the enzyme, or both. Although mtDNA is ~ 30 % depleted and COI immunostaining is about 50 % decreased in the striatum of Glasgow HD mice, the striatal neurons might still be able to maintain their ATP production. Therefore, it is more likely that mtDNA depletion and decreased COI levels in the striatum of HD mice may be the consequences, rather than the cause, of increased oxidative stress. Striatal mtDNA depletion could also be caused by decreased mtDNA replication. Although altered levels of *Tfam* mRNA and mtTFA protein in the striatum of HD mice could not be detected in the present study, the possibility of reduced expression or activity of other mtDNA replication-related factors cannot be excluded. Therefore, further studies to investigate whether these factors are involved in the depletion of mtDNA detected in HD mouse striatum, are warranted.

This is the first time that evidence of increased oxidative stress in a "knock in" HD mouse model has been shown. It is not known whether the increased oxidative stress is present when the HD mice are yonger than 24 months of age. In the future, it will be important to investigate the onset of increased oxidative stress in HD mice and its relationship with other molecular changes and clinical phenotypes, because the relationship will determine what benefits may be obtained from treatments that prevent increased oxidative damage.

So what causes the increased oxidative stress in the striatum of HD mice? Possible links between mutant huntingtin and oxidative damage have been discussed in previous section (section 8.2.6). Future studies on these links and other aspects may help to dissect out the HD pathogenesis and identify potential novel therapeutic targets.

References

Albin, R. L., Young, A. B., Penney, J. B., Handelin, B., Balfour, R., Anderson, K. D., Markel, D. S., Tourtellotte, W. W., and Reiner, A. (1990). Abnormalities of striatal projection neurons and N-methyl-D-aspartate receptors in presymptomatic Huntington's disease. N Engl J Med *322*, 1293-1298.

Alavi, A., Dann, R., Chawluk, J., Alavi, J., Kushner, M., and Reivich, M. (1986). Positron emission tomography imaging of regional cerebral glucose metabolism. Semin Nucl Med *16*, 2-34.

Ambrose, C. M., Duyao, M. P., Barnes, G., Bates, G. P., Lin, C. S., Srinidhi, J., Baxendale, S., Hummerich, H., Lehrach, H., Altherr, M., *et al.* (1994). Structure and expression of the Huntington's disease gene: evidence against simple inactivation due to an expanded CAG repeat. Somat Cell Mol Genet *20*, 27-38.

Andreu, A. L., Arbos, M. A., Perez-Martos, A., Lopez-Perez, M. J., Asin, J., Lopez, N., Montoya, J., and Schwartz, S. (1998). Reduced mitochondrial DNA transcription in senescent rat heart. Biochem Biophys Res Commun *252*, 577-581.

Andrew, S. E., Goldberg, Y. P., Kremer, B., Squitieri, F., Theilmann, J., Zeisler, J., Telenius, H., Adam, S., Almquist, E., Anvret, M., and et al. (1994). Huntington disease without CAG expansion: phenocopies or errors in assignment? Am J Hum Genet *54*, 852-863.

Andrews, T. C., and Brooks, D. J. (1998). Advances in the understanding of early Huntington's disease using the functional imaging techniques of PET and SPET. Mol Med Today *4*, 532-539.

Annex, B. H., and Williams, R. S. (1990). Mitochondrial DNA structure and expression in specialized subtypes of mammalian striated muscle. Mol Cell Biol *10*, 5671-5678.

Antonetti, D. A., Reynet, C., and Kahn, C. R. (1995). Increased expression of mitochondrial-encoded genes in skeletal muscle of humans with diabetes mellitus. J Clin Invest *95*, 1383-1388.

Aronin, N., Chase, K., Young, C., Sapp, E., Schwarz, C., Matta, N., Kornreich, R., Landwehrmeyer, B., Bird, E., Beal, M. F., *et al.* (1995). Cag Expansion Affects the Expression Of Mutant Huntingtin In the Huntingtons Disease Brain. Neuron *15*, - 1193-1201.

Auerbach, W., Hurlbert, M. S., Hilditch-Maguire, P., Wadghiri, Y. Z., Wheeler, V. C., Cohen, S. I., Joyner, A. L., MacDonald, M. E., and Turnbull, D. H. (2001). The HD mutation causes progressive lethal neurological disease in mice expressing reduced levels of huntingtin. Hum Mol Genet *10*, 2515-2523.

Augood, S. J., Faull, R. L., Love, D. R., and Emson, P. C. (1996). Reduction in enkephalin and substance P messenger RNA in the striatum of early grade Huntington's disease: a detailed cellular in situ hybridization study. Neuroscience *72*, 1023-1036.

Bao, J., Sharp, A. H., Wagster, M. V., Becher, M., Schilling, G., Ross, C. A., Dawson, V. L., and Dawson, T. M. (1996). Expansion of polyglutamine repeat in huntingtin leads to abnormal protein interactions involving calmodulin. Proc Natl Acad Sci U S A *93*, 5037-5042.

Barazzoni, R., Short, K. R., and Nair, K. S. (2000). Effects of aging on mitochondrial DNA copy number and cytochrome c oxidase gene expression in rat skeletal muscle, liver, and heart. J Biol Chem *275*, 3343-3347.

Barbaro, G., Di Lorenzo, G., Asti, A., Ribersani, M., Belloni, G., Grisorio, B., Filice, G., and Barbarini, G. (1999). Hepatocellular mitochondrial alterations in patients with chronic hepatitis C: ultrastructural and biochemical findings. Am J Gastroenterol *94*, 2198-2205.

Barnes, G. T., Duyao, M. P., Ambrose, C. M., McNeil, S., Persichetti, F., Srinidhi, J., Gusella, J. F., and MacDonald, M. E. (1994). Mouse Huntington's disease gene homolog (Hdh). Somat Cell Mol Genet *20*, 87-97.

Beal, M. F. (1995). Aging, energy, and oxidative stress in neurodegenerative diseases. Ann Neurol *38*, 357-366.

Beal, M. F. (1996). Mitochondria, free radicals, and neurodegeneration. Curr Opin Neurobiol *6*, 661-666.

Beal, M. F. (1998). Mitochondrial dysfunction in neurodegenerative diseases. Biochimica Et Biophysica Acta Bioenergetics *1366*, - 211-223.

Beal, M. F., Ferrante, R. J., Swartz, K. J., and Kowall, N. W. (1991). Chronic quinolinic acid lesions in rats closely resemble Huntington's disease. J Neurosci *11*, 1649-1659.

Becher, M. W., Kotzuk, J. A., Sharp, A. H., Davies, S. W., Bates, G. P., Price, D. L., and Ross, C. A. (1998). Intranuclear neuronal inclusions in Huntington's disease and dentatorubral and pallidoluysian atrophy: Correlation between the density of inclusions and IT15 CAG triplet repeat length. Neurobiol Dis *4*, - 387-397.

Beckman, J. S., and Crow, J. P. (1993). Pathological implications of nitric oxide, superoxide and peroxynitrite formation. Biochem Soc Trans *21*, 330-334.

Benbrik, E., Chariot, P., Bonavaud, S., Ammi-Said, M., Frisdal, E., Rey, C., Gherardi, R., and Barlovatz-Meimon, G. (1997). Cellular and mitochondrial toxicity of zidovudine (AZT), didanosine (ddI) and zalcitabine (ddC) on cultured human muscle cells. J Neurol Sci *149*, 19-25.

Bence, N. F., Sampat, R. M., and Kopito, R. R. (2001). Impairment of the ubiquitin-proteasome system by protein aggregation. Science *292*, 1552-1555.

Benitez, J., Robledo, M., Ramos, C., Ayuso, C., Astarloa, R., Garcia Yebenes, J., and Brambati, B. (1995). Somatic stability in chorionic villi samples and other Huntington fetal tissues. Hum Genet *96*, 229-232.

Bennett, J. L., Jeong-Yu, S., and Clayton, D. A. (1992). Characterization of a Xenopus laevis ribonucleoprotein endoribonuclease. Isolation of the RNA component and its expression during development. J Biol Chem *267*, 21765-21772.

Berger, A., Bruschek, M., Grethen, C., Sperl, W., and Kofler, B. (2001). Poor storage and handling of tissue mimics mitochondrial DNA depletion. Diagn Mol Pathol *10*, 55-59.

Bogdanov, M. B., Andreassen, O. A., Dedeoglu, A., Ferrante, R. J., and Beal, M. F. (2001). Increased oxidative damage to DNA in a transgenic mouse model of Huntington's disease. J Neurochem *79*, 1246-1249.

Bonni, A., Brunet, A., West, A. E., Datta, S. R., Takasu, M. A., and Greenberg, M. E. (1999). Cell survival promoted by the Ras-MAPK signaling pathway by transcription-dependent and -independent mechanisms. Science *286*, 1358-1362.

Borlongan, C. V., Nishino, H., and Sanberg, P. R. (1997). Systemic, but not intraparenchymal, administration of 3 nitropropionic acid mimics the neuropathology of Huntington's disease: A speculative explanation. Neurosci Res *28*, 185-189.

Boutell, J. M., Thomas, P., Neal, J. W., Weston, V. J., Duce, J., Harper, P. S., and Jones, A. L. (1999). Aberrant interactions of transcriptional repressor proteins with the Huntington's disease gene product, huntingtin. Hum Mol Genet *8*, 1647-1655.

Boutell, J. M., Wood, J. D., Harper, P. S., and Jones, A. L. (1998). Huntingtin interacts with cystathionine beta synthase. Hum Mol Genet *7*, 371-378.

Braak, H., Del Tredici, K., Sandmann-Kiel, D., Rub, U., and Schultz, C. (2001). Nerve cells expressing heat-shock proteins in Parkinson's disease. Acta Neuropathol (Berl) *102*, 449-454.

Bradley, J. L., Blake, J. C., Chamberlain, S., Thomas, P. K., Cooper, J. M., and Schapira, A. H. (2000). Clinical, biochemical and molecular genetic correlations in Friedreich's ataxia. Hum Mol Genet *9*, 275-282.

Brandt, J., Bylsma, F. W., Gross, R., Stine, O. C., Ranen, N., and Ross, C. A. (1996). Trinucleotide Repeat Length and Clinical Progression In Huntingtons Disease. Neurology *46*, - 527-531.

Brennan, W. A., Jr., Bird, E. D., and Aprille, J. R. (1985). Regional mitochondrial respiratory activity in Huntington's disease brain. J Neurochem *44*, 1948-1950.

Brinkman, R. R., Mezei, M. M., Theilmann, J., Almqvist, E., and Hayden, M. R. (1997). The likelihood of being affected with huntington disease by a particular age, for a specific CAG size. Am J Hum Genet *60*, 1202-1210.

Brossas, J. Y., Barreau, E., Courtois, Y., and Treton, J. (1994). Multiple deletions in mitochondrial DNA are present in senescent mouse brain. Biochem Biophys Res Commun *202*, 654-659.

Browne, S. E., Bowling, A. C., MacGarvey, U., Baik, M. J., Berger, S. C., Muqit, M. M., Bird, E. D., and Beal, M. F. (1997). Oxidative damage and metabolic dysfunction in Huntington's disease: selective vulnerability of the basal ganglia. Ann Neurol *41*, 646-653.

Browne, S. E., Ferrante, R. J., and Beal, M. F. (1999). Oxidative stress in Huntington's disease. Brain Pathol *9*, 147-163.

Burke, J. R., Enghild, J. J., Martin, M. E., Jou, Y. S., Myers, R. M., Roses, A. D., Vance, J. M., and Strittmatter, W. J. (1996). Huntington and DRPLA Proteins Selectively Interact With the Enzyme Gapdh. Nature Medicine *2*, - 347-350.

Calabresi, P., Centonze, D., Pisani, A., Sancesario, G., Gubellini, P., Marfia, G. A., and Bernardi, G. (1998). Striatal spiny neurons and cholinergic interneurons express differential ionotropic glutamatergic responses and vulnerability: Implications for ischemia and Huntington's disease. Ann Neurol *43*, - 586-597.

Calabresi, P., Gubellini, P., Picconi, B., Centonze, D., Pisani, A., Bonsi, P., Greengard, P., Hipskind, R. A., Borrelli, E., and Bernardi, G. (2001). Inhibition of mitochondrial complex II induces a long-term potentiation of NMDA-mediated synaptic excitation in the striatum requiring endogenous dopamine. J Neurosci *21*, 5110-5120.

Callen, J. C., Tourte, M., Dennebouy, N., and Mounolou, J. C. (1983). Changes in D-loop frequency and superhelicity among the mitochondrial DNA molecules in relation to organelle biogenesis in oocytes of Xenopus laevis. Exp Cell Res *143*, 115-125.

Cardozo-Pelaez, F., Song, S., Parthasarathy, A., Hazzi, C., Naidu, K., and Sanchez-Ramos, J. (1999). Oxidative DNA damage in the aging mouse brain. Mov Disord *14*, 972-980.

Carter, R. J., Lione, L. A., Humby, T., Mangiarini, L., Mahal, A., Bates, G. P., Dunnett, S. B., and Morton, A. J. (1999). Characterization of progressive motor deficits in mice transgenic for the human Huntington's disease mutation. J Neurosci *19*, 3248-3257.

Castellani, R., Smith, M. A., Richey, P. L., Kalaria, R., Gambetti, P., and Perry, G. (1995). Evidence for oxidative stress in Pick disease and corticobasal degeneration. Brain Res *696*, 268-271.

Castellani, R., Smith, M. A., Richey, P. L., and Perry, G. (1996). Glycoxidation and oxidative stress in Parkinson disease and diffuse Lewy body disease. Brain Res *737*, 195-200.

Cataldo, A. M., Hamilton, D. J., Barnett, J. L., Paskevich, P. A., and Nixon, R. A. (1996). Abnormalities of the endosomal-lysosomal system in Alzheimer's disease: relationship to disease pathogenesis. Adv Exp Med Biol *389*, 271-280.

Cepeda, C., Ariano, M. A., Calvert, C. R., Flores-Hernandez, J., Chandler, S. H., Leavitt, B. R., Hayden, M. R., and Levine, M. S. (2001). NMDA receptor function in mouse models of Huntington disease. J Neurosci Res *66*, 525-539.

Chai, Y., Koppenhafer, S. L., Bonini, N. M., and Paulson, H. L. (1999). Analysis of the role of heat shock protein (Hsp) molecular chaperones in polyglutamine disease. J Neurosci *19*, 10338-10347.

Chang, C. M., Yu, Y. L., Fong, K. Y., Wong, M. T., Chan, Y. W., Ng, T. H., Leung, C. M., and Chan, V. (1994). Huntington's disease in Hong Kong Chinese: epidemiology and clinical picture. Clin Exp Neurol *31*, 43-51.

Chang, D. D., and Clayton, D. A. (1984). Precise identification of individual promoters for transcription of each strand of human mitochondrial DNA. Cell *36*, 635-643.

Chang, D. D., Hauswirth, W. W., and Clayton, D. A. (1985). Replication priming and transcription initiate from precisely the same site in mouse mitochondrial DNA. Embo J *4*, 1559-1567.

Chariot, P., Drogou, I., de Lacroix-Szmania, I., Eliezer-Vanerot, M. C., Chazaud, B., Lombes, A., Schaeffer, A., and Zafrani, E. S. (1999). Zidovudine-induced mitochondrial disorder with massive liver steatosis, myopathy, lactic acidosis, and mitochondrial DNA depletion. J Hepatol *30*, 156-160.

Chen, B., Kubelik, A. R., Mohr, S., and Breitenberger, C. A. (1996). Cloning and characterization of the Neurospora crassa cyt-5 gene. A nuclear-coded mitochondrial RNA polymerase with a polyglutamine repeat. J Biol Chem *271*, 6537-6544.

Chen, M., Ona, V. O., Li, M., Ferrante, R. J., Fink, K. B., Zhu, S., Bian, J., Guo, L., Farrell, L. A., Hersch, S. M., *et al.* (2000). Minocycline inhibits caspase-1 and caspase-3 expression and delays mortality in a transgenic mouse model of Huntington disease. Nat Med *6*, 797-801.

Chen, Z., and Pickart, C. M. (1990). A 25-kilodalton ubiquitin carrier protein (E2) catalyzes multi- ubiquitin chain synthesis via lysine 48 of ubiquitin. J Biol Chem *265*, 21835-21842.

Chun, W., Lesort, M., Tucholski, J., Ross, C. A., and Johnson, G. V. (2001). Tissue transglutaminase does not contribute to the formation of mutant huntingtin aggregates. J Cell Biol *153*, 25-34.

Clayton, D. A. (1982). Replication of animal mitochondrial DNA. Cell *28*, 693-705.

Clayton, D. A. (1991). Replication and transcription of vertebrate mitochondrial DNA. Annu Rev Cell Biol *7*, 453-478.

Cooper, A. J. L., Sheu, K. F. R., Burke, J. R., Onodera, O., Strittmatter, W. J., Roses, A. D., and Blass, J. P. (1997). Polyglutamine domains are substrates of tissue transglutaminase: Does transglutaminase play a role in expanded CAG/poly Q neurodegenerative diseases? J Neurochem *69*, - 431-434.

Cooper, J. K., Schilling, G., Peters, M. F., Herring, W. J., Sharp, A. H., Kaminsky, Z., Masone, J., Khan, F. A., Delanoy, M., Borchelt, D. R., *et al.* (1998). Truncated N-terminal fragments of huntingtin with expanded glutamine repeats form nuclear and cytoplasmic aggregates in cell culture. Hum Mol Genet *7*, 783-790.

Craufurd, D., Thompson, J. C., and Snowden, J. S. (2001). Behavioral changes in Huntington Disease. Neuropsychiatry Neuropsychol Behav Neurol *14*, 219-226.

Crossthwaite, A. J., Hasan, S., and Williams, R. J. (2002). Hydrogen peroxide-mediated phosphorylation of ERK1/2, Akt/PKB and JNK in cortical neurones: dependence on Ca(2+) and PI3-kinase. J Neurochem *80*, 24-35.

Cummings, C. J., Mancini, M. A., Antalffy, B., DeFranco, D. B., Orr, H. T., and Zoghbi, H. Y. (1998). Chaperone suppression of aggregation and altered subcellular proteasome localization imply protein misfolding in SCA1 [In Process Citation]. Nat Genet *19*, 148-154.

Cummings, C. J., Sun, Y., Opal, P., Antalffy, B., Mestril, R., Orr, H. T., Dillmann, W. H., and Zoghbi, H. Y. (2001). Over-expression of inducible HSP70 chaperone suppresses neuropathology and improves motor function in SCA1 mice. Hum Mol Genet *10*, 1511-1518.

Cummings, C. J., and Zoghbi, H. Y. (2000). Fourteen and counting: unraveling trinucleotide repeat diseases. Hum Mol Genet *9*, 909-916.

Dairaghi, D. J., Shadel, G. S., and Clayton, D. A. (1995). Addition of a 29 residue carboxyl-terminal tail converts a simple HMG box-containing protein into a transcriptional activator. J Mol Biol *249*, 11-28.

Davey, G. P., Peuchen, S., and Clark, J. B. (1998). Energy thresholds in brain mitochondria. Potential involvement in neurodegeneration. J Biol Chem *273*, 12753-12757.

Davies, S. W., Turmaine, M., Cozens, B. A., DiFiglia, M., Sharp, A. H., Ross, C. A., Scherzinger, E., Wanker, E. E., Mangiarini, L., and Bates, G. P. (1997). Formation of neuronal intranuclear inclusions underlies the neurological dysfunction in mice transgenic for the HD mutation. Cell *90*, - 537-548.

Davis, A. F., Ropp, P. A., Clayton, D. A., and Copeland, W. C. (1996). Mitochondrial DNA polymerase gamma is expressed and translated in the absence of mitochondrial DNA maintenance and replication. Nucleic Acids Res *24*, 2753-2759.

Davison, F. D., Sweeney, B. J., and Scaravilli, F. (1996). Mitochondrial DNA levels in the brain of HIV-positive patients after zidovudine therapy. J Neurol *243*, 648-651.

de la Monte, S. M., Vonsattel, J. P., and Richardson, E. P., Jr. (1988). Morphometric demonstration of atrophic changes in the cerebral cortex, white matter, and neostriatum in Huntington's disease. J Neuropathol Exp Neurol *47*, 516-525.

De Rooij, K. E., De Koning Gans, P. A., Roos, R. A., Van Ommen, G. J., and Den Dunnen, J. T. (1995). Somatic expansion of the (CAG)n repeat in Huntington disease brains. Hum Genet *95*, 270-274.

Desouza, E. B. (1995). Corticotropin Releasing Factor Receptors Physiology, Pharmacology, Biochemistry and Role In Central Nervous System and Immune Disorders. Psychoneuroendocrinology *20*, - 789-819.

DiFiglia, M., Sapp, E., Chase, K., Schwarz, C., Meloni, A., Young, C., Martin, E., Vonsattel, J. P., Carraway, R., Reeves, S. A., and et al. (1995). Huntingtin is a cytoplasmic protein associated with vesicles in human and rat brain neurons. Neuron *14*, 1075-1081.

DiFiglia, M., Sapp, E., Chase, K. O., Davies, S. W., Bates, G. P., Vonsattel, J. P., and Aronin, N. (1997). Aggregation of huntingtin in neuronal intranuclear inclusions and dystrophic neurites in brain. Science *277*, - 1990-1993.

Ding, Q., and Keller, J. N. (2001). Proteasome inhibition in oxidative stress neurotoxicity: implications for heat shock proteins. J Neurochem *77*, 1010-1017.

Doda, J. N., Wright, C. T., and Clayton, D. A. (1981). Elongation of displacement-loop strands in human and mouse mitochondrial DNA is arrested near specific template sequences. Proc Natl Acad Sci U S A *78*, 6116-6120.

Doersen, C. J., Guerrier-Takada, C., Altman, S., and Attardi, G. (1985). Characterization of an RNase P activity from HeLa cell mitochondria. Comparison with the cytosol RNase P activity. J Biol Chem *260*, 5942-5949.

Dragatsis, I., Levine, M. S., and Zeitlin, S. (2000). Inactivation of Hdh in the brain and testis results in progressive neurodegeneration and sterility in mice. Nat Genet *26*, 300-306.

Dragunow, M., Faull, R. L., Lawlor, P., Beilharz, E. J., Singleton, K., Walker, E. B., and Mee, E. (1995). In situ evidence for DNA fragmentation in Huntington's disease striatum and Alzheimer's disease temporal lobes. Neuroreport *6*, 1053-1057.

Dunah, A. W., Jeong, H., Griffin, A., Kim, Y. M., Standaert, D. G., Hersch, S. M., Mouradian, M. M., Young, A. B., Tanese, N., and Krainc, D. (2002). Sp1 and TAFII130 Transcriptional Activity Disrupted in Early Huntington's Disease. Science *2*, 2.

Dunham, N. V., and Miya, T. S. (1957). A note on a simple apparatus for detecting neurological deficits in rats and mice. J Am Pharmacol Assoc XLVI, 208-209.

Dunnett, S. B., Carter, R. J., Watts, C., Torres, E. M., Mahal, A., Mangiarini, L., Bates, G., and Morton, A. J. (1998). Striatal transplantation in a transgenic mouse model of Huntington's disease. Exp Neurol *154*, - 31-40.

Duyao, M., Ambrose, C., Myers, R., Novelletto, A., Persichetti, F., Frontali, M., Folstein, S., Ross, C., Franz, M., Abbott, M., and et, a. l. (1993). Trinucleotide repeat length instability and age of onset in Huntington's disease [see comments]. Nat Genet *4*, 387-392.

Duyao, M. P., Auerbach, A. B., Ryan, A., Persichetti, F., Barnes, G. T., McNeil, S. M., Ge, P., Vonsattel, J. P., Gusella, J. F., Joyner, A. L., and MacDonald, M. E. (1995). Inactivation of the mouse Huntington's disease gene homolog Hdh. Science *269*, - 407-410.

Dyer, R. B., and McMurray, C. T. (2001). Mutant protein in Huntington disease is resistant to proteolysis in affected brain. Nat Genet *29*, 270-278.

Dykens, J. A. (1994). Isolated cerebral and cerebellar mitochondria produce free radicals when exposed to elevated CA2+ and Na+: implications for neurodegeneration. J Neurochem *63*, 584-591.

Elliott, R. M., Southon, S., and Archer, D. B. (1999). Oxidative insult specifically decreases levels of a mitochondrial transcript. Free Radic Biol Med *26*, 646-655.

Emond, M., Lepage, G., Vanasse, M., and Pandolfo, M. (2000). Increased levels of plasma malondialdehyde in Friedreich ataxia. Neurology *55*, 1752-1753.

Esposito, L. A., Melov, S., Panov, A., Cottrell, B. A., and Wallace, D. C. (1999). Mitochondrial disease in mouse results in increased oxidative stress. Proc Natl Acad Sci U S A *96*, 4820-4825.

Faber, P. W., Alter, J. R., MacDonald, M. E., and Hart, A. C. (1999). Polyglutamine mediated dysfunction and apoptotic death of a Caenorhabditis elegans sensory neuron. Proc Natl Acad Sci U S A *96*, 179-184.

Faber, P. W., Barnes, G. T., Srinidhi, J., Chen, J., Gusella, J. F., and MacDonald, M. E. (1998). Huntingtin interacts with a family of WW domain proteins. Hum Mol Genet *7*, 1463-1474.

Feinberg, A. P., and Vogelstein, B. (1983). A technique for radiolabeling DNA restriction endonuclease fragments to high specific activity. Anal Biochem *132*, 6-13.

Fernandez-Funez, P., Nino-Rosales, M. L., de Gouyon, B., She, W. C., Luchak, J. M., Martinez, P., Turiegano, E., Benito, J., Capovilla, M., Skinner, P. J., *et al.* (2000). Identification of genes that modify ataxin-1-induced neurodegeneration. Nature *408*, 101-106.

Ferrante, R. J., Andreassen, O. A., Jenkins, B. G., Dedeoglu, A., Kuemmerle, S., Kubilus, J. K., Kaddurah-Daouk, R., Hersch, S. M., and Beal, M. F. (2000). Neuroprotective effects of creatine in a transgenic mouse model of Huntington's disease. J Neurosci *20*, 4389-4397.

Ferrante, R. J., Gutekunst, C. A., Persichetti, F., McNeil, S. M., Kowall, N. W., Gusella, J. F., MacDonald, M. E., Beal, M. F., and Hersch, S. M. (1997). Heterogeneous topographic and cellular distribution of Huntington expression in the normal human neostriatum. J Neurosci *17*, 3052-3063.

Ferrante, R. J., Kowall, N. W., Cipolloni, P. B., Storey, E., and Beal, M. F. (1993). Excitotoxin lesions in primates as a model for Huntington's disease: histopathologic and neurochemical characterization. Exp Neurol *119*, 46-71.

Ferrer, I., Goutan, E., Marin, C., Rey, M. J., and Ribalta, T. (2000). Brain-derived neurotrophic factor in Huntington disease. Brain Res *866*, 257-261.

Figueredo-Cardenas, G., Anderson, K. D., Chen, Q., Veenman, C. L., and Reiner, A. (1994). Relative survival of striatal projection neurons and interneurons after intrastriatal injection of quinolinic acid in rats. Exp Neurol *129*, 37-56.

Fisher, R. P., Lisowsky, T., Parisi, M. A., and Clayton, D. A. (1992). DNA wrapping and bending by a mitochondrial high mobility group-like transcriptional activator protein. J Biol Chem *267*, 3358-3367.

Foran, D. R., Hixson, J. E., and Brown, W. M. (1988). Comparisons of ape and human sequences that regulate mitochondrial DNA transcription and D-loop DNA synthesis. Nucleic Acids Res *16*, 5841-5861.

Freeland, K., Boxer, L. M., and Latchman, D. S. (2001). The cyclic AMP response element in the Bcl-2 promoter confers inducibility by hypoxia in neuronal cells. Brain Res Mol Brain Res *92*, 98-106.

Furtado, S., Suchowersky, O., Rewcasle, N. B., Graham, L., Klimek, M. L., and Garber, A. (1996). Relationship Between Trinucleotide Repeats and Neuropathological Changes In Huntingtons Disease. Ann Neurol *39*, - 132-136.

Garseth, M., Sonnewald, U., White, L. R., Rod, M., Zwart, J. A., Nygaard, O., and Aasly, J. (2000). Proton magnetic resonance spectroscopy of cerebrospinal fluid in neurodegenerative disease: indication of glial energy impairment in Huntington chorea, but not Parkinson disease. J Neurosci Res *60*, 779-782.

Gervais, F. G., Singaraja, R., Xanthoudakis, S., Gutekunst, C. A., Leavitt, B. R., Metzler, M., Hackam, A. S., Tam, J., Vaillancourt, J. P., Houtzager, V., *et al.* (2002). Recruitment and activation of caspase-8 by the Huntingtin-interacting protein Hip-1 and a novel partner Hippi. Nat Cell Biol *4*, 95-105.

Giovannone, B., Sabbadini, G., Di Maio, L., Calabrese, O., Castaldo, I., Frontali, M., Novelleto, A., and Squitieri, F. (1997). Analysis of (CAG)n size heterogeneity in somatic and sperm cell DNA from intermediate and expanded Huntington disease gene carriers. Hum Mutat *10*, 458-464.

Goldberg, Y. P., Nicholson, D. W., Rasper, D. M., Kalchman, M. A., Koide, H. B., Graham, R. K., Bromm, M., Kazemi-Esfarjani, P., Thornberry, N. A., Vaillancourt, J. P., and Hayden, M. R. (1996). Cleavage of huntingtin by apopain, a proapoptotic cysteine protease, is modulated by the polyglutamine tract [see comments]. Nat Genet *13*, 442-449.

Goto, I., Taniwaki, T., Hosokawa, S., Otsuka, M., Ichiya, Y., and Ichimiya, A. (1993). Positron emission tomographic (PET) studies in dementia. J Neurol Sci *114*, 1-6.

Gourfinkel-An, I., Vila, M., Faucheux, B., Duyckaerts, C., Viallet, F., Hauw, J. J., Brice, A., Agid, Y., and Hirsch, E. C. (2002). Metabolic changes in the basal ganglia of patients with Huntington's disease: an in situ hybridization study of cytochrome oxidase subunit I mRNA. J Neurochem *80*, 466-476.

Gray, H., and Wong, T. W. (1992). Purification and identification of subunit structure of the human mitochondrial DNA polymerase. J Biol Chem *267*, 5835-5841.

Gu, M., Gash, M. T., Mann, V. M., Javoyagid, F., Cooper, J. M., and Schapira, A. H. V. (1996). Mitochondrial Defect In Huntingtons Disease On Caudate Nucleus. Annals Of Neurology *39*, - 385-389.

Guidetti, P., Charles, V., Chen, E. Y., Reddy, P. H., Kordower, J. H., Whetsell, W. O., Jr., Schwarcz, R., and Tagle, D. A. (2001). Early degenerative changes in transgenic mice expressing mutant huntingtin involve dendritic abnormalities but no impairment of mitochondrial energy production. Exp Neurol *169*, 340-350.

Gutekunst, C. A., Levey, A. I., Heilman, C. J., Whaley, W. L., Yi, H., Nash, N. R., Rees, H. D., Madden, J. J., and Hersch, S. M. (1995). Identification and localization of huntingtin in brain and human lymphoblastoid cell lines with anti-fusion protein antibodies. Proc Natl Acad Sci U S A *92*, 8710-8714.

Gutekunst, C. A., Li, S. H., Yi, H., Mulroy, J. S., Kuemmerle, S., Jones, R., Rye, D., Ferrante, R. J., Hersch, S. M., and Li, X. J. (1999). Nuclear and neuropil aggregates in Huntington's disease: relationship to neuropathology. J Neurosci *19*, 2522-2534.

Guyot, M. C., Hantraye, P., Dolan, R., Palfi, S., Maziere, M., and Brouillet, E. (1997). Quantifiable bradykinesia, gait abnormalities and Huntington's disease like striatal lesions in rats chronically treated with 3 nitropropionic acid. Neuroscience *79*, - 45-56.

Hackam, A. S., Yassa, A. S., Singaraja, R., Metzler, M., Gutekunst, C. A., Gan, L., Warby, S., Wellington, C. L., Vaillancourt, J., Chen, N., *et al.* (2000). Huntingtin interacting protein 1 induces apoptosis via a novel caspase- dependent death effector domain. J Biol Chem *275*, 41299-41308.

Hansson, O., Castilho, R. F., Korhonen, L., Lindholm, D., Bates, G. P., and Brundin, P. (2001). Partial resistance to malonate-induced striatal cell death in transgenic mouse models of Huntington's disease is dependent on age and CAG repeat length. J Neurochem *78*, 694-703.

Hansson, O., Peters n, A., Leist, M., Nicotera, P., Castilho, R. F., and Brundin, P. (1999). Transgenic mice expressing a Huntington's disease mutation are resistant to quinolinic acid-induced striatal excitotoxicity. Proc Natl Acad Sci U S A *96*, 8727-8732.

Hantraye, P., Riche, D., Maziere, M., and Isacson, O. (1990). A primate model of Huntington's disease: behavioral and anatomical studies of unilateral excitotoxic lesions of the caudate-putamen in the baboon. Exp Neurol *108*, 91-104.

Harper, P. (1996). Huntington's Disease, W.B. Saunders Company Ltd.).
Hayakawa, M., Torii, K., Sugiyama, S., Tanaka, M., and Ozawa, T. (1991). Age-associated accumulation of 8-hydroxydeoxyguanosine in mitochondrial DNA of human diaphragm. Biochem Biophys Res Commun *179*, 1023-1029.

Hayden, M. R., Martin, W. R., Stoessl, A. J., Clark, C., Hollenberg, S., Adam, M. J., Ammann, W., Harrop, R., Rogers, J., Ruth, T., and et al. (1986). Positron emission tomography in the early diagnosis of Huntington's disease. Neurology *36*, 888-894.

HDCRG (2001). A randomized, placebo-controlled trial of coenzyme Q10 and remacemide in Huntington's disease. Neurology *57*, 397-404.

(HDCRG), T. H. s. D. C. R. G. (1993). A novel gene containing a trinucleotide repeat that is expanded and unstable on Huntington's disease chromosomes. The Huntington's Disease Collaborative Research Group [see comments]. Cell *72*, 971-983.

Heddi, A., Stepien, G., Benke, P. J., and Wallace, D. C. (1999). Coordinate induction of energy gene expression in tissues of mitochondrial disease patients. J Biol Chem *274*, 22968-22976.

Hedreen, J.C., and Folsten S.E. (1995). Early losss of neostriatal striosome neurons in Huntington's disease. J Neuropathol Exp neurol *54,* 105-120

Hehman, G. L., and Hauswirth, W. W. (1992). DNA helicase from mammalian mitochondria. Proc Natl Acad Sci U S A *89*, 8562-8566.

Hirai, K., Aliev, G., Nunomura, A., Fujioka, H., Russell, R. L., Atwood, C. S., Johnson, A. B., Kress, Y., Vinters, H. V., Tabaton, M., *et al.* (2001). Mitochondrial abnormalities in Alzheimer's disease. J Neurosci *21*, 3017-3023.

Hirakura, Y., Azimov, R., Azimova, R., and Kagan, B. L. (2000). Polyglutamine-induced ion channels: a possible mechanism for the neurotoxicity of Huntington and other CAG repeat diseases. J Neurosci Res *60*, 490-494.

Ho, L. W., Brown, R., Maxwell, M., Wyttenbach, A., and Rubinsztein, D. C. (2001). Wild type Huntingtin reduces the cellular toxicity of mutant Huntingtin in mammalian cell models of Huntington's disease. J Med Genet *38*, 450-452.

Hodgson, J. G., Agopyan, N., Gutekunst, C. A., Leavitt, B. R., LePiane, F., Singaraja, R., Smith, D. J., Bissada, N., McCutcheon, K., Nasir, J., *et al.* (1999). A YAC mouse model for

Huntington's disease with full-length mutant huntingtin, cytoplasmic toxicity, and selective striatal neurodegeneration. Neuron *23*, 181-192.

Hodgson, J. G., Smith, D. J., McCutcheon, K., Koide, H. B., Nishiyama, K., Dinulos, M. B., Stevens, M. E., Bissada, N., Nasir, J., Kanazawa, I., *et al.* (1996). Human Huntingtin Derived From Yac Transgenes Compensates For Loss Of Murine Huntingtin By Rescue Of the Embryonic Lethal Phenotype. Hum Mol Genet *5*, 1875-1885.

Holmes, S. E., O'Hearn, E., Rosenblatt, A., Callahan, C., Hwang, H. S., Ingersoll-Ashworth, R. G., Fleisher, A., Stevanin, G., Brice, A., Potter, N. T., *et al.* (2001). A repeat expansion in the gene encoding junctophilin-3 is associated with Huntington disease-like 2. Nat Genet *29*, 377-378.

Hood, D. A., Zak, R., and Pette, D. (1989). Chronic stimulation of rat skeletal muscle induces coordinate increases in mitochondrial and nuclear mRNAs of cytochrome-c-oxidase subunits. Eur J Biochem *179*, 275-280.

Horton, T. M., Graham, B. H., CorralDebrinski, M., Shoffner, J. M., Kaufman, A. E., Beal, M. F., and Wallace, D. C. (1995). Marked increase in mitochondrial DNA deletion levels in the cerebral cortex of Huntington's disease patients. Neurology *45*, - 1879-1883.

Huang, Q., Zhou, D., Sapp, E., Aizawa, H., Ge, P., Bird, E. D., Vonsattel, J. P., and DiFiglia, M. (1995). Quinolinic acid-induced increases in calbindin D28k immunoreactivity in rat striatal neurons in vivo and in vitro mimic the pattern seen in Huntington's disease. Neuroscience *65*, 397-407.

Hughes, R. E., Lo, R. S., Davis, C., Strand, A. D., Neal, C. L., Olson, J. M., and Fields, S. (2001). Altered transcription in yeast expressing expanded polyglutamine. Proc Natl Acad Sci U S A *98*, 13201-13206.

Ide, K., Nukina, N., Masuda, N., Goto, J., and Kanazawa, I. (1995). Abnormal gene product identified in Huntington's disease lymphocytes and brain. Biochem Biophys Res Commun *209*, 1119-1125.

Illarioshkin, S. N., Igarashi, S., Onodera, O., Markova, E. D., Nikolskaya, N. N., Tanaka, H., Chabrashwili, T. Z., Insarova, N. G., Endo, K., Ivanova-Smolenskaya, I. A., and et al. (1994). Trinucleotide repeat length and rate of progression of Huntington's disease. Ann Neurol *36*, 630-635.

Ishiguro, H., Yamada, K., Sawada, H., Nishii, K., Ichino, N., Sawada, M., Kurosawa, Y., Matsushita, N., Kobayashi, K., Goto, J., *et al.* (2001). Age-dependent and tissue-specific CAG repeat instability occurs in mouse knock-in for a mutant Huntington's disease gene. J Neurosci Res *65*, 289-297.

Itakura, K., Rossi, J. J., and Wallace, R. B. (1984). Synthesis and use of synthetic oligonucleotides. Annu Rev Biochem *53*, 323-356.

Iwaki, T., Wisniewski, T., Iwaki, A., Corbin, E., Tomokane, N., Tateishi, J., and Goldman, J. E. (1992). Accumulation of alpha B-crystallin in central nervous system glia and neurons in pathologic conditions. Am J Pathol *140*, 345-356.

Jackson, G. R., Salecker, I., Dong, X., Yao, X., Arnheim, N., Faber, P. W., MacDonald, M. E., and Zipursky, S. L. (1998). Polyglutamine-expanded human huntingtin transgenes induce degeneration of Drosophila photoreceptor neurons. Neuron *21*, 633-642.

Jana, N. R., Tanaka, M., Wang, G., and Nukina, N. (2000). Polyglutamine length-dependent interaction of Hsp40 and Hsp70 family chaperones with truncated N-terminal huntingtin: their role in suppression of aggregation and cellular toxicity. Hum Mol Genet *9*, 2009-2018.

Jenkins, B. G., Koroshetz, W. J., Beal, M. F., and Rosen, B. R. (1993). Evidence for impairment of energy metabolism in vivo in Huntington's disease using localized 1H NMR spectroscopy. Neurology *43*, 2689-2695.

Jou, Y. S., and Myers, R. M. (1995). Evidence from antibody studies that the CAG repeat in the Huntington disease gene is expressed in the protein. Hum Mol Genet *4*, 465-469.

Kagan, B. L., Hirakura, Y., Azimov, R., and Azimova, R. (2001). The channel hypothesis of Huntington's disease. Brain Res Bull *56*, 281-284.

Kahlem, P., Green, H., and Djian, P. (1998). Transglutaminase as the agent of neurodegenerative diseases due to polyglutamine expansion. Pathol Biol (Paris) *46*, 681-682.

Kahlem, P., Terre, C., Green, H., and Djian, P. (1996). Peptides containing glutamine repeats as substrates for transglutaminase-catalyzed cross-linking: relevance to diseases of the nervous system [see comments]. Proc Natl Acad Sci U S A *93*, 14580-14585.

Kalchman, M. A., Graham, R. K., Xia, G., Koide, H. B., Hodgson, J. G., Graham, K. C., Goldberg, Y. P., Gietz, R. D., Pickart, C. M., and Hayden, M. R. (1996). Huntingtin is ubiquitinated and interacts with a specific ubiquitin conjugating enzyme. Journal of Biological Chemistry *271*, - 19385-19394.

Kalchman, M. A., Koide, H. B., McCutcheon, K., Graham, R. K., Nichol, K., Nishiyama, K., KazemiEsfarjani, P., Lynn, F. C., Wellington, C., Metzler, M., *et al.* (1997). HIP1, a human homologue of S cerevisiae Sla2p, interacts with membrane associated huntingtin in the brain. Nature Genetics *16*, - 44-53.

Kambouris, M., Bohlega, S., Al-Tahan, A., and Meyer, B. F. (2000). Localization of the gene for a novel autosomal recessive neurodegenerative Huntington-like disorder to 4p15.3. Am J Hum Genet *66*, 445-452.

Karpuj, M. V., Garren, H., Slunt, H., Price, D. L., Gusella, J., Becher, M. W., and Steinman, L. (1999). Transglutaminase aggregates huntingtin into nonamyloidogenic polymers, and its enzymatic activity increases in Huntington's disease brain nuclei [In Process Citation]. Proc Natl Acad Sci U S A *96*, 7388-7393.

Kazantsev, A., Preisinger, E., Dranovsky, A., Goldgaber, D., and Housman, D. (1999). Insoluble detergent-resistant aggregates form between pathological and nonpathological lengths of polyglutamine in mammalian cells. Proc Natl Acad Sci U S A *96*, 11404-11409.

Kazantsev, A., Walker, H. A., Slepko, N., Bear, J. E., Preisinger, E., Steffan, J. S., Zhu, Y. Z., Gertler, F. B., Housman, D. E., Marsh, J. L., and Thompson, L. M. (2002). A bivalent Huntingtin binding peptide suppresses polyglutamine aggregation and pathogenesis in Drosophila. Nat Genet *30*, 367-376 .

Kazemi-Esfarjani, P., and Benzer, S. (2000). Genetic suppression of polyglutamine toxicity in Drosophila. Science *287*, 1837-1840.

Kegel, K. B., Kim, M., Sapp, E., McIntyre, C., Castano, J. G., Aronin, N., and DiFiglia, M. (2000). Huntingtin expression stimulates endosomal-lysosomal activity, endosome tubulation, and autophagy. J Neurosci *20*, 7268-7278.

Kennedy, L., and Shelbourne, P. F. (2000). Dramatic mutation instability in HD mouse striatum: does polyglutamine load contribute to cell-specific vulnerability in Huntington's disease? Hum Mol Genet *9*, 2539-2544.

Kieburtz, K., MacDonald, M., Shih, C., Feigin, A., Steinberg, K., Bordwell, K., Zimmerman, C., Srinidhi, J., Sotack, J., Gusella, J., and et al. (1994). Trinucleotide repeat length and progression of illness in Huntington's disease. J Med Genet *31*, 872-874.

Kim, M., Lee, H. S., LaForet, G., McIntyre, C., Martin, E. J., Chang, P., Kim, T. W., Williams, M., Reddy, P. H., Tagle, D., *et al.* (1999a). Mutant huntingtin expression in clonal striatal cells: dissociation of inclusion formation and neuronal survival by caspase inhibition. J Neurosci *19*, 964-973.

Kim, Y. J., Yi, Y., Sapp, E., Wang, Y., Cuiffo, B., Kegel, K. B., Qin, Z. H., Aronin, N., and DiFiglia, M. (2001). Caspase 3-cleaved N-terminal fragments of wild-type and mutant huntingtin are present in normal and Huntington's disease brains, associate with membranes, and undergo calpain-dependent proteolysis. Proc Natl Acad Sci U S A *98*, 12784-12789.

King, T. C., and Low, R. L. (1987). Mitochondrial DNA displacement loop structure depends on growth state in bovine cells. J Biol Chem *262*, 6214-6220.

Kish, S. J., LopesCendes, I., Guttman, M., Furukawa, Y., Pandolfo, M., Rouleau, G. A., Ross, B. M., Nance, M., Schut, L., Ang, L., and DiStefano, L. (1998). Brain glyceraldehyde 3 phosphate dehydrogenase activity in human trinucleotide repeat disorders. Arch Neurol *55*, 1299-1304.

Klement, I. A., Skinner, P. J., Kaytor, M. D., Yi, H., Hersch, S. M., Clark, H. B., Zoghbi, H. Y., and Orr, H. T. (1998). Ataxin 1 nuclear localization and aggregation: Role in polyglutamine induced disease in SCA1 transgenic mice. Cell *95*, - 41-53.

Klingenspor, M., Ivemeyer, M., Wiesinger, H., Haas, K., Heldmaier, G., and Wiesner, R. J. (1996). Biogenesis of thermogenic mitochondria in brown adipose tissue of Djungarian hamsters during cold adaptation. Biochem J *316*, 607-613.

Kovtun, I. V., and McMurray, C. T. (2001). Trinucleotide expansion in haploid germ cells by gap repair. Nat Genet *27*, 407-411.

Kremer, B., Goldberg, P., Andrew, S., Theilman, J., Telenius, H., Zeisler, J., Squitieri, F., Lin, B., Bassett, A., Almqvist, E., *et al.* (1994). A Worldwide Study of the Huntington's Disease Mutation. N Engl J Med *330*, 1401-1406.

Krobitsch, S., and Lindquist, S. (2000). Aggregation of huntingtin in yeast varies with the length of the polyglutamine expansion and the expression of chaperone proteins. Proc Natl Acad Sci U S A *97*, 1589-1594.

Kruse, B., Narasimhan, N., and Attardi, G. (1989). Termination of transcription in human mitochondria: identification and purification of a DNA binding protein factor that promotes termination. Cell *58*, 391-397.

Kuemmerle, S., Gutekunst, C. A., Klein, A. M., Li, X. J., Li, S. H., Beal, M. F., Hersch, S. M., and Ferrante, R. J. (1999). Huntington aggregates may not predict neuronal death in Huntington's disease. Ann Neurol *46*, 842-849.

Laforet, G. A., Sapp, E., Chase, K., McIntyre, C., Boyce, F. M., Campbell, M., Cadigan, B. A., Warzecki, L., Tagle, D. A., Reddy, P. H., *et al.* (2001). Changes in cortical and striatal neurons predict behavioral and electrophysiological abnormalities in a transgenic murine model of Huntington's disease. J Neurosci *21*, 9112-9123.

Lalonde, R. (1987a). Motor abnormalities in weaver mutant mice. Exp Brain Res *65*, 479-481.

Lalonde, R. (1987b). Motor abnormalities in staggerer mutant mice. Exp Brain Res *68*, 417-420.

Landwehrmeyer, G. B., McNeil, S. M., Dure, L. S. t., Ge, P., Aizawa, H., Huang, Q., Ambrose, C. M., Duyao, M. P., Bird, E. D., Bonilla, E., and et al. (1995). Huntington's disease gene: regional and cellular expression in brain of normal and affected individuals. Ann Neurol *37*, 218-230.

Lange, K. W., Sahakian, B. J., Quinn, N. P., Marsden, C. D., and Robbins, T. W. (1995). Comparison of executive and visuospatial memory function in Huntington's disease and dementia of Alzheimer type matched for degree of dementia. J Neurol Neurosurg Psychiatry *58*, 598-606.

Larsson, N. G., Oldfors, A., Holme, E., and Clayton, D. A. (1994). Low levels of mitochondrial transcription factor A in mitochondrial DNA depletion. Biochem Biophys Res Commun *200*, 1374-1381.

Larsson, N. G., Wang, J., Wilhelmsson, H., Oldfors, A., Rustin, P., Lewandoski, M., Barsh, G. S., and Clayton, D. A. (1998). Mitochondrial transcription factor A is necessary for mtDNA maintenance and embryogenesis in mice [see comments]. Nat Genet *18*, 231-236.

Lawrence, A. D., Hodges, J. R., Rosser, A. E., Kershaw, A., ffrench-Constant, C., Rubinsztein, D. C., Robbins, T. W., and Sahakian, B. J. (1998). Evidence for specific cognitive deficits in preclinical Huntington's disease. Brain *121*, 1329-1341.

Lawrence, A. D., Sahakian, B. J., Hodges, J. R., Rosser, A. E., Lange, K. W., and Robbins, T. W. (1996). Executive and mnemonic functions in early Huntington's disease. Brain *119*, 1633-1645.

Lawrence, A. D., Watkins, L. H., Sahakian, B. J., Hodges, J. R., and Robbins, T. W. (2000). Visual object and visuospatial cognition in Huntington's disease: implications for information processing in corticostriatal circuits. Brain *123*, 1349-1364.

Leary, S. C., Battersby, B. J., Hansford, R. G., and Moyes, C. D. (1998). Interactions between bioenergetics and mitochondrial biogenesis. Biochim Biophys Acta *1365*, 522-530.

Leavitt, B. R., Guttman, J. A., Hodgson, J. G., Kimel, G. H., Singaraja, R., Vogl, A. W., and Hayden, M. R. (2001). Wild-type huntingtin reduces the cellular toxicity of mutant huntingtin in vivo. Am J Hum Genet *68*, 313-324.

Ledoux, S. P., Shen, C. C., Grishko, V. I., Fields, P. A., Gard, A. L., and Wilson, G. L. (1998). Glial cell-specific differences in response to alkylation damage. Glia *24*, 304-312.

Lee, D. Y., and Clayton, D. A. (1997). RNase mitochondrial RNA processing correctly cleaves a novel R loop at the mitochondrial DNA leading-strand origin of replication. Genes Dev *11*, 582-592.

Lee, H. C., Lu, C. Y., Fahn, H. J., and Wei, Y. H. (1998). Aging- and smoking-associated alteration in the relative content of mitochondrial DNA in human lung. FEBS Lett *441*, 292-296.

Lee, M. H., Hyun, D. H., Jenner, P., and Halliwell, B. (2001). Effect of proteasome inhibition on cellular oxidative damage, antioxidant defences and nitric oxide production. J Neurochem *78*, 32-41.

Leeflang, E. P., Zhang, L., Tavare, S., Hubert, R., Srinidhi, J., MacDonald, M. E., Myers, R. H., De Young, M., Wexler, N. S., Gusella, J. F., and Arnheim, N. (1995). Single sperm analysis of the trinucleotide repeats in the Huntington's disease gene: Quantification of the mutation frequency spectrum. Hum Mol Genet *4*, 1519-1526.

Lesort, M., Chun, W., Johnson, G. V., and Ferrante, R. J. (1999). Tissue transglutaminase is increased in Huntington's disease brain. J Neurochem *73*, 2018-2027.

Leung, A. C., and McKee, E. E. (1990). Mitochondrial protein synthesis during thyroxine-induced cardiac hypertrophy. Am J Physiol *258*, E511-518.

Levine, M. S., Klapstein, G. J., Koppel, A., Gruen, E., Cepeda, C., Vargas, M. E., Jokel, E. S., Carpenter, E. M., Zanjani, H., Hurst, R. S., *et al.* (1999). Enhanced sensitivity to N-methyl-D-aspartate receptor activation in transgenic and knockin mouse models of Huntington's disease. J Neurosci Res *58*, 515-532.

Lewis, W., Copeland, W. C., and Day, B. J. (2001). Mitochondrial dna depletion, oxidative stress, and mutation: mechanisms of dysfunction from nucleoside reverse transcriptase inhibitors. Lab Invest *81*, 777-790.

Li, H., Li, S. H., Cheng, A. L., Mangiarini, L., Bates, G. P., and Li, X. J. (1999b). Ultrastructural localization and progressive formation of neuropil aggregates in Huntington's disease transgenic mice. Hum Mol Genet *8*, 1227-1236.

Li, H., Li, S. H., Johnston, H., Shelbourne, P. F., and Li, X. J. (2000a). Amino-terminal fragments of mutant huntingtin show selective accumulation in striatal neurons and synaptic toxicity. Nat Genet *25*, 385-389.

Li, S. H., Cheng, A. L., Li, H., and Li, X. J. (1999c). Cellular defects and altered gene expression in PC12 cells stably expressing mutant huntingtin. J Neurosci *19*, 5159-5172.

Li, S. H., Cheng, A. L., Zhou, H., Lam, S., Rao, M., Li, H., and Li, X. J. (2002). Interaction of Huntington disease protein with transcriptional activator Sp1. Mol Cell Biol *22*, 1277-1287.

Li, S. H., Lam, S., Cheng, A. L., and Li, X. J. (2000b). Intranuclear huntingtin increases the expression of caspase-1 and induces apoptosis. Hum Mol Genet *9*, 2859-2867.

Li, S. H., and Li, X. J. (1998). Aggregation of N-terminal huntingtin is dependent on the length of its glutamine repeats. Hum Mol Genet *7*, 777-782.

Li, X. J., Li, S. H., Sharp, A. H., Nucifora, F. C., Schilling, G., Lanahan, A., Worley, P., Snyder, S. H., and Ross, C. A. (1995). A Huntingtin Associated Protein Enriched In Brain With Implications For Pathology. Nature *378*, - 398-402.

Li, X. J., Sharp, A. H., Li, S. H., Dawson, T. M., Snyder, S. H., and Ross, C. A. (1996). Huntingtin-associated protein (HAP1): discrete neuronal localizations in the brain resemble those of neuronal nitric oxide synthase. Proc Natl Acad Sci U S A *93*, 4839-4844.

Li, Z., Karlovich, C. A., Fish, M. P., Scott, M. P., and Myers, R. M. (1999a). A putative Drosophila homolog of the Huntington's disease gene. Hum Mol Genet *8*, 1807-1815.

Lievens, J. C., Woodman, B., Mahal, A., Spasic-Boscovic, O., Samuel, D., Kerkerian-Le Goff, L., and Bates, G. P. (2001). Impaired glutamate uptake in the R6 Huntington's disease transgenic mice. Neurobiol Dis *8*, 807-821.

Lin, B., Rommens, J. M., Graham, R. K., Kalchman, M., MacDonald, H., Nasir, J., Delaney, A., Goldberg, Y. P., and Hayden, M. R. (1993). Differential 3' polyadenylation of

the Huntington disease gene results in two mRNA species with variable tissue expression. Hum Mol Genet 2, 1541-1545.

Lin, C. H., Tallaksen-Greene, S., Chien, W. M., Cearley, J. A., Jackson, W. S., Crouse, A. B., Ren, S., Li, X. J., Albin, R. L., and Detloff, P. J. (2001). Neurological abnormalities in a knock-in mouse model of Huntington's disease. Hum Mol Genet *10*, 137-144.

Lin, X., Antalffy, B., Kang, D., Orr, H. T., and Zoghbi, H. Y. (2000). Polyglutamine expansion down-regulates specific neuronal genes before pathologic changes in SCA1. Nat Neurosci *3*, 157-163.

Lione, L. A., Carter, R. J., Hunt, M. J., Bates, G. P., Morton, A. J., and Dunnett, S. B. (1999). Selective discrimination learning impairments in mice expressing the human Huntington's disease mutation. J Neurosci *19*, 10428-10437.

Liu, V. W., Zhang, C., and Nagley, P. (1998). Mutations in mitochondrial DNA accumulate differentially in three different human tissues during ageing. Nucleic Acids Res *26*, 1268-1275.

Ludolph, A. C., Seelig, M., Ludolph, A. G., Sabri, M. I., and Spencer, P. S. (1992). ATP deficits and neuronal degeneration induced by 3-nitropropionic acid. Ann N Y Acad Sci *648*, 300-302.

Luesse, H. G., Schiefer, J., Spruenken, A., Puls, C., Block, F., and Kosinski, C. M. (2001). Evaluation of R6/2 HD transgenic mice for therapeutic studies in Huntington's disease: behavioral testing and impact of diabetes mellitus. Behav Brain Res *126*, 185-195.

Luthi-Carter, R., Strand, A., Peters, N. L., Solano, S. M., Hollingsworth, Z. R., Menon, A. S., Frey, A. S., Spektor, B. S., Penney, E. B., Schilling, G., *et al.* (2000). Decreased expression of striatal signaling genes in a mouse model of Huntington's disease. Hum Mol Genet *9*, 1259-1271.

Maat-Schieman, M. L., Dorsman, J. C., Smoor, M. A., Siesling, S., Van Duinen, S. G., Verschuuren, J. J., den Dunnen, J. T., Van Ommen, G. J., and Roos, R. A. (1999). Distribution of inclusions in neuronal nuclei and dystrophic neurites in Huntington disease brain. J Neuropathol Exp Neurol *58*, 129-137.

MacDonald, M. E., Barnes, G., Srinidhi, J., Duyao, M. P., Ambrose, C. M., Myers, R. H., Gray, J., Conneally, P. M., Young, A., Penney, J., and et al. (1993). Gametic but not somatic instability of CAG repeat length in Huntington's disease. J Med Genet *30*, 982-986.

Mandel, H., Szargel, R., Labay, V., Elpeleg, O., Saada, A., Shalata, A., Anbinder, Y., Berkowitz, D., Hartman, C., Barak, M., *et al.* (2001). The deoxyguanosine kinase gene is mutated in individuals with depleted hepatocerebral mitochondrial DNA. Nat Genet *29*, 337-341.

Mangiarini, L., Sathasivam, K., Mahal, A., Mott, R., Seller, M., and Bates, G. P. (1997). Instability of highly expanded CAG repeats in mice transgenic for the Huntington's disease mutation. Nat Genet *15*, 197-200.

Mangiarini, L., Sathasivam, K., Seller, M., Cozens, B., Harper, A., Hetherington, C., Lawton, M., Trottier, Y., Lehrach, H., Davies, S. W., and Bates, G. P. (1996). Exon 1 Of the Hd Gene With an Expanded Cag Repeat Is Sufficient to Cause a Progressive Neurological Phenotype In Transgenic Mice. Cell *87*, 493-506.

Manley, K., Shirley, T. L., Flaherty, L., and Messer, A. (1999). Msh2 deficiency prevents in vivo somatic instability of the CAG repeat in Huntington disease transgenic mice. Nat Genet *23*, 471-473.

Mansouri, A., Demeilliers, C., Amsellem, S., Pessayre, D., and Fromenty, B. (2001). Acute ethanol administration oxidatively damages and depletes mitochondrial dna in mouse liver, brain, heart, and skeletal muscles: protective effects of antioxidants. J Pharmacol Exp Ther *298*, 737-743.

Mansouri, A., Gaou, I., De Kerguenec, C., Amsellem, S., Haouzi, D., Berson, A., Moreau, A., Feldmann, G., Letteron, P., Pessayre, D., and Fromenty, B. (1999). An alcoholic binge causes massive degradation of hepatic mitochondrial DNA in mice [see comments]. Gastroenterology *117*, 181-190.

Margolis, R. L., O'Hearn, E., Rosenblatt, A., Willour, V., Holmes, S. E., Franz, M. L., Callahan, C., Hwang, H. S., Troncoso, J. C., and Ross, C. A. (2001). A disorder similar to Huntington's disease is associated with a novel CAG repeat expansion. Ann Neurol *50*, 373-380.

Markesbery, W. R. (1997). Oxidative stress hypothesis in Alzheimer's disease. Free Radic Biol Med *23*, 134-147.

Martindale, D., Hackam, A., Wieczorek, A., Ellerby, L., Wellington, C., McCutcheon, K., Singaraja, R., KazemiEsfarjani, P., Devon, R., Kim, S. U., *et al.* (1998). Length of huntingtin and its polyglutamine tract influences localization and frequency of intracellular aggregates. Nat Genet *18*, 150-154.

Mazzola, J. L., and Sirover, M. A. (2001). Reduction of glyceraldehyde-3-phosphate dehydrogenase activity in Alzheimer's disease and in Huntington's disease fibroblasts. J Neurochem *76*, 442-449.

McCampbell, A., and Fischbeck, K. H. (2001a). Polyglutamine and CBP: fatal attraction? Nat Med *7*, 528-530.

McCampbell, A., Taye, A. A., Whitty, L., Penney, E., Steffan, J. S., and Fischbeck, K. H. (2001b). Histone deacetylase inhibitors reduce polyglutamine toxicity. Proc Natl Acad Sci U S A *98*, 15179-15184.

McDowell, D. G., Burns, N. A., and Parkes, H. C. (1998). Localised sequence regions possessing high melting temperatures prevent the amplification of a DNA mimic in competitive PCR. Nucleic Acids Res *26*, 3340-3347.

McNeil, S. M., Novelletto, A., Srinidhi, J., Barnes, G., Kornbluth, I., Altherr, M. R., Wasmuth, J. J., Gusella, J. F., MacDonald, M. E., and Myers, R. H. (1997). Reduced penetrance of the Huntington's disease mutation. Hum Mol Genet *6*, 775-779.

Menalled, L., Zanjani, H., MacKenzie, L., Koppel, A., Carpenter, E., Zeitlin, S., and Chesselet, M. F. (2000). Decrease in striatal enkephalin mRNA in mouse models of Huntington's disease. Exp Neurol *162*, 328-342.

Mende-Mueller, L. M., Toneff, T., Hwang, S. R., Chesselet, M. F., and Hook, V. Y. (2001). Tissue-specific proteolysis of Huntingtin (htt) in human brain: evidence of enhanced levels of N- and C-terminal htt fragments in Huntington's disease striatum. J Neurosci *21*, 1830-1837.

Metzler, M., Legendre-Guillemin, V., Gan, L., Chopra, V., Kwok, A., McPherson, P. S., and Hayden, M. R. (2001). HIP1 functions in clathrin-mediated endocytosis through binding to clathrin and adaptor protein 2. J Biol Chem *276*, 39271-39276.

Michikawa, Y., Mazzucchelli, F., Bresolin, N., Scarlato, G., and Attardi, G. (1999). Aging-dependent large accumulation of point mutations in the human mtDNA control region for replication. Science *286*, 774-779.

Miranda, S., Foncea, R., Guerrero, J., and Leighton, F. (1999). Oxidative stress and upregulation of mitochondrial biogenesis genes in mitochondrial DNA-depleted HeLa cells. Biochem Biophys Res Commun *258*, 44-49.

Monoi, H., Futaki, S., Kugimiya, S., Minakata, H., and Yoshihara, K. (2000). Poly-L-glutamine forms cation channels: relevance to the pathogenesis of the polyglutamine diseases. Biophys J *78*, 2892-2899.

Moraes, C. T., Kenyon, L., and Hao, H. (1999). Mechanisms of human mitochondrial DNA maintenance: the determining role of primary sequence and length over function. Mol Biol Cell *10*, 3345-3356.

Morales, L. M., Estevez, J., Suarez, H., Villalobos, R., Chacin de Bonilla, L., and Bonilla, E. (1989). Nutritional evaluation of Huntington disease patients. Am J Clin Nutr *50*, 145-150.

Morel, F., Mazet, F., Touraille, S., and Alziari, S. (1995). Changes in the respiratory chain complexes activities and in the mitochondrial DNA content during ageing in D. subobscura. Mech Ageing Dev *84*, 171-181.

Myers, R. H., Leavitt, J., Farrer, L. A., Jagadeesh, J., McFarlane, H., Mastromauro, C. A., Mark, R. J., and Gusella, J. F. (1989). Homozygote for Huntington disease. Am J Hum Genet *45*, 615-618.

Myers, R. H., MacDonald, M. E., Koroshetz, W. J., Duyao, M. P., Ambrose, C. M., Taylor, S. A., Barnes, G., Srinidhi, J., Lin, C. S., Whaley, W. L., and et al. (1993). De novo expansion of a (CAG)n repeat in sporadic Huntington's disease. Nat Genet *5*, 168-173.

Myers, R. H., Vonsattel, J. P., Stevens, T. J., Cupples, L. A., Richardson, E. P., Martin, J. B., and Bird, E. D. (1988). Clinical and neuropathologic assessment of severity in Huntington's disease. Neurology *38*, 341-347.

Nakashima, K., Watanabe, Y., Kusumi, M., Nanba, E., Maeoka, Y., Nakagawa, M., Igo, M., Irie, H., Ishino, H., Fujimoto, A., *et al.* (1996). Epidemiological and genetic studies of Huntington's disease in the San-in area of Japan. Neuroepidemiology *15*, 126-131.

Nasir, J., Floresco, S. B., O'Kusky, J. R., Diewert, V. M., Richman, J. M., Zeisler, J., Borowski, A., Marth, J. D., Phillips, A. G., and Hayden, M. R. (1995). Targeted disruption of the Huntington's disease gene results in embryonic lethality and behavioral and morphological changes in heterozygotes. Cell *81*, 811-823.

Nicholls, D. G., and Budd, S. L. (1998). Neuronal excitotoxicity: the role of mitochondria. Biofactors *8*, 287-299.

Nishino, I., Spinazzola, A., and Hirano, M. (1999). Thymidine phosphorylase gene mutations in MNGIE, a human mitochondrial disorder. Science *283*, 689-692.

Nucifora, F. C., Jr., Sasaki, M., Peters, M. F., Huang, H., Cooper, J. K., Yamada, M., Takahashi, H., Tsuji, S., Troncoso, J., Dawson, V. L., *et al.* (2001). Interference by huntingtin and atrophin-1 with cbp-mediated transcription leading to cellular toxicity. Science *291*, 2423-2428.

O'Kusky, J. R., Nasir, J., Cicchetti, F., Parent, A., and Hayden, M. R. (1999). Neuronal degeneration in the basal ganglia and loss of pallido- subthalamic synapses in mice with targeted disruption of the Huntington's disease gene. Brain Res *818*, 468-479.

O'Neill (1995). The meaurement of brain ascorbate in vivo and its link with excitatory amino acid neurotransmission. In: Neuromethods: voltametric methods in brain systems (Clifton, NJ, Humana).

Ohsawa, Y., Isahara, K., Kanamori, S., Shibata, M., Kametaka, S., Gotow, T., Watanabe, T., Kominami, E., and Uchiyama, Y. (1998). An ultrastructural and immunohistochemical study of PC12 cells during apoptosis induced by serum deprivation with special reference to autophagy and lysosomal cathepsins. Arch Histol Cytol *61*, 395-403.

Ona, V. O., Li, M., Vonsattel, J. P., Andrews, L. J., Khan, S. Q., Chung, W. M., Frey, A. S., Menon, A. S., Li, X. J., Stieg, P. E., *et al.* (1999). Inhibition of caspase-1 slows disease progression in a mouse model of Huntington's disease [see comments]. Nature *399*, 263-267.

Ostronoff, L. K., Izquierdo, J. M., Enriquez, J. A., Montoya, J., and Cuezva, J. M. (1996). Transient activation of mitochondrial translation regulates the expression of the mitochondrial genome during mammalian mitochondrial differentiation. Biochem J *316*, 183-191.

Pawson, T. (1995). Protein-tyrosine kinases. Getting down to specifics. Nature *373*, 477-478.

Penney, J. B., Vonsattel, J. P., MacDonald, M. E., Gusella, J. F., and Myers, R. H. (1997). CAG repeat number governs the development rate of pathology in Huntington's disease. Ann Neurol *41*, 689-692.

Perez-Severiano, F., Rios, C., and Segovia, J. (2000). Striatal oxidative damage parallels the expression of a neurological phenotype in mice transgenic for the mutation of Huntington's disease. Brain Res *862*, 234-237.

Persichetti, F., Ambrose, C. M., Ge, P., McNeil, S. M., Srinidhi, J., Anderson, M. A., Jenkins, B., Barnes, G. T., Duyao, M. P., Kanaley, L., and et al. (1995). Normal and expanded Huntington's disease gene alleles produce distinguishable proteins due to translation across the CAG repeat. Mol Med *1*, 374-383.

Persichetti, F., Carlee, L., Faber, P. W., McNeil, S. M., Ambrose, C. M., Srinidhi, J., Anderson, M., Barnes, G. T., Gusella, J. F., and MacDonald, M. E. (1996). Differential expression of normal and mutant Huntington's disease gene alleles. Neurobiology of Disease *3*, - 183-190.

Perutz, M. F. (1996). Glutamine repeats and inherited neurodegenerative diseases: Molecular aspects. Current Opinion in Structural Biology *6*, 848-858.

Pesce, V., Cormio, A., Marangi, L. C., Guglielmi, F. W., Lezza, A. M., Francavilla, A., Cantatore, P., and Gadaleta, M. N. (2002). Depletion of mitochondrial DNA in the skeletal muscle of two cirrhotic patients with severe asthenia. Gene *286*, 143-148.

Peters, M. F., and Ross, C. A. (2001). Isolation of a 40-kDa Huntingtin-associated protein. J Biol Chem *276*, 3188-3194.

Petersen, A., Chase, K., Puschban, Z., DiFiglia, M., Brundin, P., and Aronin, N. (2002). Maintenance of susceptibility to neurodegeneration following intrastriatal injections of quinolinic acid in a new transgenic mouse model of Huntington's disease. Exp Neurol *175*, 297-300.

Petersen, A., Hansson, O., Puschban, Z., Sapp, E., Romero, N., Castilho, R. F., Sulzer, D., Rice, M., DiFiglia, M., Przedborski, S., and Brundin, P. (2001). Mice transgenic for exon 1 of the Huntington's disease gene display reduced striatal sensitivity to neurotoxicity induced by dopamine and 6- hydroxydopamine. Eur J Neurosci *14*, 1425-1435.

Polidori, M. C., Mecocci, P., Browne, S. E., Senin, U., and Beal, M. F. (1999). Oxidative damage to mitochondrial DNA in Huntington's disease parietal cortex. Neurosci Lett *272*, 53-56.

Porntadavity, S., Xu, Y., Kiningham, K., Rangnekar, V. M., Prachayasitikul, V., and St Clair, D. K. (2001). TPA-activated transcription of the human MnSOD gene: role of transcription factors Sp-1 and Egr-1. DNA Cell Biol *20*, 473-481.

Portera-Cailliau, C., Hedreen, J. C., Price, D. L., and Koliatsos, V. E. (1995). Evidence for apoptotic cell death in Huntington disease and excitotoxic animal models. J Neurosci *15*, 3775-3787.

Poulton, J., Morten, K., Freeman-Emmerson, C., Potter, C., Sewry, C., Dubowitz, V., Kidd, H., Stephenson, J., Whitehouse, W., Hansen, F. J., and et al. (1994). Deficiency of the human mitochondrial transcription factor h-mtTFA in infantile mitochondrial myopathy is associated with mtDNA depletion. Hum Mol Genet *3*, 1763-1769.

Poyton, R. O., and McEwen, J. E. (1996). Crosstalk between nuclear and mitochondrial genomes. Annu Rev Biochem *65*, 563-607.

Pratley, R. E., Salbe, A. D., Ravussin, E., and Caviness, J. N. (2000). Higher sedentary energy expenditure in patients with Huntington's disease. Ann Neurol *47*, 64-70.

Rachamim, N., Latter, H., Malinin, N., Asher, C., Wald, H., and Garty, H. (1995). Dexamethasone enhances expression of mitochondrial oxidative phosphorylation genes in rat distal colon. Am J Physiol *269*, C1305-1310.

Ranen, N. G., Stine, O. C., Abbott, M. H., Sherr, M., Codori, A. M., Franz, M. L., Chao, N. I., Chung, A. S., Pleasant, N., Callahan, C., *et al.* (1995). Anticipation and instability of IT 15 (CAG)(N) repeats in parent offspring pairs with Huntington disease. Am J Hum Genet *57*, 593-602.

Ravikumar, B., Duden, R., and Rubinsztein, D. C. (2002). Aggregate-prone proteins with polyglutamine and polyalanine expansions are degraded by autophagy. Hum Mol Genet *11*, 1107-1117.

Rebec, G. V., Barton, S. J., and Ennis, M. D. (2002). Dysregulation of ascorbate release in the striatum of behaving mice expressing the Huntington's disease gene. J Neurosci *22*, RC202.

Reddy, P. H., Williams, M., Charles, V., Garrett, L., PikeBuchanan, L., Whetsell, W. O., Miller, G., and Tagle, D. A. (1998). Behavioural abnormalities and selective neuronal loss in HD transgenic mice expressing mutated full length HD cDNA. Nat Genet *20*, 198-202.

Reiner, A., Albin, R. L., Anderson, K. D., D'Amato, C. J., Penney, J. B., and Young, A. B. (1988). Differential loss of striatal projection neurons in Huntington disease. Proc Natl Acad Sci U S A *85*, 5733-5737.

Renkawek, K., Stege, G. J., and Bosman, G. J. (1999). Dementia, gliosis and expression of the small heat shock proteins hsp27 and alpha B-crystallin in Parkinson's disease. Neuroreport *10*, 2273-2276.

Richfield, E. K., Maguirezeiss, K. A., Vonkeman, H. E., and Voorn, P. (1995). Preferential Loss Of Preproenkephalin Versus Preprotachykinin Neurons From the Striatum Of Huntingtons Disease Patients. Ann Neurol *38*, 852-861.

Richter, C., Park, J. W., and Ames, B. N. (1988). Normal oxidative damage to mitochondrial and nuclear DNA is extensive. Proc Natl Acad Sci U S A *85*, 6465-6467.

Rigamonti, D., Bauer, J. H., De-Fraja, C., Conti, L., Sipione, S., Sciorati, C., Clementi, E., Hackam, A., Hayden, M. R., Li, Y., *et al.* (2000). Wild-type huntingtin protects from apoptosis upstream of caspase-3. J Neurosci *20*, 3705-3713.

Rigamonti, D., Sipione, S., Goffredo, D., Zuccato, C., Fossale, E., and Cattaneo, E. (2001). Huntingtin's neuroprotective activity occurs via inhibition of procaspase-9 processing. J Biol Chem *276*, 14545-14548.

Rodriguez-Santiago, B., Casademont, J., and Nunes, V. (2001). Is mitochondrial DNA depletion involved in Alzheimer's disease? Eur J Hum Genet *9*, 279-285.

Ronai, Z. (1993). Glycolytic enzymes as DNA binding proteins. Int J Biochem *25*, 1073-1076.

Rozas, G., and Labandeira Garcia, J. L. (1997). Drug-free evaluation of rat models of parkinsonism and nigral grafts using a new automated rotarod test. Brain Res *749*, 188-199.

Rubinsztein, D. C., Leggo, J., Coles, R., Almqvist, E., Biancalana, V., Cassiman, J. J., Chotai, K., Connarty, M., Craufurd, D., Curtis, A., *et al.* (1996). Phenotypic Characterization Of Individuals With 30 40 Cag Repeats In the Huntington Disease (HD) Gene Reveals Hd Cases With 36 Repeats and Apparently Normal Elderly Individuals With 36-39 Repeats. Am J Hum Genet *59*, 16-22.

Saada, A., Shaag, A., Mandel, H., Nevo, Y., Eriksson, S., and Elpeleg, O. (2001). Mutant mitochondrial thymidine kinase in mitochondrial DNA depletion myopathy. Nat Genet *29*, 342-344.

Sambrook, J., Fritsch, E., and Maniatis, T. (1989). Molecular Cloning: A Laboratory Manual, Cold Spring Harbor Laboratory Press).

Sanchez, I., Xu, C. J., Juo, P., Kakizaka, A., Blenis, J., and Yuan, J. Y. (1999). Caspase 8 is required for cell death induced by expanded polyglutamine repeats. Neuron *22*, 623-633.

Sanger, F., Nicklen, S., and Coulson, A. R. (1977). DNA sequencing with chain-terminating inhibitors. Proc Natl Acad Sci U S A *74*, 5463-5467.

Sapp, E., Ge, P., Aizawa, H., Bird, E., Penney, J., Young, A. B., Vonsattel, J. P., and DiFiglia, M. (1995). Evidence for a preferential loss of enkephalin immunoreactivity in the external globus pallidus in low grade Huntington's disease using high resolution image analysis. Neuroscience *64*, 397-404.

Sapp, E., Penney, J., Young, A., Aronin, N., Vonsattel, J. P., and DiFiglia, M. (1999). Axonal transport of N-terminal huntingtin suggests early pathology of corticostriatal projections in Huntington disease. J Neuropathol Exp Neurol *58*, 165-173.

Sapp, E., Schwarz, C., Chase, K., Bhide, P. G., Young, A. B., Penney, J., Vonsattel, J. P., Aronin, N., and DiFiglia, M. (1997). Huntingtin localization in brains of normal and Huntington's disease patients. Ann Neurol *42*, 604-612.

Satyal, S. H., Schmidt, E., Kitagawa, K., Sondheimer, N., Lindquist, S., Kramer, J. M., and Morimoto, R. I. (2000). Polyglutamine aggregates alter protein folding homeostasis in Caenorhabditis elegans. Proc Natl Acad Sci U S A *97*, 5750-5755.

Saudou, F., Finkbeiner, S., Devys, D., and Greenberg, M. E. (1998). Huntingtin acts in the nucleus to induce apoptosis but death does not correlate with the formation of intranuclear inclusions. Cell *95*, 55-66.

Sawa, A., Wiegand, G. W., Cooper, J., Margolis, R. L., Sharp, A. H., Lawler, J. F., Jr., Greenamyre, J. T., Snyder, S. H., and Ross, C. A. (1999). Increased apoptosis of Huntington disease lymphoblasts associated with repeat length-dependent mitochondrial depolarization. Nat Med *5*, 1194-1198.

Scherzinger, E., Lurz, R., Turmaine, M., Mangiarini, L., Hollenbach, B., Hasenbank, R., Bates, G. P., Davies, S. W., Lehrach, H., and Wanker, E. E. (1997). Huntingtin encoded polyglutamine expansions form amyloid like protein aggregates in vitro and in vivo. Cell *90*, 549-558.

Schilling, G., Becher, M. W., Sharp, A. H., Jinnah, H. A., Duan, K., Kotzuk, J. A., Slunt, H. H., Ratovitski, T., Cooper, J. K., Jenkins, N. A., *et al.* (1999). Intranuclear inclusions and neuritic aggregates in transgenic mice expressing a mutant N terminal fragment of huntingtin. Hum Mol Genet *8*, 397-407.

Schilling, G., Coonfield, M. L., Ross, C. A., and Borchelt, D. R. (2001). Coenzyme Q10 and remacemide hydrochloride ameliorate motor deficits in a Huntington's disease transgenic mouse model. Neurosci Lett *315*, 149-153.

Schipper, H. M., Liberman, A., and Stopa, E. G. (1998). Neural heme oxygenase-1 expression in idiopathic Parkinson's disease. Exp Neurol *150*, 60-68.

Schwartz, A. L., and Ciechanover, A. (1999). The ubiquitin-proteasome pathway and pathogenesis of human diseases. Annu Rev Med *50*, 57-74.

Sealey, P. G., Whittaker, P. A., and Southern, E. M. (1985). Removal of repeated sequences from hybridisation probes. Nucleic Acids Res *13*, 1905-1922.

Shadel, G. S., and Clayton, D. A. (1997). Mitochondrial DNA maintenance in vertebrates. Annu Rev Biochem *66*, 409-435.

Sharp, A. H., Loev, S. J., Schilling, G., Li, S. H., Li, X. J., Bao, J., Wagster, M. V., Kotzuk, J. A., Steiner, J. P., Lo, A., and et al. (1995). Widespread expression of Huntington's disease gene (IT15) protein product. Neuron *14*, 1065-1074.

Shelbourne, P. F., Killeen, N., Hevner, R. F., Johnston, H. M., Tecott, L., Lewandoski, M., Ennis, M., Ramirez, L., Li, Z., Iannicola, C., *et al.* (1999). A Huntington's disease CAG expansion at the murine Hdh locus is unstable and associated with behavioural abnormalities in mice. Hum Mol Genet *8*, 763-774.

Shimohata, T., Nakajima, T., Yamada, M., Uchida, C., Onodera, O., Naruse, S., Kimura, T., Koide, R., Nozaki, K., Sano, Y., *et al.* (2000). Expanded polyglutamine stretches interact with TAFII130, interfering with CREB-dependent transcription. Nat Genet *26*, 29-36.

Shuman, S. (1994). Novel approach to molecular cloning and polynucleotide synthesis using vaccinia DNA topoisomerase. J Biol Chem *269*, 32678-32684.

Siebert, P. D., and Larrick, J. W. (1992). Competitive PCR. Nature *359*, 557-558.

Sieradzan, K., Mann, D. M. A., and Dodge, A. (1997). Clinical presentation and patterns of regional cerebral atrophy related to the length of trinucleotide repeat expansion in patients with adult onset Huntington's disease. Neurosci Lett *225*, 45-48.

Sieradzan, K. A., Mechan, A. O., Jones, L., Wanker, E. E., Nukina, N., and Mann, D. M. A. (1999). Huntington's disease intranuclear inclusions contain truncated, ubiquitinated huntingtin protein. Exp Neurol *156*, 92-99.

Sitte, N., Merker, K., von Zglinicki, T., and Grune, T. (2000). Protein oxidation and degradation during proliferative senescence of human MRC-5 fibroblasts. Free Radic Biol Med *28*, 701-708.

Sittler, A., Walter, S., Wedemeyer, N., Hasenbank, R., Scherzinger, E., Eickhoff, H., Bates, G. P., Lehrach, H., and Wanker, E. E. (1998). SH3GL3 associates with the Huntingtin exon 1 protein and promotes the formation of polygln-containing protein aggregates. Mol Cell *2*, 427-436.

Southern, E. M. (1975). Detection of specific sequences among DNA fragments separated by gel electrophoresis. J Mol Biol *98*, 503-517.

Steffan, J. S., Bodai, L., Pallos, J., Poelman, M., McCampbell, A., Apostol, B. L., Kazantsev, A., Schmidt, E., Zhu, Y. Z., Greenwald, M., *et al.* (2001). Histone deacetylase inhibitors arrest polyglutamine-dependent neurodegeneration in Drosophila. Nature *413*, 739-743.

Steffan, J. S., Kazantsev, A., Spasic-Boskovic, O., Greenwald, M., Zhu, Y. Z., Gohler, H., Wanker, E. E., Bates, G. P., Housman, D. E., and Thompson, L. M. (2000). The Huntington's disease protein interacts with p53 and CREB-binding protein and represses transcription. Proc Natl Acad Sci U S A *97*, 6763-6768.

Stenoien, D. L., Cummings, C. J., Adams, H. P., Mancini, M. G., Patel, K., DeMartino, G. N., Marcelli, M., Weigel, N. L., and Mancini, M. A. (1999). Polyglutamine-expanded androgen receptors form aggregates that sequester heat shock proteins, proteasome components and SRC-1, and are suppressed by the HDJ-2 chaperone. Hum Mol Genet *8*, 731-741.

Stine, O. C., Pleasant, N., Franz, M. L., Abbott, M. H., Folstein, S. E., and Ross, C. A. (1993). Correlation between the onset age of Huntington's disease and length of the trinucleotide repeat in IT-15. Hum Mol Genet *2*, 1547-1549.

Strong, T. V., Tagle, D. A., Valdes, J. M., Elmer, L. W., Boehm, K., Swaroop, M., Kaatz, K. W., Collins, F. S., and Albin, R. L. (1993). Widespread expression of the human and rat Huntington's disease gene in brain and nonneural tissues. Nat Genet *5*, 259-265.

Suggs, S. V., Wallace, R. B., Hirose, T., Kawashima, E. H., and Itakura, K. (1981). Use of synthetic oligonucleotides as hybridization probes: isolation of cloned cDNA sequences for human beta 2-microglobulin. Proc Natl Acad Sci U S A *78*, 6613-6617.

Sun, Y., and Oberley, L. W. (1996). Redox regulation of transcriptional activators. Free Radic Biol Med *21*, 335-348.

Sun, Y., Savanenin, A., Reddy, P. H., and Liu, Y. F. (2001). Polyglutamine-expanded huntingtin promotes sensitization of N-methyl-D- aspartate receptors via post-synaptic density 95. J Biol Chem *276*, 24713-24718.

Susin, S. A., Lorenzo, H. K., Zamzami, N., Marzo, I., Snow, B. E., Brothers, G. M., Mangion, J., Jacotot, E., Costantini, P., Loeffler, M., *et al.* (1999). Molecular characterization of mitochondrial apoptosis-inducing factor. Nature *397*, 441-446.

Suzuki, H., Kumagai, T., Goto, A., and Sugiura, T. (1998). Increase in intracellular hydrogen peroxide and upregulation of a nuclear respiratory gene evoked by impairment of mitochondrial electron transfer in human cells. Biochem Biophys Res Commun *249*, 542-545.

Tabrizi, S. J., Cleeter, M. W., Xuereb, J., Taanman, J. W., Cooper, J. M., and Schapira, A. H. (1999). Biochemical abnormalities and excitotoxicity in Huntington's disease brain. Ann Neurol *45*, 25-32.

Tabrizi, S. J., Workman, J., Hart, P. E., Mangiarini, L., Mahal, A., Bates, G., Cooper, J. M., and Schapira, A. H. (2000). Mitochondrial dysfunction and free radical damage in the Huntington R6/2 transgenic mouse. Ann Neurol *47*, 80-86.

Tanhauser, S. M., and Laipis, P. J. (1995). Multiple deletions are detectable in mitochondrial DNA of aging mice. J Biol Chem *270*, 24769-24775.

Taraboulos, A., Raeber, A. J., Borchelt, D. R., Serban, D., and Prusiner, S. B. (1992). Synthesis and trafficking of prion proteins in cultured cells. Mol Biol Cell *3*, 851-863.

Telenius, H., Kremer, B., Goldberg, Y. P., Theilmann, J., Andrew, S. E., Zeisler, J., Adam, S., Greenberg, C., Ives, E. J., Clarke, L. A., and et al. (1994). Somatic and gonadal mosaicism of the Huntington disease gene CAG repeat in brain and sperm [published erratum appears in Nat Genet 1994 May;7(1):113]. Nat Genet *6*, 409-414.

Tellez-Nagel, I., Johnson, A. B., and Terry, R. D. (1974). Studies on brain biopsies of patients with Huntington's chorea. J Neuropathol Exp Neurol *33*, 308-332.

Thomas, L. B., Gates, D. J., Richfield, E. K., Obrien, T. F., Schweitzer, J. B., and Steindler, D. A. (1995). DNA end labeling (TUNEL) in Huntington's disease and other neuropathological conditions. Experimental Neurology *133*, - 265-272.

Toyokuni, S. (1999). *Reactive oxygen species-induced molecular damage and its application in pathology.* Pathol Int *49*, 91-102.

Trottier, Y., Biancalana, V., and Mandel, J. L. (1994). Instability of CAG repeats in Huntington's disease: relation to parental transmission and age of onset. J Med Genet *31*, 377-382.

Trottier, Y., Devys, D., Imbert, G., Saudou, F., An, I., Lutz, Y., Weber, C., Agid, Y., Hirsch, E. C., and Mandel, J. L. (1995). Cellular localization of the Huntington's disease protein and discrimination of the normal and mutated form [see comments]. Nat Genet *10*, 104-110.

Tukamoto, T., Nukina, N., Ide, K., and Kanazawa, I. (1997). Huntington's disease gene product, huntingtin, associates with microtubules in vitro. Brain Res Mol Brain Res *51*, 8-14.

Usdin, M. T., Shelbourne, P. F., Myers, R. M., and Madison, D. V. (1999). Impaired synaptic plasticity in mice carrying the Huntington's disease mutation. Hum Mol Genet *8*, 839-846.

Van Tuyle, G. C., and Pavco, P. A. (1985). The rat liver mitochondrial DNA-protein complex: displaced single strands of replicative intermediates are protein coated. J Cell Biol *100*, 251-257.

Velier, J., Kim, M., Schwarz, C., Kim, T. W., Sapp, E., Chase, K., Aronin, N., and DiFiglia, M. (1998). Wild-type and mutant huntingtins function in vesicle trafficking in the secretory and endocytic pathways. Exp Neurol *152*, 34-40.

Virbasius, J. V., and Scarpulla, R. C. (1994). Activation of the human mitochondrial transcription factor A gene by nuclear respiratory factors: a potential regulatory link between nuclear and mitochondrial gene expression in organelle biogenesis. Proc Natl Acad Sci U S A *91*, 1309-1313.

Vis, J. C., Verbeek, M. M., De Waal, R. M., Ten Donkelaar, H. J., and Kremer, H. P. (1999). 3-Nitropropionic acid induces a spectrum of Huntington's disease-like neuropathology in rat striatum. Neuropathol Appl Neurobiol *25*, 513-521.

Vonsattel, J. P., Myers, R. H., Stevens, T. J., Ferrante, R. J., Bird, E. D., and Richardson, E. P., Jr. (1985). Neuropathological classification of Huntington's disease. J Neuropathol Exp Neurol *44*, 559-577.

Vonsattel, J. P. G., and DiFiglia, M. (1998). Huntington disease. J Neuropathol Exp Neurol *57*, 369-384.

Waelter, S., Scherzinger, E., Hasenbank, R., Nordhoff, E., Lurz, R., Goehler, H., Gauss, C., Sathasivam, K., Bates, G. P., Lehrach, H., and Wanker, E. E. (2001). The huntingtin interacting protein HIP1 is a clathrin and alpha-adaptin- binding protein involved in receptor-mediated endocytosis. Hum Mol Genet *10*, 1807-1817.

Wallace, D. C. (1999). Mitochondrial diseases in man and mouse. Science *283*, 1482-1488.

Wanker, E. E., Rovira, C., Scherzinger, E., Hasenbank, R., Walter, S., Tait, D., Colicelli, J., and Lehrach, H. (1997). HIP I: A huntingtin interacting protein isolated by the yeast two hybrid system. Hum Mol Genet *6*, 487-495.

Warrick, J. M., Chan, H. Y., Gray-Board, G. L., Chai, Y., Paulson, H. L., and Bonini, N. M. (1999). Suppression of polyglutamine-mediated neurodegeneration in Drosophila by the molecular chaperone HSP70. Nat Genet *23*, 425-428.

Wellington, C. L., Ellerby, L. M., Hackam, A. S., Margolis, R. L., Trifiro, M. A., Singaraja, R., McCutcheon, K., Salvesen, G. S., Propp, S. S., Bromm, M., *et al.* (1998). Caspase cleavage of gene products associated with triplet expansion disorders generates truncated fragments containing the polyglutamine tract. J Biol Chem *273*, 9158-9167.

Wellington, C. L., Singaraja, R., Ellerby, L., Savill, J., Roy, S., Leavitt, B., Cattaneo, E., Hackam, A., Sharp, A., Thornberry, N., *et al.* (2000). Inhibiting caspase cleavage of huntingtin reduces toxicity and aggregate formation in neuronal and nonneuronal cells. J Biol Chem *275*, 19831-19838.

Wexler, N. S., Young, A. B., Tanzi, R. E., Travers, H., Starosta-Rubinstein, S., Penney, J. B., Snodgrass, S. R., Shoulson, I., Gomez, F., Ramos Arroyo, M. A., and et al. (1987). Homozygotes for Huntington's disease. Nature *326*, 194-197.

Wheeler, V. C., Auerbach, W., White, J. K., Srinidhi, J., Auerbach, A., Ryan, A., Duyao, M. P., Vrbanac, V., Weaver, M., Gusella, J. F., *et al.* (1999). Length dependent gametic CAG repeat instability in the Huntington's disease knock in mouse. Hum Mol Genet *8*, 115-122.

Wheeler, V. C., Gutekunst, C. A., Vrbanac, V., Lebel, L. A., Schilling, G., Hersch, S., Friedlander, R. M., Gusella, J. F., Vonsattel, J. P., Borchelt, D. R., and MacDonald, M. E. (2002). Early phenotypes that presage late-onset neurodegenerative disease allow testing of modifiers in Hdh CAG knock-in mice. Hum Mol Genet *11*, 633-640.

Wheeler, V. C., White, J. K., Gutekunst, C. A., Vrbanac, V., Weaver, M., Li, X. J., Li, S. H., Yi, H., Vonsattel, J. P., Gusella, J. F., *et al.* (2000). Long glutamine tracts cause nuclear localization of a novel form of huntingtin in medium spiny striatal neurons in HdhQ92 and HdhQ111 knock- in mice. Hum Mol Genet *9*, 503-513.

White, J. K., Auerbach, W., Duyao, M. P., Vonsattel, J. P., Gusella, J. F., Joyner, A. L., and MacDonald, M. E. (1997). Huntingtin is required for neurogenesis and is not impaired by the Huntington's disease CAG expansion. Nat Genet *17*, 404-410.

Wiesner, R. J. (1992b). Regulation of mitochondrial gene expression: transcription versus replication [letter; comment]. Trends Genet *8*, 264-265.

Wiesner, R. J., Aschenbrenner, V., Ruegg, J. C., and Zak, R. (1994). Coordination of nuclear and mitochondrial gene expression during the development of cardiac hypertrophy in rats. Am J Physiol *267*, C229-235.

Wiesner, R. J., Hornung, T. V., Garman, J. D., Clayton, D. A., O'Gorman, E., and Wallimann, T. (1999). Stimulation of mitochondrial gene expression and proliferation of mitochondria following impairment of cellular energy transfer by inhibition of the phosphocreatine circuit in rat hearts [In Process Citation]. J Bioenerg Biomembr *31*, 559-567.

Wiesner, R. J., Kurowski, T. T., and Zak, R. (1992). Regulation by thyroid hormone of nuclear and mitochondrial genes encoding subunits of cytochrome-c oxidase in rat liver and skeletal muscle. Mol Endocrinol *6*, 1458-1467.

Williams, A. J., and Kaguni, L. S. (1995). Stimulation of Drosophila mitochondrial DNA polymerase by single- stranded DNA-binding protein. J Biol Chem *270*, 860-865.

Williams, R. S. (1986). Mitochondrial gene expression in mammalian striated muscle. Evidence that variation in gene dosage is the major regulatory event. J Biol Chem *261*, 12390-12394.

Wood, J. D., Macmillan, J. C., Harper, P. S., Lowenstein, P. R., and Jones, A. L. (1996). Partial Characterization Of Murine Huntingtin and Apparent Variations In the Subcellular Localization Of Huntingtin In Human, Mouse and Rat Brain. Hum Mol Genet *5*, 481-487.

Wyttenbach, A., Carmichael, J., Swartz, J., Furlong, R. A., Narain, Y., Rankin, J., and Rubinsztein, D. C. (2000). Effects of heat shock, heat shock protein 40 (HDJ-2), and proteasome inhibition on protein aggregation in cellular models of Huntington's disease. Proc Natl Acad Sci U S A *97*, 2898-2903.

Wyttenbach, A., Sauvageot, O., Carmichael, J., Diaz-Latoud, C., Arrigo, A. P., and Rubinsztein, D. C. (2002). Heat shock protein 27 prevents cellular polyglutamine toxicity and suppresses the increase of reactive oxygen species caused by huntingtin. Hum Mol Genet *11*, 1137-1151.

Wyttenbach, A., Swartz, J., Kita, H., Thykjaer, T., Carmichael, J., Bradley, J., Brown, R., Maxwell, M., Schapira, A., Orntoft, T. F., *et al.* (2001). Polyglutamine expansions cause decreased CRE-mediated transcription and early gene expression changes prior to cell death in an inducible cell model of Huntington's disease. Hum Mol Genet *10*, 1829-1845.

Xu, B., and Clayton, D. A. (1996). RNA-DNA hybrid formation at the human mitochondrial heavy-strand origin ceases at replication start sites: an implication for RNA-DNA hybrids serving as primers. Embo J *15*, 3135-3143.

Xu, Y., Porntadavity, S., and St Clair, D. K. (2002). Transcriptional regulation of the human manganese superoxide dismutase gene: the role of specificity protein 1 (Sp1) and activating protein-2 (AP-2). Biochem J *362*, 401-412.

Yamamoto, A., Lucas, J. J., and Hen, R. (2000). Reversal of neuropathology and motor dysfunction in a conditional model of Huntington's disease. Cell *101*, 57-66.

Yamashita, T., Ando, Y., Obayashi, K., Terazaki, H., Sakashita, N., Uchida, K., Ohama, E., Ando, M., and Uchino, M. (2000). Oxidative injury is present in Purkinje cells in patients with olivopontocerebellar atrophy. J Neurol Sci *175*, 107-110.

Yoritaka, A., Hattori, N., Uchida, K., Tanaka, M., Stadtman, E. R., and Mizuno, Y. (1996). Immunohistochemical detection of 4-hydroxynonenal protein adducts in Parkinson disease. Proc Natl Acad Sci U S A *93*, 2696-2701.

Young, A. B., Penney, J. B., Starosta-Rubinstein, S., Markel, D. S., Berent, S., Giordani, B., Ehrenkaufer, R., Jewett, D., and Hichwa, R. (1986). PET scan investigations of Huntington's disease: cerebral metabolic correlates of neurological features and functional decline. Ann Neurol *20*, 296-303.

Young, A. B., Greenamyre, J. T., Hollingsworth, Z., Albin, R., D'Amato, C., Shoulson, I., and Penney, J. B. (1988). NMDA receptor losses in putamen from patients with Huntington's disease. Science *241*, 981-983.

Zeitlin, S., Liu, J. P., Chapman, D. L., Papaioannou, V. E., and Efstratiadis, A. (1995). Increased apoptosis and early embryonic lethality in mice nullizygous for the Huntington's disease gene homologue. Nat Genet *11*, 155-163.

Zeron, M. M., Chen, N., Moshaver, A., Lee, A. T., Wellington, C. L., Hayden, M. R., and Raymond, L. A. (2001). Mutant huntingtin enhances excitotoxic cell death. Mol Cell Neurosci *17*, 41-53.

Zeron, M. M., Hansson, O., Chen, N., Wellington, C. L., Leavitt, B. R., Brundin, P., Hayden, M. R., and Raymond, L. A. (2002). Increased sensitivity to N-methyl-D-aspartate

receptor-mediated excitotoxicity in a mouse model of Huntington's disease. Neuron *33*, 849-860.

Zhou, H., Li, S. H., and Li, X. J. (2001). Chaperone suppression of cellular toxicity of huntingtin is independent of polyglutamine aggregation. J Biol Chem *276*, 48417-48424.

Zuccato, C., Ciammola, A., Rigamonti, D., Leavitt, B. R., Goffredo, D., Conti, L., MacDonald, M. E., Friedlander, R. M., Silani, V., Hayden, M. R., *et al.* (2001). Loss of huntingtin-mediated BDNF gene transcription in Huntington's disease. Science *293*, 493-498.

Zuhlke, C., Riess, O., Bockel, B., Lange, H., and Thies, U. (1993). Mitotic stability and meiotic variability of the (CAG)n repeat in the Huntington disease gene. Hum Mol Genet *2*, 2063-2067.